Università degli studi di Genova

School of Mathematical, Physical and Natural Sciences

Department of Chemistry and Industrial Chemistry

Doctorate in

Sciences and Technologies of Chemistry and Materials

Curricula: Chemical Science and Technology

(XXXVI Cycle)

Synthesis, Characterization and Application of Polycaprolactone Based Systems

Supervisor

Prof.ssa Orietta Monticelli

Candidate

Giacomo Damonte

Index

Abstract

ITA: Il programma di ricerca di dottorato è stato incentrato sullo sviluppo di nuove formulazioni a base di policaprolattone (PCL) mediante l'impiego di polimeri con geometria lineare e stellare, sia commerciali che preparati *ad hoc*. Comunemente, per tutti questi sistemi, è stata investigata l'influenza della natura chimica del PCL nonché dei suoi gruppi terminali di catena, introdotti attraverso differenti tipi di funzionalizzazione chimica, sulle proprietà finali delle formulazioni studiate. In particolare, l'interesse per il PCL risiede nelle sue caratteristiche intrinseche di biodegradabilità e biocompatibilità. Inoltre, l'utilizzo di questo polimero può essere promettente in relazione allo sviluppo di nuovi materiali sostenibili poiché potenzialmente ottenibile attraverso fonti rinnovabili. Di particolare rilevanza in questo progetto di ricerca è stato l'impiego di polimeri caratterizzati da topologia molecolare stellare, comunemente definiti come "*star-shaped*", a bassa massa molecolare. Questo particolare tipo di struttura molecolare permette di poter influenzare alcune importanti proprietà fisiche dei polimeri come la cristallinità, il raggio idrodinamico e di girazione, la solubilità, la viscosità del fuso e delle soluzioni risultanti. In particolare, vale la pena sottolineare come questi sistemi siano dotati di un maggior numero di gruppi funzionali terminali per unità di massa rispetto ai polimeri lineari di peso molecolare equivalente. Infatti, una delle principali problematiche del PCL è proprio legata all'assenza di funzionalità di catena sfruttabili per la sua modificazione chimica con metodi convenzionali, rendendola di fatto possibile solo sui terminali ossidrilici. L'unione di queste caratteristiche peculiari rende dunque i sistemi *star-shaped* molto interessanti dal punto di vista di un loro impiego come additivi in sistemi polimerici, in virtù della loro miscibilità e della capacità di conferire funzionalità, tramite l'elevato numero di gruppi che è possibile introdurre tramite il loro utilizzo. Nello specifico, le attività di ricerca durante il dottorato si sono articolate attraverso sviluppo di sette differenti sistemi contenenti PCL. In particolare, due lavori hanno riguardato la preparazione di PCL lineari e *star-shaped* pirenil terminati e la loro rispettiva applicazione nello sviluppo di nanocompositi e *nanopapers* contenenti *graphene nanoplates* (GNP). Lo sfruttamento della funzionalità pirenica è stato finalizzato allo scopo di favorire le interazioni PCL/GNP attraverso l'introduzione di interazioni di *stacking* di tipo π-π con la superficie degli strati di grafite presenti nel GNP con l'obiettivo di promuovere, in un lavoro, la dispersione del GNP nei nanocompositi onde aumentarne la conducibilità elettrica, e nell'altro la reticolazione fisica del GNP nei *nanopapers* per migliorarne le proprietà termomeccaniche. Negli altri lavori, PCL lineari e *star-shaped* con diverse funzionalità terminali sono stati impiegati nella preparazione di film polimerici

sia porosi che densi nonché in idrogeli meccanicamente rinforzati e vetrimeri. Nello specifico, un lavoro è stato incentrato sullo sviluppo di film porosi con proprietà adatte al loro utilizzo come sensori ed assorbitori, tramite l'impiego di un PCL lineare ad alta massa molecolare in combinazione con acido polilattico (PLA) e GNP, con la funzione di aumentare la duttilità e manipolabilità dei film. Un altro lavoro, inerente alla preparazione di film densi a base di PLA, ha previsto l'impiego di tre diversi PCL *star-shaped* con funzionalità terminali di tipo ossidrilico (PCL-OH), carbossilico (PCL-COOH), pirenico (PCL-Pyr). Questi polimeri sono stati aggiunti al fine di investigare l'influenza delle diverse funzionalità sulle proprietà finali dei materiali ottenuti nonchè di migliorare alcune proprietà dei film come l'allungamento a rottura e la capacità assorbente nei confronti di specie cationiche. Analogamente, un lavoro affine, ha riguardato nuovamente lo sviluppo di film densi a base di PCL ad alta massa molecolare e GNP. A tale scopo, un PCL *star-shaped* con funzionalità terminali di tipo furoilico (PCL-Fur) è stato aggiunto al sistema con la funzione di promuovere la dispersione del GNP all'interno della matrice di PCL. Questo è stato possibile attraverso la formazione di legami covalenti mediante reazione di Diels-Alder tra gli anelli furanici del PCL-Fur ed i bordi dei sistemi grafenici presenti nel GNP. L'applicazione del PCL nei lavori inerenti alla preparazione di idrogeli ha previsto l'utilizzo di polimeri *star-shaped* dotati funzionalità terminali reattive nei confronti di reazioni di polimerizzazione radicalica, di tipo acrilico (PCL-TA) e maleico (PCL-COOH) in combinazione, rispettivamente, con idrossietilacrilato e N-isopropilacrilammide. Queste funzionalità sono state sfruttate per promuovere, durante il processo di polimerizzazione frontale, la reticolazione con conseguente formazione strutture copolimeriche. Queste hanno permesso di migliorare compatibilità tra i polimeri e le proprietà meccaniche del sistema. Al contempo, l'utilizzo delle funzionalità maleiche ha permesso nuovamente di introdurre capacità assorbente da parte degli idrogeli nei confronti di specie cationiche. Infine, in un ultimo lavoro, tre PCL *star-shaped* con funzionalità terminali acriliche e diversa massa e/o numero di braccia sono stati utilizzati nello sviluppo di altrettanti vetrimeri *green,* ossia senza l'utilizzo di catalizzatori e biodegradabili. Questo è stato possibile sfruttando una reazione di tipo tiolo-acrilato tra le funzionalità terminali ed i gruppi tiolici di un reticolante dinamico difunzionale contente esteri boronici. In definitiva, si può affermare come i risultati riportati in questa tesi mettano nuovamente in evidenza la versatilità applicativa del PCL, un poliestere alifatico di notevole interesse applicativo. Tale ricerca ha inoltre provato come questa bioplastica risulti ancora essere capace di possedere, a quasi un secolo dalla sua scoperta, caratteristiche promettenti per lo sviluppo di nuovi materiali sostenibili in sistemi dove le sue potenzialità non sono ancora state del tutto pienamente sfruttate.

ENG: The PhD research program focused on the development of new formulations based on polycaprolactone (PCL) using polymers with linear and star geometry, commercially and *ad hoc* synthesized. For all these systems, the influence of the chemical nature of PCL as well as its chain terminal groups, introduced by different types of chemical functionalization, on the final properties of the studied formulations was investigated. The interest in PCL lies particularly in its intrinsic characteristics of biodegradability and biocompatibility. In addition, the use of this polymer can be promising with regard to the development of new sustainable materials, as it can potentially be obtained from renewable sources. Of particular relevance in this research project was the use of polymers characterized by star molecular topology, commonly defined as "star-shaped", with low molecular weight. In general, this type of molecular structure allows to influence some important physical properties of polymers, such as crystallinity, hydrodynamic and gyration radius, solubility, viscosity of the melt and the resulting solutions. In particular, it is worth noting that these systems have a greater number of terminal functional groups per unit mass than linear polymers of equivalent molecular weight. Indeed, one of the main problems of linear PCL is the lack of chain functionalities that can be exploited for chemical modification by conventional methods, which is only possible at the hydroxyl end groups. The combination of these peculiar features therefore makes star-shaped systems very interesting in terms of their use as additives in polymer systems, due to their miscibility and ability to confer functionality through the high number of groups. Specifically, the research activities during the PhD were articulated through the development of seven different systems containing PCL. In particular, two projects focused on the preparation of linear and star-shaped pyrenyl-terminated PCLs and their application in the development of nanocomposites and nanopapers containing graphene nanoplates (GNPs). The exploitation of pyrene functionality aimed at promoting PCL/GNP interactions by introducing π-π stacking interactions between the polymer functionalities and the surface of the graphite layers of GNP. In one work, the above property was applied to promote the dispersion of GNP in polymer nanocomposites and consequently their electrical conductivity, while in another system, namely a nanopaper, the specific PCL/GNP interactions were used to improve its thermomechanical properties by the physical cross-linking of GNP. The PhD work also dealt with the application of linear and star-shaped PCLs with different end functionalities in the preparation of porous and dense films as well as hydrogels and vitrimers. Specifically, one work focused on the development of porous films with properties suitable for their use as sensors and absorbers, exploiting a high molecular weight linear PCL in combination with polylactic acid (PLA) and GNP to increase the ductility and manipulability of the films. In another study on the preparation of dense PLA-based films, three types of star-shaped PCLs with hydroxyl (PCL-OH), carboxyl (PCL-COOH) and pyrenic (PCL-Pyr) end groups were used. Indeed, the influence of the different

functionalities on the final properties of the materials was investigated as well as the improvement of some properties of the films, such as elongation at break and the adsorption capacity towards cationic species. A related work also dealt with the development of dense films based on high molecular mass PCL and GNP. For this purpose, a star-shaped PCL with furoyl-type terminal functionalities (PCL-Fur) was added to the system to promote the GNP dispersion within the PCL matrix. This was achieved by the occurrence of covalent bonds through Diels-Alder reaction between the furan rings of PCL-Fur and the edges of the graphene systems. In the application of PCL in the preparation of hydrogels, star-shaped polymers with reactive end functionalities against radical polymerization reactions were used, namely acrylic (PCL-TA) and maleic (PCL-COOH), in combination with hydroxyethyl acrylate and N-isopropyl acrylamide, respectively. These functionalities were exploited to promote cross-linking with consequent formation of copolymers during the frontal polymerization process used. In particular, the effect of the above-mentioned copolymers on the compabilization of the two polymer phases and consequently on the hydrogel mechanical properties was investigated. At the same time, the use of maleic functions has in turn enabled the adsorption capacity of hydrogels towards cationic species. Finally, in a last work, three star-shaped PCLs with acrylic functionalities and different mass and/or number of arms were used for the development of catalyst-free biodegradable vitrimers. This was possible by exploiting a thiol-acrylate cross-linking reaction between the terminal PCL functionalities and the thiol groups of a dynamic bifunctional crosslinker containing boronic esters. In conclusion, the results reported in this thesis highlight the versatility of PCL, and prove that, almost a century after its discovery, this bioplastic has promising characteristics for the development of new sustainable materials in systems where its potential has not yet been fully exploited.

Outline

Chapter 1: Introduction

In this chapter, some of the general characteristics of PCL ad PCL-related materials are discussed, as well as some of their most important applications, giving a complete vision to the reader of the possible applications of this bioplastic nowadays. In addition, a more specific focus is made on the synthetical methods currently in use to produce monomers, precursors of PCL, as well as an in-depth discussion of their polymerization techniques. In this part some general notes will also be provided regarding the state-of-the-art about the preparation of polymers with star topology including some of their practical applications that can be found in the current literature.

Chapter 2: On the development of an effective method to produce conductive PCL films

In this chapter the effects of a low molecular weight, pyrenyl terminated PCL (Pyr-PCL) in the preparation of nanocomposites were investigated. Pyr-PCL was designed to be an effective promoter of the dispersion of graphene nanoplates (GNP) in PCL-based nanocomposites prepared through a melt blending approach. The exploitation, in Pyr-PCL, of the pyrenyl moiety coupled to a PCL chain was crucial to promote, at the same time, the formation of π-π stacking interactions with the surface of graphene layers and ensure their homogeneous dispersion and compatibilization throughout the polymeric matrix thanks to the same chemical composition of the polymer chains. A comparison between different PCL-GNP nanocomposites, prepared with and without the additive, was made with a particular focus on their thermal and electrical properties. It has been found that the addition of Pyr-PCL significantly increases the electrical conductivity of the material thanks to a better exfoliation and dispersion of the graphite within the polymer matrix. This allows an improvement in the ability to form the percolative network that underlies the conduction process.

Chapter 3: Synthesis and characterization of a novel star polycaprolactone to be applied in the development of graphite nanoplates-based nanopapers

The focus of this work was to design and synthesize a polymeric material capable to improve thermomechanical properties of GNP-based nanopapers, i.e., films characterized

by a very high GNP content (up to 90%). With this aim, a star-shaped PCL was end-capped with pyrenic functionalities using a three-step procedure (PCL-star-4-Pyr) to interact with the graphite surface and facilitate physical networking among GNP layers by providing, like in the previous work, π-π stacking bridges. Specifically, GNP-based nanopapers were prepared using a solution blending approach followed by filtration and hot pressing. The increased interactions between polymer and GNP provided by the functionalities allowed to introduce a greater quantity of PCL respect to nanopapers prepared using a conventional linear high molecular weight PCL. The incorporation of pyrenyl moieties decreased polymer crystallinity compared to the starting hydroxyl terminated PCL, enhancing at the same time its thermal stability. The increased interactions between functionalized PCL and GNP resulted in nanopapers with remarkable heat-spreading capacity and good thermomechanical stability, well above PCL melting point, making them high performance sustainable materials.

Chapter 4: On novel hydrogels based on poly(2-hydroxyethyl acrylate) and polycaprolactone with improved mechanical properties prepared by frontal polymerization

This study aimed to improve the mechanical performances, in terms of stiffness and compressive strength, of poly(2-hydroxyethyl acrylate) (PHEA)-based hydrogels by using a star-shaped, acryloyl terminated PCL (PCL-TA) in place of a traditional cross-linker, pentaerythritol tetraacrylate (PE-TA). The hydrogels were prepared by varying concentrations of PCL-TA using frontal (FP) and bulk polymerization (BP), and their properties were compared. The use of a low molecular weight polymer was crucial to obtain the formation of a starting homogeneous mixture which was possible only by taking advantage of PCL-TA solubility in 2-hydroxyethyl acrylate. This was critical due to the non-miscibility between PCL and PHEA, to obtain the highest possible degree of dispersion of PCL domains during the polymerization phase. Interestingly, the use of PCL-TA enabled to obtain the formation of stable polymerization fronts in FP samples. Thermal analysis of PHEA/PCL hydrogels revealed the formation of a partially miscible copolymeric system between PCL and PHEA that was confirmed by comparing the thermal behaviour of hydrogels polymerized in the presence of a hydroxyl terminated PCL without active functional end groups. This was reflected by the mechanical behaviour of PCL-containing hydrogels which exhibited higher modulus than PE-TA crosslinked PHEA, remaining structurally stable even under high compressive loads. The combination

of striking mechanical properties, fast and efficient frontal polymerization approach and the environmentally friendly nature of PCL make these hydrogels promising materials for practical applications.

Chapter 5: Multifunctional Porous Films Based on Polylactic Acid

In this chapter the preparation of porous PLA-based films using phase inversion to be employed in the development of sensors is discussed. Some features such as ductility and electrical conductivity of the films were obtained by addition to the system, during its preparation, of PCL and GNP respectively. Phase inversion process was optimized by studying the cause-effect relation between polymer concentration, viscosity of the solutions and porosity of the obtained films. Interestingly, morphological analysis of PCL-containing films revealed a homogeneous PCL dispersion in PLA with GNP flakes completely adhered to the polymer matrix. In a further step, surface amino functionalities, to provide ionic interactions with negatively charged species, were introduced through aminolysis of the polymer films using an ethylenediamine solution. After this treatment, the films exhibited high capacity to adsorb fluorescein, a model dye, demonstrating their retaining ability. Mechanical characterization revealed a 3-fold increase in the elongation at break in PCL-containing films respect neat PLA ones. Optimized, surface-functionalized, PLA/PCL-GNP containing films were tested positively as effective electrodes for voltammetric determination of ascorbic acid making the materials attractive for further applications.

Chapter 6: On the effective application of star-shaped polycaprolactones with different end functionalities to improve the properties of polylactic acid blend films

The purpose of this work was to improve the mechanical properties of a widely employed commodity bioplastic PLA, which shows poor elongation at break, by adding a ductile polymer like PCL. In detail, star-shaped, hydroxyl (PCL-OH), carboxyl (PCL-COOH) and pyrenyl (PCL-Pyr) terminated PCL were employed as additives (20% -wt.%) in the preparation of PLA-based dense films by solvent casting technique. The choice of the use of low molecular weight star-shaped PCLs was done by considering the intrinsic immiscibility between PLA and PCL, to improve their blending. At the same time, the inclusion of PCL with different functionalities enabled an improvement in its phase dispersion and adhesion within the PLA matrix. As expected, when observed through FE-SEM, star PCLs-containing films showed smaller and better-adhered PCL domains in

comparison to those prepared with high molecular weight linear PCL. Indeed, as revealed by thermal characterization, the properties of PCL domains were influenced by the different chain-end functionalities. Remarkably, PLA films containing star-shaped PCLs displayed superior elongation at break, up to 40% ca., while preserving an acceptable level of stiffness for practical applications. Contact angle measurements revealed an increased wettability of PCL-COOH containing films. These, in a dye adsorption test, showed the highest capacity to retain the cationic dye, indicating ionic interactions with positively charged molecules. Enzymatic degradation test using cutinase, an enzyme with high affinity towards PCL, demonstrated that star PCLs containing films were characterized by slower and more controlled hydrolysis compared to PLA/high molecular PCL systems, with the possibility of tuning the kinetics by varying star PCL end functionality.

Chapter 7: Star-shaped furoate-PCL: An effective compound for the development of graphite nanoplatelets-based films

In this chapter, the dispersion of graphite nanoplatelets (GNP) in high molecular weight linear PCL (PCL-L) films prepared by solvent casting was improved using a star-shaped, PCL-based additive end-capped with furoyl terminal moietes (PCL-Fur). This additive was synthesized with the aim of interacting and forming covalent bonds with the edges of graphene layers through Diels-Alder reactions. The reactivity of furoyl groups to GNP was demonstrated by studying the thermal behaviour of the GNP/methyl-2-furoate system. In particular, when combined with PCL (PCL-L) and high molecular weight GNP, PCL-Fur has been shown to improve GNP dispersion, as demonstrated through DSC and UV-Vis measurements of the prepared blends. In fact, SEM characterization of the resulting composite films revealed excellent dispersion and adhesion of GNP flakes to the polymer matrix. The homogeneous distribution of the conductive material, provided by PCL-Fur, resulted in significantly higher electrical conductivity values in films containing PCL-L/PCL-Fur/GNP compared to pure PCL-L/GNP films.

Chapter 8: Mechanically-reinforced biocompatible hydrogels based on poly(N-isopropylacrylamide) and star-shaped polycaprolactones

In this chapter some properties of thermoresponsive poly(N-isopropyl acrylamide) (PNIPAAm) hydrogels prepared by FP, in terms of functionality and mechanical behaviour, were improved by incorporation of a star-shaped PCL (PCL-COOH) to keep

unaltered the biocompatibility of the materials. Specifically, this additive, was tailored to be at the same time: easy to synthesize, soluble in the reactive mixture, capable of participating in the formation of cross-links during the radical FP reaction and capable to introduce ionizable negatively charged groups for non-specific interactions with drugs. For these systems the obtaining of stable polymerization fronts up to 25% wt% of PCL-COOH was verified. The presence of this additive influenced the morphology, swelling and mechanical properties of the prepared hydrogels. In particular, PCL-COOH decreased mean pore size and swelling ratio of hydrogels without affecting their thermoresponsive behaviour. Thermal analysis revealed a partial miscibility between PCL and PNIPAAM with the possible formation of a mixed copolymer settled at their interphase. A dye retention test showed higher loading capacity of the PCL-containing hydrogels. Cytotoxicity of the materials was evaluated using SH-SY5Y cell line which demonstrated complete biocompatibility of the hydrogels making them promising materials for biomedical applications.

Chapter 9: On novel sustainable vitrimers based on polycaprolactones

This work aimed to develop novel biodegradable PCL-based boronic ester vitrimers to meet the current demand for a sustainable economy. Three different star-shaped, acrylated tetra- and hexafunctional polymers, with different molecular weight, were prepared and cross-linked in bulk by exploiting a thiol-acrylate reaction with a bifunctional boronic ester dithiol, namely [2,2′-(1,4-phenylene)-bis[4-mercaptan-1,3,2-dioxaborolane] (DBEDT), which synthesis is easy and can be performed under mild conditions. For all the prepared vitrimers, the formation of a cross-linked network was testified by the high values of gel fraction measured, around 80%. Mechanical and rheological characterization revealed the existence of dynamic covalent networks capable of rapid relaxation phenomena. Specifically, rheological measurements showed activation energies for the relaxation process in the range of 44-62 kJ/mol, which makes these materials comparable to other boronic ester vitrimers. Moreover, complete enzymatic hydrolysis within 12 days was proven for the developed systems, highlighting their excellent degradability. In addition, all the vitrimers demonstrated good recyclability and exhibited self-healing properties when processed at 180 °C opening the possibility to extend material lifecycle and reduce their environmental impact.

Chapter 1: Introduction

1.1 Poly(ε-caprolactone)

Poly(ε-caprolactone), generally referred as polycaprolactone (PCL), is a semicrystalline, aliphatic, saturated polyester composed by several 6-hydroxyhexanoic repetition units which structure is reported in **Figure 1.1**. Its crystallinity degree can reach values up to 70% which is generally reduced by increasing the molecular weight due chain folding phenomena [1]; for example, in linear samples with molecular weight of approximately 200 $kg \cdot mol^{-1}$ a crystallinity reduction to 33% is observed [2]. In detail, the unit cell structure of PCL crystalline phase (**Figure 1.2**) is orthorhombic (space group $P2_12_12_1$-D_2^4) with lattice constants of: **a** = 7.496±0.002 A˚, **b** = 4.974±0.001 A˚ and **c** = 17.297±0.023 A˚, with **c** being the fibre axis [3].

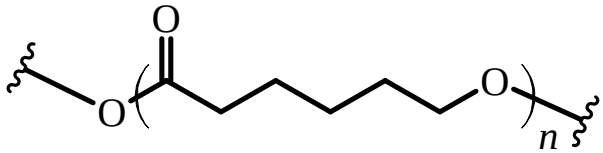

Figure 1.1. *Chemical structure of PCL.*

The polymer, due to the low glass transition (-60 °C ca.) and melting temperature of crystalline phase (56-65 °C) in addition to the good rheological properties is easily processable and can be used to fabricate highly structured forms such as foams prepared, for example by using super-critical CO_2 [4].This polymer, thanks to its strong hydrophobicity, is readily soluble in a wide range of medium and low polarity solvents such as chloroform, dichloromethane, carbon tetrachloride, benzene, toluene, cyclohexanone and 2-nitropropane while is slightly soluble in acetone, 2-butanone, ethyl acetate, dimethylformamide and acetonitrile and completely insoluble in completely apolar or polar solvents like petroleum ether, diethyl ether, water or alcohols [5]. These last one together with *n*-hexane or petroleum ether are often used for its precipitation from its solutions. Due to its physicochemical properties displays an exceptional blend compatibility when combined with polymers like PVC, ABS, PC, nitrocellulose, and cellulose butyrate where it is often employed as plasticizer. Considering its structure, PCL possess the lowest O/C ratio when compared to other two largely diffused biodegradable polymers, PLA and PGA, which indirectly indicates its higher hydrophobicity [6]. This character is also reflected by the values of the Hildebrand parameters (**Table 1.1**), which show higher dispersive (δ_d), lower polar (δ_p) and hydrogen bonding (δ_h) and similar total

solubility parameter (δ_T) components for PCL, when compared to other polymers such as poly(lactic acid) (PLA) and poly(ethylene glycol) PEG [7]. Thanks to the presence of the ester moiety, it appears to be a fairly biodegradable material, however the degradation is generally slow and depends on different parameters such as the surface area to volume ratio, molecular weight and geometry of the specimen [8] being degraded on a timescale ranging from a few months to several years, especially when hydrolysis is conducted in water or phosphate buffered saline (PBS) solution [8,9]. As generally reported for biodegradable aliphatic polyesters, the degradation usually occurs through bulk or surface hydrolysis [10]. For this reason, the high hydrophobicity and the important crystallinity value displayed by PCL hinder the access of water molecules in the amorphous fraction in the bulk slowing down the whole process.

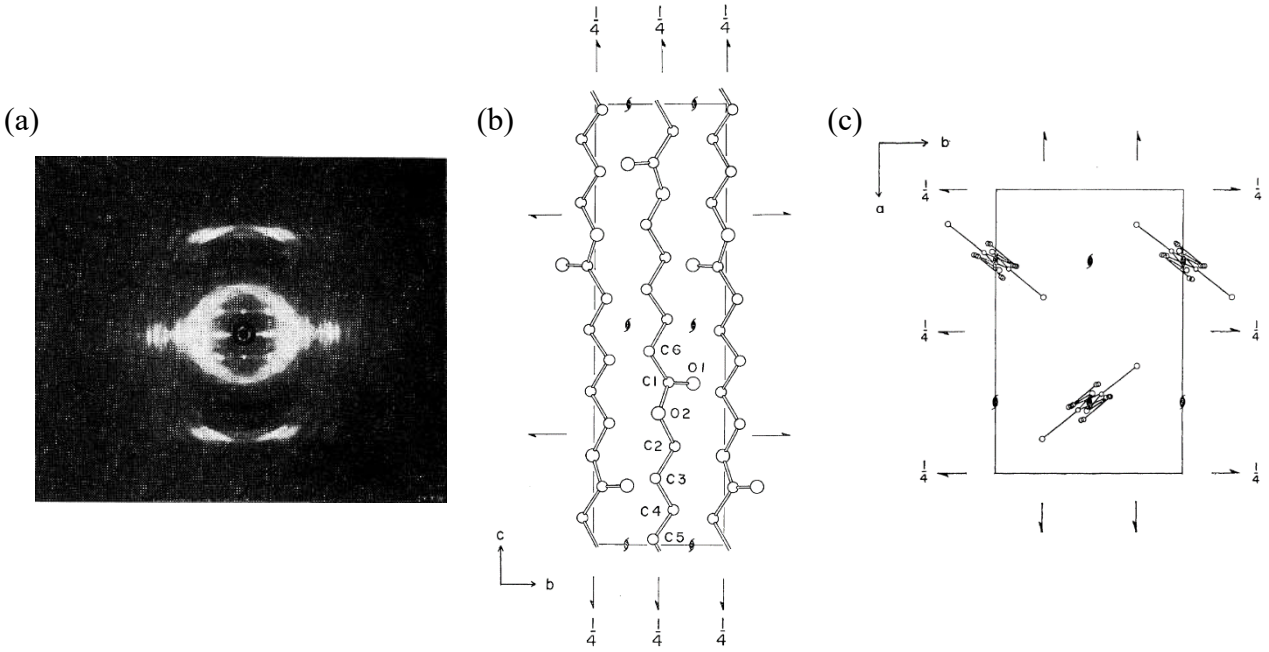

Figure 1.2. *X-Ray photograph of PCL fiber (a), projection of the crystal structure of viewed along a axis (b) and c axis (c). Adapted from [3].*

Specifically, the hydrolysis reaction is autocatalytic; once the polymer starts to be hydrolysed, the carboxylic groups derived from the newly formed chain terminals and from the 6-hydroxyhexanoic acid, also known as hydroxycaproic acid, and other hydroxyacids promote further hydrolysis [10,11]. This is especially true when the diffusion of the acid species into the surrounding degradation medium is limited, and the acid species remain trapped in the polymer bulk. In this case, a concentration gradient of the acid species is generated, and the degradation in the bulk occurs at an exponential rate [12]. However, when PCL is compared to other aliphatic biodegradable polyesters such as polyglycolides [13,14] or polylactides [14,15], the production of acidic hydrolysis byproducts per

unit of mass of polymer is lower. This is due to the reduced number of ester bond along the chains which affects the degradation rate of the structure, causing less inflammatory responses in implant materials produced using this polymer [1].

Table 1.1. *Hildebrand solubility parameters for PCL, PLA and PEG, in MPa. Adapted from [7].*

Polymer type	δ_d	δ_p	δ_h	δ_T
PCL	21.2±0.6	3.4±0.9	5.3±0.8	22.1±0.8
PLA	20.0±0.6	5.9±0.7	7.6±0.9	22.2±0.7
PEG	20.8±0.6	8.4±0.7	9.4±0.9	24.3±0.7

PCL hydrolytic degradation process is pH dependent and can be accelerated under strongly acidic or basic pH conditions with the degradation being far more significant in strongly basic environments [16] or using enzymes [17]. In the literature there is a large list of the latter capable of accelerating the degradation of polycaprolactone. Among these, some, such as cutinases or lipases, are particularly effective due to the similarity between the structure of PCL and their natural substrates [18]. For example, complete degradation of PCL films (thickness = 0.1 mm) in the presence of *Pseudomonas* lipase has been observed within 4 days [19]. Other lipases such as those from *Rhizopus delemer* [20], *Rhizopus arrhizus* [21], *Pseudomonas PS* [22] and *Candida antarctica* [18] can be employed. On the other hand, in vivo degradation occurs due to various phenomena such as the normal degradation of the polymer in a physiological environment combined with the action of enzymes such as esterases and lipases [23]. PCL degradation studies in female Wistar rats have shown a duration of the process of about 3 years [24]. The implanted capsules (2.5/2.3 mm outer/internal diameter, 23 mm length), containing polymer with an initial molecular mass of 66 kDa, remained intact, in shape, during the first two years, starting to disintegrate after that time. In particular, the molecular weight of the polymer went from 22 kDa after 16 months of implantation to 15 kDa after 24 months. This further dropped to 8 kDa by 30 months where the implants became fragile and without mechanical strength. After 36 months, the tested implants were found as small pieces and could not be collected anymore. The results, in **Figure 1.3**, showed an almost linear relationship between the log M_w vs. time, which was in good accordance with the random hydrolytic chain scission mechanism of the ester bonds. This study is a clear example of the hydrolytic stability and long permanence in the body that can generally be obtained by exploiting the use of PCL. Thanks to these properties, this material is used in the production of biomedical devices such as scaffolds for tissue engineering and in long-term drug delivery systems [5,25–28]. Other significant applications are found in the field of microelectronics, adhesives, and packaging [29]. In particular, the latter application area is the most studied for PCL-

based materials which, despite their slightly higher costs than polyolefins, have found a certain degree of diffusion.

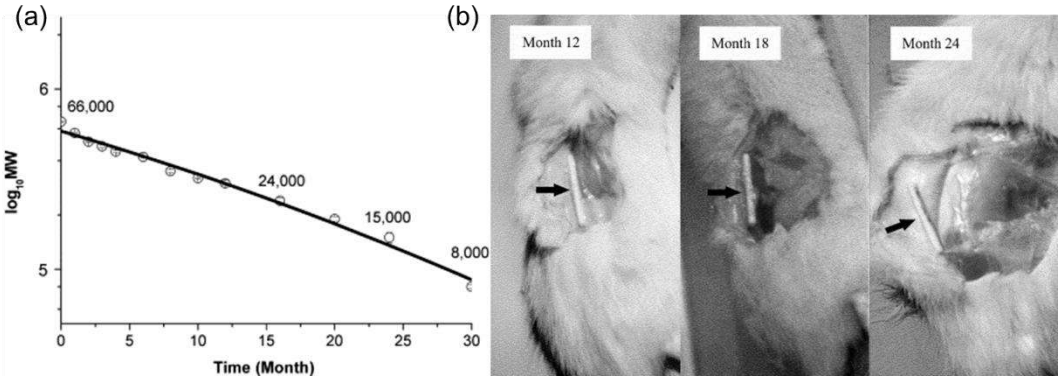

Figure 1.3. *M_w of PCL capsules vs. time after subcutaneous implantation in rats (a) and images of PCL capsules in rats taken at different times, black arrows indicate the implanted PCL capsules (b). Adapted from [24].*

For these applications, PCL is generally used alone or blended with other biodegradable polymers to give laminated or extruded materials capable of showing good biodegradability qualities [30]. For this purpose, it is often mixed with inexpensive thermoplastic biopolymers starch (TPS) or zein (TPZ), a corn derived protein, to obtain good biodegradable materials at a low price used in many commodities [31–34]. For example, in 1990 Novamont patented Mater-Bi®, a biodegradable thermoplastic material prepared from starch, PCL and PBAT [35] which was further used to replace polyolefin-based plastic bags following the entry into force, in 2010, of a regulation which has imposed the gradual replacement of plastic bags on the market with bioplastic ones compliant with the UNI EN 13432 standard. On the other hand, some PCL/thermoplastic zein (TPZ) blends has proved to possess excellent features such as the adhesion in laminated packaging structures and due to the combination of specific performances allowed by each layer of the film, bags made from this material were found to be suitable for high pressure pasteurization treatments [34]. As evidenced by the authors, high pressure tests in **Figure 1.4**, up to 700 MPa, performed on multilayer packaging, did not promote any detectable change of oxygen and water vapor barrier properties of films confirming the possibility to industrially use such systems for food packaging applications. All these desirable properties are corroborated by the fact that this material has a relatively low cost and is very easy to prepare. As previously mentioned, blending with other polymers also allows to obtain a whole range of mixtures with different properties capable of covering a wide range of applications.

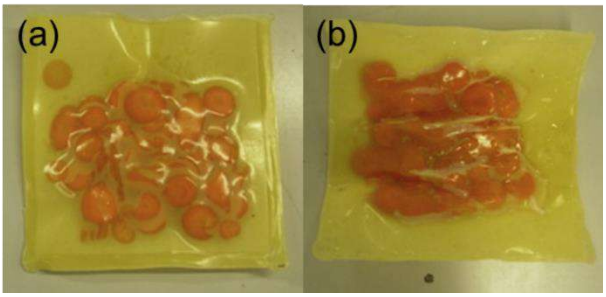

Figure 1.4. *Zein–PCL package for food applications before (a) and after (b) high pressure pasteurization at 700 MPa. Adapted from [34].*

A clear example is demonstrated by blends in combination with PLA form PLA/PCL blends, of which there is an abundance in the literature [36–38]. In a very schematic work, Delgado-Aguilar et al. studied thoroughly the properties of PLA/PCL blends (**Figure 1.5a**), prepared by compounding at 190 °C, over the whole compositional range, by using two commercially available, high molecular weight polymers [36]. The authors found that that the Young's modulus of the material evolved linearly with PCL content, indicating a good dispersion of the blend components. For blends containing more than 20 wt% of PCL, unnotched specimens did not break when their impact strength was measured using a Charpy's pendulus revealing a very good resilience, displayed also during the stress-strain characterization in **Figure 1.5b**.

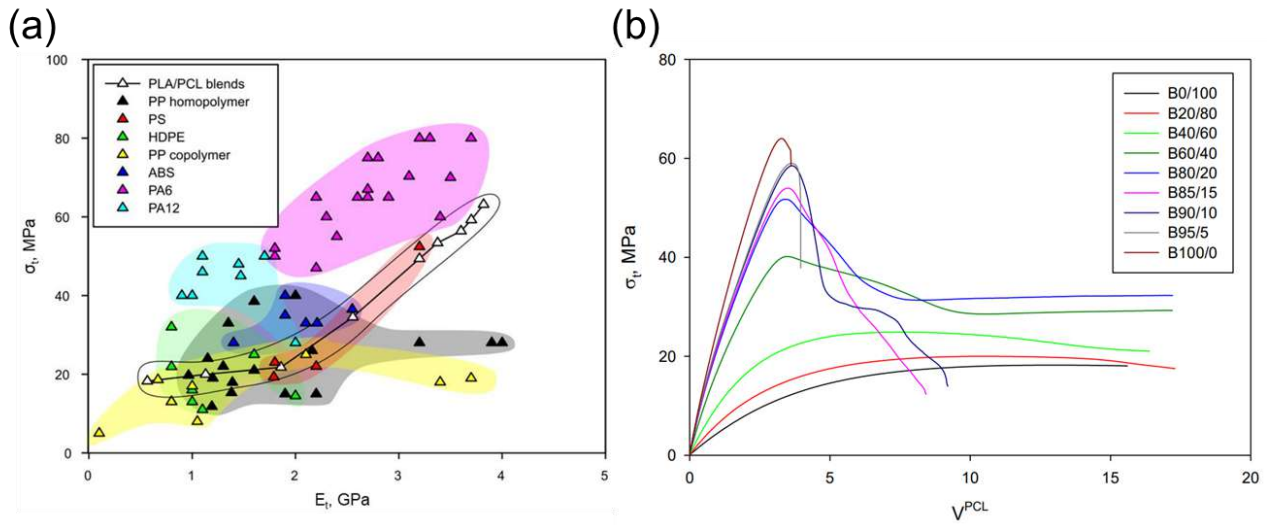

Figure 1.5. *Ashby's plot (a) for tensile strength (σ_t) against Young's modulus (E_t) for the PLA/PCL blends with different polymer ratios compared to other commodity polymers. Stress-strain curves (b) of the PLA/PCL blends and B0/100 stands for neat PCL while B100/0 represents neat PLA. Adapted from [36].*

Overall, it was found how these blends constitute an effective environmentally friendly alternative to oil-based commodity materials such as polyethylene and polystyrene. As about structural applications, PCL-based materials face many limitations due to its low glass transition temperature

and elastic properties when compared to other biodegradable polymers like PLA or polyhydroxybutirrate (PHB). A general approach used to enhance stiffness for load-bearing applications, involves the reinforcement of PCL and its blends with high aspect ratio fillers like short fibers or fabrics, thus broadening its potential use in such applications [30]. Remarkable efforts have been made towards the investigation of PCL composites reinforced with inorganic or organic natural fibers, after appropriate chemical modification, to increase the adhesion between the hydrophilic fibers and hydrophobic matrix and preserve the sustainability [39–44].

1.2 Monomers production

As previously mentioned, the most important production method for commercial PCL production lies in the ROP reaction of ε-caprolactone (ε-CL). Generally, the most used synthetical route to produce this monomer, on an industrial scale, consists of the Bayer-Villiger reaction of cyclohexanone using peracids, such as peracetic acid, in the so-called UCC process [45]. This currently produces more than 10,000 tons/year of ε-CL precursor for polymer synthesis with associated toxicity, ecology, and safety drawbacks. In particular, cyclohexanone, the starting substrate for ε-CL synthesis, is in turn obtained through different industrial processes such as the partial hydrogenation of phenol [46], the partial reduction of benzene in the Asahi process [47], or more commonly, through partial oxidation of cyclohexane [48] (**Figure 1.6**).

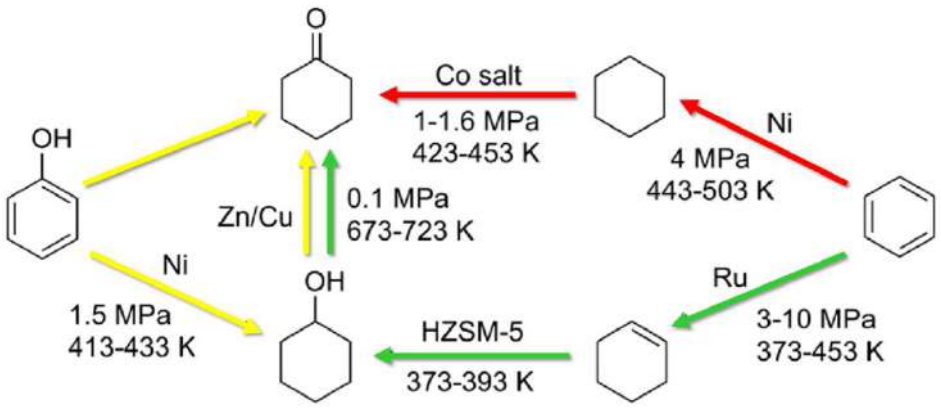

Figure 1.6. *Cyclohexanone production processes: Partial hydrogenation of phenol (yellow arrows), Asahi process (green arrows), cyclohexane oxidation (red arrows). Scheme revised and adapted from [49].*

However, the main use of cyclohexanone remains linked to the production of ε-caprolactam and adipic acid, respectively intended for the synthesis of the two most widespread polyamides on the market, Nylon-6 and Nylon-6,6.

1.2.1 Partial hydrogenation of phenol

In this process, ε-CL is obtained by direct hydrogenation of phenol to cyclohexanone with complete conversion and high selectivity (93.6%) under mild conditions (80 °C, 1 MPa hydrogen pressure). This has been studied by using a composite catalytic system prepared with Pd/C and a heteropolyacid. It has been found that a synergetic effect between Pd/C and heteropolyacid enhanced the catalytic performance of the composite system and suppressed the undesired hydrogenation of cyclohexanone to cyclohexanol [50].

1.2.2 Asahi process

During 1990 in Japan, a new process was patented and commercialized by Asahi to produce cyclohexanol with a 100 t/y plant. This is still the most used process nowadays in the industry to produce cyclohexanol. This process can be divided in three macroscopic steps that consist in the selective hydrogenation of benzene, the separation of the formed cyclohexene and finally its hydration to form cyclohexanol. The first hydrogenation step is performed by using a heterogeneous Ni catalyst, stopping the conversion to a 50% to afford a mixture composed by 35% cyclohexene, 15% cyclohexane, and 50% residual benzene. After separation through extractive distillation the cyclohexene is hydrated, in a slurry reactor over a heterogeneous catalyst, to give only the 14% of cyclohexanol due to the reaction constant value. In this sense, several additives to increase the conversion to cyclohexanol in this step were tested and patented. The overall yield of this process is extremely high, greater than 95% [51]. The formed cyclohexanol is then catalytically oxidised to cyclohexanone.

1.2.3 Partial oxidation of cyclohexane

As in the latter case, cyclohexane (Cy-H) is in turn prepared through the catalytic hydrogenation of benzene and is oxidized by using O_2 and H_2O_2 in controlled conditions (1-1.5 MPa, 120-165 °C), in order to maintain a low conversion, which is necessary to avoid the formation of polyoxygenated by-products (in the specific, cyclohexanedione, epoxycyclohexane and cyclohexylcarboxylic acid can be formed). This leads to the production of a cyclohexanol/cyclohexanone mixture nicknamed "*KA oil*" to highlight the concomitant presence of ketone and alcohol. This reaction is supposed to be initiated by the action of the ·OH radical, capable of abstracting hydrogen atoms to form the Cy· radical which would then be able to give the hydroperoxide Cy-OO· by reaction with oxygen molecules. Cy-OO· radicals then turn out to be able to give dismutation to form Cy-OH and Cy=O.

1.2.4 Monomer production from green processes

Considering how the contribution of greenhouse gas (GHG) emissions resulting from the use of fossil substrates is a global concern due to climate change, the decoupling of industrial production from these resources is increasingly becoming a necessity to reach carbon neutrality. In this sense, important efforts are made by the scientific community to create, improve, implement, and evolve green processes with the aim of gradually bringing them closer to the needs of the actual industrial production. In the literature, many example of environmentally friendly syntheses for ε-CL and other monomer precursors were reported over years [52–54]. These may concern the use of substrates coming from biomasses, with some of them still developed on the use fossils derived molecules, and although they do not yet represent processes applicable on an industrial scale for reasons related to costs and efficiency, their development is nevertheless very important for their future application to replace the processes that are currently in use for the monomer production. Despite scalability or cost problems, biocatalytic approaches provide a greater number of advantages over conventional catalytic systems, with enzymatic reactions being more environmentally friendly due to the absence of organic solvents and milder reaction conditions resulting in lower energy and sewage depuration costs. To cite some examples, Srinivasamurthy et al. set on point a whole-cell biocatalytic conversion of cyclohexanol to ε-caprolactone by using modified *Escherichia coli* cells capable to express two different enzymes, alcohol dehydrogenase (ADH) from *Lactobacillus kefir* and cyclohexanone monooxygenase from *Acinetobacter calcoaceticus* in a batch-fed process. By applying a parameter optimisation and using a cyclohexanone monooxygenase mutated variant (CHMO M15), a 98% conversion and 20 g/L product titre in ε-CL were obtained (**Figure 1.7**) [55]. It is worth to emphasize that, to improve the sustainability of this process, cyclohexanol can be obtained from lignin-based compounds, potentially allowing the practicability of a totally green synthesis [56]. Another work focused on the production of ε-CL using the Baeyer–Villiger monooxygenase (BVMO) enzymes included the use CHMO from *Acinetobacter calcoaceticus*, to directly catalyze cyclohexanone oxidation to ε-CL in the presence of O_2, but this approach suffered from low productivity and stability of CHMO over time, which is also affected by substrate and product inhibition. In this case, the product inhibition was bypassed by adding *Candida antarctica* lipase to perform directly, *in situ*, ROP of the formed ε-CL to keep low its concentration [54]. This conducted to the formation of more than 20 g/L of low molecular weight PCL oligomers starting from 200 mM cyclohexanol concentration.

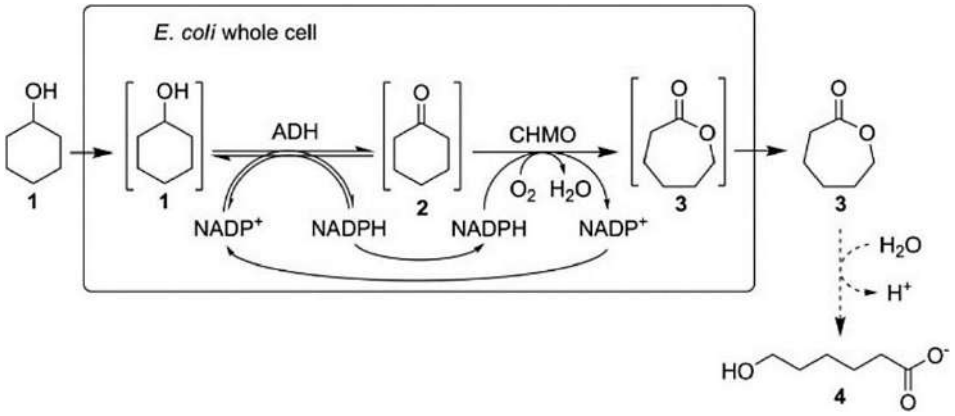

Figure 1.7. *Enzyme cascade to produce ε-caprolactone from cyclohexanol. Adapted from [55].*

Similarly, Tian et al. exploited the use of these two enzymes, alcohol dehydrogenase (ADH) from *Lactobacillus kefir* to oxidise cyclohexanol to cyclohexanone, and mutated CHMO to transform cyclohexanone in ε-CL, which were displayed separately onto the surface of different Gram-negative bacteria, *Escherichia coli*, after their modification, to produce ε-CL from cyclohexanol [57]. The results indicated that the activity of surface displayed ADH was the limiting factor due to the strong inhibitory effect of the initial substrate, cyclohexanol, on CHMO activity. To cite an example, 50 mM cyclohexanol generated a decrease CHMO activity to less than 12%. Therefore, the authors proposed to reduce the number of total cells and increase the ratio of ADH displaying cells to CHMO displaying cells far beyond 10:1 to increase the overall chemical yield. Another solution proposed was related to the continuous feeding of cyclohexanol to reduce its inhibitory effect on CHMO activity. Although there are still limitations to overcome, these results indicate the potential of surface displayed enzymes to perform cascade reactions. Differently, Bretschneider et al. evidenced the possibility to directly produce another important PCL precursor, 6-hydroxy-hexanoic acid, from one pot bacterial oxidation of cyclohexane, by recombinant *Pseudomonas taiwanensis* harboring a 4-step enzymatic cascade without the accumulation of any intermediate (**Figure 1.8**). In detail, the bacteria were supplemented with 0.5% (w/v) glucose as the sole carbon and energy source. Also in this case, product inhibition and substrate toxification were identified as the main limiting factors of the biocatalytic performance of this system. In a recent review, other synthetic routes based on the catalytic hydrogenation of biobased molecules from renewable resources, such as 5-hydroxymethylfurfural (HMF) to prepare 1,6-hexanediol (1,6-HD) as substrate for the mass production of important 6-carbon chemicals such as 6-hydroxy hexanoic acid (6-HHA), adipic acid (AA) and ε-CL are reported (**Figure 1.9**). For example, 1,6-HD can be used in turn to produce ε-CL through chemical or enzymatic processes. Specifically, Pyo et al. used *Gluconobacter oxydans* to oxidize 1,6-hexanediol selectively at pH 6–7 to 6-hydroxyhexanoic acid. This was subsequently converted to ε-caprolactone by catalytic

cyclization, by using reusable 4 Å zeolites and acidic ion exchange resin, in dimethylformamide at 130–160 °C. The combination of the heterogeneous catalysts provided the formation of ε-CL with 74.4% selectivity and 98.3% 6-HHA conversion after 6 hours of reaction [52].

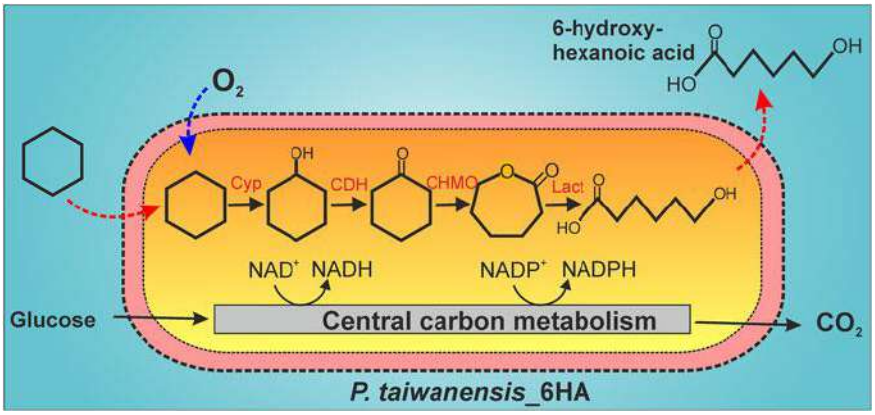

Figure 1.8. *Biocatalytic cascade for 6-hydroxyhexanoic acid (6HA) synthesis from cyclohexane with P. taiwanensis_6HA. Adapted from [58].*

Starting from this diol, Kara et al. reported oxidative lactonization of 1,6-HD in a two-liquid phase system, composed by water and diisopropyl ether, using horse liver alcohol dehydrogenase (HLADH), obtaining a 26% yield of ε-CL after 96 hours.In another paralled study about the use of biomass derived feedstocks, Thaore et al. presented a techno-economic analysis of ε-CL production from corn stover via HMF and 1,6-HD where a process model for the conversion of biomass to caprolactone via glucose and HMF was developed [59].

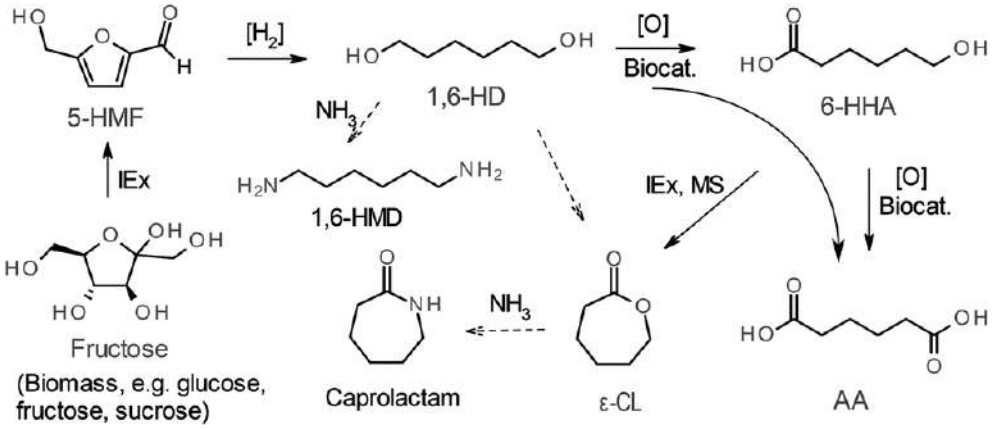

Figure 1.9. *Integrated microbial-chemical synthetical pathways to produce biobased 6-hydroxyhexanoic acid (6-HHA), adipic acid (AA), and ε-caprolactone (ε-CL) via 5-hydroxymethylfurfural (5-HMF) and 1,6-hexanediol (1,6-HD). IEx: ion exchange catalyst. The route can also be used to produce ε-caprolactam and 1,6-hexamethylenediamine (1,6-HMD) through amination steps (dotted arrows). Adapted from [52].*

In this case two crucial points such as overall sustainability in terms of economic and environmental impact factor, i.e. GHG emissions, were addressed. From this study it was possible to predict a competitive minimum sale price for the biobased monomer, which was estimated to be between 1618-1815 US $/tonne, being comparable with the actual price for the ε-CL available on the market.

1.3 Polymer Synthesis

The first attempt of preparation of PCL was performed in 1934 by Van Natta et al. by simple thermal treatment of ε-CL [60]. Other syntheses were performed by polycondensation of 6-hydroxycaproic acid and by radical ring opening (RROP) of 2-methylene-1,3-dioxepane (MDO) [30]. Even if many work were focused on the last two approaches, PCL is still mainly prepared by metal-catalyzed ring opening (ROP) of the lactone with the polycondensation and the RROP routes being the less used (**Figure 1.10**).

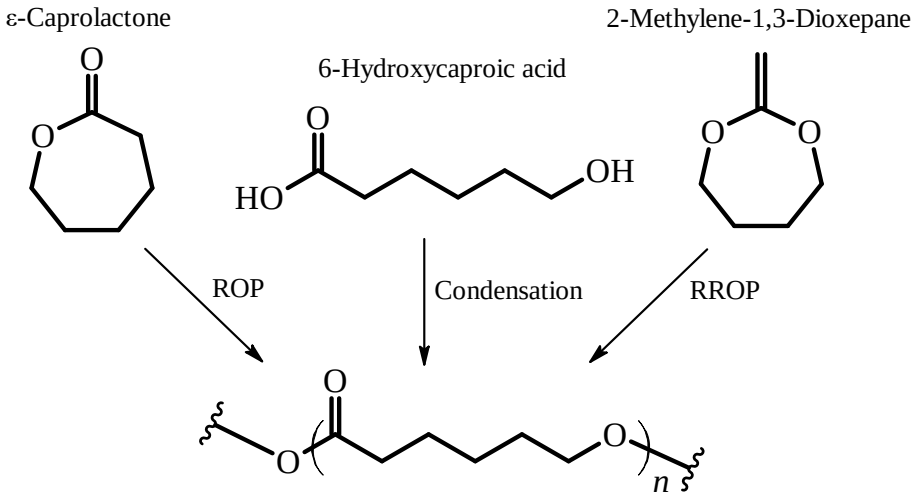

Figure 1.10. *PCL synthesis routes: ROP of ε-caprolactone, polycondensation of 6-hydroxycaproic acid, RROP of 2-methylenedioxepane. Adapted from [30].*

In particular, polycondensation is based on an equilibrium esterification process which generates water that needs to be removed, e.g., under reduced pressure in order to reach high molecular weights during the polymerization, making the process economically disadvantageous.

1.3.1 Polycondensation

The polycondensation reaction of 6-hydroxycaproic acid appears to be the least widely used synthetic pathway to produce PCL, despite the large number of patents describing the preparation of aliphatic polyesters from hydroxycarboxylic acids. To date, there are no industrial uses for this type of process,

and even on a laboratory scale it is one of the least favoured methods. Since it is based on an esterification process, i.e., on an equilibrium reaction and with the formation of water as by-product, this would have to be continuously removed from the reactive mixture during the polymerization process to move the equilibrium towards polymer formation [61]. This operation, which must be performed under reduced pressure, would make it difficult to obtain polymers with high molecular weight making the whole process disadvantageous from an economic point of view. The only example of classical hydroxyacid polycondensation reaction reported to date in the literature refers to the preparation, by Braud et al., of PCL oligomers by polycondensation of 6-hydroxyhexanoic acid under vacuum, without the addition of catalyst, by increasing the temperature from 80 to 150 °C over the course of 6 hours [62]. Few other examples where enzymatic polycondensation of the hydroxyacid or their respective hydroxyesters can be mentioned. Mahapatro et al. prepared PCL with an average molecular weight of 9000 g/mol and a polydispersity below 1.5 by polymerization of 6-hydroxycaproic acid in bulk at 90 °C for 48 hours using a 10% wt respect the monomer of supported *Candida antartica* lipase B (Novozym 435®) and applying a 10 mbar of continuous vacuum to the system to remove the formed water [63]. Dong et al. obtained an average molecular weight of 5400 g mol^{-1} and a polydispersity of 2.26 after 20 days with 82% monomer conversion by polymerization of 10 mmol of ethyl 6-hydroxycaproate at 45 °C for 20 days using 40 mg of *Pseudomonas sp.* lipase without removal of the formed ethanol [64]. These results demonstrate that it is generally not possible to obtain high molecular weight polymers through this synthetic pathway. Indeed, in this is work is remarked that the polymerizations using lactones instead of hydroxyacids/hydroxyesters as the monomers are superior, with the only exception of γ-butyrolactone [64]. However, it is still important to consider that there are no reported examples of PCL preparation through the use of Lewis acid catalyzed polycondensation of 6-hydroxycaproic acid, which could potentially lead to higher molecular weights and satisfactory yields.

1.3.2 Radical Ring Opening Polymerization (RROP)

This type of approach, first developed by Bailey et al. in 1982 [65], has a high synthetic potential since it allows to combine, in different ways, the typical PCL repetition unit deriving from the radical ring opening of the 2-methylene-1,3-dioxepane (MDO) with different vinyl monomers to originate a whole series of biodegradable poly(vinyl-co-esters). Some examples of monomers that can be used in the copolymerization with MDO are propargyl acrylate, methyl acrylate, methyl methacrylate, dimethylaminoethyl methacrylate, glycidyl methacrylate and styrene. In this type of reactions, conventional thermally activated radical initiators such as azo-bis-isobutyronitrile (AIBN) [66] or organic peroxides such as tert-butyl peroxide are generally used. In addition to MDO, other cyclic

ketene acetals monomers such as 2-methylene-1,3-dioxe-5-pene (MDE) [67] and 2-methylene-1,3,6-trioxocane (MTC) [68] are often employed in radical copolymerizations to introduce hydrolysable segments in the polyacrylate backbone. This class of monomers can also be employed in controlled reversible addition-fragmentation chain transfer (RAFT) and radical atom transfer polymerization (ATRP) reactions, which makes possible to prepare systems characterized by well-defined molecular geometries and masses [69,70]. It has been observed that the chain sequence of produced pseudo-PCL copolymers, as well as the reaction mechanism is strongly dependent on the type of cyclic acetal ketene and vinyl compound used, their ratio and the temperature used [30]. For example, by using 7-membered cycles ketene acetals it is possible to obtain quantitative yields even at 50 °C, a relatively low temperature. This synthetic way allows to produce very interesting polymers since it enables the introduction of different functional groups along the PCL chains, a polymer devoid of chain functionalities. In this sense, it is also equally important to observe that the structure of the PCL obtained from RROP on MDO is completely different from that of PCL obtained by conventional metal-catalyzed ROP of ε-CL, due to the presence of ramifications generated by 1,4 and 1,7 H-transfer radical reactions (**Figure 1.11**). These occur during the polymerization step and can lead to a branching density that in some cases can reach 20%. Moreover, by modifying the reaction conditions, it is also possible to completely suppress 1,4 H-transfer reactions and obtain, in a selective way, only ramification generated only by 1,7-H transfer reactions. As conceivable, the high number of pendant groups generated in this way hinders the development of crystallinity, enabling the production of highly amorphous PCL. Some works have demonstrated how blends containing amorphous PCLs prepared by RROP, mixed with linear semicrystalline PCLs synthesized from classical ROP had improved degradability due to the greater speed of degradation of the amorphous component. In this sense, Agarwal et al. prepared solvent casted PCL films with improved compostability for packaging applications, by blending, over the entire concentration range, conventional PCL (M_n = 42500 g/mol) with a totally amorphous PCL obtained from RROP of MDO with AIBN (PCLB). The addition of even low % PCLB was able to increase the transparency and improve dramatically the degradation of the material without affecting its thermal stability [71]. The presence of PCLB also affected the crystallinity content and the spherulite size of crystalline domains of the resulting films, reducing their tensile strength and modulus.

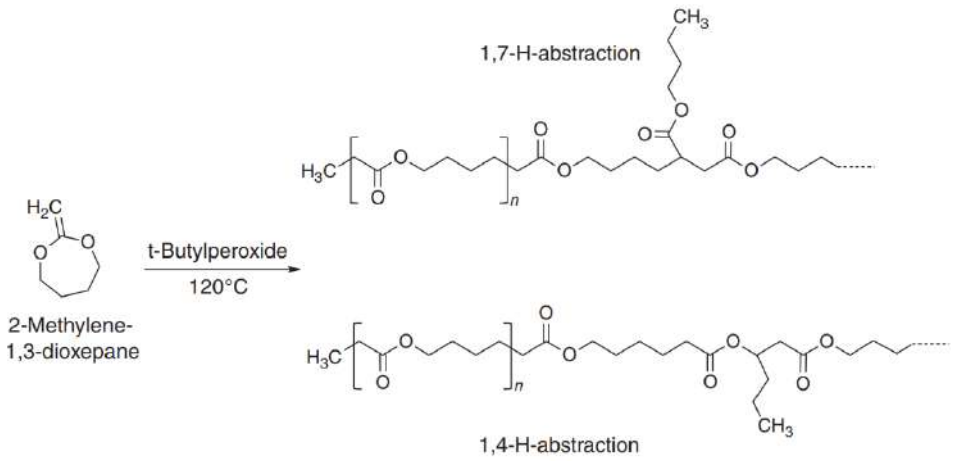

Figure 1.11. *Branched structures found in PCL obtained by RROP of MDO through 1,7- and 1,4-H- abstraction. Adapted from [30].*

1.3.3 Metal-Ring Opening Polymerization (ROP)

As previously mentioned, the most synthetically used methodology to produce PCL, due to the low costs and high efficiency, is based on the metal-catalyzed ROP reaction of ε-CL, placing this synthetic route in perfect overlap with what is used in the industrial production of some other polyesters/polycarbonates [72–74]. Curiously, towards the first half of the 1970s, some multinational oil companies, driven by the wide commercial availability of lactones and lactides, invested huge resources in the search for the most suitable catalyst for their polymerization, so much so that for this type of reaction it was possible claim that catalytic systems have been developed with almost all the elements of the periodic table. From a purely theoretical point of view, this type of polymerization reaction is applicable to any type of cyclic lactone; in practice, factors such as thermodynamics and kinetics of the process play a key role. As widely reported in the literature, for almost all cyclic esters the driving force that makes their polymerization possible is given by the ring strain [75]. It reflects the energy present in excess in the molecule and due to some factors, such as the variation of bond angles and lengths compared to those of equilibrium or the presence of non-bonding interactions (e.g., repulsive) between various substituent groups. In case the monomer-polymer-solvent interactions can be neglected, the polymerization enthalpy, shown in **Figure 1.12**, is directly dependent on the ring strain. As about entropy, in these processes it is always negative due to the granting of the degrees of translational freedom since we go from single molecules to a single macromolecule. As shown in **Figure 1.13**, the exergonicity of the process is guaranteed only when $|\Delta H_p| > T\Delta S_p$ and it turns out that the higher is the strain, the lower is the monomer concentration at equilibrium at a given temperature [75].

Monomer	Ring size	xy	ΔH_p° [a] (kJ mol^{-1})	ΔS_p° [a] (J mol^{-1} K^{-1})	$[M]_{eq}$ [b] (mol l^{-1})
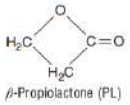 β-Propiolactone (PL)	4	Ic'	−82.3	−74	3×10^{-11}
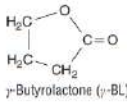 γ-Butyrolactone (γ-BL)	5	Ic	5.1	−29.9	3.3×10^{3}
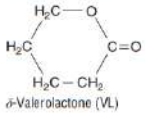 δ-Valerolactone (VL)	6	Ic'	−27.4	−65.0	3.9×10^{-1}
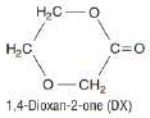 1,4-Dioxan-2-one (DX)	6	Is	−13.8 [c]	−45 [c]	2.5 [d]
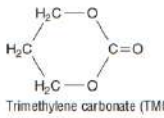 Trimethylene carbonate (TMC)	6	ss	−26.4 [e]	−44.8 [e]	5.1×10^{-3}

Monomer	Ring size	xy	ΔH_p° [a] (kJ mol^{-1})	ΔS_p° [a] (J mol^{-1} K^{-1})	$[M]_{eq}$ [b] (mol l^{-1})
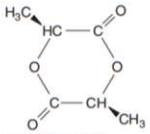 L,L-Lactide (L,L-LA)	6	ss	−22.9 [f]	−41.1 [f]	1.2×10^{-2}
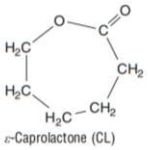 ε-Caprolactone (CL)	7	Ic'	−28.8	−53.9	5.1×10^{-2}
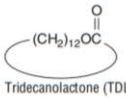 Tridecanolactone (TDL)	14	II	−8	26	2.3×10^{-2} [g]
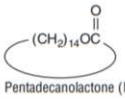 Pentadecanolactone (PDL)	16	II	3	23	0.70 [h]

Figure 1.12. *Thermodynamic polymerization parameters characteristic of some cyclic lactones. Adapted from [75].*

In the case of ε-CL, the main reason of ring strain is attributable to the presence of the carbonyl group, due to its planar geometry, and to some steric interactions between the methylene unit hydrogens that lead to a distortion of the natural bond angles in the 7-membered cycle. Because of the aforementioned reasons, γ-BL, a lactone devoid of ring strain, is incapable of reaching high molecular weights during polymerization [75].

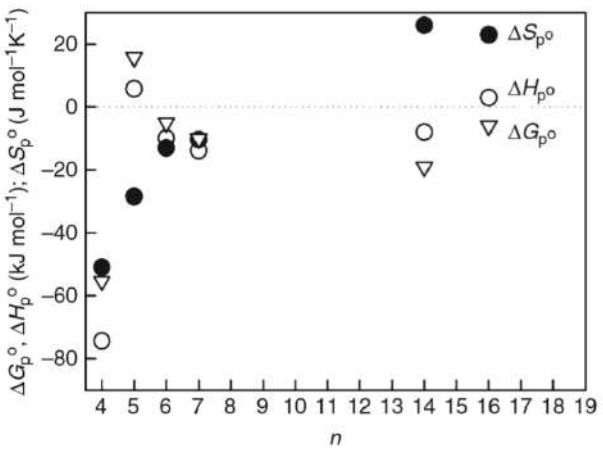

Figure 1.13. *ΔG_p, ΔH_p, and ΔS_p values for some lactones as a function of ring size, considering a temperature between 350-430K, with molten monomer and polymer. Adapted from [75].*

As far as kinetics are concerned, the reaction rate constant k_p is dependent on $\Delta G_p^{\ddagger}$ according to **Equation 1.1**.

$$k_p = \frac{k_b T}{h} \exp\left(-\frac{\Delta G_p^{\neq}}{RT}\right) = \frac{k_b T}{h} \exp\left(-\frac{\Delta H_p^{\neq}}{RT} + \frac{\Delta S_p^{\neq}}{R}\right)$$

Equation 1.1. *k_p = polymerization rate constant, k_b = Boltzmann constant, h = Planck constant, $\Delta G_p^{\ddagger}$ = Gibbs activation energy for the polymerization process, $\Delta H_p^{\ddagger}$ = activation enthalpy, $\Delta S_p^{\ddagger}$ = activation entropy, R = gas constant. Adapted from [75].*

In metal-catalyzed ROP processes, the conformation of the lactone plays a key role in the kinetics since the reaction passes through the attack of nuclophilic active species on the carbonyl. Any type of steric hindrance around is capable of significantly increase the $\Delta S_p^{\ddagger}$, reducing the rate of the process. This is what occurs in very planar systems such as β-BL, where despite the presence of sufficient ring strain, carbonyl is more difficult to be attacked. Conversely, in ε-CL this phenomenon is reduced thanks to its slightly puckered conformation, shown in detail in **Figure 1.14**. Experimentally, for these two monomers, a comparison was made by performing ROP in THF at 80 °C with $[M_0]$ = 2 M and $Al(OiPr)_3$ as catalyst/initiator which resulted in huge difference in the k_p value: k_p(β-BL) = $4 \cdot 10^{-3}$ L $mol^{-1}s^{-1}$ and k_p(ε-CL) = 30 L $mol^{-1}s^{-1}$.

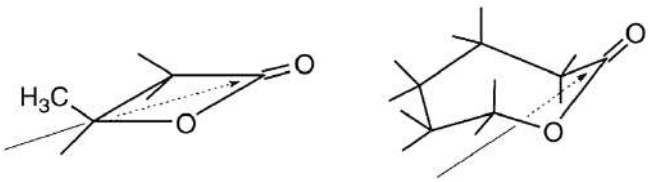

Figure 1.14. *β-BL planar (left) and ε-CL puckered (right) conformations. Adapted from [75].*

In other studies, it has been experimentally observed that for larger lactones, the polymerization rate decreases and remains constant in cycles from 12 to 17 terms. This feature is once again attributable to the strain, which is partially relieved during the transition state, leading to a drop in the $\Delta H_p^{\ddagger}$ [75]. As far as the number of catalysts and initiators that can be used in this process is concerned, there are many and every year a few dozens are discovered; for this reason, metal-catalyzed ROP can therefore be ideally divided into many subcategories. While relatively weak nucleophiles such as carboxylates of alkali metals such as Li^+, Na^+, K^+ can be used for particularly stressed esters such as propiolactone, these are not sufficient for less tensioned rings such as ε-CL which requires stronger and more reactive species such as alkoxides. In these cases, the reaction can be defined as anionic ROP and uses covalent alkoxides of metals with an acidic Lewis character (Ti^{4+}, Sn^{2+}, Sn^{4+}, Al^{3+}, Zn^{2+}, etc.). Depending on

the substituents of the alkoxy residue, they can initiate the reaction in two ways; those that are more sterically hindered favor a deprotonation process on the α position adjacent to the carbonyl of the lactone with the formation of an enolate ion which in turn acts as an initiator, conversely, those with less bulky substituents are able to directly attack the carbonyl carbon, through an S_NAc mechanism. All this is presumably assisted at the same time by coordination processes, in relation to the type of cation involved. If, on the other hand, carboxylates or acetylacetones of these metals are used, it is necessary to use a co-initiator which is generally a basic species of Lewis, in particular an alcohol or amine. There is also a curious difference in reactivity between β-lactones and larger lactones when initiating such reactions using alkoxides. As shown in **Figure 1.15**, the former can undergo ester bond breaking from the carbonyl side via S_NAc and from the alkyl side via S_N2 in a ratio of 1:1, while the latter can only be broken from the carbonyl side via S_NAc [75].

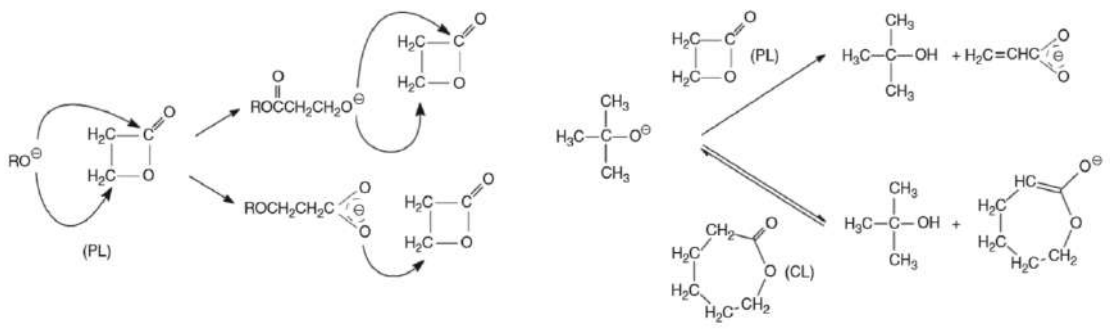

Figure 1.15. *Effect of the attack of different alkoxides without (left) and with (right) steric hindrance on β-propiolactone and ε-CL. Revised and adapted from [75].*

The use of strongly basic species, on one hand favours the process due to their reactivity, on the other hand it puts in front of the possibility of having undesired side reactions, therefore it is also necessary to consider the selectivity which is generally defined as the k_p/k_{tr} ratio. The subscript "tr" refers to the transesterification reactions that can occur between the terminal of the alkoxy chain (reactive species that propagates polymerization) and the ester bonds present in the already formed chains. These detrimental processes are the basis of an increase in the polydispersity index during the polymerization process. In this case, covalent alkoxides and carboxylates of transition metals, thanks to their very good coordinating properties, possess a greater selectivity than their non-covalent alkali counterpart. This allows them to be used in the synthesis of polymers with complex molecular geometries, where high degree of control over the polymerization process and molecular weight are required [75]. In the polymerization of lactides and ε-CL, a covalent tin carboxylate, tin(II) 2-ethylhexanoate, namely tin octanoate, $Sn(Oct)_2$ (**Figure 1.16**) is widely employed. It exerts its action

through the interaction with a species that acts as a co-initiator, which can be present as an impurity or voluntarily added to the system in a controlled manner. The co-initiator is generally a hydroxyl (water, alcohols, carboxylic acids, etc.) or amino containg species, and participates in the formation of a mixed complex with the catalyst.

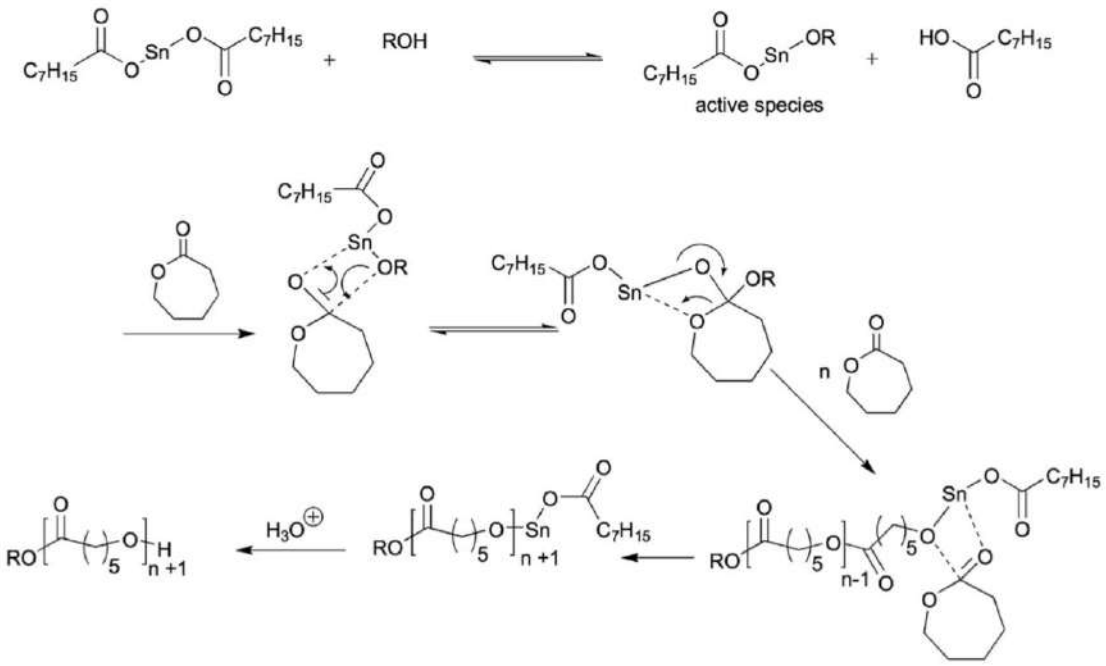

Figure 1.16. *$Sn(Oct)_2$ catalyzed ROP assisted by coordination-insertion reaction mechanism. Adapted from [1].*

This mixed complex arises from the exchange of ligands on tin octanoate and produces alkoxy ligands capable of to initiate the reaction in the same way as when using real alkoxides. Kowalski et al., by means of MALDI-TOF spectrometry studies on the ROP of (L,L)-lactide and ε-CL using $Sn(Oct)_2$ and n-BuOH as initiators, were able to prove the existence of a certain population of linear and cyclic macromolecules containing bonded tin atoms. This finding, combined with observations on the polymerization kinetics, allowed to confirm an active chain end character possessed by this mechanism. Under typical polymerization conditions, species such as OctSnOR, and $Sn(OR)_2$ have been observed in addition to all those having as an alkoxy group the one deriving from the macromolecular chain terminal [76,77].

1.3.4 Enzyme-catalyzed ROP (eROP)

Enzymatic polymerizations are nowadays considered a pinnacle in the field of polymer synthesis since they can represent a real alternative to the previously introduced organo-metallic catalysts (e.g. through Zn, Al, Sn or Ge compounds) which are known to be often cytotoxic to cellular systems and difficult to remove from polyesters due to their oxyphilic character [78,79]. When compared with transition metal catalyst polymerizations, enzymatic polymerizations are more attractive for biomedical applications due to the possibility to produce a metal-free polymer containing less by-products and having a good biocompatibility. However, nowadays, the industrial application of eROP is still absent due to intrinsic limitations related to the scarce availability of enzymes on a large scale and their high cost as well as the limited molecular weights that can be generally obtained with this type of catalysis [80]. Indeed, eROP of lactones is affected by some limitations in the kinetics, which is usually slow and in the number of monomers that can be polymerized [81]. For this purpose, lipases, a class of enzymes very abundant in the animal kingdom, would appear to be the best enzymes for catalyzing ROP reactions, especially of lactones and cyclic carbonates, as well as polycondensation reactions, as shown in the related paragraph. In detail, lipases are a class of serine hydrolases enzymes which are capable, under physiological conditions, to speed up the hydrolysis reaction of triglycerides, to release free glycerol and fatty acids, in biological systems. Varying the environment by placing them in organic systems without water allows them, by shifting the reaction equilibrium, to be able to operate in the opposite direction, i.e., by catalyzing the formation of ester bonds. Historically, lipase-catalyzed ROP was developed by Kobayashi et al. to synthesize poly(ε-caprolactone) (PCL) by exploiting *Pseudomonas fluorescens* lipase [82]. Nowadays, among the most used lipases we can include *Candida antarctica* lipase B (CalB) [64,83–85], which active site is reported in **Figure 1.17**. Some important studies have focused on the effect of the solvent in the polymerization of ε-CL in the presence of CalB. Kumar et al. observed that the use of solvents with a higher logP (between 1.9 and 4.5) allows the speed of molecular weight propagation and conversion to be increased. In particular, the best results were observed with toluene, because it behaves as a solvent towards both the monomer and the polymer. It was also hypothesized how it could stabilize the structure of CalB, allowing it to work even at a temperature of 90 °C in the place of the 70 °C studied, reaching a conversion of 90% in 2 hours using 1% of Novozym 435 respect monomer weight [83]. Furthermore, this approach, like ROP and RROP, gives the possibility to incorporate during the polymerization, other cyclic or linear monomers. As demonstrated by Dong et al., ε-CL can be copolymerized efficiently, in presence of *Pseudomonas sp.* lipase with some cyclic and linear monomers except for γ-BL.

As reported in **Table 1.2**, its combination with cyclopentadecanolide, a 15-carbon atoms macrocyclic lactone, afforded the highest molecular weight product (8.4 kDa) even though the monomer conversion of cyclopentadecanolide was limited (67%).

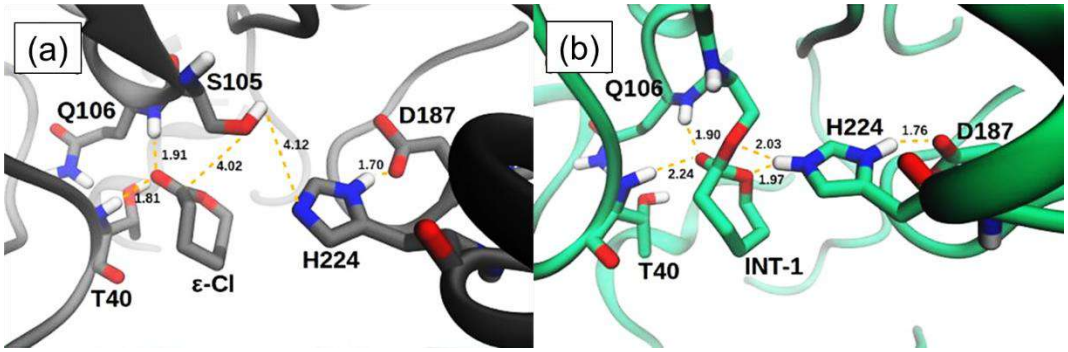

Figure 1.17. *CalB active site pocket: ε-CL substrate in the reactive complex (RC) (a) and intermediate structures (INT-1) (b), where the lactone is attacked by a serine residue to form a tetrahedral intermediate. Adapted from [86].*

Interestingly, it was also found that the copolymerizations of ε-CL with lactones produced higher molecular weight polymers than those with corresponding linear ethyl hydroxyesters. The copolymerization of ε-CL with γ-BL and ethyl 4-hydroxybutyrate gave an opposite result, probably for the low strain that characterize this lactone which, as discussed in the metal-catalyzed ROP paragraph, negatively affects the thermodynamic of polymerization. The results also indicate that the macrocyclic lactone was more easily copolymerized with ε-caprolactone compared with small ring lactone, lactide and γ-butyrolactone.

Table 1.2. *Copolymerization of ε-CL with different monomers catalyzed by Pseudomonas sp. lipase. Adapted from [64].*

	Copolymerization[b]		Monomer Conversion (%)	
Copolymerization Monomers	Mn (kDa)	Molecular Weight Distribution	ε-Caprolactone	Others
ethyl lactate[c]	2.8	2.45	100	87
lactide	5.1	2.22	100	57
γ-butyrolactone	2.9	2.16	56	3
ethyl 4-hydroxybutyrate	4.5	2.68	89	100
cyclopentadecanolide	8.4	2.77	100	67
ethyl 15-hydroxypentadecanoate	4.7	2.82	91	52
lactide and cyclopentadecanolide[c]	6.2	2.93	100	28/34

a. The reaction time was 20 days. b. Determined by GPC. c. The mole ratio of ε-caprolactone to other monomers was 4:1 and the ratio between ε-caprolactone, lactide and cyclopentadecanolide was 8:1:1.

1.3.5 Organocatalyzed ROP

Organocatalyzed ROPs, like previously mentioned eROPs, are highly valuable synthetical methods when there is the need to produce metal-free polymers. In this section, only some of the most important catalytic systems will be mentioned since there are dozens of classes of compounds capable to catalyze ROP of lactones that were reported in the literature over the years. Among the most used molecules, a special mention goes to different types of bicyclic and aromatic [87,88] amines and other nitrogen containing compounds such as ureas [89], thioureas [90,91], imidazolium compounds [92] and N-heterocyclic carbene (NHC) [93]. Many studies focused on the use of 1,8-diazabicyclo[5.4.0]undec-7-ene (DBU) and 1,5,7-triazabicyclo[4.4.0]dec-5-ene (TBD), two non-nucleophilic bases characterized by different modes of action that are widely used in organic synthesis as catalysts. TBD is reported to be a highly active ROP catalyst in conjunction with alcohol initiators and it is for the preparation of polyesters with well-defined structures in short time under mild conditions. For example, Dzienia et al. compared water-initiated ROP over a broad range of temperature and pressure conditions using DBU and TBD [94]. However, it was found that the activity of TBD can be disrupted when water is used as initiator leading to the complete loss of control over the reaction due to enhanced termination processes, even at high pressures. It was thought that water can suppress its double catalytic activity by protonation. Differently, DBU shows only sufficient activity in the polymerization of lactides and poor activity in the polymerization of lactones under ordinary conditions and has a low degradation temperature (353 K). A completely different situation was evidenced under pressure (p = 500 MPa, T = 393 K) where DBU showed increased thermal stability and the possibility to catalyze ROP of ε-CL with a linear increase of molecular weight with conversion to form polymers with moderate dispersity (Đ = 1.03–1.56) and molecular weight values (M_n = 16.7 kg/mol) due to the enhanced protonation (**Figure 1.18**).

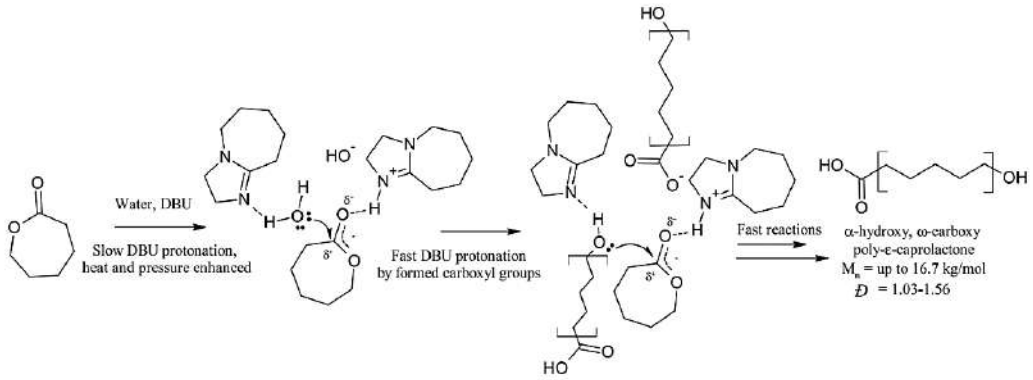

Figure 1.18. *Plausible mechanism for DBU/water system via an acid-conjugated base pair. Adapted from [94].*

Furthermore, MALDI-TOF characterization showed that the synthesized polymers were telechelic with a variable content of cyclic side products that was dependent on the reaction conditions used caused by an augmentation of the chain transfer reactions in a high viscosity regime.In another work, Chen et al. were able to validate the efficacy of DBU as catalyst in the polymerization/copolymerization of ε-CL, lactide (LA), valerolactone (VL) and trimethylene carbonate (TMC) by using different initiators and conditions, to obtain telechelic polymers with different end functionalities. In particular, PCLs with narrow dispersity, controlled molecular weight and good conversion were obtained. DFT calculations attested that a 22 kcal/mol energetic barrier exists for the monomer attack step in ROP process (**Figure 1.19**) which explains why its catalytic activity is displayed only at relatively high temperature (above 80 °C). Moreover, the high activity displayed by DBU towards ROP of LA, VL, TMC disclose its application in the preparation of biodegradable and biocompatible copolymers.

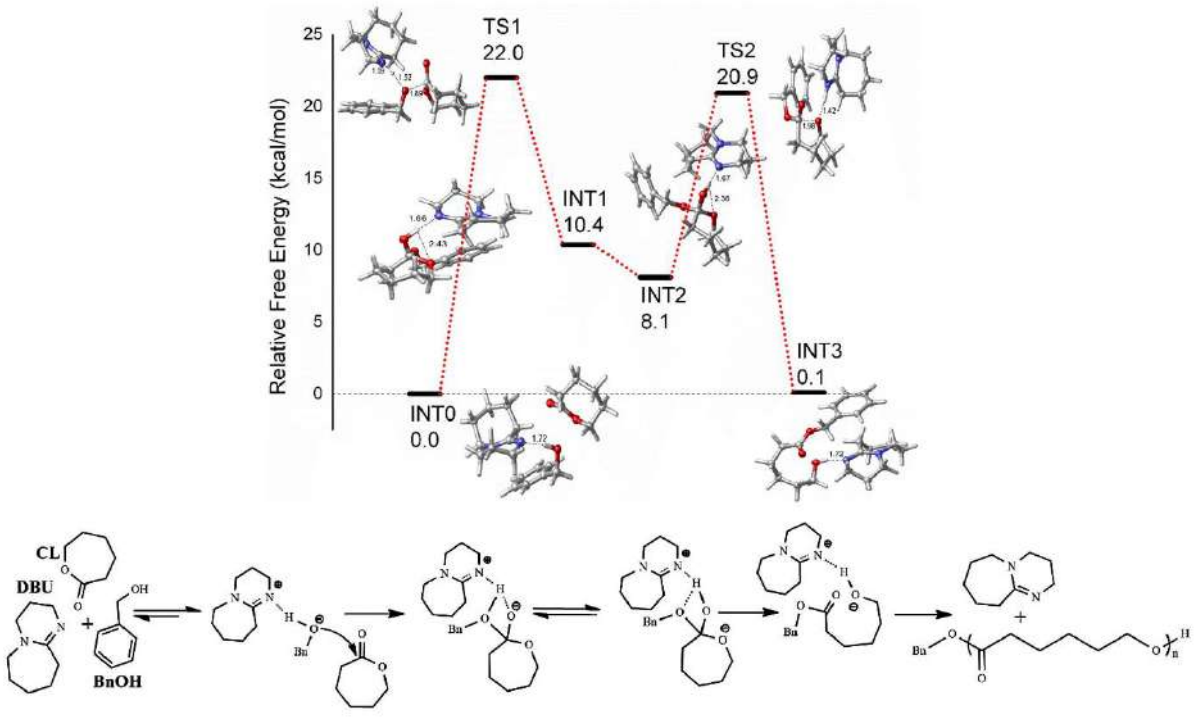

Figure 1.19. *Density functional theory (DFT) calculations (M06-2X/6-311++G(d,p)/IEFPCM level of theory) for the plausible activated alcohol initiator/chain-end mechanism in the DBU catalyzed ROP reaction. Adapted from [95].*

Other novel and efficient bifunctional organocatalysts, such as phosphoramidimidates (PADI), were employed by Zhang et al. in the ring opening polymerization of ε-CL to obtain metal-free PCL with narrow dispersity (1.06-1.22) and high molecular weight (> 60 kg/mol) in mild conditions through a living and controlled polymerization process [96]. In this work, polymerization of ε-CL was studied by comparing the activity of some catalysts such as diphenyl phosphoric acid (DPP) and

imidodiphosphorimidate (IDPi) with PADIs characterized by different structures (**Figure 1.20**), using a ratio $[M]_0/[I]_0/[catalyst]_0$ of 100/1/0.1, at room temperature. In three hours, a conversion of 44% and 76% was observed for DPP and IDPi respectively, while PADIs provided values between 88-93%.

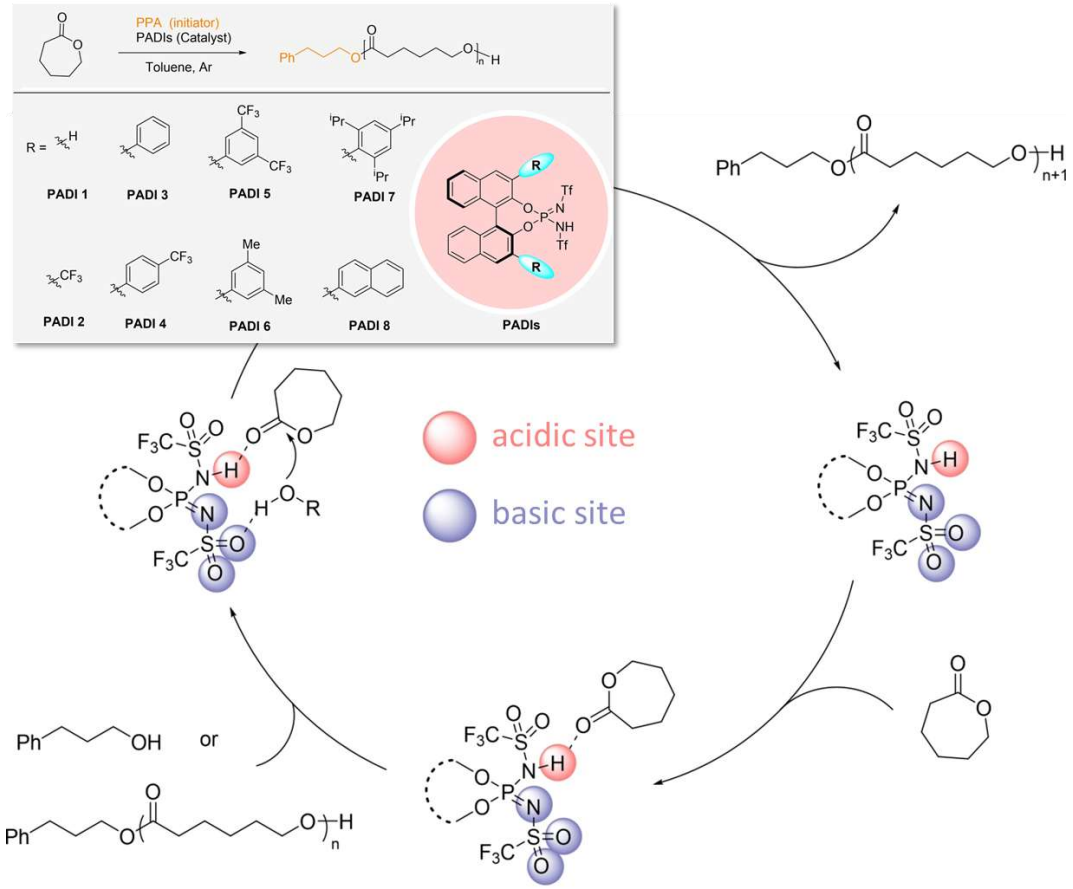

Figure 1.20. *PADI acid catalysts tested for the ROP of ϵ-CL and their proposed catalytic mechanism on this monomer. Adapted from [96].*

Furthermore, the living character of the polymerization catalyzed by PADI 5 was proven by extension of low molecular weight linear PCLs through further addition of ε-CL or δ-VL in the reaction mixture, to form copolymers. The versatility of PADI 5 was exploited also in the preparation of linear and star shaped polymers with 2, 3 and 4 arms characterized by low molecular weight and narrow dispersity using δ-VL and ε-CL in presence of 2-ethyl-2-(hydroxymethyl)propane-1,3-diol and pentaerythritol as initiators. Another study by Li et al. reported the synthesis of PCL by using ethyl diphenylphosphinite (EDPP) as an initiator and diphenyl phosphate (DPP) as a dual role organocatalyst [97]. The ROP in the DPP/EDPP system proceeded through an activated monomer mechanism supported by the reversible chain end activation/deactivation process provided by the equilibrium reaction between a phosphinite active center and its protonated dormant form. This shows living properties typical of group transfer polymerizations, which were proved by chain extension

experiments. Furthermore, it is believed that, given the ability of the phosphinite group to be preserved at the chain end after purification with non-nucleophilic solvents, these functionalized polyesters are characterized by auto-antioxidant properties, which are very important for industrial applications. Interestingly, these could be kept unchanged using bulk polymerization, without the need of any additional purification step enabling the development of a green chemistry compliant process. Another interesting class of compounds was used by Cheechana et al. which synthesized and employed bis(N-(N′-butylimidazolium)alkane dicationic ionic liquids (DIL) with different structures as non-toxic catalyst in the ROP of ε-CL, in bulk, using 1-butanol as initiator. For these systems, the authors reported, in the best conditions used (120 °C, 72 hours), conversions up to 95% with M_w of PCL 20130 g/mol (Đ~1.80). It was found that the polymerization rate of ε-CL was inversely correlated with the linker chain length of DILs. A DFT mechanistic study was performed using B3LYP (6–31G(d,p)) revealed a stepwise coordination/insertion mechanism for this process in which the rate-determining step is the alkoxide insertion. The authors found that the effectiveness of the synthesized DILs was equivalent, under the condition used in this work, to the conventional catalytic system based on $Sn(Oct)_2$. Moreover, based on cytotoxicity tests against monkey kidney epithelial cells, the synthesized DILs exhibited less cytotoxicity than 1% DMSO, used as standard, enabling these catalysts to be used in the preparation of metal-free biomedical grade polycaprolactones.

1.4 Star-shaped polymers: synthetical approaches

Star-shaped polymers, the main object of this thesis, include a wide range of macromolecules with complex macromolecular geometry and linear chains which compose the shell, more than 3 in number, starting from a central area called the core. Thanks to their shell-core structure, it is therefore possible, in some cases, to obtain different types of molecular architecture, presented in **Figure 1.21**. In fact, the great interest in stellar polymers is attributed to their unique topological structures, maintaining spatial characteristics that deviate strongly from linear polymers, which leads to interesting physical/chemical properties, including lower viscosity in dilute solutions, better encapsulation capacity, different internal and peripheral functionality and greater response to stimuli [98].

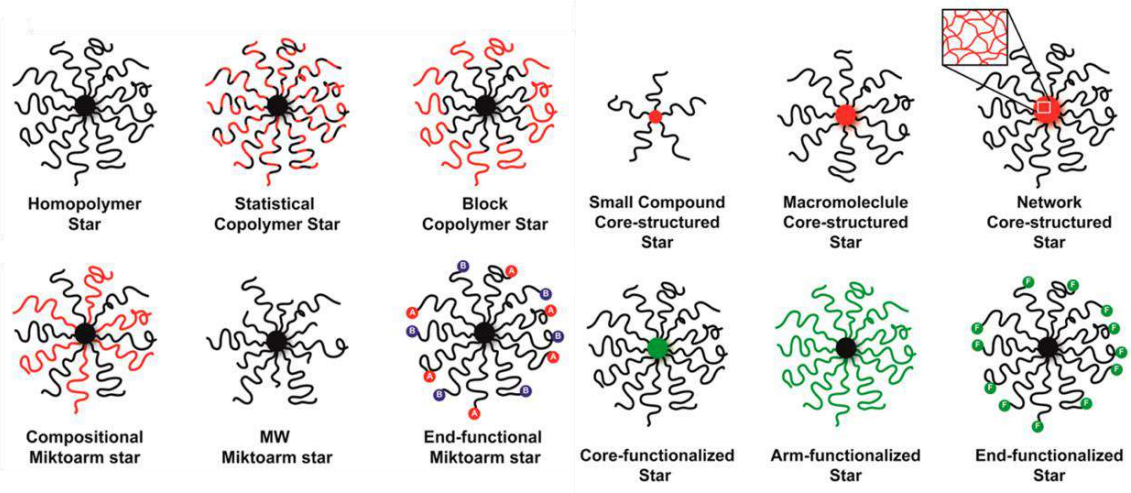

Figure 1.21. *Main structural classes of star polymers. Adapted from [99].*

The most widely used approaches in their synthesis are countless and can be grouped into three main types as carried out in a comprehensive review by Ren et al.: core-first, arm-first and grafting-onto also defined as coupling-onto [99]. The choice of one method over the others is usually dictated by the type of star structure to be obtained, the type of chemical precursors of cores and arms and the type of synthetic approach that is decided to be used during the various phases of construction of the macromolecule.

1.4.1 Core-first approach

The core-first method is based on the use of a multifunctional initiator, in which there must be reactive sites, characterized by high and identical reactivity, necessary to generate an equal number of arms and to allow the start of polymerization process as synchronous as possible **Figure 1.22**. Moreover, to obtain arms of the same identical molecular weight, the reaction rate between reactive groups (I) and the first monomer molecule (A) that is added must be much greater than the propagation rate of the chains. The main advantages of this method are the good yield, which is generally high, and the ease of separation of the product, which can often be recovered by non-solvent precipitation techniques.

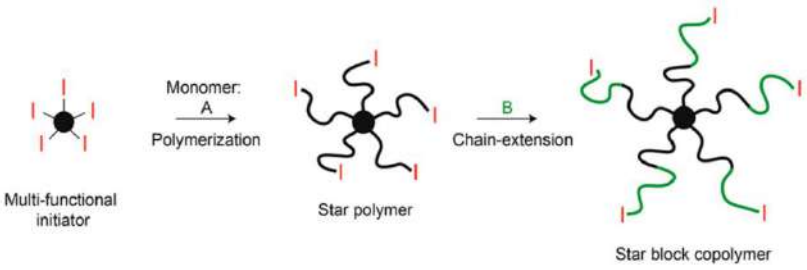

Figure 1.22. *Schematization of the synthetic core-first approach. Adapted from [99].*

Some disadvantages include the impossibility of producing miktoarm-type structures unless orthogonally reactive or protection groups are used. Moreover, on these systems it is impossible to directly determine the molecular weight of the individual arms, except in cases where they can be selectively detached from the core. This type of approach is generally not recommended to obtain polymers through classical radical polymerization reactions as they could lead to disproportionation reactions of the chain terminal radical or to the termination between radicals belonging to the arms of different molecules. Consequently, it could result in the formation of products of star-star coupling, cyclic structures, and loss of control over the molecular weight to form structures literally called "ill stars". On the other hand, this method lends itself very well to the preparation of star systems by ROP reactions on LA, ε-CL and other lactones with very good results [99].

1.4.2 Arm-first approach

This method is diametrically opposed to the previously described one, since it is convergent in nature, it in turn consists of three subgroups illustrated in **Figure 1.23**: macroinitiator (MI), macromonomer (MM) and self-assembly cross-linking (SC). The first step, common to all these categories, involves the preparation of the linear macromolecules that will make up the so-called arms. Depending on the category, these chains will have at the end: an initiating group (MI), a polymerizable group (MM) or a group capable of generating cross-linking (SC). In the preparation of arms, polymerization techniques capable to provide a high control over the molecular weight of the functionalized linear chains are preferred. In the second step, called "star formation", a polymerization reaction is started by the terminals which behave as initiators (MI), monomers (MM) or cross-linkers, depending on the case. Often the arms are studied and designed to be able to aggregate autonomously in micellar geometries to facilitate the formation of the core and decrease the probability of undesirable star-star coupling side reactions. In the MI category, the core is generated only if a monomer with at least two reactive functional groups on the end is polymerized (or even better if there are more than two, to facilitate cross-linking and the formation of the core). Differently, for MM, only a small molecule is needed to act as an initiator. In SC, coupling reactions are widely used in the formation of the core, with the preference of having small and multifunctional *ad hoc* prepared molecules inserted as terminal groups of the linear chains. For this purpose, many click reactions such as thiol-yne reaction and a large part of copper click chemistry (e.g., Huisgen 1,3 DCA, CuAAC etc.) are widely used. A great advantage that characterizes this method is related to the possibility to check and verify the actual size of the arms before their use. Among the disadvantages, the lack of control over the number of arms that form the core can be mentioned. This dependends on several parameters including

arms/crosslinker ratio and reaction time. Other drawbacks are related to the yields that are sometimes limited since not all arms are able to take part in the star formation process and to an additional separation step, required to separate the star product from the reaction mixture, that need the use of chromatography, precipitation or dialysis. Another remarkable aspect of this method lie in the possibility of using very long chains (with $M_w > 10^6$ g/mol) and in high number (>100). Interestingly, the cross-linked macromolecular structure of the core of the star structures produced with this method can reach values up to 30% of the total mass of the system [99].

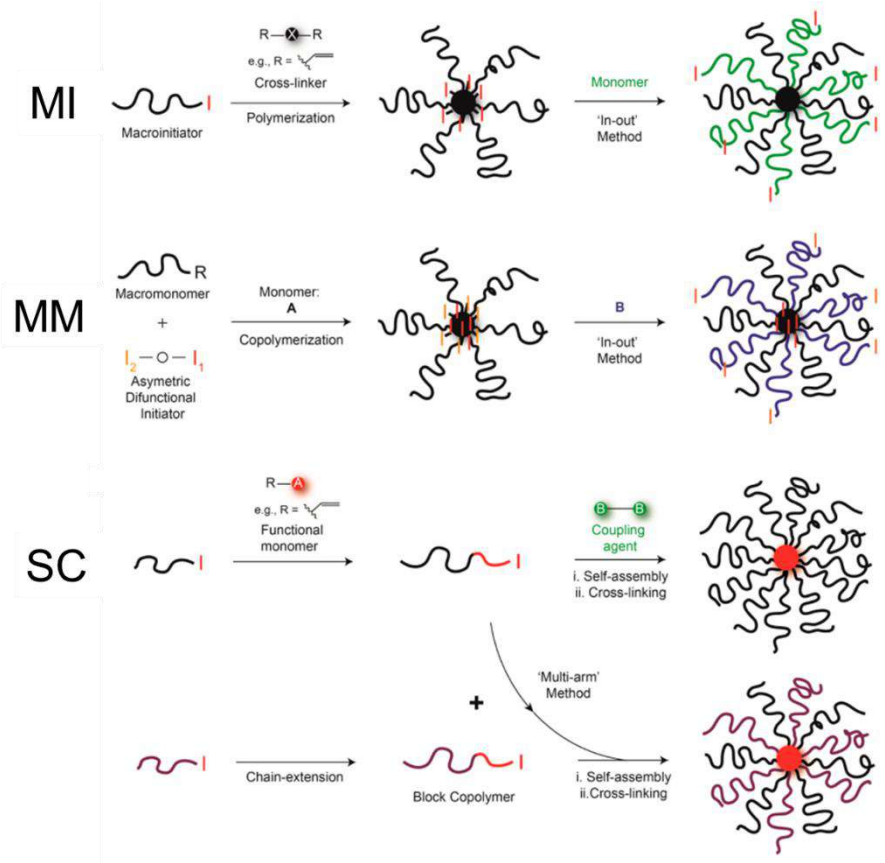

Figure 1.23. *Subcategories of arm-first approach: macroinitiator (MI), macromonomer (MM) and self-assembly cross-linking (SC). Adapted from [99].*

1.4.3 Grafting-onto/coupling-onto

Among the three methods described, it is the one that allows to have the highest degree of structural control, since cores and arms are synthesized separately and therefore can be characterized before the final coupling reaction. Typically, structures with relatively small cores and low arm count are prepared, depending on the number of reactive sites (4 to 8). Due to the limits imposed by the number of the latter and the relative steric bulk, which can be generated during the coupling phase with the chains, it is difficult to be able to covalently tie more than 20 arms on the same core. To partially limit

this steric-entropic phenomenon, the reaction can be carried out using an excess of arms compared to the stoichiometric quantity and for longer times. Similar to the arm-first method, the product recovery step requires careful separation from unreacted chains. Like the previous one, it lends itself very well to the preparation of miktoarm stars using a mixture of different chains having the same terminal reactive group. The use of cores containing sets of reactive groups orthogonal to each other opens the possibility of hybrid synthesis, such as the one shown in **Figure 1.24**, which can sometimes even become one pot. One of the problems encountered as in the previous case is related to the steric encumbrance of the chains, which in cases of hybrid synthesis could affect the number and polydispersity of the chains that are generated in successive steps. Generally, even in this case, the grafting efficiency is related to the geometry and surface density of the sites present on the core. It has been demonstrated that large and rigid cores, such as those of a fullerene nature, allow to achieve, with click reactions catalyzed by Cu(I), particularly high efficiencies [99].

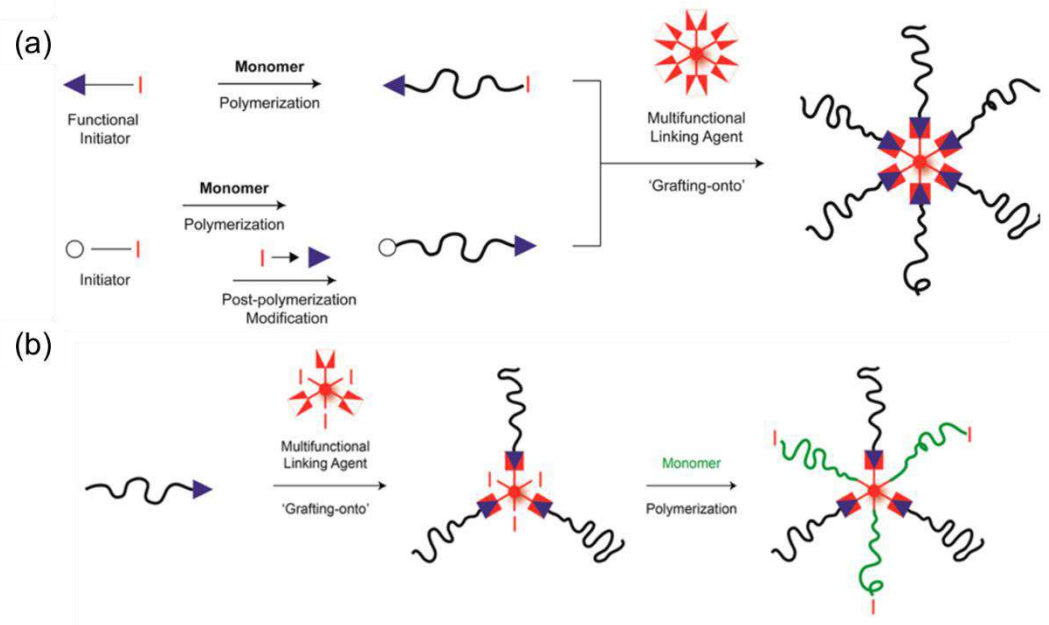

Figure 1.24. *Main subcategories of the grafting-onto (a) and core-first/grafting-onto hybrid approaches (b). Adapted from [99].*

1.5 Star-shaped PCL: applications

To highlight the great versatility of star-shaped PCL-based systems, in this section, some of their major applications are reported by discussing some of the most cited examples taken from the current literature. In a particularly intriguing study, He. et al. applied a biomimetic approach to PCL by trying to exploit catecholic groups to produce a biocompatible glue [100]. These moieties, naturally contained in mussel glue proteins, allow them to adhere perfectly to organic and inorganic substrates. Recently, it has been discovered that this kind of adhesion also occurs against biological tissues with the formation of covalent bonds between catechol moieties and the various amino and thiol groups found in proteins. For this purpose, a 19-arm star PCL was prepared using β-cyclodextrin as initiator. Subsequently, through several steps, catecholic groups were introduced to the chain terminals to form a functionalized star-shaped polymer defined as s-PCL_{19}-CA_9 (**Figure 1.25a**). The adhesive strength of the material was then studied on porcine skin samples by using $NaIO_4$ solution with different concentrations, to provide partial oxidation of the catechol groups and generate cross-links (**Figure 1.25b** and **Figure 1.25c**).

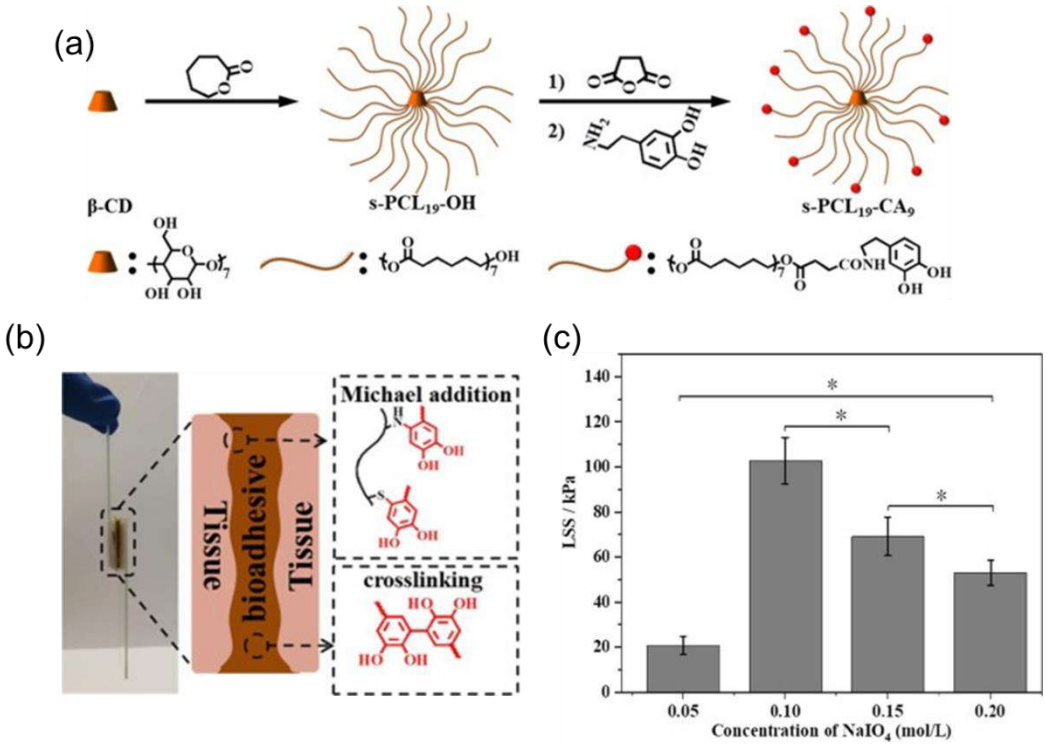

Figure 1.25. *Synthesis of s-PCL_{19}-CA_9 (a). Illustration of s-PCL_{19}-CA_9 adhesive mechanism (b) and lap shear strength of s-PCL_{19}-CA_9 after oxidation by $NaIO_4$ in different concentration (*p < 0.05)(c). Adapted from [100].*

Surprisingly, this was found to be up to 102 ± 10 kPa, a value higher than commercially available PEG or fibrin-based bio-adhesives. In another comparable work, different star-shaped tetrafunctional PCLs, with molecular weights ranging from 6 to 20 kDa, were functionalized, by using a similar multi-step approach, with N-hydroxy succinimide (NHS) end groups to be used as biocompatible melt adhesives for wound closure (star-PCL-NHS) (**Figure 1.26a** and **Figure 1.26b**). This kind of functional groups, which contain a reactive NHS ester, can promote the formation of covalent links between PCL chain and the proteins of the tissues. The material was developed to possess a low melting point, very close to human body temperature, in order to avoid damage to nearby tissue and biologic molecules when applied through the use a hot glue gun.

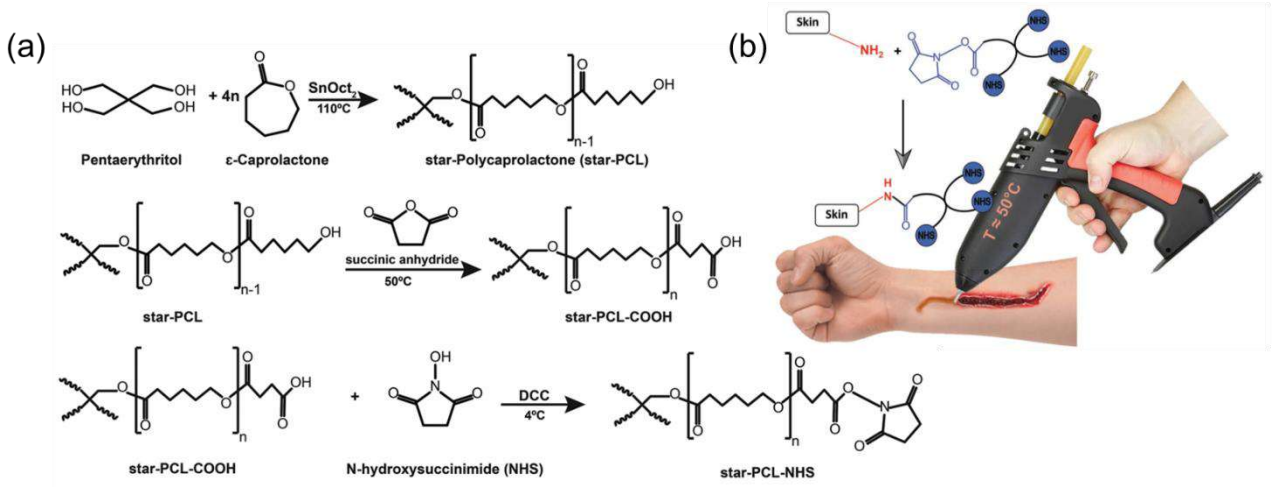

Figure 1.26. *Synthesis of star-PCL-NHS (a). Illustration of the delivery of star-PCL-NHS adhesive directly extruded from the heated nozzle, which then solidifies upon cooling, closing exposed cuts and wounds (b). Adapted from [101].*

The results showed that star-PCL-NHS provide a range of adhesive strengths that are significantly higher than other bioadhesive systems and possess up to 50% of the adhesive strength of surgical cyanoacrylate glue while being less cytotoxic and fully biocompatible. Among the samples, the 13 kDa star-PCL-NHS displayed better properties for tissue adhesion due to its melting temperature, of ca. 45 °C, which is sufficiently above the body temperature. Upon cooling to body temperature, it solidifies and maintains good elasticity and adhesion properties [101]. Another biomedical application of PCL-based star-shaped polymers can be found in the preparation of micelles for drug delivery applications. Gao et al. prepared star-shaped PCL/PEG micelles (SSMPEG-PCL) for the delivery of doxorubicin (Dox) in the treatment of colon cancer [102]. The micelles were prepared starting by an acrylated monomethoxy poly(ethylene glycol)-poly(caprolactone) (AMPEG-PCL) diblock copolymer which self-assembled into micelles when contacted with water. Thanks to the

core-shell structure obtained in this process it was possible to exploit the double bonds at the end of the PCL blocks for the cross-linking to form 25 nm in diameter star-shaped SSMPEG-PCL micelles. The loading of Dox was performed in PBS buffer with high efficiency, with Dox that self-assembled into the hydrophobic cores of the SSMPEG-PCL micelles due to its hydrophobic behaviour at that pH value (**Figure 1.27a**). Cytotoxicity of micelle-encapsulated Dox (Dox/SSMPEG-PCL) on the colon cancer CT-26 cell line was evaluated in vitro and in vivo on tumour bearing mice inoculated with CT26 cells. Results indicated that a single 5 mg/kg Dox/SSMPEG-PCL micelles dose resulted in smaller tumours volume, over time, compared with free Dox or unloaded micelles (**Figure 1.27b**). As clearly observed by the authors, after 25 days, the tumours in the group treated with Dox/SSMPEG-PCL micelles were significantly smaller than those of the other mice groups employed for the test (**Figure 1.27c**). Interestingly, the Dox/SSMPEG-PCL micelle was shown to enhance anticancer activity of Dox and might be a novel carrier for anticancer agents.

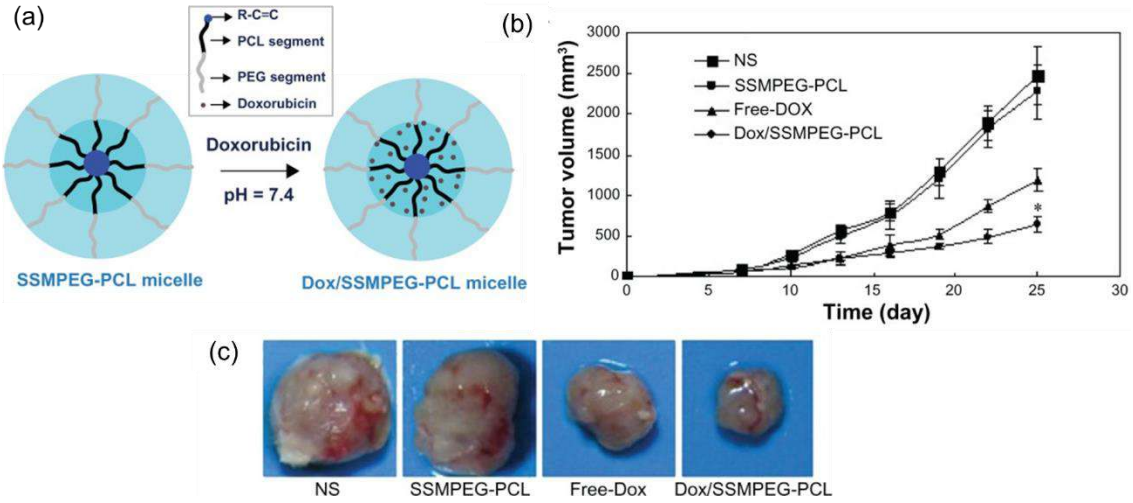

Figure 1.27. *Structure and Dox-loading of SSMPEG-PCL nanoparticles (a) and tumour growth over time in mice (b). On day 0, C-26 cells were inoculated into the animals. After 7 days, the mice were divided in four groups which were injected intravenously with saline (NS), empty SSMPEG-PCL micelles, free Dox, and Dox/SSMPEG-PCL nanoparticles. Photos of tumours in each group removed after 25 days (c). Adapted from [102].*

An additional application of star-shaped PCLs in the biomedical context was presented by Ekapakul et al. that prepared bioactive composite hydrogels made of chitosan (CS) and star-shaped polycaprolactone (stPCL) for wound dressing and bone tissue engineering (**Figure 1.28**) [103]. The addition of stPCL was done to impart good mechanical properties and stability to the composite hydrogels. Specifically, the bioactivity was referred to the antibacterial activity, cell viability, skin irritation, decomposability, and ability to attach ions for apatite nucleation displayed by the materials. The hydrogels were prepared by using a solution approach where a starting CS solution in succinic acid was mixed with carboxyl terminated star-shaped PCL (stPCL-COOH) in different ratios at 60 °C.

Then the crosslinking with the formation of a covalent network was obtained by adding the conjugating agents, 1-ethyl-3-(3-dimetilaminopropyl) carbodiimide (EDC) and N-hydroxysuccinimide (NHS) and pouring the mix into a mold, overnight at 4 °C. The prepared hydrogels showed good transparency and could inhibit bacterial growth of *Escherichia coli* and *Staphilococcus epidermis*. In addition, extract solution from hydrogels and composite hydrogels showed no toxic effects NIH/3T3 fibroblasts, showing cell viabilities above 80%. Skin irritation tests conducted on rabbits, revealed no remarkable signs of edema or erythema reactions after two days from the injection of hydrogels extract in saline (polar extract) and propylene glycol (non-polar extract), confirming the safety of the material for biomedical use on both animals and humans.

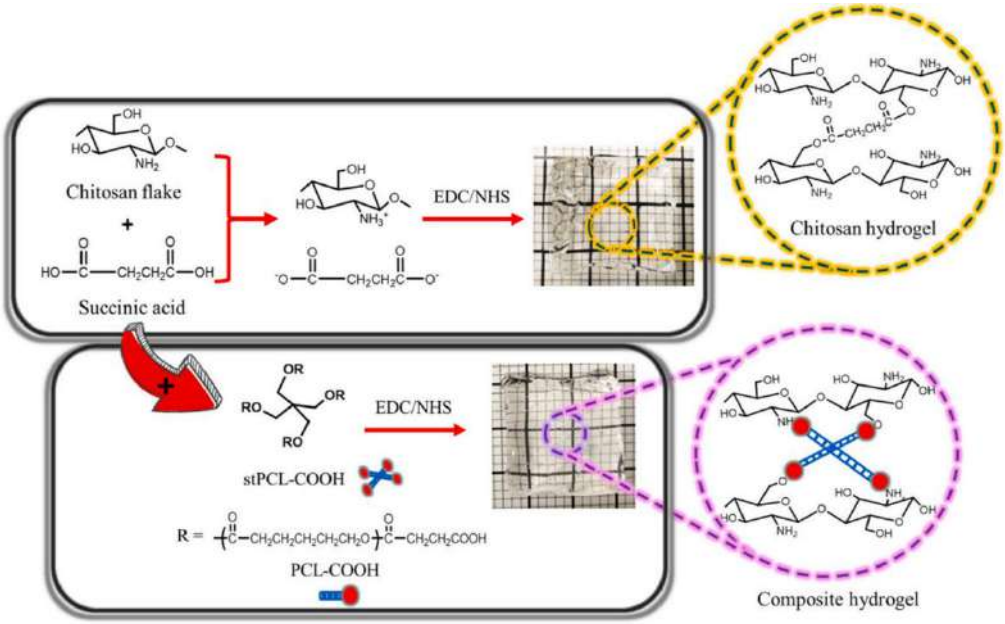

Figure 1.28. *Preparation scheme of chitosan hydrogel (CS) and chitosan/star-shaped PCL hydrogels (stPCL-COOH/CS). Adapted from [103].*

Moreover, the materials underwent complete degradation after 2 days in a soil burial test, highlighting their biodegradable nature. Additionally, calcium and phosphate ions could be induced to grow on the hydrogel porous structure by soaking samples in simulated body fluid (SBF). SEM, EDS and XRD analyses supported the formation of calcium phosphate and the Ca/P ratio which on the surface of composite hydrogel was 1.26 times higher than the neat chitosan hydrogel and was supposed to be promoted by the improved interactions between the ionized carboxylic groups of stPCL-COOH and calcium ions proving the potential to develop for wound dressing and bone tissue engineering applications. Other uses of star-shaped PCL polymers, in virtue of their branched multifunctional structure, are in the preparation of polymer additives. For example, Jeong et al. used PCL in the preparation of three different, star-shaped PCL-b-PDLA biodegradable diblock copolymeric plasticizers, with molecular weights of 5, 10 and 15 kDa respectively, with the aim to improve the

ductility of poly(lactic-*co*-glycolic acid) (PLGA) [104]. To study their influence, these additives were added to PLGA in different concentration, ranging from 0.25 to 2% wt%, to prepare PLGA/star-shaped PCL-b-PDLA thin films by solvent casting technique (**Figure 1.29**). The addition of these additives to the PLGA films disclosed the possibility to obtain a significant increase in mechanical properties in terms of elongation at break, without sacrificing some characteristics such as the elastic modulus and the yield strength of the starting material. Specifically, the authors pointed out that even just the addition of 0.5 wt% of the 5 kDa PCL-b-PDLA additive, dramatically increased the elongation at break of the blend which reached approximately 248%. This result was accounted to a strong adhesion between PLGA matrix and PDLA segment of PCL-b-PDLA composites due to the presence of stereocomplexation, which enhanced interfacial adhesion between the plasticizers and the PLGA matrix. This was then confirmed by a morphological characterization which revealed the formation of a fibrillated structure and the homogenous dispersion of the additive due to very good level of interfacial adhesion obtained.

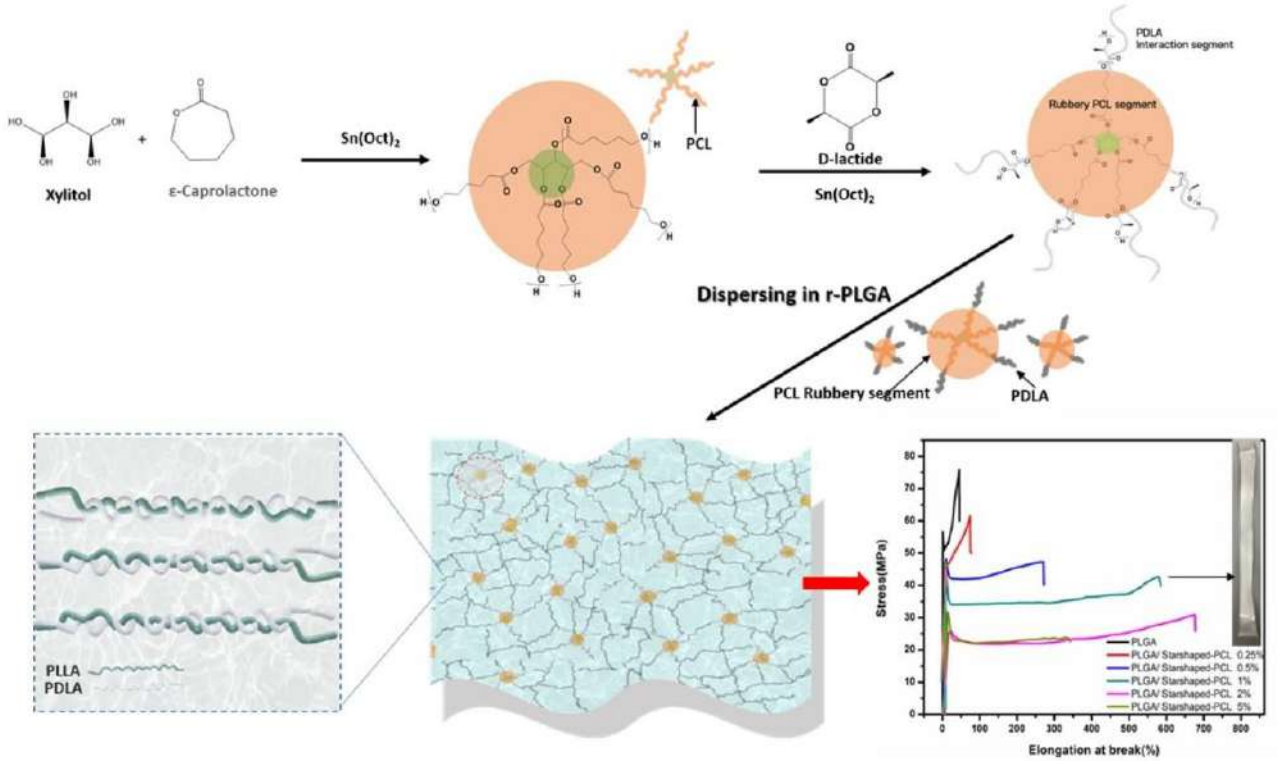

Figure 1.29. *Schematic representation of PCL-b-PDLA additive synthesis and their application in the development of plasticized PLGA/star-shaped PCL-b-PDLA blends. Adapted from [104].*

Moreover, PLGA/star-shaped PCL-b-PDLA blends exhibited good transparency in the UV-vis range, facilitating, in fact, their applicability in the field of packaging. Lyu et al., in another study, prepared star-shaped polyhedral oligomeric silsesquioxane (SPOSS)-based multi-arm PCLs with different molecular weight for the development of shape-memory (SM) materials [105]. SM behaviour was

obtained thanks to the semicrystalline nature of PCL which, when crosslinked in a certain initial shape, e.g., like in this work to form polyurethanes (PUs), it can be reshaped and locked into a new shape. This can be done, for example, by simple application of a mechanical stress, or by heating above the melting point of the crystalline phase, application of a mechanical stress and subsequent cooling to reform the crystalline phase, as performed by the authors of this research. The presence of crystalline domains is capable to freeze macromolecular segment motions enabling the material to stay in a metastable state, keeping the new given shape. To return to the initial shape, it is necessary to release the material from the applied stress and heat it again above the melting point of the crystalline phase to allow the macromolecular segments stretched by the previously applied stress to return to the initial shape. In particular, SM properties when combined with the biocompatibility of PCL are a valuable technology for various biomedical applications such as self-deployable medical products and drug delivery systems. In a first step, polyhedral oligomeric silsesquioxane (POSS) was end-capped with allylic alcohol and then the exposed hydroxyl groups were exploited as base for PCL grafting using ROP of ε-CL. Star-shaped POSS PCL were then used in the preparation of a set of SM cross-linked polyurethanes (SPOSS-PU) by successive reaction with hexamethylene diisocyanate (HMDI) in presence of dibutyltin dilaurate (DBTDL) as catalyst (**Figure 1.30a**). For these systems it was found that thermal actuation properties were significantly affected by PCL arm length of SPOSS-PU with free strain recovery onset temperatures increasing with the content of the soft segment, i.e., molecular weight PCL, as showed also by the melting temperatures found in the DSC analysis. Stress–strain–temperature diagrams with free-strain (**Figure 1.30b**) and fixed-strain recovery (**Figure 1.30c**) performed in the range from 20 to 70 °C show in detail the thermo-mechanical behaviour of one of the examined SPOSS-PU (SPOSS-PU 160) when subjected to 5 different working cycles, done by heating repeatedly the material to 70 °C and then cooling down to 20 °C, to evidence its shape memory properties. In particular, the authors found that an increase in the molecular weight of PCL chains between cross-links resulted in a lower stiffness of the network, in terms of Young's modulus measured well above PCL melting point at 70 °C, while shorter chains lead to a steeper increase in stress leading to a more crosslinked material. This was accompanied by a decrease in load stresses during the first cycle, indicating a reduced resistance to strain (**Figure 1.30c**). Free-strain recovery data reported in the work showed a modest increase in shape fixity at higher POSS contents i.e. lower soft segment content, i.e., molecular weight of PCL chains, and a decrease by decreasing cross-linking density.

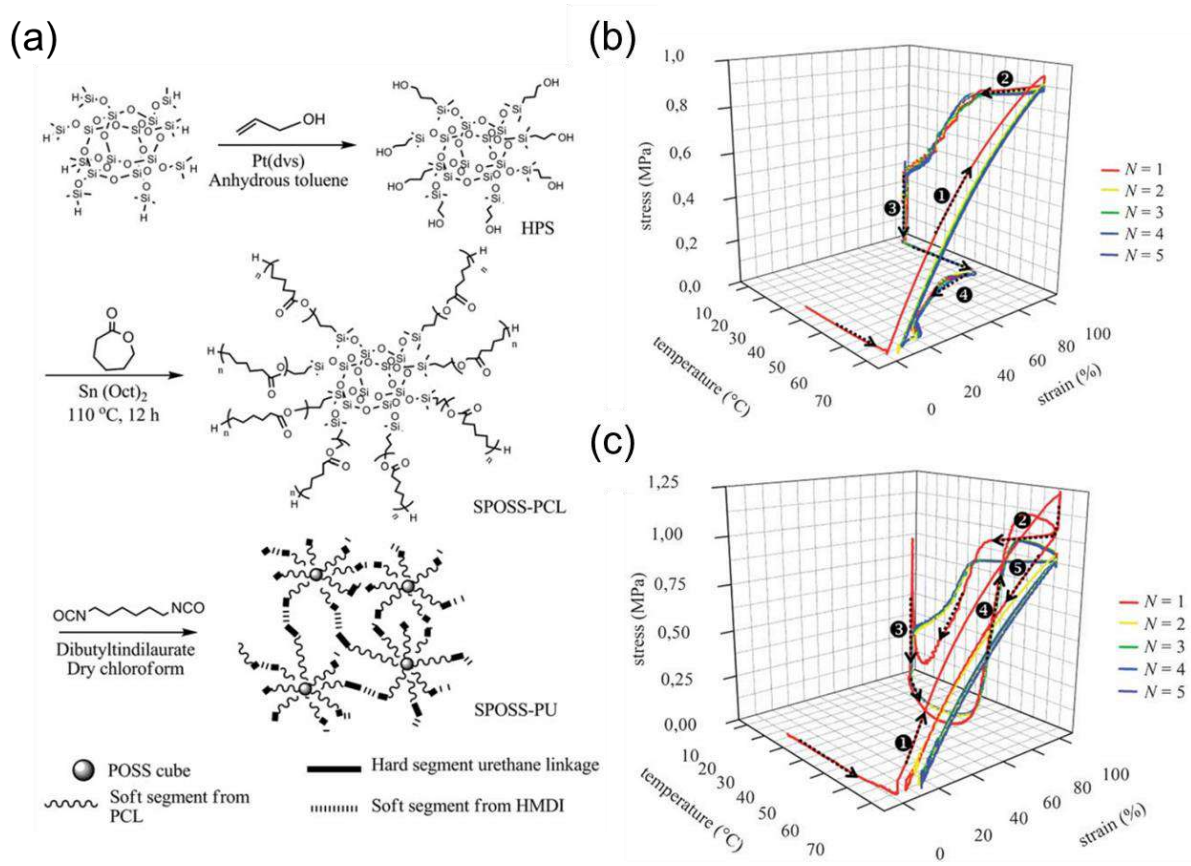

Figure 1.30. *Synthetic route for star-shaped PU networks (a). Cyclic thermo-mechanical measurements (CTM) test protocols for SPOSS-PU 160 ($M_{n,theo}$ = 19742 g/mol) showed as 3D stress–strain–temperature graphs. CTM recovery method I display the free-strain recovery profiles (b) while CTM recovery method II shows the fixed-strain (c). Five differently coloured thermo-mechanical cycles are reported (ε_m = 100%). For the sake of clarity, the relevant steps in CTM are numbered: specimen deformation (1), shape fixing (2) and unloading (3), constrained stress recovery responses of the material (4), followed by unloading to zero stress (5). Adapted from [105].*

For the best performing systems, impressive strain (98%) and stress recovery (100%) values were found disclosing their possible practical use. Ultimately, it can be stated that the wide field of application of star-shaped PCL as illustrated in this paragraph, from biocompatible adhesives to their role in shape memory systems, demonstrates their versatility of use and makes them valuable starting substrates for the development of advanced sustainable materials.

1.6 References

[1] A.L. Sisson, D. Ekinci, A. Lendlein, The contemporary role of ε-caprolactone chemistry to create advanced polymer architectures, Polymer 54 (2013) 4333–4350. https://doi.org/10.1016/j.polymer.2013.04.045.

[2] M.J. Jenkins, K.L. Harrison, The effect of molecular weight on the crystallization kinetics of polycaprolactone, Polym. Adv. Technol. 17 (2006) 474–478. https://doi.org/10.1002/pat.733.

[3] H. Bittiger, R.H. Marchessault, W.D. Niegisch, Crystal structure of poly-ε-caprolactone, Acta Crystallogr. Sect. B Struct. Crystallogr. Cryst. Chem. 26 (1970) 1923–1927. https://doi.org/10.1107/s0567740870005198.

[4] M. Karimi, M. Heuchel, T. Weigel, M. Schossig, D. Hofmann, A. Lendlein, Formation and size distribution of pores in poly(ε-caprolactone) foams prepared by pressure quenching using supercritical CO2, J. Supercrit. Fluids. 61 (2012) 175–190. https://doi.org/10.1016/j.supflu.2011.09.022.

[5] V.R. Sinha, K. Bansal, R. Kaushik, R. Kumria, A. Trehan, Poly-ϵ-caprolactone microspheres and nanospheres: an overview, Int. J. Pharm. 278 (2004) 1–23. https://doi.org/10.1016/j.ijpharm.2004.01.044.

[6] X. Zhang, Science and Principles of Biodegradable and Bioresorbable Medical Polymers: Materials and Properties, Elsevier 2016.

[7] K. Adamska, A. Voelkel, A. Berlińska, The solubility parameter for biomedical polymers—application of inverse gas chromatography, J. Pharm. Biomed. Anal. 127 (2016) 202–206. https://doi.org/10.1016/j.jpba.2016.04.014.

[8] L.A. Bosworth, S. Downes, Physicochemical characterisation of degrading polycaprolactone scaffolds, Polym. Degrad. Stab. 95 (2010) 2269–2276. https://doi.org/10.1016/j.polymdegradstab.2010.09.007.

[9] M. Nevoralová, M. Koutný, A. Ujčić, Z. Starý, J. Šerá, H. Vlková, M. Šlouf, I. Fortelný, Z. Kruliš, Structure characterization and biodegradation rate of poly(ε-caprolactone)/starch blends, Front. Mater. 7 (2020) 1–14. https://doi.org/10.3389/fmats.2020.00141.

[10] A. Göpferich, Mechanisms of polymer degradation and erosion, Biomaterials 17 (1996) 103–114. https://doi.org/10.1016/0142-9612(96)85755-3.

[11] C.G. Pitt, F.I. Chasalow, Y.M. Hibionada, D.M. Klimas, A. Schindler, Aliphatic polyesters. I. the degradation of poly(ϵ-caprolactone) in vivo, J. Appl. Polym. Sci. 26 (1981) 3779–3787. https://doi.org/10.1002/app.1981.070261124.

[12] M.A. Woodruff, D.W. Hutmacher, The return of a forgotten polymer - polycaprolactone in the 21st century, Prog. Polym. Sci. 35 (2010) 1217–1256. https://doi.org/10.1016/j.progpolymsci.2010.04.002.

[13] K. Ceonzo, A. Gaynor, L. Shaffer, K. Kojima, C.A. Vacanti, G.L. Stahl, Polyglycolic acid-induced inflammation: role of hydrolysis and resulting complement activation, Tissue Eng. 12 (2006) 301–308. https://doi.org/10.1089/ten.2006.12.301.

[14] K.-W. Ko, B. Choi, E.Y. Kang, S.-W. Shin, S.-W. Baek, D.K. Han, The antagonistic effect of magnesium hydroxide particles on vascular endothelial activation induced by acidic PLGA degradation products, Biomater. Sci. 9 (2021) 892–907. https://doi.org/10.1039/D0BM01656J.

[15] F. Yang, X. Niu, X. Gu, C. Xu, W. Wang, Y. Fan, biodegradable magnesium-incorporated poly(l-lactic acid) microspheres for manipulation of drug release and alleviation of inflammatory response, ACS Appl. Mater. Interfaces. 11 (2019) 23546–23557. https://doi.org/10.1021/acsami.9b03766.

[16] J.H. Jung, M. Ree, H. Kim, Acid- and base-catalyzed hydrolyses of aliphatic polycarbonates and polyesters, Catal. Today. 115 (2006) 283–287. https://doi.org/10.1016/j.cattod.2006.02.060.

[17] C.J. Blackwell, K. Haernvall, G.M. Guebitz, M. Groombridge, D. Gonzales, E. Khosravi, Enzymatic degradation of star poly(ε-caprolactone) with different central units, Polymers 10 (2018). https://doi.org/10.3390/polym10111266.

[18] K. Shi, J. Jing, L. Song, T. Su, Z. Wang, Enzymatic hydrolysis of polyester: degradation of poly(ε-caprolactone) by candida antarctica lipase and fusarium solani cutinase, Int. J. Biol. Macromol. 144 (2020) 183–189. https://doi.org/10.1016/j.ijbiomac.2019.12.105.

[19] Z. Gan, D. Yu, Z. Zhong, Q. Liang, X. Jing, Enzymatic degradation of poly(ε-caprolactone)/poly(dl-lactide) blends in phosphate buffer solution, Polymer 40 (1999) 2859–2862. https://doi.org/10.1016/S0032-3861(98)00549-7.

[20] M. Mochizuki, M. Hirano, Y. Kanmuri, K. Kudo, Y. Tokiwa, Hydrolysis of polycaprolactone fibers by lipase: effects of draw ratio on enzymatic degradation, J. Appl. Polym. Sci. 55 (1995) 289–296. https://doi.org/10.1002/app.1995.070550212.

[21] Z. Gan, Q. Liang, J. Zhang, X. Jing, Enzymatic degradation of poly(ε-caprolactone) film in phosphate buffer solution containing lipases, Polym. Degrad. Stab. 56 (1997) 209–213. https://doi.org/10.1016/S0141-3910(96)00208-X.

[22] S. Li, M. Pignol, F. Gasc, M. Vert, Synthesis, characterization, and enzymatic degradation of copolymers prepared from ε-caprolactone and β-butyrolactone, Macromolecules 37 (2004) 9798–9803. https://doi.org/10.1021/ma0489422.

[23] M. Bartnikowski, T.R. Dargaville, S. Ivanovski, D.W. Hutmacher, Degradation mechanisms of

polycaprolactone in the context of chemistry, geometry and environment, Prog. Polym. Sci. 96 (2019) 1–20. https://doi.org/10.1016/j.progpolymsci.2019.05.004.
[24] H. Sun, L. Mei, C. Song, X. Cui, P. Wang, The in vivo degradation, absorption and excretion of pcl-based implant, Biomaterials 27 (2006) 1735–1740. https://doi.org/10.1016/j.biomaterials.2005.09.019.
[25] C.X.F. Lam, S.H. Teoh, D.W. Hutmacher, comparison of the degradation of polycaprolactone and polycaprolactone-(β-tricalcium phosphate) scaffolds in alkaline medium, Polym. Int. 56 (2007) 718–728. https://doi.org/10.1002/pi.2195.
[26] J. Kim, Isovolemic degradation of polycaprolactone particles and calculation of their original size from human biopsy, Plast. Reconstr. Surg. - Glob. Open. 8 (2020) E2866. https://doi.org/10.1097/GOX.0000000000002866.
[27] M.J. Jenkins, K.L. Harrison, M.M.C.G. Silva, M.J. Whitaker, K.M. Shakesheff, S.M. Howdle, Characterisation of microcellular foams produced from semi-crystalline PCL using supercritical carbon dioxide, Eur. Polym. J. 42 (2006) 3145–3151. https://doi.org/10.1016/j.eurpolymj.2006.07.022.
[28] D.W. Hutmacher, T. Schantz, I. Zein, K.W. Ng, S.H. Teoh, K.C. Tan, Mechanical properties and cell cultural response of polycaprolactone scaffolds designed and fabricated via fused deposition modeling, J. Biomed. Mater. Res. 55 (2001) 203–216. https://doi.org/10.1002/1097-4636(200105)55:2<203::AID-JBM1007>3.0.CO;2-7.
[29] M. Labet, W. Thielemans, Synthesis of polycaprolactone: a review, Chem. Soc. Rev. 38 (2009) 3484. https://doi.org/10.1039/b820162p.
[30] V. Guarino, G. Gentile, L. Sorrentino, L. Ambrosio, Polycaprolactone: synthesis, properties, and applications, Enc. Polym. Sci. Tech. (2017). https://doi.org/10.1002/0471440264.pst658.
[31] R.. Singh, J.. Pandey, D. Rutot, P. Degée, P. Dubois, Biodegradation of poly(ε-caprolactone)/starch blends and composites in composting and culture environments: the effect of compatibilization on the inherent biodegradability of the host polymer, Carbohydr. Res. 338 (2003) 1759–1769. https://doi.org/10.1016/S0008-6215(03)00236-2.
[32] P. Dubois, M. Krishnan, R. Narayan, Aliphatic polyester-grafted starch-like polysaccharides by ring-opening polymerization, Polymer 40 (1999) 3091–3100. https://doi.org/10.1016/S0032-3861(98)00110-4.
[33] C.R. Di Franco, V.P. Cyras, J.P. Busalmen, R.A. Ruseckaite, A. Vázquez, Degradation of polycaprolactone/starch blends and composites with sisal fibre, Polym. Degrad. Stab. 86 (2004) 95–103. https://doi.org/10.1016/j.polymdegradstab.2004.02.009.
[34] G. Mensitieri, E. Di Maio, G.G. Buonocore, I. Nedi, M. Oliviero, L. Sansone, S. Iannace, Processing and shelf life issues of selected food packaging materials and structures from renewable resources, Trends Food Sci. Technol. 22 (2011) 72–80. https://doi.org/10.1016/j.tifs.2010.10.001.
[35] M. Aldas, E. Rayón, J. López-Martínez, M.P. Arrieta, A deeper microscopic study of the interaction between gum rosin derivatives and a mater-bi type bioplastic, Polymers 12 (2020). https://doi.org/10.3390/polym12010226.
[36] M. Delgado-Aguilar, R. Puig, I. Sazdovski, P. Fullana-i-Palmer, Polylactic acid/polycaprolactone blends: on the path to circular economy, substituting single-use commodity plastic products, Materials 13 (2020) 2655. https://doi.org/10.3390/ma13112655.
[37] M. Rizzuto, L. Marinetti, D. Caretti, A. Mugica, M. Zubitur, A.J. Müller, Can poly(ε-caprolactone) crystals nucleate glassy polylactide?, CrystEngComm. 19 (2017) 3178–3191. https://doi.org/10.1039/C7CE00578D.
[38] L. Magazzini, S. Grilli, S.E. Fenni, A. Donetti, D. Cavallo, O. Monticelli, The blending of poly(glycolic acid) with polycaprolactone and poly(l-lactide): promising combinations, Polymers 13 (2021) 2780. https://doi.org/10.3390/polym13162780.
[39] G. Bogoeva-Gaceva, M. Avella, M. Malinconico, A. Buzarovska, A. Grozdanov, G. Gentile, M.E. Errico, Natural fiber eco-composites, Polym. Compos. 28 (2007) 98–107. https://doi.org/10.1002/pc.20270.
[40] T. Gurunathan, S. Mohanty, S.K. Nayak, A review of the recent developments in biocomposites based on natural fibres and their application perspectives, Compos. Part A Appl. Sci. Manuf. 77 (2015) 1–25. https://doi.org/10.1016/j.compositesa.2015.06.007.
[41] J. Biagiotti, D. Puglia, J.M. Kenny, A review on natural fibre-based composites — part II, J. Nat. Fibers. 1 (2004) 37–68.
[42] K. Van De Velde, P. Kiekens, Biopolymers: overview of several properties and consequences on their applications, Polym. Test. 21 (2002) 433–442. https://doi.org/10.1016/S0142-9418(01)00107-6.
[43] J.S. Lyu, J.-S. Lee, J. Han, Development of a biodegradable polycaprolactone film incorporated with an antimicrobial agent via an extrusion process, Sci. Rep. 9 (2019) 20236. https://doi.org/10.1038/s41598-019-56757-5.
[44] R.A. Ilyas, M.Y.M. Zuhri, M.N.F. Norrrahim, M.S.M. Misenan, M.A. Jenol, S.A. Samsudin, N.M. Nurazzi, M.R.M. Asyraf, A.B.M. Supian, S.P. Bangar, R. Nadlene, S. Sharma, A.A.B. Omran, Natural fiber-reinforced polycaprolactone green and hybrid biocomposites for various advanced applications, Polymers 14 (2022). https://doi.org/10.3390/polym14010182.
[45] K. Weissermel, H. Arpe, Industrial organic chemistry, Wiley, 2003.
[46] D. Yin, Q. Xin, S. Yu, L. Jiang, L. Li, C. Xie, Q. Wu, H. Yu, Y. Liu, Y. Liu, S. Liu, Selective hydrogenation of

phenol to cyclohexanone over a highly stable core-shell catalyst with pd-lewis acid sites, J. Phys. Chem. C. 125 (2021) 27241–27251. https://doi.org/10.1021/acs.jpcc.1c08616.
[47] H. Nagahara, M. Ono, M. Konishi, Y. Fukuoka, Partial hydrogenation of benzene to cyclohexene, Appl. Surf. Sci. 121–122 (1997) 448–451. https://doi.org/10.1016/S0169-4332(97)00325-5.
[48] U. Schuchardt, D. Cardoso, R. Sercheli, R. Pereira, R.S. da Cruz, M.C. Guerreiro, D. Mandelli, E. V. Spinacé, E.L. Pires, Cyclohexane oxidation continues to be a challenge, Appl. Catal. A Gen. 211 (2001) 1–17. https://doi.org/10.1016/S0926-860X(01)00472-0.
[49] J. Zhong, J. Chen, L. Chen, Selective hydrogenation of phenol and related derivatives, Catal. Sci. Technol. 4 (2014) 3555–3569. https://doi.org/10.1039/c4cy00583j.
[50] S. Liu, J. Han, Q. Wu, B. Bian, L. Li, S. Yu, J. Song, C. Zhang, A.J. Ragauskas, Hydrogenation of phenol to cyclohexanone over bifunctional pd/c-heteropoly acid catalyst in the liquid phase, Catal. Letters. 149 (2019) 2383–2389. https://doi.org/10.1007/s10562-019-02852-1.
[51] I. Marchante, A.E.B. Ruiz, V. Plesu, J. Bonet-Ruiz, P. Iancu, J. Llorens, Hydration of cyclohexene to cyclohexanol in a hybrid reactive distillation with a side decanter, Chem. Eng. Trans. 76 (2019) 25–30. https://doi.org/10.3303/CET1976005.
[52] S.H. Pyo, J.H. Park, V. Srebny, R. Hatti-Kaul, A sustainable synthetic route for biobased 6-hydroxyhexanoic acid, adipic acid and ϵ-caprolactone by integrating bio- and chemical catalysis, Green Chem. 22 (2020) 4450–4455. https://doi.org/10.1039/d0gc01454k.
[53] W. Zhang, Y. Zheng, M. Lang, Simple separation operation improved enzyme-catalyzed ε-caprolactone yield, J. Mol. Struct. (2023) 136638. https://doi.org/10.1016/j.molstruc.2023.136638.
[54] S. Schmidt, C. Scherkus, J. Muschiol, U. Menyes, T. Winkler, W. Hummel, H. Gröger, A. Liese, H.-G. Herz, U.T. Bornscheuer, An enzyme cascade synthesis of ε-caprolactone and its oligomers, Angew. Chemie Int. Ed. 54 (2015) 2784–2787. https://doi.org/10.1002/anie.201410633.
[55] V.S.T. Srinivasamurthy, D. Böttcher, J. Engel, S. Kara, U.T. Bornscheuer, A whole-cell process for the production of ε-caprolactone in aqueous media, Process Biochem. 88 (2020) 22–30. https://doi.org/10.1016/j.procbio.2019.10.009.
[56] S. Gundekari, B. Biswas, T. Bhaskar, K. Srinivasan, Preparation of cyclohexanol from lignin-based phenolic concoction using controlled hydrogen delivery tool over in-situ Ru catalyst, Biomass and Bioenergy. 161 (2022) 106448. https://doi.org/10.1016/j.biombioe.2022.106448.
[57] H. Tian, C. Furtmann, F. Lenz, V. Srinivasamurthy, U.T. Bornscheuer, J. Jose, Enzyme cascade converting cyclohexanol into ε-caprolactone coupled with NADPH recycling using surface displayed alcohol dehydrogenase and cyclohexanone monooxygenase on E. coli, Microb. Biotechnol. 15 (2022) 2235–2249. https://doi.org/10.1111/1751-7915.14062.
[58] L. Bretschneider, I. Heuschkel, M. Wegner, M. Lindmeyer, K. Bühler, R. Karande, B. Bühler, Conversion of cyclohexane to 6-hydroxyhexanoic acid using recombinant pseudomonas taiwanensis in a stirred-tank bioreactor, Front. Catal. 1 (2021). https://doi.org/10.3389/fctls.2021.683248.
[59] V. Thaore, D. Chadwick, N. Shah, Sustainable production of chemical intermediates for nylon manufacture: A techno-economic analysis for renewable production of caprolactone, Chem. Eng. Res. Des. 135 (2018) 140–152. https://doi.org/10.1016/j.cherd.2018.05.026.
[60] F.J. Van Natta, J.W. Hill, W.H. Carothers, studies of polymerization and ring formation. XXIII. ε-caprolactone and its polymers, J. Am. Chem. Soc. 56 (1934) 455–457. https://doi.org/10.1021/ja01317a053.
[61] Y.M. Harshe, G. Storti, M. Morbidelli, S. Gelosa, D. Moscatelli, Polycondensation kinetics of lactic acid, Macromol. React. Eng. 1 (2007) 611–621. https://doi.org/10.1002/mren.200700019.
[62] C. Braud, R. Devarieux, A. Atlan, C. Ducos, Michel Vert, Capillary zone electrophoresis in normal or reverse polarity separation modes for the analysis of hydroxy acid oligomers in neutral phosphate buffer, in: J. Chromatogr. B Biomed. Appl., 1998: pp. 73–82. https://doi.org/10.1016/S0378-4347(97)00468-4.
[63] A. Mahapatro, A. Kumar, R.A. Gross, Mild, solvent-free ω-hydroxy acid polycondensations catalyzed by candida antarctica lipase b, Biomacromolecules 5 (2004) 62–68. https://doi.org/10.1021/bm0342382.
[64] H. Dong, H. Da Wang, S.G. Cao, J.C. Shen, Lipase-catalyzed polymerization of lactones and linear hydroxyesters, Biotechnol. Lett. 20 (1998) 905–908. https://doi.org/10.1023/A:1005482232687.
[65] W.J. Bailey, Z. Ni, S.R. Wu, Free radical ring-opening polymerization of 4,7-dimethyl-2-methylene-1,3-dioxepane and 5,6-benzo-2-methylene-1,3-dioxepane, Macromolecules 15 (1982) 711–714. https://doi.org/10.1021/ma00231a006.
[66] J. Undin, A. Finne-Wistrand, A.C. Albertsson, Copolymerization of 2-methylene-1,3-dioxepane and glycidyl methacrylate, a well-defined and efficient process for achieving functionalized polyesters for covalent binding of bioactive molecules, Biomacromolecules 14 (2013) 2095–2102. https://doi.org/10.1021/bm4004783.
[67] P. Peter, T. Therese, F.W. Anna, A.C. Albertsson, Mapping the characteristics of the radical ring-opening polymerization of a cyclic ketene acetal towards the creation of a functionalized polyester, J. Polym. Sci. Part A Polym. Chem. 47 (2009) 4587–4601. https://doi.org/10.1002/pola.23511.
[68] J. Undin, P. Plikk, A. Finne-Wistrand, A.C. Albertsson, Synthesis of amorphous aliphatic polyester-ether homo- and copolymers by radical polymerization of ketene acetals, J. Polym. Sci. Part A Polym. Chem. 48 (2010)

4965–4973. https://doi.org/10.1002/pola.24292.
[69] J.Y. Yuan, C.Y. Pan, Block copolymerization of 5,6-benzo-2-methylene-1,3-dioxepane with conventional vinyl monomers by ATRP method, Eur. Polym. J. 38 (2002) 1565–1571. https://doi.org/10.1016/S0014-3057(02)00023-X.
[70] P. Xu, X. Huang, X. Pan, N. Li, J. Zhu, X. Zhu, Hyperbranched polycaprolactone through RAFT polymerization of 2-methylene-1,3-dioxepane, Polymers 11 (2019). https://doi.org/10.3390/polym11020318.
[71] S. Agarwal, C. Speyerer, Degradable blends of semi-crystalline and amorphous branched poly(caprolactone): effect of microstructure on blend properties, Polymer 51 (2010) 1024–1032. https://doi.org/10.1016/j.polymer.2010.01.020.
[72] L.G. Li, Q.Y. Wang, Q.Y. Zheng, F.S. Du, Z.C. Li, Tough and thermally recyclable semiaromatic polyesters by ring-opening polymerization of benzo-thia-caprolactones, Macromolecules 54 (2021) 6745–6752. https://doi.org/10.1021/acs.macromol.1c00497.
[73] A.S. Narmon, L.M. Jenisch, L.M. Pitet, M. Dusselier, Ring-opening polymerization strategies for degradable polyesters, Biodegrad. Polym. Circ. Plast. Econ. (2022) 205–271. https://doi.org/10.1002/9783527827589.ch7.
[74] Z.A. Baki, H. Dib, T. Sahin, Overview: polycarbonates via ring-opening polymerization, differences between six- and five-membered cyclic carbonates: inspiration for green alternatives, Polymers 14 (2022). https://doi.org/10.3390/polym14102031.
[75] A. Duda, ROP of cyclic esters: mechanisms of ionic and coordination processes, Polym. Sci. A Compr. Ref. 10 Vol. Set, Elsevier (2012) 213–246. https://doi.org/10.1016/B978-0-444-53349-4.00104-7.
[76] A. Kowalski, A. Duda, S. Penczek, Mechanism of cyclic ester polymerization initiated with tin(ii) octoate. 2. macromolecules fitted with tin(II) alkoxide species observed directly in maldi-tof spectra, Macromolecules 33 (2000) 689–695. https://doi.org/10.1021/ma9906940.
[77] A. Kowalski, A. Duda, S. Penczek, Kinetics and mechanism of cyclic esters polymerization initiated with tin(II) octoate. 3. polymerization of l,l-dilactide, Macromolecules 33 (2000) 7359–7370. https://doi.org/10.1021/ma000125o.
[78] M.C. Tanzi, P. Verderio, M.G. Lampugnani, M. Resnati, E. Dejana, E. Sturani, Cytotoxicity of some catalysts commonly used in the synthesis of copolymers for biomedical use, J. Mater. Sci. Mater. Med. 5 (1994) 393–396. https://doi.org/10.1007/BF00058971.
[79] K.A. Winship, Toxicity of tin and its compounds, Advers. Drug React. Acute Poisoning Rev. 7 (1988) 19–38.
[80] C. Ulker, N. Gokalp, Y. Guvenilir, Enzymatic synthesis and characterization of polycaprolactone by using immobilized lipase onto a surface-modified renewable carrier, Polish J. Chem. Technol. 18 (2016) 134–140. https://doi.org/10.1515/pjct-2016-0060.
[81] J. Pleiss, M. Fischer, R.D. Schmid, Anatomy of lipase binding sites: The scissile fatty acid binding site, Chem. Phys. Lipids (1998) 67–80. https://doi.org/10.1016/S0009-3084(98)00030-9.
[82] H. Uyama, S. Kobayashi, Enzymatic ring-opening polymerization of lactones catalyzed by lipase, Chem. Lett. 22 (1993) 1149–1150. https://doi.org/10.1246/cl.1993.1149.
[83] A. Kumar, R.A. Gross, Candida antartica lipase b catalyzed polycaprolactone synthesis: effects of organic media and temperature, Biomacromolecules 1 (2000) 133–138. https://doi.org/10.1021/bm990510p.
[84] S.W. Duchiron, E. Pollet, S. Givry, L. Avérous, Enzymatic synthesis of poly(ε-caprolactone-co-ε-thiocaprolactone), Eur. Polym. J. 87 (2017) 147–158. https://doi.org/10.1016/j.eurpolymj.2016.12.024.
[85] F.C. Loeker, C.J. Duxbury, R. Kumar, W. Gao, R.A. Gross, S.M. Howdle, Enzyme-catalyzed ring-opening polymerization of ε-caprolactone in supercritical carbon dioxide, Macromolecules 37 (2004) 2450–2453. https://doi.org/10.1021/ma0349884.
[86] P.R. Figueiredo, B.C. Almeida, D.F.A.R. Dourado, A.F. Sousa, A.J.D. Silvestre, A.T.P. Carvalho, Enzymatic synthesis of poly(caprolactone): a qm/mm study, ChemCatChem. 12 (2020) 4845–4852. https://doi.org/10.1002/cctc.202000780.
[87] A. Basterretxea, E. Gabirondo, C. Jehanno, H. Zhu, O. Coulembier, D. Mecerreyes, H. Sardon, Stereoretention in the bulk rop of l -lactide guided by a thermally stable organocatalyst, Macromolecules 54 (2021) 6214–6225. https://doi.org/10.1021/acs.macromol.1c01060.
[88] G. Gontard, A. Amgoune, D. Bourissou, Ring-opening polymerization of ε-caprolactone catalyzed by ionic hydrogen bond activation with bis-pyridiniums, J. Polym. Sci. Part A Polym. Chem. 54 (2016) 3253–3256. https://doi.org/10.1002/pola.28238.
[89] K. V. Fastnacht, S.S. Spink, N.U. Dharmaratne, J.U. Pothupitiya, P.P. Datta, E.T. Kiesewetter, M.K. Kiesewetter, Bis- and tris-urea h-bond donors for ring-opening polymerization: unprecedented activity and control from an organocatalyst, ACS Macro Lett. 5 (2016) 982–986. https://doi.org/10.1021/acsmacrolett.6b00527.
[90] L. Zhou, Z. Wang, G. Xu, C. Lv, Q. Wang, Structure and activity relationship studies of N-heterocyclic olefin and thiourea/urea catalytic systems: application in ring-opening polymerization of lactones, Polym. Chem. 12 (2021) 1806–1815. https://doi.org/10.1039/d0py01747g.
[91] X. Li, Q. Zhang, Z. Li, X. Wang, J. Liu, S. Cui, S. Xu, C. Zhao, C. Chen, K. Guo, Thiourea binding with carboxylic acid promoted cationic ring-opening polymerization, Polymer 84 (2016) 293–303.

https://doi.org/10.1016/j.polymer.2015.12.057.
[92] M.J. Leite, T. Agner, F. Machado, B.A.D. Neto, P.H.H. Araujo, C. Sayer, E-caprolactone ring-opening polymerization catalyzed by imidazolium-based ionic liquid under mild reaction conditions, J. Polym. Res. 29 (2022). https://doi.org/10.1007/s10965-022-02891-0.
[93] O. Coulembier, P. Degée, J.L. Hedrick, P. Dubois, From controlled ring-opening polymerization to biodegradable aliphatic polyester: especially poly(β-malic acid) derivatives, Prog. Polym. Sci. 31 (2006) 723–747. https://doi.org/10.1016/j.progpolymsci.2006.08.004.
[94] A. Dzienia, P. Maksym, B. Hachuła, M. Tarnacka, T. Biela, S. Golba, A. Zięba, M. Chorążewski, K. Kaminski, M. Paluch, Studying the catalytic activity of dbu and tbd upon water-initiated rop of ϵ-caprolactone under different thermodynamic conditions, Polym. Chem. 10 (2019) 6047–6061. https://doi.org/10.1039/c9py01134j.
[95] Y. Chen, J. Zhang, W. Xiao, A. Chen, Z. Dong, J. Xu, W. Xu, C. Lei, Reinvestigation of the ring-opening polymerization of ε-caprolactone with 1,8-diazacyclo[5.4.0]undec-7-ene organocatalyst in bulk, Eur. Polym. J. 161 (2021) 110861. https://doi.org/10.1016/j.eurpolymj.2021.110861.
[96] X. Zhang, P. Sun, Y. Jiang, S. Liao, Organocatalytic ring-opening polymerization of ϵ-caprolactone with phosphoramidimidates (padis) as a bifunctional brønsted acid catalyst, Chem. - An Asian J. 18 (2023). https://doi.org/10.1002/asia.202201127.
[97] Y. Li, S. Xu, J. Ling, K. Pan, Y. Liu, Y. Chen, Diphenyl phosphate/ethyl diphenylphosphinite as an efficient organocatalytic system for ring-opening polymerization of ϵ-caprolactone and δ-valerolactone, Polym. Chem. 13 (2022) 545–557. https://doi.org/10.1039/d1py01289d.
[98] W. Wu, W. Wang, J. Li, Star polymers: advances in biomedical applications, Prog. Polym. Sci. 46 (2015) 55–85. https://doi.org/10.1016/j.progpolymsci.2015.02.002.
[99] J.M. Ren, T.G. McKenzie, Q. Fu, E.H.H. Wong, J. Xu, Z. An, S. Shanmugam, T.P. Davis, C. Boyer, G.G. Qiao, Star Polymers, Chem. Rev. 116 (2016) 6743–6836. https://doi.org/10.1021/acs.chemrev.6b00008.
[100] Y. He, J. Chen, I. Rafique, Z. Lu, Star-shaped polycaprolactone bearing mussel-inspired catechol end-groups as a promising bio-adhesive, Eur. Polym. J. 139 (2020). https://doi.org/10.1016/j.eurpolymj.2020.110025.
[101] A. Shagan, W. Zhang, M. Mehta, S. Levi, D.S. Kohane, B. Mizrahi, Hot glue gun releasing biocompatible tissue adhesive, Adv. Funct. Mater. 30 (2020). https://doi.org/10.1002/adfm.201900998.
[102] X. Gao, B.L. Wang, X.W. Wei, W. Rao, F. Ai, F. Zhao, K. Men, B. Yang, X. Liu, M. Huang, M. Gou, Z.Y. Qian, N. Huang, Y. Wei, Preparation, characterization and application of star-shaped pcl/peg micelles for the delivery of doxorubicin in the treatment of colon cancer, Int. J. Nanomedicine 8 (2013) 971–982. https://doi.org/10.2147/IJN.S39532.
[103] N. Ekapakul, C. Sinthuvanich, H. Ajiro, C. Choochottiros, Bioactivity of star-shaped polycaprolactone/chitosan composite hydrogels for biomaterials, Int. J. Biol. Macromol. 212 (2022) 420–431. https://doi.org/10.1016/j.ijbiomac.2022.05.139.
[104] J. Jeong, S. Yoon, X. Yang, Y.J. Kim, Super-tough and biodegradable poly(lactide-co-glycolide) (plga) transparent thin films toughened by star-shaped pcl-b-pdla plasticizers, Polymers 15 (2023). https://doi.org/10.3390/polym15122617.
[105] K.Y. Mya, H.B. Gose, T. Pretsch, M. Bothe, C. He, Star-shaped poss-polycaprolactone polyurethanes and their shape memory performance, J. Mater. Chem. 21 (2011) 4827–4836. https://doi.org/10.1039/c0jm04459h.

Chapter 2: On the development of an effective method to produce conductive PCL films

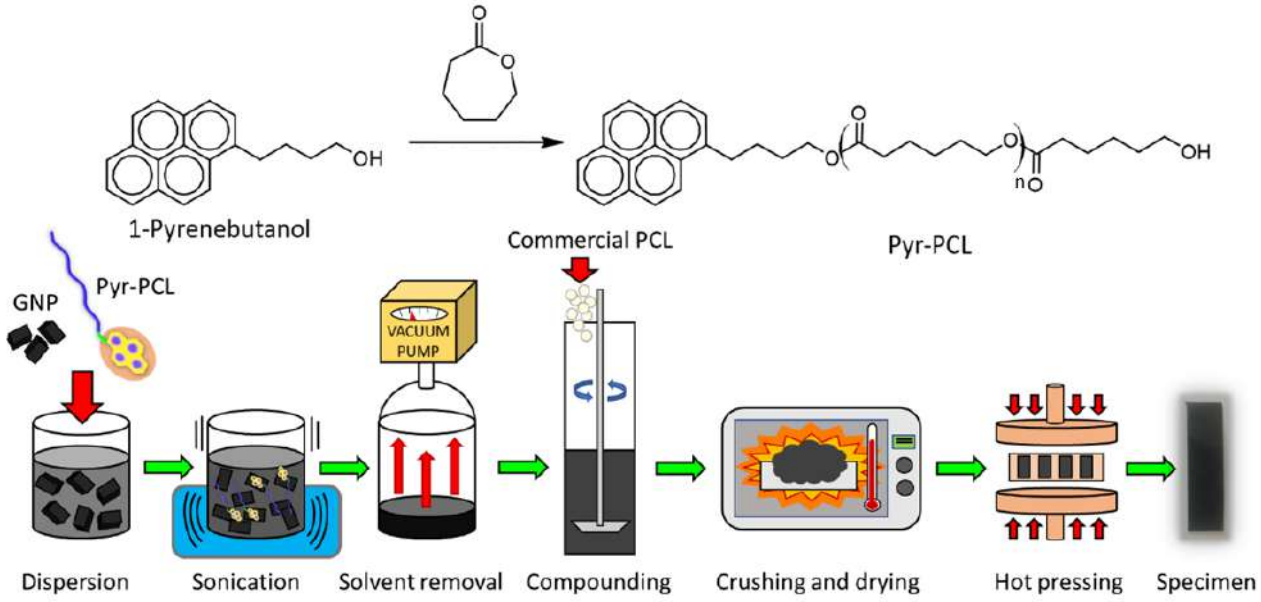

nanomaterials

MDPI

Article

On the Development of an Effective Method to Produce Conductive PCL Film

Giacomo Damonte [1], Alberto Vallin [1], Alberto Fina [2] and Orietta Monticelli [1,*]

[1] Dipartimento di Chimica e Chimica Industriale, Università degli studi di Genova, Via Dodecaneso 31, 16146 Genoa, Italy; giacomo.damonte@edu.unige.it (G.D.); berto.vallin@gmail.com (A.V.)
[2] Dipartimento di Scienza Applicata e Tecnologia, Politecnico di Torino-sede di Alessandria, Viale Teresa Michel, 5, 15121 Alessandria, Italy; alberto.fina@polito.it
* Correspondence: orietta.monticelli@unige.it

Abstract: The aim of this work was to develop an effective approach to improve the graphite dispersion and, consequently, the electrical conductivity of nanocomposites based on polycaprolactone (PCL) and graphite nanoplates (GNP). With this aim, a polymeric additive was designed to be compatible with the polymer matrix and capable of interacting with the graphite layers. Indeed, the compound consists of a low molecular mass PCL ending with a pyrene group (Pyr-PCL). The exploitation of such a molecule is expected to promote from one side specific interactions of the pyrene terminal group with the surface of graphite layers and from the other to guarantee the compatibility with PCL, having a chain with the same nature as the matrix. The features of the nanocomposites prepared by directly blending PCL with GNP were compared with those of the same systems also containing the additive. Moreover, a neat mixture, based on PCL and PCL-Pyr, was prepared and characterized. The specific interactions between the ad hoc synthesized compound and graphite were verified by UV measurements, while SEM characterization demonstrated a finer dispersion of GNP in the samples containing Pyr-PCL. GNP nucleating effect, proved by the increase in the crystallization temperature, was observed in all the samples containing the nanofiller. Moreover, a significant improvement of the electrical conductivity was found in the systems based on the pyrenyl terminated PCL. This peculiar and interesting phenomenon was related to the optimized nanofiller dispersion and to the ameliorated compatibility with the polymer matrix.

Keywords: PCL; nanocomposites; graphite nanoplates; compatibilization; melt blending; electrical conductivity

Citation: Damonte, G.; Vallin, A.; Fina, A.; Monticelli, O. On the Development of an Effective Method to Produce Conductive PCL Film. *Nanomaterials* **2021**, *11*, 1385. https://doi.org/10.3390/nano11061385

Academic Editor: Lavinia Balan

Received: 5 April 2021
Accepted: 22 May 2021
Published: 24 May 2021

1. Introduction

The combination of graphene and graphene-related materials (GRM) [1] with biopolymers represents an appealing and effective approach to enlarge the exploitation of such systems, which represent a valid alternative to polymers from fossil sources [2–4]. Indeed, on one hand, the addition of the above nanoparticles could potentially improve the features of the polymer matrix and disclose novel properties and on the other, the low environmental impact of both the components make the resulting composite/nanocomposites "green". Clearly, in the development of these materials it is necessary to consider the exploitation of preparation methods capable of facilitating the nanoparticle dispersion, easily applicable and sustainable. With regard to the latter aspect, the combination of GRM with the biopolymers was generally carried out by using solution-mixing approaches [2] or via melt blending [2,3], which is highly recommended for industrial viability. The layered carbon filler dispersion, such as graphite nanoplates (GNP), which is the object of the present work may be challenging and depends on the affinity towards the polymer matrix. Partial oxidation of graphite using strong acids and oxidating agents was widely used to prepare graphite oxide or graphene oxide (GO) [5,6], which may enhance the affinity towards polar polymers. In the case of the investigated biopolymer, namely poly(ε-caprolactone) (PCL),

it was mainly combined with GO by applying the solution blending [7] or the in-situ polymerization method [8,9]. Thanks to the filler functionalities, by using the latter approach, a direct grafting of the macromolecular chains onto the surface of GO was achieved, allowing a strong interfacial interaction between GO and the PCL matrix. Moreover, studies on the crystallization of PCL/GO nanocomposites, prepared by using the in-situ polymerization method, showed that the crystallization temperature of the polymer was significantly enhanced with respect to the neat polymer, without affecting the crystalline structure [8]. As demonstrated by Wang et al. [9], the direct PCL grafting improved not only graphene dispersion in the polymer matrix, but also the mechanical properties of the resultant composites. Electrospinning is another approach exploited to combine GO with PCL: in a pioneering work, describing the preparation of PCL/GO nanocomposites by applying the above method, a significant increase in the mechanical strength by the incorporation of GO was found, which phenomenon was directly related to the changes in the fiber morphology [10]. Furthermore, the composite nanofiber mats turned out to be suitable scaffolds, showing high bioactivity [11,12]. Despite the potentialities of such materials, it is worth underlining that in order to restore high electrical and thermal conductivity, reduction of GO has to be accomplished, which requires the use of strong chemical reducing agents and/or extremely high temperature [13]. As such, thermally reduced graphene oxide (TRGO) was incorporated in a PCL matrix via the conventional solution casting method [7]. The developed nanocomposites were characterized by a fine dispersion of TRGO throughout the PCL matrix, which lead to a significant improvement in the storage modulus. The combination of GRM with PCL was also used in the development of blends with polylactic acid (PLA) [14–17]. Indeed, nanoparticles were found to be capable of decreasing the surface tension between the two polymers, thus acting as a compatibilizer. In particular, using GNP, the electron microscopy measurements indicated a predominant localization of nanoplates in the PCL phase [14]. It is worth underlining that GRM dispersion represents a key issue for the above systems, as it is necessary to reach a fine distribution to transfer the properties of the nanofiller to the polymer matrix. In this respect, while the oxidation of graphite and possible subsequent organic functionalization may allow better interaction with the polymer matrix, enabling easier nanofiller dispersion, the chemical modification of GRM introduces disruptions of the sp^2 structure, thus affecting their physical properties, particularly in terms of electrical and thermal conductivity. An alternative approach to guarantee strong interactions between non functionalized GRM is the modification of the chemical structure of the macromolecules to promote non-covalent bonding with graphitic surfaces. As such, taking into account the specific interactions that occur between pyrene molecules and the surface of the graphite lamellae [18,19], polymers bearing these functionalities were developed and used for the preparation of composite systems [20–22]. In particular, considering biopolymers, in a recent work of ours we reported on the development of nanocomposites based on poly(L-lactide) (PLLA) by synthesizing initiators, constituted by a pyrene end group and a poly(D-lactide) (PDLA) chain, capable of interacting with the surface of GNP layers as well as forming stereoblocks during the ring opening polymerization of L-lactide [22]. Clearly, the application of the pyrene-based functionalization to other biopolymers by using environmentally friendly routes with sustainable and scalable processing to obtain graphite nanocomposites is of great interest. Within this scenario, this work represents the first report on PCL-based pyrene (Pyr-PCL) systems to be used as additives in the preparation of PCL/GNP nanocomposites. In order to maintain the sustainability of the whole process, the synthesis of Pyr-PCL was carried out without using solvents and the blends were prepared via a simple and industrially viable melt blending procedure. The developed materials were characterized by using DSC, TGA, FE-SEM and electrical conductivity measurements.

2. Materials and Methods

2.1. Materials

From Sigma Aldrich® (Milan, Italy), ε-caprolactone (purity ≥ 97%), dimethylformamide (DMF) (purity ≥ 99%), 1-pyrenebutanol (purity ≥ 99%), 1-dodecanol (purity ≥ 99%), tin octanoate ($Sn(Oct)_2$) (purity ≥ 96%), toluene (anhydrous, purity 99.7%), dichloromethane (stabilized with 0.002% 2-methyl-2-butene), and methanol (99.9%) were purchased. GNP was provided by Avanzare Innovación Tecnólogica (Navarrete (La Rioja), Spain), prepared according to a previously reported procedure [23]. Commercial PCL CAPA® 6500 (M_w = 50,000 g/mol) was purchased from Perstorp (Malmö, Sweden). The ε-caprolactone was purified prior to use by vacuum distillation over CaH_2. All the other reagents were of analytical grade and used without purification.

2.2. Synthesis of Pyr-PCL and Dod-PCL

The synthesis of 1-pyrenyl terminated PCL (referred to as Pyr-PCL) was carried out using the ring opening polymerization (ROP) reaction in bulk, a method widely reported in the literature for the preparation of polycaprolactone [24–26]. Briefly, 3.650 g (31.978 mmol) of ε-caprolactone was placed in a 50 mL round bottom flask equipped with a magnetic stirrer under argon atmosphere, then 0.500 g (1.822 mmol) of 1-pyrenebutanol was added and the system was slowly heated to 80 °C and stirred until complete dissolution of the initiator. The polymerization reaction was started by increasing the temperature to 120 °C followed by the addition of the catalyst, namely 26 µL of a freshly prepared 100 mg/mL solution (6.417 µmol) of tin octanoate ($Sn(Oct)_2$) in anhydrous toluene (ratio [ε-CL]/[$Sn(Oct)_2$] = 5000). The reaction mixture was maintained at 120 °C for 24 h under stirring. After cooling, the warm crude product was dissolved in 2 mL of CH_2Cl_2 and precipitated by adding the viscous solution obtained dropwise into 200 mL of cold methanol under slow stirring. After precipitation, the product was filtered on a Buchner funnel, washed with small amounts of ice cold methanol and then dried at 40 °C under vacuum for 72 h. 1-dodecyl terminated PCL (referred to as Dod-PCL) was synthesized by adjusting the initiator amount, namely 1-dodecanol, to obtain a polymer characterized by the same molecular mass as that of Pyr-PCL. The synthesis of Dod-PCL, with a theoretical M_n of 2000 g/mol, was performed using the same method applied for the preparation of the pyrenyl terminated PCL. In this case, the ROP was performed using 3.260 g (28.561 mmol) of ε-caprolactone and 0.304 g (1.631 mmol) of 1-Dodecanol. The polymerization reaction was started by adding 23 µL of tin octanoate solution.

2.3. Preparation PCL/GNP Nanocomposites

Neat mixture (referred to as PCL/Pyr-PCL) was prepared by mixing a commercial PCL (referred to as PCL) with the ad hoc synthesized 1-pyrenyl terminated PCL, using a ratio PCL/Pyr-PCL of 80/20. Before blending at 120 °C for 30 min, the polymers were dried overnight at 40 °C under vacuum. The mixture was prepared by using a laboratory internal mixer equipped with a mechanical stirrer, type RZR1 (Heidolph Instruments GmbH & Co, Schwabach, Germany), which was connected to a vacuum line and evacuated for 30 min at room temperature, followed by purging with Argon for 30 min (the above operations were repeated at least three times, to be sure to avoid humidity coming in contact with the reagents). The reactor was heated at 120 °C and stirred for 5 min at 160 rpm under inert atmosphere. GNP at two different concentrations (1 and 2 wt.-%) was added to the 80/20 blends to prepare composite systems, which were assigned names indicating the quantity of the mixed graphite (as an example PCL/Pyr-PCL/G1 indicates a sample based on a ratio PCL/Pyr-PCL 80/20 and a percentage of GNP of 1 wt.-%). Before mixing the nanofiller with the polymer matrix, it was pre-dispersed into a round bottom flask with toluene using a sonicating bath at 40 kHz for 60 min. Successively the solvent was removed, using a rotavapor, and the sonicated material was collected. The same conditions were applied for the composites, which were prepared by mixing the polymers and graphite. The neat mixture and the composites were dried under vacuum at 40 °C for 72 h. In order to

evidence the effect of the pyrenyl-based additive on the composite characteristics, samples were prepared by adding the graphite directly to the neat commercial PCL, by using the same equipment and conditions previously described.

2.4. Polymers Characterization

^{1}H-NMR measurements were recorded on a Varian "Mercury 300"(Palo_Alto, CA, USA)operating at a frequency of 300 MHz. All the samples were dissolved in $CDCl_3$ in 10 mm NMR tubes at room temperature. The sample concentration used was 30 mg/mL. The thermal properties were measured using a Mettler Toledo "DSC1 STARe System" (Milan, Italy) differential scanning calorimeter (DSC) in the temperature range from −100 to 150 °C under a nitrogen flow of 20 mL/min and employing 40 µL aluminum crucibles with pin. The heating and cooling rates were +10 (heating) and −10 (cooling) °C/min. The thermogravimetric analysis (TGA) was performed using a Mettler Toledo "DSC1 STARe System" in the temperature range from 30 to 800 °C, at a heating rate of 10 °C/min under a nitrogen atmosphere. The FT–IR spectra were acquired with a Bruker "Vertex 70" operating in ATR mode with a diamond crystal, from 400 to 4000 cm^{-1}. UV–Vis measurement were performed using a Shimadzu "UV-1800" (Milan, Italy) spectrometer equipped with short path quartz cells (0.2 cm, slit: 1 nm, scan speed: very slow). In particular, in order to evaluate the interaction between Pyr-terminated PCL and graphite, 0.1 mg of Pyr-PCL was dissolved into a test tube with 2 mL of DMF, then different amounts of GNP (0, 0.5, 1, 2, and 5 mg) were added. The five samples were sonicated using a sonicating bath (40 kHz, maximum power) for one hour. After sonication, the dispersed samples were left to sedimentate at room temperature for one week. The solution surnatant was collected and analyzed spectroscopically from 270 to 1100 nm to show the content of pyrenic units.

Surface conductivity tests were performed at room temperature by applying a picoammeter (Keithley Instruments, Solon, OH, USA) and by using films of 12 × 10 mm (with a thickness of ca. 0.2 mm). Two rectangles of conductive tape (10 × 1 mm, 3M electrically conductive "ECATT" adhesive tape 9707), spaced 10 mm apart, were deposited on the films surface in order to form the electrical contact. For the measurements, a ddp. of 150 V cc. was applied.

3. Results and Discussion

3.1. Synthesis and Characterization of Pyr-PCL

3.1.1. H-NMR Analysis

This work has been primarily focused on the fine-tuning of the synthesis of a pyrenyl terminated PCL (Pyr-PCL), prepared by applying the ROP of ε-caprolactone and by using 1-pyrenebutanol as initiator. In order to evidence the influence of the pyrenyl group on the specific features of the above polymer, a dodecyl terminated PCL (Dod-PCL) was also synthesized, adjusting the initiator/monomer ratio to obtain two polymers characterized by the same molar mass, namely 2000 g/mol, but different end groups. It is worth underlining that Dod-PCL was not applied in the nanocomposite preparation. In order to calculate the molar mass (M_{nNMR}), as well as to confirm the synthesized polymer structures, ^{1}H-NMR measurements were performed. Figure 1 shows the ^{1}H-NMR spectrum of Pyr-PCL. Indeed, M_{nNMR} was calculated using the ratio between the intensities of the triplet peaks around 2.29 ppm and (E) 3.63 ppm. The value found for both the polymers was ca. 2000 g/mol, which is in accordance with the theoretical number for the average molecular weight, thus demonstrating the fine control of the polymerization reaction. It was also possible to recognize the other signals correlated to the methylenic couples of protons in PCL repetition units at 4.05 (t), 1.64 (m), 1.38 (m). The Pyr-PCL sample also displayed a distinct pattern around 8 ppm (Pyr) given by the aromatic pyrene protons, along with the presence of four butylic chain signals (A) 4.14 (t), (D) 3.37 (t), (B) 1.92 (quint), and (C) 1.80 (quint) ppm. The chemical shift value of the signal A confirmed that all the initiators reacted to form covalent links with PCL chains.

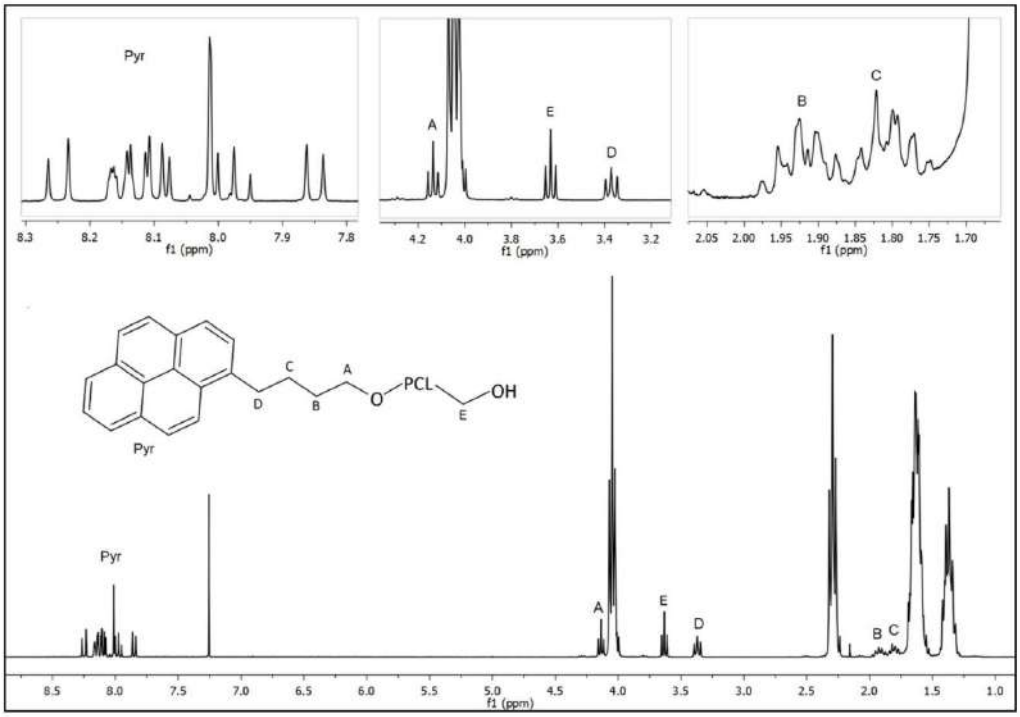

Figure 1. ^{1}H-NMR spectra of Pyr-PCL in $CDCl_3$.

3.1.2. FT-IR Analysis

In order to further corroborate the chemical structure of the two polymers, FTIR measurements were performed. The comparison of the Pyr-PCL and Dod-PCL spectra is reported in Figure 2. For both samples, it is possible to recognize the signals typical of PCL chains [27] at 3400 cm^{-1} (O–H hydroxyl moiety stretching); 2950 cm^{-1} and 2870 cm^{-1} (symmetrical/unsymmetrical stretching Csp^3-H bonds in methylenic unit); 1728 cm^{-1} (carbonyl stretching); 1296 cm^{-1} (C–O and C–C stretching); and at 1241 cm^{-1} and 1170 cm^{-1} (unsimmetrical/simmetrical C–O–C stretching). In the pyrenyl terminated sample novel bands appear at 3047 cm^{-1} (Csp^2-H stretching); 1600 cm^{-1} (breathing of the pyrenic unit); 845 cm^{-1}, 820 cm^{-1}, 684 cm^{-1}, and 622 cm^{-1} related to the complex vibrational motions of pyrene.

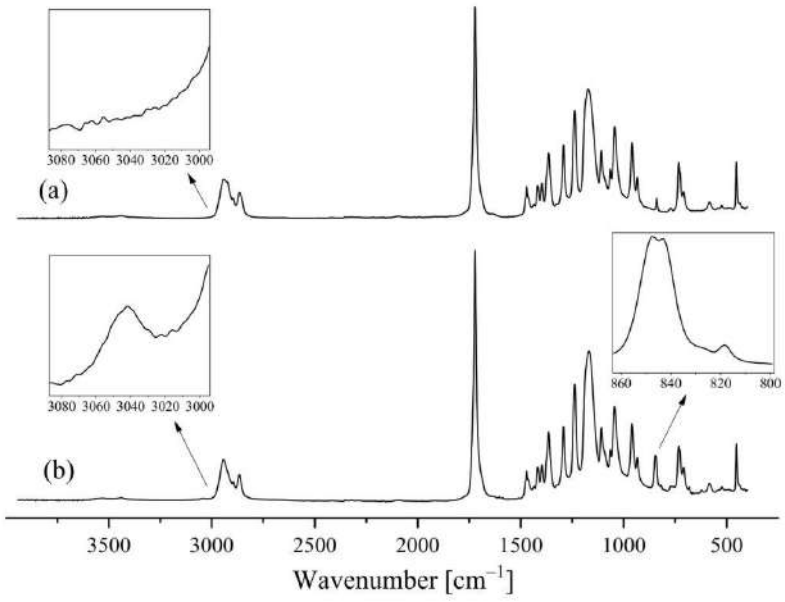

Figure 2. FT-IR spectra of Dod-PCL (**a**) and Pyr-PCL (**b**).

3.1.3. DSC Measurements

In order to evidence the effect of the functionalization and molecular mass on the polymer thermal properties, Dod-PCL, Pyr-PCL and a commercial PCL were analyzed by means of DSC. Figure 3 shows the cooling and heating traces for the above three samples, while the thermal data are summarized in Table 1. Differences in the thermal behavior can be noticed by comparing the DSC traces of two polymers which hold similar molecular mass, but different end groups. Indeed, while the melting temperature (T_m) is similar for both Dod-PCL and Pyr-PCL, ca. 50 °C (Figure 3a), Pyr-PCL holds a double melting peak. This phenomenon is related to the crystal lamellae thickness distribution produced during crystallization [28,29], which is possibly affected by the presence of bulky pyrene moieties as chain ends on relatively short PCL chains. It is worth noting that the commercial PCL has a higher melting temperature (ca. 56 °C), reflecting its high molar mass [30]. Furthermore, Pyr-PCL shows a significantly lower crystallization temperature (T_c) and crystallinity (χ_c) with compared with Dod-PCL. This result can be related to the steric hindrance of the pyrenyl group, which may affect the polymer structuring. The specific effect of the initiator on the crystallization behavior of PCL has also been reported in the literature for other kind of systems [30,31]. In the case of the commercial PCL, the lower crystallinity and T_c can be ascribed to the higher molecular mass with respect to both Pyr-PCL and Dod-PCL.

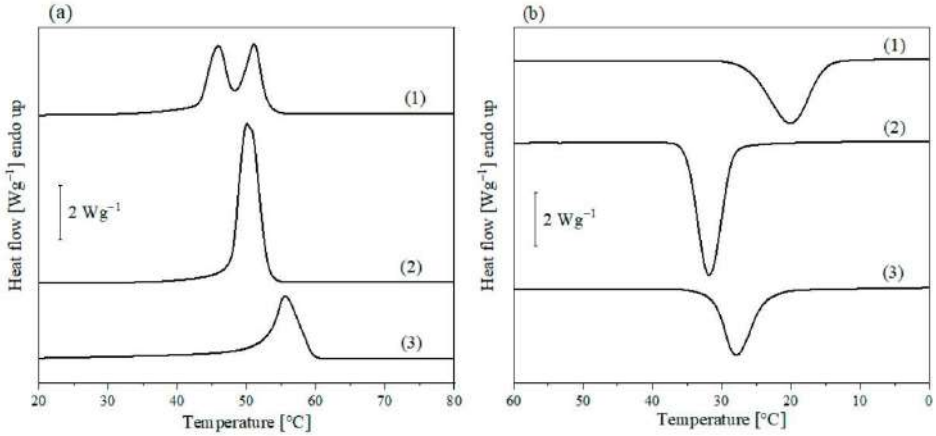

Figure 3. DSC thermograms of linear PCL, second heating (**a**) and cooling (**b**): (1) Pyr-PCL, (2) Dod-PCL, (3) PCL.

Table 1. DSC, TGA and surface conductivity measurement results.

Sample	ΔH_c [J/g]	T_c [°C]	ΔH_m [J/g]	T_m [°C]	χ_c [%]	$T_{onset\ 5\%}$ [°C]	T_{Vmax1} [°C]	T_{Vmax2} [°C]	σ [S·m^{-1}]
Pyr-PCL	−79	20	83	51	60	298	367	-	-
Dod-PCL	−99	32	102	50	73	301	352	425	-
PCL	−63	28	72	56	51	394	-	426	$<10^{-11}$
PCL/G1	−64	36	78	57	56	396	-	426	$1.7 \cdot 10^{-10}$
PCL/G2	−59	37	69	57	51	395	-	426	$8.3 \cdot 10^{-11}$
PCL/Pyr-PCL	−74	28	82	56	59	378	-	427	$<10^{-11}$
PCL/Pyr-PCL/G1	−70	36	78	56	57	375	-	427	$4.0 \cdot 10^{-8}$
PCL/Pyr-PCL/G2	−79	38	87	56	64	376	-	429	$5.0 \cdot 10^{-2}$

ΔH_c = crystallization enthalpy, T_c = crystallization temperature, ΔH_m = melting enthalpy, T_m = melting temperature, χ_c = crystallinity percentage, $T_{onset\ 5\%}$ = temperature of 5% mass loss, T_{Vmax1} = temperature of the maximum degradation rate (first step), T_{Vmax2} = temperature of the maximum degradation rate (second step), σ = specific conductance.

3.1.4. TGA Measurements

The TGA curves of Pyr-PCL, Dod-PCL and PCL are reported in Figure 4. While Dod-PCL shows two degradation steps, the TGA profiles of Pyr-PCL and PCL are characterized by only one decomposition step. In order to elucidate this finding, it is necessary to consider the specific degradation behavior of polycaprolactone. As reported in the literature [32–34], the decomposition of this polymer follows two concurring mechanisms, namely unzipping, which requires a nucleophilic terminal chain group such as hydroxyl functionalities, and β-elimination, which needs at least a hydrogen atom onto the β-carbon in the alcoholic side of the ester moiety. The commercial PCL decomposes in one weight loss step (400–450 °C), suggesting the effect of terminal OH groups is negligible, in accordance with its high molecular mass. On the other hand, in the case of the low molecular mass polymers, the high concentration of hydroxyl groups is likely to promote the unzipping mechanism, leading to an anticipation of the weight loss onset. However, while Pyr-PCL is completely volatilized before 400 °C is reached, Dod-PCL also displays a second weight loss step at higher temperature (ca. 425 °C), which may be related to the β-elimination, apparently hindered for Pyr-PCL because of the pyrenyl end group.

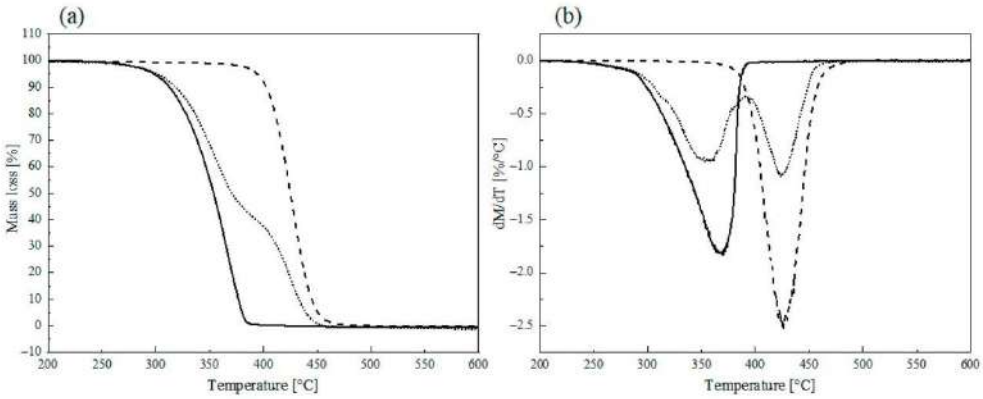

Figure 4. TGA (**a**) and DTG thermogram (**b**): Pyr-PCL (continuous line), Dod-PCL (dotted), PCL (dashed).

3.2. Study of the Graphite Dispersion

The capacity of the pyrenyl terminated polymer to disperse and stabilize GNP in a liquid medium was primarily evaluated by comparing two dispersions in DMF, one containing only GNP and the other GNP and Pyr-PCL. Figure 5 shows the photos of the two dispersions after a sonication and centrifugation treatment. Indeed, the neat DMF was not capable of stabilizing the GNP as evidenced by the transparency of the liquid. Moreover, in the mild sonication conditions used, GNP is not expected to exfoliate in DMF and leads to a poorly stable suspension which fully precipitates after several hours.

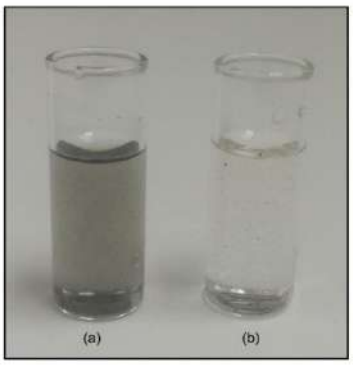

Figure 5. Pyr-PCL DMF solution + GNP (**a**), neat DMF + GNP (**b**); both after bath sonication for 1 h and 24 h of sedimentation. Quantity used: 3 mL of DMF, 50 mg of polymer and 5 mg of graphite.

Conversely, the suspension containing Pyr-PCL, appears slightly grey even after 24 h, thus demonstrating that the polymer promoted stabilization of the GNP suspension. A more detailed analysis of the specific interactions between graphite and the pyrenyl terminated polymer was obtained by UV measurements. Figure 6 shows the UV spectra of the surnatants, which were prepared by adding Pyr-PCL and different amounts of graphite to DMF. In the acquired spectra it is possible to observe, in the range 310–350 nm, strong adsorption bands characteristic of the pyrenic unit [35], whose intensity significantly decreased by increasing the graphite amount. This finding suggests the adsorption of Pyr-PCL onto the surface of graphite flakes, likely due to the pyrenic unit π-stacking interactions [36]. Another interesting piece of information comes from the shoulder of the band at 280 nm, which can be ascribed to the absorption produced by the dispersed graphite

flakes. This signal started to be noticeable in the sample containing 0.5 mg of graphite. This phenomenon demonstrated that Pyr-PCL promotes the dispersion of graphite when the ratio of Pyr-PCL/graphite reaches a critical value, which allows the adsorption of the molecule on the surface of the flakes as well as maintaining the GNP dispersed in DMF, thus avoiding its coalescence. The proven adsorbance of Pyr-PCL onto GNP suggests the possibility to exploit this as a compatibilizer in PCL nanocomposites [22].

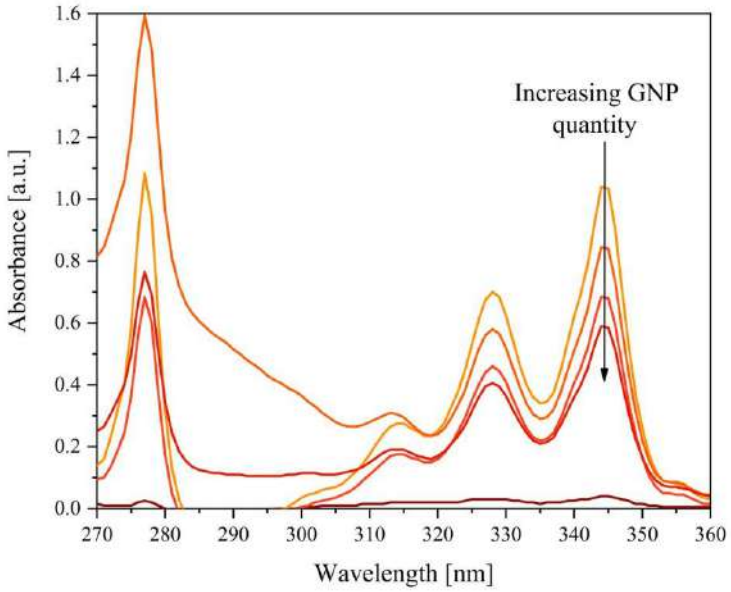

Figure 6. UV-Vis spectra of Pyr-PCL DMF solution surnatant with different amounts of GNP, after sonication and 7 days of sedimentation: neat, 0.5 mg, 1 mg, 2 mg, 5 mg from orange to brown.

3.3. Preparation and Characterization of PCL/GNP Nanocomposites

FE-SEM micrographs of the samples PCL/G1 and PCL/Pyr-PCL/G1 are given in Figure 7. The former composite, prepared by adding directly GNP to the PCL, was characterized by an inhomogeneous dispersion of the filler and by the presence of several voids, formed by the GNP removal during the fracture (see insert in the Figure 7a).

This phenomenon can be related to the poor adhesion between the polymer matrix and the filler. Conversely, a more homogeneous distribution of GNP was found in the Pyr-PCL-based sample, whose micrograph evidenced the strong adhesion of the GNP with PCL (see insert in the Figure 7b). This result clearly demonstrates that the previously mentioned interactions, occurring between the pyrenyl terminated polymer and graphite, also promote the filler dispersion in the molten system as well as the adhesion of the PCL to the GNP. It is worth underlining that very similar morphologies were also found for the composites based on 2 wt.-% of GNP. In Table 1, thermal data of the neat samples (Pyr-PCL, Dod-PCL and PCL) are compared with the system based on PCL and Pyr-PCL (PCL/Pyr-PCL) as well as with those containing GNP, prepared by directly adding the nanoplates to the PCL or to the blended PCL/Pyr-PCL. Neat PCL/Pyr-PCL exhibited the same crystallization temperature (T_c) as PCL but was characterized by a higher crystallinity (χ_c). This result can be related to the presence of the low molecular mass polymer, which might reduce the viscosity of the molten system, thus helping the polymer structuring. For all the composite samples, a significant increase in T_c and a slight enhancement of the crystallization with respect to PCL were observed. These phenomena, already reported in the literature [37], indicate that GNP acts as a nucleating agent for the PCL structuring. Concerning the

thermal decomposition of the prepared compounds, T_{onset} of the systems based on Pyr-PCL showed a slight decrease with respect to the neat PCL, which phenomenon might be accounted for by the presence of the low molecular mass polymer. Nevertheless, it is worth underlining that T_{max} was found to be constant for all the analyzed systems.

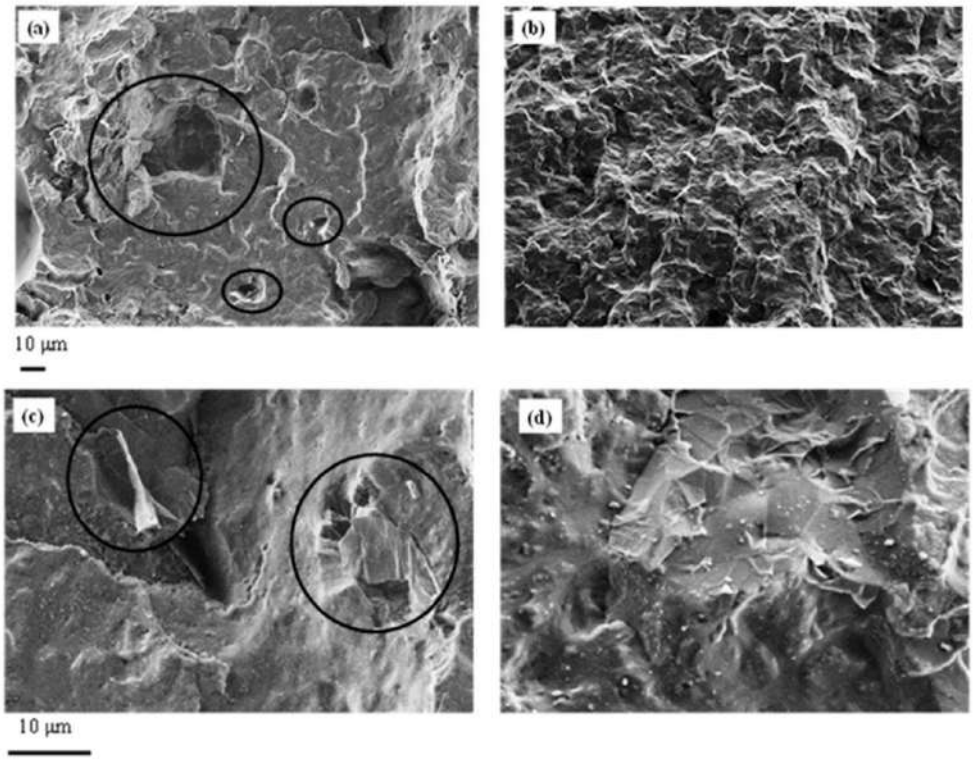

Figure 7. FE-SEM micrographs at different magnifications of: (**a**,**c**) PCL/G1 and (**b**,**d**) PCL/Pyr-PCL/G1.

The effect of GNP on the electrical properties of the prepared systems was evaluated by comparing the conductivity (σ) of the neat samples with those of the composites (Table 1). While the polymer matrices are electrically insulating with σ in the range of 10^{-11} S·m^{-1}, the addition of GNP to PCL led to an increase in the electrical conductivity. In the case of the samples prepared by directly adding GNP to PCL, σ turned out to be similar, the conductivity values only slightly decreasing by increasing the graphite content, passing from $1.7 \cdot 10^{-10}$ to $8.3 \cdot 10^{-11}$ in the samples containing 1 and 2 wt.-% of GNP, respectively.

On the other hand, samples based on Pyr-PCL showed a much higher σ, thus confirming better dispersion of GNP. For these nanocomposites, the conductivity was found to increase by increasing the amount of GNP, reaching a value of $5 \cdot 10^{-2}$ for the sample PCL/Pyr-PCL/G2. The different behavior found in the nanocomposites based on the neat PCL with respect to those containing the additive, can be explained by taking into account that Pyr-PCL renders GNP more compatible with the polymer matrix, allowing the addition of a greater quantity of the nanofiller before reaching its coalescence, a phenomenon which generally leads to a reduction in the material final properties.

While conductive systems based on PCL were generally prepared by using reduced graphene oxide (rGO) and by applying the solution mixing method [38,39], in this work, we demonstrated an alternative approach. Indeed, the exploitation of the ad-hoc synthesized additive on one hand avoids the use of oxidized forms of graphite, and on the other, allows

preparation via melt blending, which is more easily scalable and environmental friendly compared to solution processing. Moreover, the conductivity, which was 10^{-5} in the case of a system reported in the literature [38], based on PCL and containing comparable amounts of graphite, turned out to be lower than the values found in our composites based on Pyr-PCL (Figure 8). These relevant results corroborate the active role of the synthesized pyrenyl terminated polymer in the graphite dispersion and consequently in the formation of an effective percolative network.

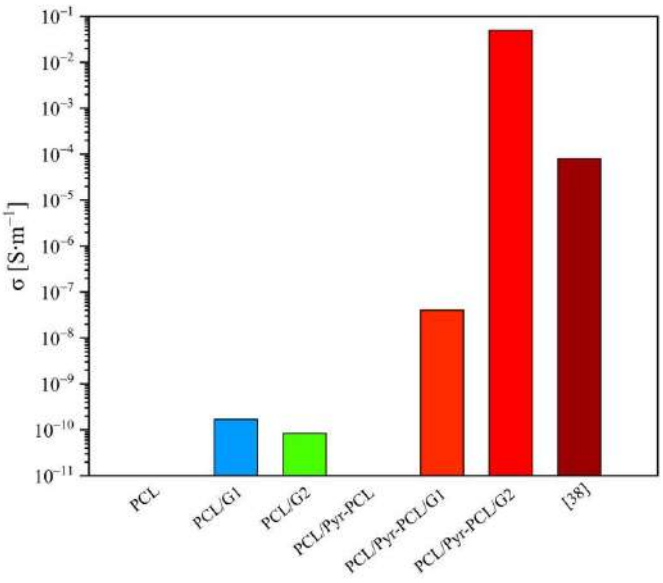

Figure 8. Surface conductivity of a commercial PCL, of our developed samples and of a PCL-based system reported in the literature.

4. Conclusions

A novel polymer additive, consisting of a low molecular mass polycaprolactone ending with a pyrene group (Pyr-PCL), to be applied in the preparation of composites based on a commercial PCL and graphite nanoplates, was developed. The structure of the polymer, synthesized by applying the ROP of ε-caprolactone and by using 1-pyrenebutanol as initiator, was confirmed by ^{1}H-NMR and FT-IR analysis. The comparison of the thermal behavior of Pyr-PCL with that of a dodecyl terminated PCL, characterized by the same molecular mass, evidenced that the pyrenyl group limits the polymer crystallization. The specific interactions, which occur between the pyrenyl terminated PCL and graphite flakes, as confirmed by UV measurements, turned out to affect the GNP dispersion in the nanocomposites. Indeed, with respect to the systems prepared by directly adding GNP to the molten polymer, the addition of Pyr-PCL allowed to obtain a finer dispersion and stronger adhesion of GNP to the polymer matrix. Pyr-PCL-compatibilized nanocomposites exhibited better electrical conductivity than that reported in the literature for other PCL/graphite systems. This was obtained by the use of poorly oxidized forms of graphite, by the design of Pyr-PCL as a compabilizer, and by exploiting an easily scalable melt blending process, opening up the possibility to use this biopolymer in novel and attractive applications.

Author Contributions: Investigation, G.D. and A.V.; Writing—original draft preparation, G.D., Conceptualization, A.F. and O.M.; Writing—review and editing, A.F. and O.M.; Supervision, O.M. All authors have read and agreed to the published version of the manuscript.

Funding: This research received no external funding.

Conflicts of Interest: The authors declare no conflict of interest.

References

1. Huang, X.; Yin, Z.; Wu, S.; Qi, X.; He, Q.; Zhang, Q.; Yan, Q.; Boey, F.; Zhang, H. Graphene-based materials: Synthesis, characterization, properties, and applications. *Small* **2011**, *7*, 1876–1902. [CrossRef] [PubMed]
2. Huang, X.; Qi, X.; Boey, F.; Zhang, H. Graphene-based composites. *Chem. Soc. Rev.* **2012**, *41*, 666–686. [CrossRef] [PubMed]
3. Gardella, L.; Colonna, S.; Fina, A.; Monticelli, O. A novel electrostimulated drug delivery system based on PLLA composites exploiting the multiple functions of graphite nanoplatelets. *ACS Appl. Mater. Interfaces* **2016**, *8*, 24909–24917. [CrossRef] [PubMed]
4. Rouf, T.B.; Kokini, J.L. Biodegradable biopolymer–graphene nanocomposites. *J. Mater. Sci.* **2016**, *51*, 9915–9945. [CrossRef]
5. Hummers, W.S.; Offeman, R.E. Preparation of graphitic oxide. *J. Am. Chem. Soc.* **1958**, *80*, 1339. [CrossRef]
6. Fathy, M.; Gomaa, A.; Taher, F.A.; El-Fass, M.M.; Kashyout, A.E.H.B. Optimizing the preparation parameters of GO and rGO for large-scale production. *J. Mater. Sci.* **2016**, *51*, 5664–5675. [CrossRef]
7. Zhang, J.; Qiu, Z. Morphology, crystallization behavior, and dynamic mechanical properties of biodegradable poly(ε-caprolactone)/thermally reduced graphene nanocomposites. *Ind. Eng. Chem. Res.* **2011**, *50*, 13885–13891. [CrossRef]
8. Wang, R.; Wang, X.; Chen, S.; Jiang, G. In Situ polymerization approach to poly(ε-caprolactone)-graphene oxide composites. *Des. Monomers Polym.* **2012**, *15*, 303–310. [CrossRef]
9. Wang, G.S.; Wei, Z.Y.; Sang, L.; Chen, G.Y.; Zhang, W.X.; Dong, X.F.; Qi, M. Morphology, crystallization and mechanical properties of poly(ε-caprolactone)/graphene oxide nanocomposites. *Chin. J. Polym. Sci.* **2013**, *31*, 1148–1160. [CrossRef]
10. Wan, C.; Chen, B. Poly(ε-caprolactone)/graphene oxide biocomposites: Mechanical properties and bioactivity. *Biomed. Mater.* **2011**, *6*, 1–8. [CrossRef]
11. Song, J.; Gao, H.; Zhu, G.; Cao, X.; Shi, X.; Wang, Y. The preparation and characterization of polycaprolactone/graphene oxide biocomposite nanofiber scaffolds and their application for directing cell behaviors. *Carbon* **2015**, *95*, 1039–1050. [CrossRef]
12. Bagheri, M.; Mahmoodzadeh, A. Polycaprolactone/graphene nanocomposites: Synthesis, characterization and mechanical properties of electrospun nanofibers. *J. Inorg. Organomet. Polym. Mater.* **2020**, *30*, 1566–1577. [CrossRef]
13. Pei, S.; Cheng, H.M. The reduction of graphene oxide. *Carbon* **2012**, *50*, 3210–3228. [CrossRef]
14. Kelnar, I.; Kratochvíl, J.; Kaprálková, L.; Zhigunov, A.; Nevoralová, M. Graphite nanoplatelets-modified PLA/PCL: Effect of blend ratio and nanofiller localization on structure and properties. *J. Mech. Behav. Biomed. Mater.* **2017**, *71*, 271–278. [CrossRef]
15. Kelnar, I.; Kratochvíl, J.; Fortelný, I.; Kaprálková, L.; Zhigunov, A.; Nevoralová, M. Effect of graphite nanoplatelets on melt drawing and properties of PCL/PLA microfibrillar composites. *Polym. Compos.* **2018**, *39*, 3147–3156. [CrossRef]
16. Luyt, A.S.; Kelnar, I. Effect of blend ratio and nanofiller localization on the thermal degradation of graphite nanoplatelets-modified PLA/PCL. *J. Therm. Anal. Calorim.* **2019**, *136*, 2373–2382. [CrossRef]
17. Forouharshad, M.; Gardella, L.; Furfaro, D.; Galimberti, M.; Monticelli, O. A low-environmental-impact approach for novel bio-composites based on PLLA/PCL blends and high surface area graphite. *Eur. Polym. J.* **2015**, *70*, 28–36. [CrossRef]
18. Zhang, Y.; Liu, C.; Shi, W.; Wang, Z.; Dai, L.; Zhang, X. Direct measurements of the interaction between pyrene and graphite in aqueous media by single molecule force spectroscopy: Understanding the π-π interactions. *Langmuir* **2007**, *23*, 7911–7915. [CrossRef]
19. Duan, D.; Ye, H.; Meng, N.; Xu, C.; Han, B.; Chen, Y.; Zhong, M.; Xu, L. Efficient exfoliation of graphite in chloroform with a pyrene-containing hyperbranched polyethylene as stabilizer to render pyrene-functionalized high-quality graphene. *Carbon* **2018**, *136*, 417–429. [CrossRef]
20. Luo, Z.; Ye, H.; Hu, J.; Hu, T.; Zhang, B.; Zhang, X.; Xu, L. Synthesis of a pyrene-functionalized hyperbranched polyethylene ternary copolymer for efficient graphite exfoliation in chloroform and formation of ethylene-vinyl acetate/graphene nanocomposites. *J. Appl. Polym. Sci.* **2020**, *137*, 1–15. [CrossRef]
21. Gkermpoura, S.S.; Papadimitriou, K.D.; Skountzos, E.N.; Polyzos, I.; Pastore Carbone, M.G.; Kotrotsos, A.; Mavrantzas, V.G.; Galiotis, C.; Tsitsilianis, C. 3-Arm star pyrene-functional PMMAs for efficient exfoliation of graphite in chloroform: Fabrication of graphene-reinforced fibrous veils. *Nanoscale* **2019**, *11*, 915–931. [CrossRef] [PubMed]
22. Fina, A.; Colonna, S.; Maddalena, L.; Tortello, M.; Monticelli, O. Facile and low environmental impact approach to prepare thermally conductive nanocomposites based on polylactide and graphite nanoplatelets. *ACS Sustain. Chem. Eng.* **2018**, *6*, 14340–14347. [CrossRef] [PubMed]
23. Colonna, S.; Bernal, M.M.; Gavoci, G.; Gomez, J.; Novara, C.; Saracco, G.; Fina, A. Effect of processing conditions on the thermal and electrical conductivity of poly (butylene terephthalate) nanocomposites prepared via ring-opening polymerization. *Mater. Des.* **2017**, *119*, 124–132. [CrossRef]
24. Labet, M.; Thielemans, W. Synthesis of polycaprolactone: A review. *Chem. Soc. Rev.* **2009**, *38*, 3484–3504. [CrossRef] [PubMed]
25. Duda, A. ROP of cyclic esters: Mechanisms of ionic and coordination processes. In *Polymer Science: A Comprehensive Reference*; Elsevier: Amsterdam, The Netherlands, 2012; Volume 4, pp. 213–246. ISBN 9780080878621.
26. Dzienia, A.; Maksym, P.; Hachuła, B.; Tarnacka, M.; Biela, T.; Golba, S.; Zięba, A.; Chorążewski, M.; Kaminski, K.; Paluch, M. Studying the catalytic activity of DBU and TBD upon water-initiated ROP of ε-caprolactone under different thermodynamic conditions. *Polym. Chem.* **2019**, *10*, 6047–6061. [CrossRef]

27. Azizi, M.; Azimzadeh, M.; Afzali, M.; Alafzadeh, M.; Mirhosseini, S.H. Characterization and optimization of using calendula officinalis extract in the fabrication of polycaprolactone/gelatin electrospun nanofibers for wound dressing applications. *J. Adv. Mater. Process.* **2018**, *6*, 34–46.
28. Kong, Y.; Hay, J.N. Multiple melting behaviour of poly(ethylene terephthalate). *Polymer* **2002**, *44*, 623–633. [CrossRef]
29. Yasuniwa, M.; Tsubakihara, S.; Sugimoto, Y.; Nakafuku, C. Thermal analysis of the double-melting behavior of poly(L-lactic acid). *J. Polym. Sci. Part B Polym. Phys.* **2004**, *42*, 25–32. [CrossRef]
30. Wang, J.L.; Dong, C.M. Physical properties, crystallization kinetics, and spherulitic growth of well-defined poly(ε{lunate}-caprolactone)s with different arms. *Polymer* **2006**, *47*, 3218–3228. [CrossRef]
31. Atanase, L.I.; Glaied, O.; Riess, G. Crystallization kinetics of PCL tagged with well-defined positional triazole de-fects generated by click chemistry. *Polymer* **2011**, *52*, 3074–3081. [CrossRef]
32. Persenaire, O.; Alexandre, M.; Degée, P.; Dubois, P. Mechanisms and kinetics of thermal degradation of poly(ε-caprolactone). *Biomacromolecules* **2001**, *2*, 288–294. [CrossRef]
33. Unger, M.; Vogel, C.; Siesler, H.W. Molecular weight dependence of the thermal degradation of poly(ε-caprolactone): A thermogravimetric differential thermal fourier transform infrared spectroscopy study. *Appl. Spectrosc.* **2010**, *64*, 805–809. [CrossRef]
34. Sivalingam, G.; Karthik, R.; Madras, G. Kinetics of thermal degradation of poly(ε-caprolactone). *J. Anal. Appl. Pyrolysis* **2003**, *70*, 631–647. [CrossRef]
35. Duhamel, J. Pyrene florescence to study polymeric systems. *Mol. Interfacial Phenom. Polym. Biopolym.* **2005**, 214–248. [CrossRef]
36. Zhang, J.; Xu, Y.; Cui, L.; Fu, A.; Yang, W.; Barrow, C.; Liu, J. Mechanical properties of graphene films enhanced by homo-telechelic functionalized polymer fillers via π-π stacking interactions. *Compos. Part A Appl. Sci. Manuf.* **2015**, *71*, 1–8. [CrossRef]
37. Lv, Q.; Wu, D.; Qiu, Y.; Chen, J.; Yao, X.; Ding, K.; Wei, N. Crystallization of poly(ε-caprolactone) composites with graphite nanoplatelets: Relations between nucleation and platelet thickness. *Thermochim. Acta* **2015**, *612*, 25–33. [CrossRef]
38. Correa, E.; Moncada, M.E.; Gutiérrez, O.D.; Vargas, C.A.; Zapata, V.H. Characterization of polycaprolactone/rGO nanocomposite scaffolds obtained by electrospinning. *Mater. Sci. Eng. C* **2019**, *103*, 109773. [CrossRef]
39. Vijayavenkataraman, S.; Thaharah, S.; Zhang, S.; Lu, W.F.; Fuh, J.Y.H. 3D-printed PCL/rGO conductive scaffolds for peripheral nerve injury repair. *Artif. Organs* **2019**, *43*, 515–523. [CrossRef]

Chapter 3: Synthesis and characterization of a novel star polycaprolactone to be applied in the development of graphite nanoplates-based nanopapers

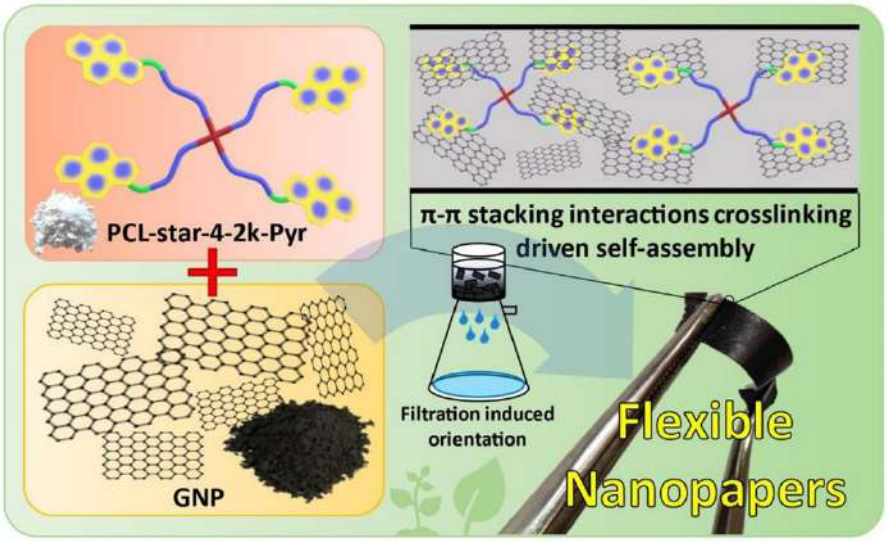

Reactive and Functional Polymers 167 (2021) 105019

Contents lists available at ScienceDirect

Reactive and Functional Polymers

journal homepage: www.elsevier.com/locate/react

Perspective Article

Synthesis and characterization of a novel star polycaprolactone to be applied in the development of graphite nanoplates-based nanopapers

Giacomo Damonte [a], Alberto Vallin [a], Daniele Battegazzore [b], Alberto Fina [b], Orietta Monticelli [a,*]

[a] Dipartimento di Chimica e Chimica Industriale, Università degli studi di Genova, Via Dodecaneso 31, 16146 Genoa, Italy
[b] Dipartimento di Scienza Applicata e Tecnologia, Politecnico di Torino-sede di Alessandria, Viale Teresa Michel, 5, 15121 Alessandria, Italy

ARTICLE INFO

Keywords:
PCL
Pyrenic functionalities
GNP nanopapers
Thermomechanical resistance
Thermal diffusivity

ABSTRACT

The work was focused on the synthesis and characterization of a polymer designed with suitable features to be applied in the development of graphite nanoplates (GNP)-based nanopapers, prepared by using a solution blending approach, followed by filtration, drying and pressing treatments. Indeed, the polymer was tailored to possess: i) pyrenic functionalities, potentially capable of interacting with the graphite surface; ii) a star shape to promote the formation of a physical networking among the GNP layers; iii) arms made of a semicrystalline biopolymer, namely polycaprolactone (PCL), to obtain a mechanically robust and sustainable system. The polymer structure, synthesized by applying a three-step procedure, was validated by IR and ^{1}H NMR measurements. The presence of the pyrenic end groups turned out to decrease the crystallinity of the polymer, compared to the starting PCL with hydroxylic and carboxylic functionalities, while significantly increasing its thermal stability at high temperature. The star shape structure of the synthesized PCL, together with its pyrene functionality, allowed introducing into the nanopapers structure a greater amount of polymer than that which can be inserted by using a high-molecular weight linear PCL. Moreover, GNP was found to promote significantly the pyrenic-PCL crystallization, acting as a nucleating agent. The strong interaction between the functionalized PCL and GNP delivered nanopapers exhibiting remarkable thermomechanical stability, up to well above the PCL melting temperature, coupled with noticeable heat spreading performance. Indeed, the developed nanopapers, being also based on a biopolymer, represent novel promising high performance and sustainable materials.

1. Introduction

Nanopapers are promising materials made by tightly packed particles, whose orientation are induced by flow-directed filtration [1–5], layer by layer self assembly [6] or tape casting [7]. Indeed, the peculiar structure, based on highly oriented particles or fibers, allowed obtaining remarkable mechanical, electrical and thermal properties [8,9]. On this basis, the application of nanopapers could potentially cover several fields, including flexible electronics [10,11] and energy harvesting applications [12]. Moreover, the good biocompatibility of some type of nanopapers, towards different cellular lines [3,12,13], expanded their application also to the biomedical field. Nanopapers based on nanocellulose [14–21], metals nanowires [14], clay [15,22], carbon nanotubes (CNT) [23] and graphene related materials (GRM) [9,16,22–25] were successfully obtained. In particular, considering the latter systems, generally graphene oxide (GO) [2,22,26,27], reduced graphene oxide (rGO) and graphite nanoplates (GNP) [22,25] were exploited. The use of a polymer binder in combination with GRM was previously proposed, with the aim of producing flexible systems [28–30], while retaining high electrical and thermal conductivity. Indeed, in the development of these materials, the specific interactions occurring between the graphite surface and the polymer has to be taken into account, as the performances of the composite resulted to be strongly affected by this feature [9,31]. In an ideal system, the polymer should act as a binder between GRM, to promote the formation of a dense and tightly packed structures. With this respect, the application of multifunctional polymers, bearing groups capable of interacting with the graphite appears particularly suitable. Beside mechanical properties, strong connections between GRM flakes may also enhance thermal conductivity properties, by creating preferential channels for phonon transmission, usually referred to as molecular junctions [32]. Indeed, the concept of molecular junctions between edge-functionalized GNP flakes was previously validated for the

* Corresponding author.
E-mail addresses: alberto.fina@polito.it (A. Fina), orietta.monticelli@unige.it (O. Monticelli).

https://doi.org/10.1016/j.reactfunctpolym.2021.105019
Received 29 July 2021; Received in revised form 24 August 2021; Accepted 25 August 2021
Available online 27 August 2021

enhancement of thermal conductivity within nanopapers [33]. Furthermore, Ferraro et al. reported the use of bispyrene molecules with various chain length as non-covalent molecular junctions to enhance thermal conductivity within GNP nanopapers, exploiting well known π-π stacking interactions [34–38] between bispyrene groups and GNP flakes [9]. Based on this background, a pyrene-terminated *star*-shaped polymer was designed in this work to provide mechanical reinforcement while retaining high heat transfer performance. As an added value, the functional polymer was designed on polycaprolactone (PCL), being a biodegradable and biocompatible polymer of relevant industrial interest. In particular, the pyrenic end capped star PCL was synthesized by applying a three-step procedure, starting from the preparation of a star PCL hydroxyl terminated, by using pentaerythritol as initiator of the ring opening polymerizarion of ε-caprolactone and tin octanoate as catalyst. In the second step, the esterification with maleic anhydride was carried out to introduce carboxylic end groups, which were converted into pyrenic functionalities in the last step. The features of the obtained products were studied by means of FT-IR, ^{1}H NMR, DSC and TGA measurements, while the specific interactions occurring between the graphite and polymer were evaluated by UV–Vis spectroscopy. Finally, nanopapers based on GNP and the synthesized pyrenic end capped star PCL, which were prepared by a solution blending approach, followed by filtration, drying and pressing treatments (Fig. 1), were characterized in terms of thermal and thermomechanical properties.

2. Materials and methods

2.1. Materials

ε-caprolactone (purity ≥97%), 1-pyrenebutanol (purity ≥99%), pentaerythritol (purity 99%), tin octanoate ($Sn(Oct)_2$) (purity ≥96%), toluene (anhydrous, purity 99,7%), dichloromethane (stabilized with 0.002% 2-methyl-2-butene) (DCM), methanol (99,9%), maleic anhydride (≥ 99%), N,N′-dcyclohexylcarbodiimide (DCC) and 4-Dimethylaminopyridine (DMAP) were purchased from Sigma Aldrich®. Graphene nanoplatelets (GNP) was provided by Avanzare Innovación Tecnológica (Spain), prepared according to a previously reported procedure [39]. This product is constituted by large (tens of μm) and wavy foils a few nm thickness, obtained after the expansion of graphite. Full characterization (Field Emission electron microscopy, Raman spectroscopy, X-ray Photoelectron Spectroscopy and specific surface area) of this product is reported elsewhere [40]. ε-caprolactone was purified prior to use by vacuum distillation over CaH_2. All the other reagents were of analytical grade and used without purification.

2.2. Synthesis of 1-pyrenic end capped star PCL

The synthesis of 1-pyrenic end-capped star PCL (referred to as PCL-star-4-2 k-Pyr) was performed by following a three-step procedure (Fig. 2). In the first, the preparation of PCL hydroxyl terminated substrate (referred to as PCL-star-4-2 k-OH) was accomplished. Subsequently, an esterification with maleic anhydride was carried out to introduce carboxylic end groups (the obtained polymer is referred to as PCL-*star*-4-2 k-COOH). In the last step, a Steglich esterification was applied to produce the pyrenic functionalized polymer (referred to as PCL-*star*-4-2 k-Pyr), by the reaction between the carboxylic functionalities of PCL-star-4-2 k-COOH and the hydroxyl group of 1-pyrenebutanol. In the following the details about the procedure are given.

2.2.1. Synthesis of PCL-star-4-2k-OH

PCL-star-4-2 k-OH was synthesized by the ring-opening polymerization (ROP) of ε-caprolactone using pentaerythritol as initiator and $Sn(Oct)_2$ as catalyst. The amount of initiator was adjusted to obtain a molecular mass of 2000 g mol^{-1}. In detail, 8.340 g of ε-caprolactone (73.06 mmol) together with 142 mg of pentaerythritol (1.04 mmol) were introduced into a 50 mL round bottomed flask under argon atmosphere and were gently heated at 80 °C under stirring, in order to ensure the complete solubilization of the initiator in the liquid monomer. Then, the mixture was heated in a thermostated oil bath at 120 °C and 60 μL of a freshly prepared solution of $Sn(Oct)_2$ in anhydrous toluene ($[\varepsilon\text{-CL}]/[Sn(Oct)_2] = 5000$) were added under argon. The reaction was allowed to proceed for 24 h, under inert atmosphere. After this time, the reaction mixture was cooled down to room temperature, the crude product was dissolved in 2 mL of DCM and precipitated in 200 mL of cold methanol, under vigorous stirring. The product was then filtered on buchner funnel, washed several times with cold methanol and dried under vacuum at 40 °C for 72 h.

2.2.2. Synthesis of PCL-star-4-2k-COOH

995 mg of the synthesized PCL-star-4-2k-OH and 196 mg of maleic anhydride (1.99 mmol, 4 eq. respect to the hydroxyls groups) were dissolved in 3 mL of anhydrous toluene into a 50 mL two necks round bottomed flask under inert argon atmosphere. The temperature was increased up to 80 °C and the system was left at this temperature under mixing for 24 h. The crude polymer solution was precipitated in 200 mL of cold methanol, washed, filtered and dried as done in the previous step.

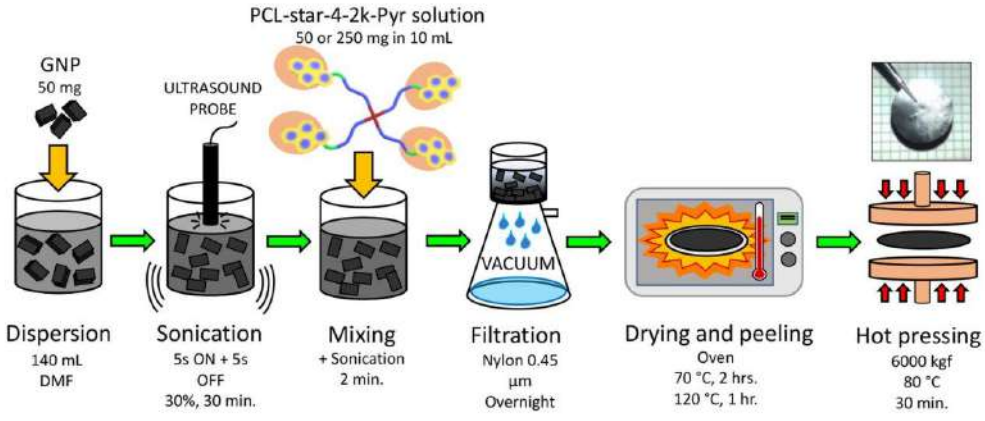

Fig. 1. Scheme of the preparation procedure of the nanopapers.

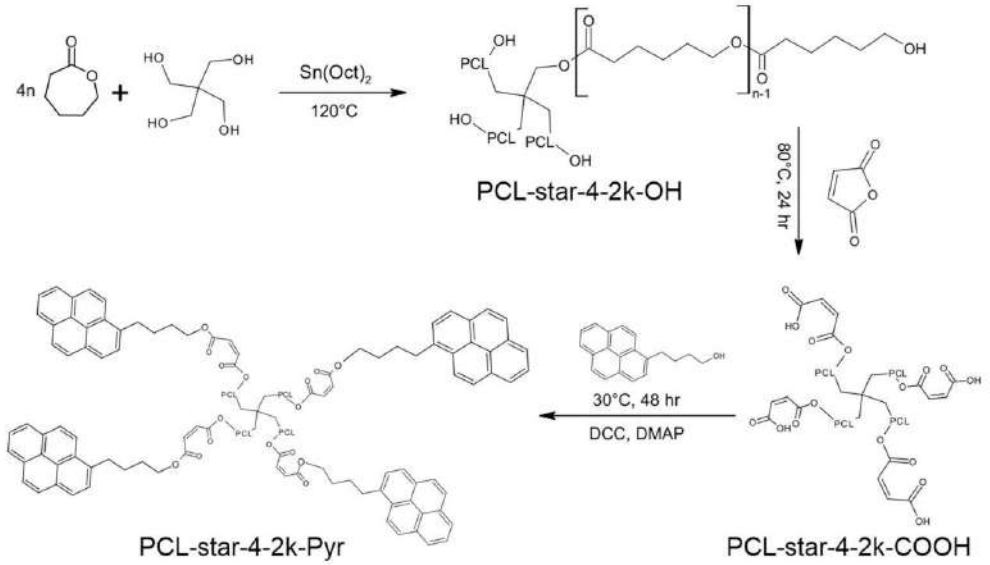

Fig. 2. Synthetic pathway of PCL-star-4-2 k-Pyr.

2.2.3. Synthesis of PCL-star-4-2k-Pyr

900 mg of PCL-star-4-2 k-COOH, 96 mg of DCC (1.1 eq., 465 μmol), 5.7 mg of DMAP (46.5 μmol, 10 mol% respect to DCC) and 124 mg of 1-pyrenebutanol (1.07 eq., 451 μmol) were introduced with 3.4 mL of anhydrous DCM into a 50 mL two necks round bottomed flask under inert argon atmosphere. The mixture was maintained at 30 °C under stirring for 48 h. The formed byproduct, namely dicyclohexylurea, was removed by filtration over a buchner funnel, washing the filter with 2 mL of DCM. The solution was collected and reduced by rotavapor to a volume of 2 mL. The functionalized polymer was precipitated by slowly dripping the solution into 200 mL of cold methanol. The final product was recovered by vacuum filtration, washed several times, with small amount of cold methanol, and dried under vacuum at 40 °C for 72 h.

2.3. Nanopaper preparation

Nanopapers were prepared by filtration following the procedure shown in Fig. 1. In detail, two different amounts of PCL-star-4-2 k-Pyr (50 or 250 mg) were dissolved in 10 mL DMF at room temperature for 1 h. GNP powder (50 mg) was sonicated in 140 mL DMF to obtain an homogeneous suspensions (with no obvious big GNP particles). The PCL solution was added to the sonicated GNP and further sonicated for 2 min. The sonication treatment was always the same and set in pulsed mode (5 s on and 5 s off) for 30 min with power set at 30% of the full output (500 W), accomplished with an ultra-sonication probe (Sonics Vibracell VC-505, Sonics &Materials Inc.) with a 13 mm diameter Ti-alloy tip. The suspension was filtered by using a polyamide PA supported membrane (0.45 μm nominal pore size, diameter 47 mm, Whatman) and left for filtration overnight. After filtration, the cake, containing GNP and adsorbed PCL over the nylon membrane, was dried in two steps, firstly at 70 °C for 2 h to remove most of the solvent and later at 120 °C for 1 h to complete solvent removal. Indeed, drying was carried out in two steps in order to avoid cracking of the film. Finally, nanopapers were obtained by applying a 6 tons load for 30 min at 80 °C on the PCL-GNP cakes after being peeled off from the nylon membrane at room temperature.

2.4. Characterization

The FT-IR analysis was performed with a Bruker "Vertex 70®" operating in ATR mode, from 400 to 4000 cm^{-1} using powdered sample. ^1H NMR spectra were recorded using a Varian "Mercury 300", operating at a frequency of 300 MHz. The samples, which were dissolved in $CDCl_3$ at a concentration of 30 mg/mL, were analyzed in 10 mm NMR tubes at room temperature. The polymers thermal properties were measured by using a Mettler Toledo "DSC1 STAR^e System®" differential scanning calorimeter (DSC), in the temperature range from 0 to 100 °C, at a heating rate of 10 °C/min, under a nitrogen flow of 20 mL/min. The crystallinity (X_c) of PCL following Eq. (1):

$$X_c(\%) = \frac{\Delta H_m}{\Delta H_m^0} \times 100\% \quad (1)$$

where ΔH_m is the measured heat of fusion and $\Delta H_m{}^0$ is melting enthalpy of the 100% crystalline PCL (139 J/g) [41]. Thermogravimetric analysis (TGA) was performed using a Mettler Toledo "DSC1 STAR^e System®" in the temperature range from 30 to 800 °C, with a heating rate of 10 °C/min, under a 80 mL/min nitrogen flow. UV–Vis measurement were carried out by applying a Shimadzu "UV-1800®" spectrometer equipped with short path quartz cells (b = 0.2 cm, slit: 1 nm, scan speed: very slow). To evaluate the interaction between pyrene-based polymer and GNP, 0.1 mg of PCL-star-4-2 k-Pyr were dissolved into a test tube with 2 mL of DMF. Then, different amounts of GNP (from 0.5 to 5 mg) were added. The obtained samples were sonicated using a sonicating bath Falc "Labsonic LBS-2®" (40 kHz, maximum power) for one hour. After sonication, the dispersed samples were left to sedimentate at room temperature for 7 days. The surnatant was collected and analyzed spectroscopically from 270 nm to 1100 nm. The nanopapers thermal diffusivity (α) was measured at 25 °C using light flash analysis (LFA, Netzsch 467 Hyperflash). 25 mm diameter samples were measure in the in-plane sample holder, heating the sample in the central region and measuring the temperature rise in time, on the outer region of the sample. Measurements were repeated five times for each sample and averaged to obtain representative thermal diffusivity values. Deformation under constant load tests (referred to as creep tests) were carried

out in tensile mode on a Q800 Dynamic Mechanical Analyzer by TA instrument, using 5 × 20 mm^2 specimens obtained from nanopapers. Condition were selected at 100 °C and 3 MPa (which are representative of a low temperature heat exchanger under moderate stress), for 8 h, followed by deformation recovery at zero load and the same temperature for 8 h.

3. Results and discussion

The synthesis of pyrenic functionalized star PCL was accomplished by applying a three-step procedure, which consisted in the preliminary preparation of a hydroxyl terminated polymer and in two following reactions to obtain carboxyl end groups, which were converted into pyrenic functionalities in the last step. In particular, concerning the latter reaction, a Steglich esterification was chosen [42,43], as it requires mild conditions, thus limiting the possible polymer decomposition, which might occur by applying the classical esterification.

3.1. FT-IR measurements

In order to evidence the chemical structure of the synthesized systems, FT-IR measurements were carried out. A comparison of the FTIR spectra of PCL-star-4-2 k-OH, PCL-star-4-2 k-COOH and PCL-star-4-2 k-Pyr is showed in Fig. 3. For all the synthesized samples, it is possible to recognize the signals typical of PCL [44] at: 2950 cm^{-1} and 2870 cm^{-1} (symmetrical/unsymmetrical stretching Csp^3-H bonds in methylenic unit), 1728 cm^{-1} (carbonyl stretching), at 1296 cm^{-1} (C—O and C—C stretching), 1241 cm^{-1} and 1170 cm^{-1} (unsimmetrical/simmetrical C-O-C stretching). In the intermediate maleated product (PCL-star-4-2 k-COOH) (Fig. 3b), two distinct novel bands appear at 1650 cm^{-1} (C=C stretching) and 815 cm^{-1} (Csp^2-H bending), which being characteristic of double bonds [45] confirm the occurrence of the polymer functionalization. For PCL-star-4-2 k-Pyr (Fig. 3c), it is possible to observe additional bands at 896 cm^{-1}, 848 cm^{-1}, 686 cm^{-1} and 623 cm^{-1} which can be ascribed to the pyrenic unit [46]. As the sample was extensively washed to remove the unreacted reagents, the presence of the pyrenic moiety is a preliminary indication of the effective esterification reaction.

3.2. ^1H NMR measurements

^1H NMR measurements were applied to confirm the chemical structure and to calculate the mean molecular weight (M_{nNMR}) of the starting PCL-based star polymer (PCL-*star*-4-2 k-OH) as well as to study the polymer functionalization. ^1H NMR spectra of the three synthesized systems are shown in Fig. 4. In the spectrum of PCL-star-4-2 k-OH (Fig. 4a), it is possible to recognize signals characteristic of the macromolecule structure at 4.05 (**5**, t), 3.63 (**5′**, t), 2.29 (**1**, m) 1.64 (**2** and **4**, m), 1.38 (**3**, m) ppm [43,47]. The mean molecular mass (M_{nNMR}) was obtained by evaluating the ratio of the areas of signal **1** and **5′**. The value found was *ca.* 2000 g mol^{-1}, which is in accordance with the theoretical number average molecular weight (M_{nth}), thus demonstrating the fine control of the polymerization reaction. Fig. 4b shows ^1H NMR spectrum of PCL star polymer treated with maleic anhydride. The complete functionalization of hydroxylic terminal groups was evidenced by a marked shift of the **5′** signal from 3.63 to 4.26 which is in perfect agreement with the values observed for monoalkyl maleates [48]. Another proof of the carboxylic end groups formation was related to the presence of two signals at 6.43 (**7**, d) and 6.31 (**6**, d), which can ascribed to double bond protons of a maleic monoester [49]. For the pyrenic terminated end-product (Fig. 4c), the complete esterification is demonstrated by several changes in the spectrum. Firstly, the merge of the signals **6** and **7** to a singlet at 6.22 ppm indicates the formation of a quasi-simmetric maleic diester that gives an equal shielding effect on the maleic double bond protons. In addition, at 8 ppm it is noticeable the characteristic pyrene (**Pyr**) signals pattern and finally, at 4.16 (**8**, t), 3.37 (**11**, t), 1.92 (**9**, quint), 1.80 (**10**, quint) ppm four butylic chain signals are clearly visible. The covalent link, between pyrenic unit and polymer in the esterification reaction, was confirmed by the chemical shift value of the signal **8**, inherent to terminal -CH_2-OH of 1-pyrenebutanol, which reached typical esters values. It is worth underling that the molecular weight of the intermediate and pyrenic terminated end product, calculated as previously reported by the integration of the NMR signals, remained identical to that of the starting material PCL-star-4-2 k-OH, demonstrating how the functionalization reaction could be carried out easily without affecting the polymer final structure.

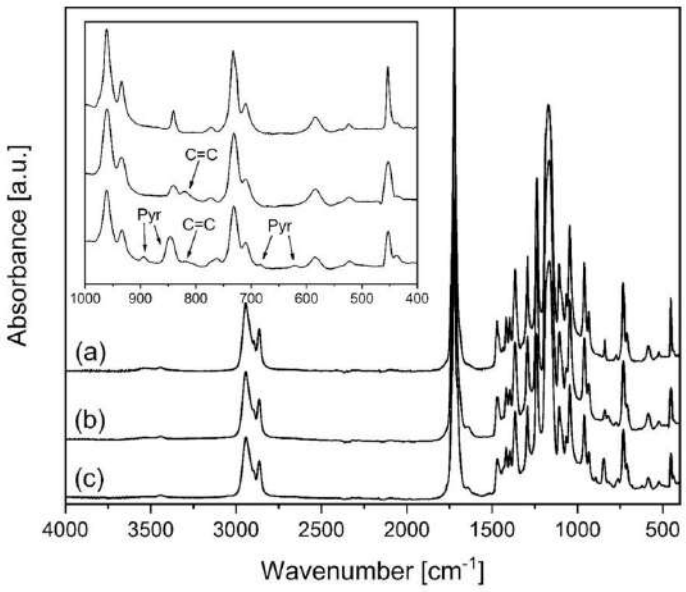

Fig. 3. FT-IR spectra of: (a) PCL-star-4-2 k-OH, (b) PCL-star-4-2 k-COOH, (c) PCL-star-4-2 k-Pyr.

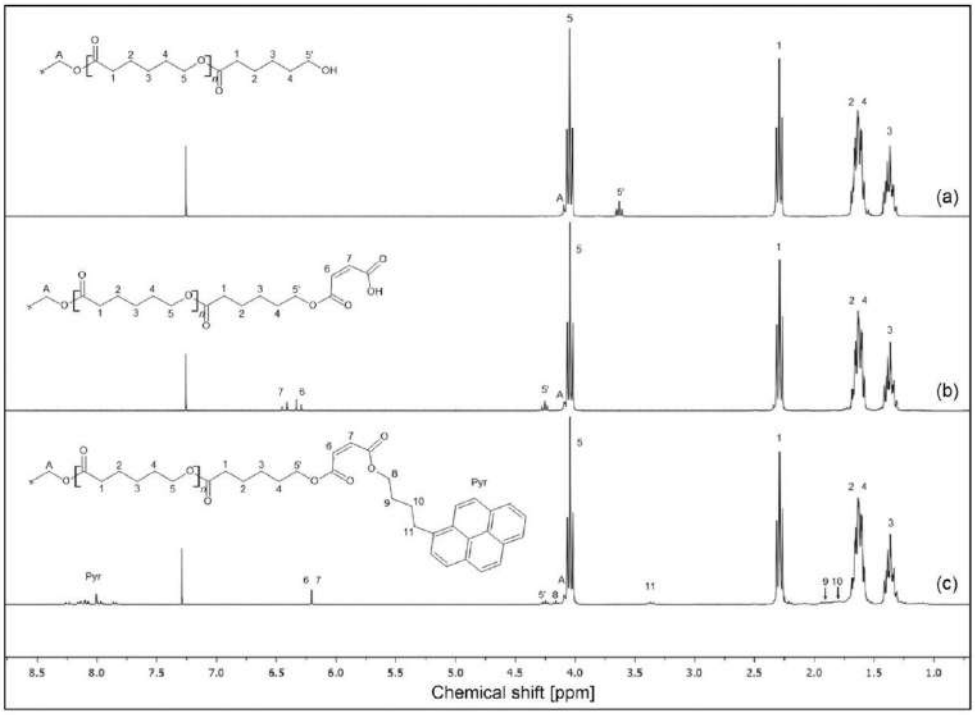

Fig. 4. ^{1}H NMR spectra of: (a) PCL-star-4-2 k-OH, (b) PCL-star-4-2 k-COOH, (c) PCL-star-4-2 k-Pyr.

3.3. Thermal properties

DSC curves of PCL-star-4-2 k-OH, PCL-star-4-2 k-COOH and PCL-star-4-2 k-Py are shown in Fig. S1, while the results are summarized in Table 1. In the cooling stage, the crystallization temperature (T_c) was observed at about 30 °C for both PCL-star-4-2 k-OH and PCL-star-4-2 k-COOH, whereas a 8 °C shift to lower temperature was found for the pyrene-terminated polymer. Moreover, PCL-star-4-Pyr showed a lower crystallinity than the other samples. Indeed, this different behaviour can be ascribed to the functional groups, all the compared polymers having the same molecular weight and a star structure. As already reported for a linear PCL ending with a pyrenic group [34], it appears that the steric hindrance of these groups as well as their π-stacking interactions may limit the polymer structuring, thus reducing the crystallinity and decreasing the crystallization temperature.

The study of the influence of the functionality on the polymer thermal properties was completed by thermogravimetric analysis. Fig. 5 compares TGA curves of PCL-star-4-2 k-OH with those of PCL-star-4-2 k-COOH and PCL-star-4-2 k-Pyr. The starting material, PCL-star-4-2 k-OH, shows only one decomposition step in the TGA curve with a maximum weight loss rate temperature (T_{max1}) at 385 °C. As reported in the literature [50,51], PCL degradation follows two concurring mechanisms, namely unzipping, which needs a nucleophilic terminal chain group, such as hydroxyl functionalities, and β-elimination, which requires at least a hydrogen atom onto the β-carbon in the alcoholic side of the ester moiety. Despite the fact that PCL is a biopolymer of significant application interest and intensely studied, its thermal degradation mechanism still remains debated. In particular, the temperature range of the above two processes has not been unanimously accepted yet. Nevertheless, the most recent work on this subject [51] and our preliminary studies on the PCL degradation demonstrated that the unzipping precedes the β-elimination. In the case of PCL-star-4-2 k-COOH, three decomposition steps were observed. As reported in the literature for other maleated polymers [52], the first degradation event, characterized by a slightly mass loss at around 200 °C, may be ascribed to maleic anhydride elimination with subsequent unlock of some hydroxylic moieties. As such, the successive two decomposition steps, which occurred with T_{max} at 365 and 427 °C, can be related to the unzipping mechanism (T_{max} at 365 °C), due to the hydroxylic groups which were formed in the previously described step, and to the statistic chain

Table 1
Thermal properties of the synthesized PCL polymers.

Sample code	ΔH_c [J/g]	T_c [°C]	ΔH_m [J/g]	T_m [°C]	χ_c [%]	T_{onset} [°C]	T_{max1} [°C]	T_{max2} [°C]
PCL-star-4-2 k-OH	−71	28	80	49	58	318	385	–
PCL-star-4-2 k-COOH	−64	22	70	44	50	253	387	428
PCL-star-4-Pyr	−56	8	56	45	40	376	–	428

The subscript m and c indicate the values measured during melting and crystallization, respectively. χ_c is the degree of crystallinity calculated by assuming the ideal enthalpies of fusion as 139 J/g. T_{onset}, T_{max1} and T_{max2} indicate the onset of the degradation temperature at a weight loss of 5%, the first stage maximum rate of degradation temperature and the second stage maximum rate of degradation temperature, respectively.

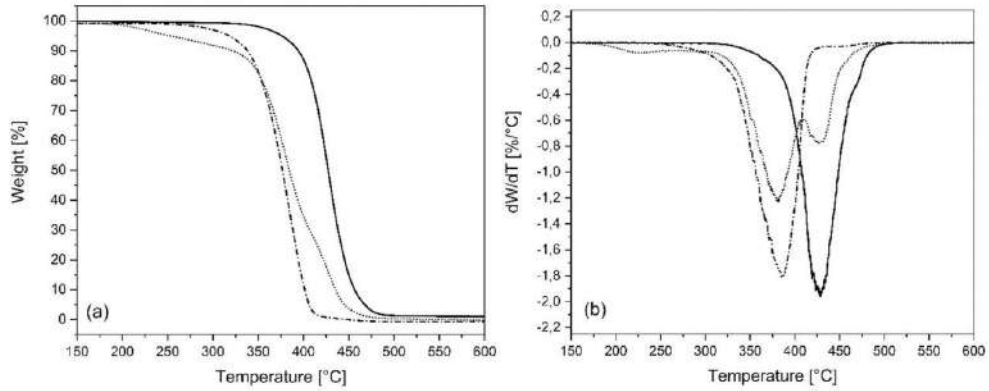

Fig. 5. TGA (a) and DTG (b) thermograms of: PCL-star-4-2 k-OH (dash dot), PCL-star-4-2 k-COOH (dot) and PCL-star-4-2 k-Pyr (continuous).

scission (T_{max} at 427 °C) related to the esterified terminals, which prevented the unzipping. Conversely, TGA curve of PCL-star-4-2 k-Pyr, which showed a T_{onset} at 376 °C, displayed a single degradation event with a T_{max} at 428 °C, which can be attributed mainly to β-elimination. Indeed, the absence of reactive terminal groups capable of promoting backbiting mechanisms directly explains the inactivation of unzipping decomposition mechanism. As such, the polymer turned out to decompose only by random chain scission and consequently to increase its thermostability with respect to the OH-terminated and COOH-terminated counterparts.

3.4. Study of PCL-star-4-2 k-Pyr interaction with GNP

To assess the interactions occurring between the developed pyrenic-based polymer with GNP, feature which might affect also the formation of tightly packed nanopapers, preliminary tests were carried out by adding PCL-*star*-4-2 k-Pyr to GNP dispersion in DMF. Indeed, GNP was sonicated in a DMF solution containing the polymer (Fig. 6a) and in the neat DMF (Fig. 6b). After sedimentation, the volumes of the suspension fraction rich in GNP, which was precipitated in the two systems, were compared. As shown in Fig. 6, the final volume of the sedimented GNP in DMF containing PCL-star-4-2 k-Pyr was almost half compare to pristine DMF. This result is a preliminary indication of the polymer capacity of acting as a physical crosslinker between the graphitic flakes, driving the formation of a GNP-based network in the solvent. A more detailed and quantitative analysis of the specific interactions occurring between graphite and PCL-star-4-2 k-Pyr was obtained by UV measurements. Fig. 7 shows the UV spectra of the surnatants, which were prepared by adding PCL-star-4-2 k-Pyr and different amounts of GNP to DMF.

Absorption bands ascribed to the electronic transitions of the pyrenic system [53] are clearly observable in Fig. 7 respectively at 345, 328, 315, 277 nm and whose intensity depends on the PCL-star-4-2 k-Pyr content in the solution. In particular, the intensity of the above peaks in the surnatant decreased by increasing the amount of GNP added to the solution, demonstrating the adsorption of PCL-star-4-2 k-Pyr onto the surface of graphite flakes, by π-π stacking interactions [38]. In the spectra of the samples containing the highest GNP amounts (1, 2 and 5 mg), a shoulder at 290 nm appeared, which can be related to absorption phenomena generated by some GNP flakes, which were not sedimented but dispersed in the solution, suggesting excess of GNP compared to the pyrene-terminated polymer, the latter being in shortage to promote

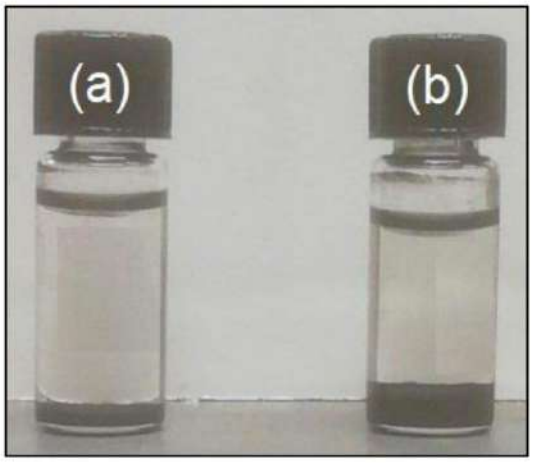

Fig. 6. Photos of the sedimented GNP in: (a) DMF containing PCL-star-4-2 k-Pyr (1.5 mL of DMF, 10 mg of PCL-star-4-2 k-Pyr and 1.5 mg of GNP) and (b) in the neat DMF (1.5 mL of DMF and 1.5 mg of GNP). Applied conditions: 1 h of sonication and 24 h of sedimentation.

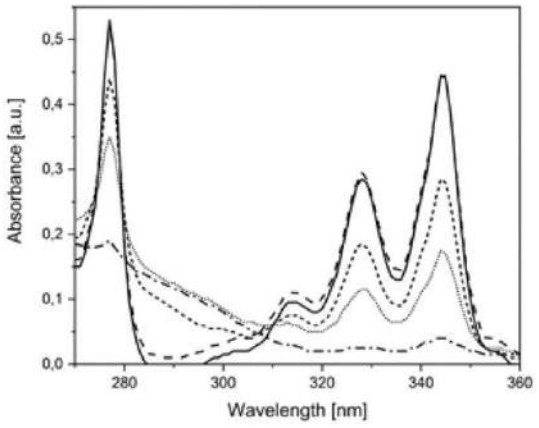

Fig. 7. UV–Vis spectra of surnatant PCL-star-4-2 k-Pyr solution with different amount of GNP, after sonication and 7 days of sedimentation: neat (continuous), 0.5 mg (dash), 1 mg (small dash), 2 mg (dot), 5 mg (dash dot).

complete GNP sedimentation.

3.5. Nanopapers preparation and characterization

Nanopapers based on GNP and the *ad-hoc* synthesized polymer were prepared by applying a solution blending, with variable polymer/GNP ratio, followed by filtration, drying and pressing treatments.

The macroscopic effect of the polymer on the mechanical properties of the nanopapers was highlighted by comparing the capability of the neat GNP-based system to resist to the bending before fracturing with that of the nanopapers containing PCL-*star*-4-2 k-Pyr. Pristine GNP nanopaper broke after the first bending (Fig. 8a), while the polymer-bound nanopapers allow multiple bending cycles without apparent damages (Fig. 8b). This qualitative result is a preliminary indication of the synthesized polymer capability of increasing the ductility of the material.

The amount of PCL retained by GNP flakes during filtration was investigated by TGA measurements. Since PCL-star-4-2 k-Pyr holds a much lower decomposition temperature (T_{max} at 428 °C) than GNP, it was indeed possible to calculate the polymer content inside the nanopapers from the residual weight at 600 °C. As only a limited fraction of the polymer can be adsorbed onto the GNP flakes and retained, its final amount in the nanopapers was clearly much lower than the polymer concentration in the suspension. Indeed, PCL-star-4-2 k-Pyr contents were approx. 9% and 12% for the nanopapers PCL-star-4-2 k-Pyr/GNP_1:1 and PCL-star-4-2 k-Pyr/GNP_5:1, respectively, suggesting saturation of the GNP retaining capability. Nevertheless, it is worth underlining that the amount of the retained polymer in the systems prepared starting from a polymer/GNP ratio of 1:1, is significantly higher, about 60% greater, than that found using a commercial high molecular mass PCL [28]. This result, demonstrates the effect of the peculiar architecture and functionality of the synthesized polymer on the capacity of interacting with GNP flakes. The thermal properties of the prepared nanopapers were analyzed by DSC measurements. Fig. 9 displays the characteristic DSC scans upon cooling and heating the samples PCL-star-4-2 k-Pyr/GNP_1:1 and PCL-star-4-2 k-Pyr/GNP_5:1, while Table 2 summarizes the results. The crystallization and melting peaks of the polymer are visible, especially in the DSC trace of PCL-*star*-4-2 k-Pyr/GNP_5:1 nanopaper, result which demonstrates the capability of the polymer of organizing crystalline structures even when confined between GNP flakes. Furthermore, it is relevant to underline that T_c turned out to be much higher than that of the neat polymer, passing from 8 °C in the case of neat PCL-star-4-2 k-Pyr to 48 °C when the polymer is between GNP in the nanopaper. This result can be ascribed to a strong nucleacting effect of GNP, phenomenon which is well documented for the systems prepared by adding graphite to PCL [54–56].

Thermomechanical properties of composites containing high volume fraction of inorganics is known to depend on the mobility of the polymer chains between inorganics flakes/fibers and the strength of interaction between the two phases. Therefore, the strongly interacting pyrene-terminated crystalline PCL represents and ideal binder for the thermo-mechanical reinforcement of GNP nanopapers. To investigate the thermomechanical resistance of polymer/GNP nanopapers, creep tests were carried out. Temperature was selected at 100 °C to represent possible application in low temperature heat exchangers, while a constant 3 MPa load was kept for 8 h, before recovery. Despite this temperature is well above melting of PCL, polymer-bound GNP nanopapers exhibited excellent creep resistance.

Indeed, upon stress application, the PCL-star-4-2 k-Pyr/GNP_5:1 nanopaper immediately deformed to a strain of only 0.8% approximately, followed by a very limited increase in strain, typical of phase I and II creep, leading to a strain of 1.4% after 8 h at 100 °C (Fig. 10). After the release of stress, strain recovery was completed after about 2 h, to a final deformation of only 1.2%.

Is important to mention that this performance is significantly better than that of the corresponding PCL-star-4-2 k-OH /GNP_5:1 nanopaper (Fig. 10), which shows 50% higher deformation at similar polymer content, proving once again the specific effect of pyrenic functionalization on the mechanical properties of the material.

Targeting application of polymer/GNP nanopapers in heat spreaders, thermal diffusivity was measured. In particular, PCL-star-4-2 k-Pyr/GNP_5:1 nanopaper exhibited a thermal diffusivity of 158 ± 6 mm^2/s, which is only slightly lower than obtained for the pristine GNP nanopaper (164 ± 4 mm^2/s) used a reference. It is worth mentioning that such value is competitive with traditional metal foils [9,57], with clear advantages for polymer/GNP nanopapers in terms of much lower density and higher flexibility compared to metals such as copper or aluminum.

3.6. Conclusions

In this work, the synthesis of a novel *star*-shaped polymer, consisting of PCL arms and pyrenic end groups (PCL-*star*-4-2 k-Pyr), was developed and exploited in the preparation of GNP-based nanopapers. The adopted synthetic procedure allowed a fine control of the polymer molecular weight as well as of the structure, leading to the complete functionalization of the end groups. Thanks to the pyrenic functionalities, PCL-star-4-2 k-Pyr turned out to possess a greater thermal stability than the two polymers which were synthesized as precursors. Furthermore, the pyrenic functionalities and the peculiar polymer shape allowed not only specific interactions with the surface of graphitic flakes but also promoted their binding, thus favouring the formation of tightly packed GNP systems. Nanopapers, prepared starting from solution containing the functional polymer, showed much higher ductility and higher

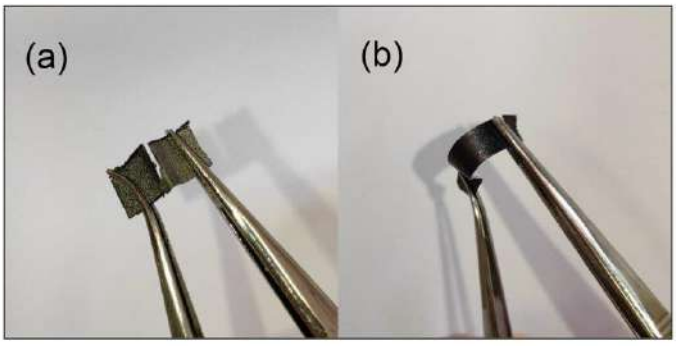

Fig. 8. Photos of: (a) folded neat GNP and (b) folded PCL-star-4-2 k-Pyr/GNP_1:1 nanopapers.

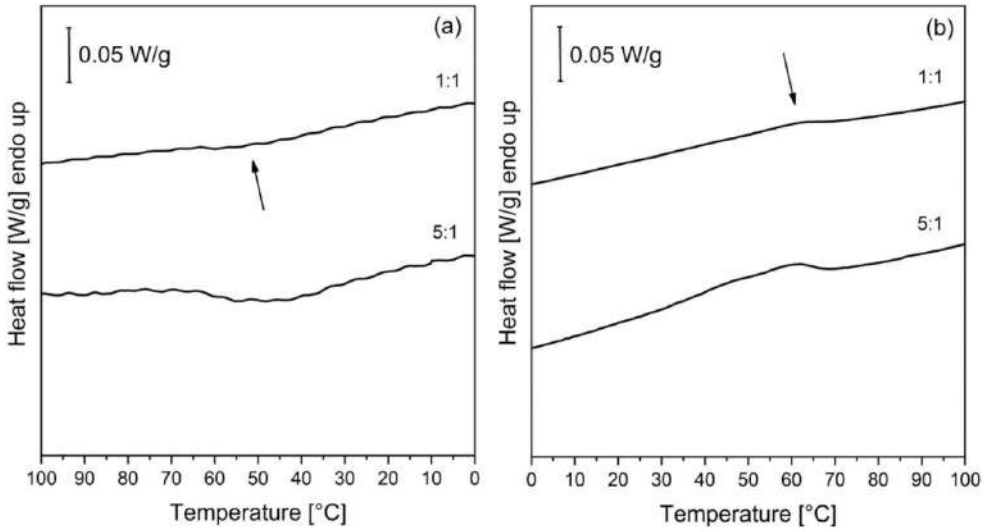

Fig. 9. DSC traces of: (a) PCL-star-4-2 k-Pyr/GNP_1:1 and (b) PCL-star-4-2 k-Pyr/GNP_5:1 nanopapers. The curves on the left refer to the cooling step (the peaks indicate the crystallization of the material), while the curves on the right represent the melting of the material.

Table 2
Characteristics of the prepared nanopapers.

Nanopaper code	ΔH_c [J/g]	T_c [°C]	ΔH_m [J/g]	T_m [°C]	PCL content [wt.-%]
PCL-star-4-2 k-Pyr/GNP_1:1	−1.1	48	1.4	60	9 ± 1
PCL-star-4-2 k-Pyr/GNP_5:1	−3.0	43	3.3	58	12 ± 2

The subscript m and c indicate the values measured during melting and crystallization, respectively.

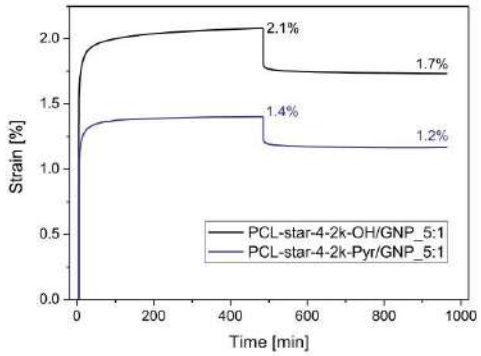

Fig. 10. Plots from creep tests at 100 °C and 3 MPa stress on PCL-star-4-2 k-OH /GNP_5:1 and PCL-star-4-2 k-Pyr/GNP_5:1 nanopapers.

thermomechanical resistance compared to those based on the neat GNP, while maintaining elevated thermal diffusivity. Beside the proposed application as low temperature heat exchanger materials, several other exploitations may be envisaged, including in the biomedical field, taking advantage of the biocompatibility and degradability of the PCL chains.

Declaration of Competing Interest

The authors declare that they have no known competing financial interests or personal relationships that could have appeared to influence the work reported in this paper.

Appendix A. Supplementary data

Supplementary data to this article can be found online at https://doi.org/10.1016/j.reactfunctpolym.2021.105019.

References

[1] H.P. Cong, J.F. Chen, S.H. Yu, Graphene-based macroscopic assemblies and architectures: an emerging material system, Chem. Soc. Rev. 43 (2014) 7295–7325, https://doi.org/10.1039/c4cs00181h.
[2] D.A. Dikin, S. Stankovich, E.J. Zimney, R.D. Piner, G.H.B. Dommett, G. Evmenenko, S.T. Nguyen, R.S. Ruoff, Preparation and characterization of graphene oxide paper, Nature 448 (2007) 457–460, https://doi.org/10.1038/nature06016.
[3] H. Chen, M.B. Müller, K.J. Gilmore, G.G. Wallace, D. Li, Mechanically strong, electrically conductive, and biocompatible graphene paper, Adv. Mater. 20 (2008) 3557–3561, https://doi.org/10.1002/adma.200800757.
[4] D. Li, M.B. Müller, S. Gilje, R.B. Kaner, G.G. Wallace, Processable aqueous dispersions of graphene nanosheets, Nat. Nanotechnol. 3 (2008) 101–105, https://doi.org/10.1038/nnano.2007.451.
[5] C.N. Yeh, K. Raidongia, J. Shao, Q.H. Yang, J. Huang, On the origin of the stability of graphene oxide membranes in water, Nat. Chem. 7 (2015) 166–170, https://doi.org/10.1038/nchem.2145.
[6] J. Shen, Y. Hu, C. Li, C. Qin, M. Shi, M. Ye, Layer-by-layer self-assembly of graphene nanoplatelets, Langmuir 25 (2009) 6122–6128, https://doi.org/10.1021/la900126g.
[7] S. Korkut, J.D. Roy-Mayhew, D.M. Dabbs, D.L. Milius, I.A. Aksay, High surface area tapes produced with functionalized graphene, ACS Nano 5 (2011) 5214–5222, https://doi.org/10.1021/nn2013723.
[8] Y. Zhou, C. Chen, S. Zhu, C. Sui, C. Wang, Y. Kuang, U. Ray, D. Liu, A. Brozena, U. H. Leiste, N. Quispe, H. Guo, A. Vellore, H.A. Bruck, A. Martini, B. Foster, J. Lou, T. Li, L. Hu, A printed, recyclable, ultra-strong, and ultra-tough graphite structural material, Mater. Today 30 (2019) 17–25, https://doi.org/10.1016/j.mattod.2019.03.016.
[9] G. Ferraro, M. Bernal, F. Carniato, C. Novara, M. Tortello, S. Ronchetti, F. Giorgis, S. Applicata, P. Torino, A. Campus, I. Tecnologica, P. Orientale, Bispyrene

functionalization drives self-assembly of graphite nanoplates into highly efficient heat spreader foils, Appl. Mater. Interfaces 13 (2021) 15509–15517, https://doi.org/10.1021/acsami.1c00319.
[10] H. Lu, Y. Liu, J. Leng, Carbon nanopaper enabled shape memory polymer composites for electrical actuation and multifunctionalization, Macromol. Mater. Eng. 297 (2012) 1138–1147, https://doi.org/10.1002/mame.201200235.
[11] B. Kim, Y. Lu, T. Kim, J.W. Han, M. Meyyappan, J. Li, Carbon nanotube coated paper sensor for damage diagnosis, ACS Nano 8 (2014) 12092–12097, https://doi.org/10.1021/nn5037653.
[12] A. Barhoum, P. Samyn, T. Öhlund, A. Dufresne, Review of recent research on flexible multifunctional nanopapers, Nanoscale 9 (2017) 15181–15205, https://doi.org/10.1039/C7NR04656A.
[13] Y. Guo, Z. Fang, M. Du, L. Yang, L. Shao, X. Zhang, L. Li, J. Shi, J. Tao, J. Wang, H. Li, Y. Fang, Flexible and biocompatible nanopaper-based electrode arrays for neural activity recording, Nano Res. 11 (2018) 5604–5614, https://doi.org/10.1007/s12274-018-2005-0.
[14] R.J.B. Pinto, M.A. Martins, J.M.F. Lucas, C. Vilela, A.J.M. Sales, L.C. Costa, P.A.A. P. Marques, C.S.R. Freire, Highly electroconductive nanopapers based on nanocellulose and copper nanowires: a new generation of flexible and sustainable electrical materials, ACS Appl. Mater. Interfaces 12 (2020) 34208–34216, https://doi.org/10.1021/acsami.0c09257.
[15] A. Liu, A. Walther, O. Ikkala, L. Belova, L.A. Berglund, Clay nanopaper with tough cellulose nanofiber matrix for fire retardancy and gas barrier functions, Biomacromolecules 12 (2011) 633–641, https://doi.org/10.1021/bm101296z.
[16] C. Yan, J. Wang, W. Kang, M. Cui, X. Wang, C.Y. Foo, K.J. Chee, P.S. Lee, Highly stretchable piezoresistive graphene-nanocellulose nanopaper for strain sensors, Adv. Mater. 26 (2014) 2022–2027, https://doi.org/10.1002/adma.201304742.
[17] M. Henriksson, L.A. Berglund, P. Isaksson, T. Lindström, T. Nishino, Cellulose nanopaper structures of high toughness, Biomacromolecules 9 (2008) 1579–1585, https://doi.org/10.1021/bm800038n.
[18] H. Yousefi, M. Faezipour, S. Hedjazi, M.M. Mousavi, Y. Azusa, A.H. Heidari, Comparative study of paper and nanopaper properties prepared from bacterial cellulose nanofibers and fibers/ground cellulose nanofibers of canola straw, Ind. Crop. Prod. 43 (2013) 732–737, https://doi.org/10.1016/j.indcrop.2012.08.030.
[19] H. Yousefi, M. Faezipour, T. Nishino, A. Shakeri, G. Ebrahimi, All-cellulose composite and nanocomposite made from partially dissolved micro-and nanofibers of canola straw, Polym. J. 43 (2011) 559–564, https://doi.org/10.1038/pj.2011.31.
[20] A.J. Benítez, A. Walther, Cellulose nanofibril nanopapers and bioinspired nanocomposites: a review to understand the mechanical property space, J. Mater. Chem. A 5 (2017) 16003–16024, https://doi.org/10.1039/c7ta02006f.
[21] B. Wang, A.J. Benitez, F. Lossada, R. Merindol, A. Walther, Bioinspired mechanical gradients in cellulose nanofibril/polymer nanopapers, Angew. Chem. 128 (2016) 6070–6074, https://doi.org/10.1002/ange.201511512.
[22] W. Huang, Nanopapers, Elsevier, Amsterdam, 2018.
[23] Y. Tang, J. Gou, Morphology, electrical conductivity of novel graphite nanoplatelets-carbon nanotube hybrid nanopaper, in: Proc. 12th Int. Conf. Eng. Sci. Constr. Oper. Challenging Environ. - Earth Sp, 2010, pp. 3657–3664, https://doi.org/10.1061/41096(366)351.
[24] J. Zhuge, J. Gou, R.H. Chen, A. Gordon, J. Kapat, D. Hart, C. Ibeh, Fire retardant evaluation of carbon nanofiber/graphite nanoplatelets nanopaper-based coating under different heat fluxes, Compos. Part B Eng. 43 (2012) 3293–3305, https://doi.org/10.1016/j.compositesb.2012.02.013.
[25] M.M. Bernal, M. Tortello, S. Colonna, G. Saracco, A. Fina, Thermally and electrically conductive nanopapers from reduced graphene oxide: effect of nanoflakes thermal annealing on the film structure and properties, Nanomaterials 7 (2017) 2–8, https://doi.org/10.3390/nano7120428.
[26] G.S. Wang, Z.Y. Wei, L. Sang, G.Y. Chen, W.X. Zhang, X.F. Dong, M. Qi, Morphology, crystallization and mechanical properties of poly(ε-caprolactone)/graphene oxide nanocomposites, Chin. J. Polym. Sci. English Ed. 31 (2013) 1148–1160, https://doi.org/10.1007/s10118-013-1278-8.
[27] T. Gong, V. Lam, R. Liu, S. Won, Y. Hwangbo, S. Kwon, J. Kim, K. Sun, J.-H. Kim, S.-M. Lee, C. Lee, Thickness dependence of the mechanical properties of free-standing graphene oxide papers, Adv. Funct. Mater. 25 (2015) 3756–3763, https://doi.org/10.1002/adfm.201500998.
[28] K. Li, D. Battegazzore, R.A. Pérez-Camargo, G. Liu, O. Monticelli, A.J. Müller, A. Fina, Polycaprolactone Adsorption and Nucleation onto Graphite Nanoplates for Highly Flexible, Thermally Conductive and Thermomechanically Stiff Nanopapers, submitted, 2021.
[29] H. Wu, L.T. Drzal, Graphene nanoplatelet paper as a light-weight composite with excellent electrical and thermal conductivity and good gas barrier properties, Carbon 50 (2012) 1135–1145, https://doi.org/10.1016/j.carbon.2011.10.026.
[30] W. Liu, N. Song, Y. Wu, Y. Gai, Y. Zhao, Preparation of layer-aligned graphene composite film with enhanced thermal conductivity, Vacuum 138 (2017) 39–47, https://doi.org/10.1016/j.vacuum.2017.01.023.
[31] M. Eleuteri, M. Bernal, M. Milanesio, O. Monticelli, A. Fina, Stereocomplexation of poly(lactic acid)s on graphite nanoplatelets: from functionalized nanoparticles to self-assembled nanostructures, Front. Chem. 7 (2019), https://doi.org/10.3389/fchem.2019.00176.
[32] D. Martinez Gutierrez, A. Di Pierro, A. Pecchia, L.M. Sandonas, R. Gutierrez, M. Bernal, B. Mortazavi, G. Cuniberti, G. Saracco, A. Fina, Thermal bridging of graphene nanosheets via covalent molecular junctions: a non-equilibrium green's functions–density functional tight-binding study, Nano Res. 12 (2019) 791–799, https://doi.org/10.1007/s12274-019-2290-2.
[33] M.M. Bernal, A. Di Pierro, C. Novara, F. Giorgis, B. Mortazavi, G. Saracco, A. Fina, Edge-grafted molecular junctions between graphene nanoplatelets: applied chemistry to enhance heat transfer in nanomaterials, Adv. Funct. Mater. 28 (2018) 2–12, https://doi.org/10.1002/adfm.201706954.
[34] G. Damonte, A. Vallin, A. Fina, O. Monticelli, On the development of an effective method to produce conductive pcl film, Nanomaterials 11 (2021) 1385, https://doi.org/10.3390/nano11061385.
[35] Z. Luo, H. Ye, J. Hu, T. Hu, B. Zhang, X. Zhang, L. Xu, Synthesis of a pyrene-functionalized hyperbranched polyethylene ternary copolymer for efficient graphite exfoliation in chloroform and formation of ethylene-vinyl acetate/graphene nanocomposites, J. Appl. Polym. Sci. 137 (2020) 1–15, https://doi.org/10.1002/app.49320.
[36] Y. Yan, J. Cui, P. Pötschke, B. Voit, Dispersion of pristine single-walled carbon nanotubes using pyrene-capped polystyrene and its application for preparation of polystyrene matrix composites, Carbon 48 (2010) 2603–2612, https://doi.org/10.1016/j.carbon.2010.03.065.
[37] Y. Zhang, C. Liu, W. Shi, Z. Wang, L. Dai, X. Zhang, Direct measurements of the interaction between pyrene and graphite in aqueous media by single molecule force spectroscopy: understanding the π-π interactions, Langmuir 23 (2007) 7911–7915, https://doi.org/10.1021/la700876d.
[38] J. Zhang, Y. Xu, L. Cui, A. Fu, W. Yang, C. Barrow, J. Liu, Mechanical properties of graphene films enhanced by homo-telechelic functionalized polymer fillers via π-π stacking interactions, Compos. Part A Appl. Sci. Manuf. 71 (2015) 1–8, https://doi.org/10.1016/j.compositesa.2014.12.013.
[39] S. Colonna, M.M. Bernal, G. Gavoci, J. Gomez, C. Novara, G. Saracco, A. Fina, Effect of processing conditions on the thermal and electrical conductivity of poly (butylene terephthalate) nanocomposites prepared via ring-opening polymerization, Mater. Des. 119 (2017) 124–132, https://doi.org/10.1016/j.matdes.2017.01.067.
[40] S. Colonna, D. Battegazzore, M. Eleuteri, R. Arrigo, A. Fina, Properties of graphene-related materials controlling the thermal conductivity of their polymer nanocomposites, Nanomaterials 10 (2020) 2167, https://doi.org/10.3390/nano10112167.
[41] M.A. Woodruff, D.W. Hutmacher, The return of a forgotten polymer - polycaprolactone in the 21st century, Prog. Polym. Sci. 35 (2010) 1217–1256, https://doi.org/10.1016/j.progpolymsci.2010.04.002.
[42] J. Gaitzsch, P.C. Welsch, J. Folini, C.A. Schoenenberger, J.C. Anderson, W.P. Meier, Revisiting monomer synthesis and radical ring opening polymerization of dimethylated MDO towards biodegradable nanoparticles for enzymes, Eur. Polym. J. 101 (2018) 113–119, https://doi.org/10.1016/j.eurpolymj.2018.02.015.
[43] A. Petrelli, R. Borsali, S. Fort, S. Halila, Redox tunable delivery systems: sweet block copolymer micelles: via thiol-(bromo)maleimide conjugation, Chem. Commun. 52 (2016) 12202–12205, https://doi.org/10.1039/c6cc07136h.
[44] M. Azizi, M. Azimzadeh, M. Afzali, M. Alafzadeh, S.H. Mirhosseini, Characterization and optimization of using calendula officinalis extract in the fabrication of polycaprolactone/gelatin electrospun nanofibers for wound dressing applications, J. Adv. Mater. Process. 6 (2018) 34–46.
[45] J.F. Jean-Pierre Fouassier, Rabek, Radiation Curing in Polymer Science and Technology vol. 2, Elsevier, Amsterdam, 1993.
[46] S. Chakraborty, G. Mulas, K. Demyk, C. Joblin, Experimental approach to the study of anharmonicity in the infrared spectrum of pyrene from 14 to 723 K, J. Phys. Chem. A 123 (2019) 4139–4148, https://doi.org/10.1021/acs.jpca.8b11016.
[47] A.M. Bhayo, R. Abdul-Karim, S.G. Musharraf, M.I. Malik, Synthesis and characterization of 4-arm star-shaped amphiphilic block copolymers consisting of poly(ethylene oxide) and poly(ε-caprolactone), RSC Adv. 8 (2018) 28569–28580, https://doi.org/10.1039/c8ra05000g.
[48] G.M. De Oca-Ramirez, L. Rios-Guerrero, J.-A. Trejo-O'Reilly, G. Flores-Rosete, A. Guyot, J. Guillot, E. Bourgeat-Lami, Synthesis and characterization of monoalkyl maleates and their use in emulsion polymerization of vinyl acetate, Macromol. Symp. 150 (2000) 161–169, https://doi.org/10.1002/1521-3900(200002)150:1<161::AID-MASY161>3.0.CO;2-H.
[49] P. Baheti, C. Bonneaud, C. Bouilhac, C. Joly-Duhamel, S.M. Howdle, P. Lacroix-Desmazes, Novel green route towards polyesters-based resin by photopolymerization of star polymers, Express Polym Lett 13 (2019) 1104–1115, https://doi.org/10.3144/expresspolymlett.2019.95.
[50] O. Persenaire, M. Alexandre, P. Degée, P. Dubois, Mechanisms and kinetics of thermal degradation of poly(ε-caprolactone), Biomacromolecules 2 (2001) 288–294, https://doi.org/10.1021/bm0056310.
[51] M. Unger, C. Vogel, H.W. Siesler, Molecular weight dependence of the thermal degradation of poly(ε-caprolactone): a thermogravimetric differential thermal fourier transform infrared spectroscopy study, Appl. Spectrosc. 64 (2010) 805–809, https://doi.org/10.1366/000370210791666309.
[52] J.W. Huang, W.C. Lu, M.Y. Yen, C.H. Lin, I.S. Tsai, Unusual thermal degradation of maleic anhydride grafted polyethylene, Polym. Eng. Sci. 48 (2008) 1550–1554, https://doi.org/10.1002/pen.21129.
[53] J. Duhamel, Pyrene florescence to study polymeric systems, Mol. Interfacial Phenom. Polym. Biopolym. (2005) 214–248, https://doi.org/10.1533/9781845690830.2.214.
[54] Q. Lv, D. Wu, Y. Qiu, J. Chen, X. Yao, K. Ding, N. Wei, Crystallization of poly (ε-caprolactone) composites with graphite nanoplatelets: relations between nucleation and platelet thickness, Thermochim. Acta 612 (2015) 25–33, https://doi.org/10.1016/j.tca.2015.05.005.
[55] I. Kelnar, J. Kratochvíl, I. Fortelný, L. Kaprálková, A. Zhigunov, M. Nevoralová, Effect of graphite nanoplatelets on melt drawing and properties of PCL/PLA

microfibrillar composites, Polym. Compos. 39 (2018) 3147–3156, https://doi.org/10.1002/pc.24322.
[56] M. Forouharshad, L. Gardella, D. Furfaro, M. Galimberti, O. Monticelli, A low-environmental-impact approach for novel bio-composites based on PLLA/PCL blends and high surface area graphite, Eur. Polym. J. 70 (2015) 28–36, https://doi.org/10.1016/j.eurpolymj.2015.06.016.
[57] F. Gong, H. Li, W. Wang, D. Xia, Q. Liu, D.V. Papavassiliou, Z. Xu, Recent advances in graphene-based free-standing films for thermal management: synthesis, properties, and applications, Coatings 8 (2018) 1–17, https://doi.org/10.3390/coatings8020063.

Chapter 4: On novel hydrogels based on poly(2-hydroxyethyl acrylate) and polycaprolactone with improved mechanical properties prepared by frontal polymerization

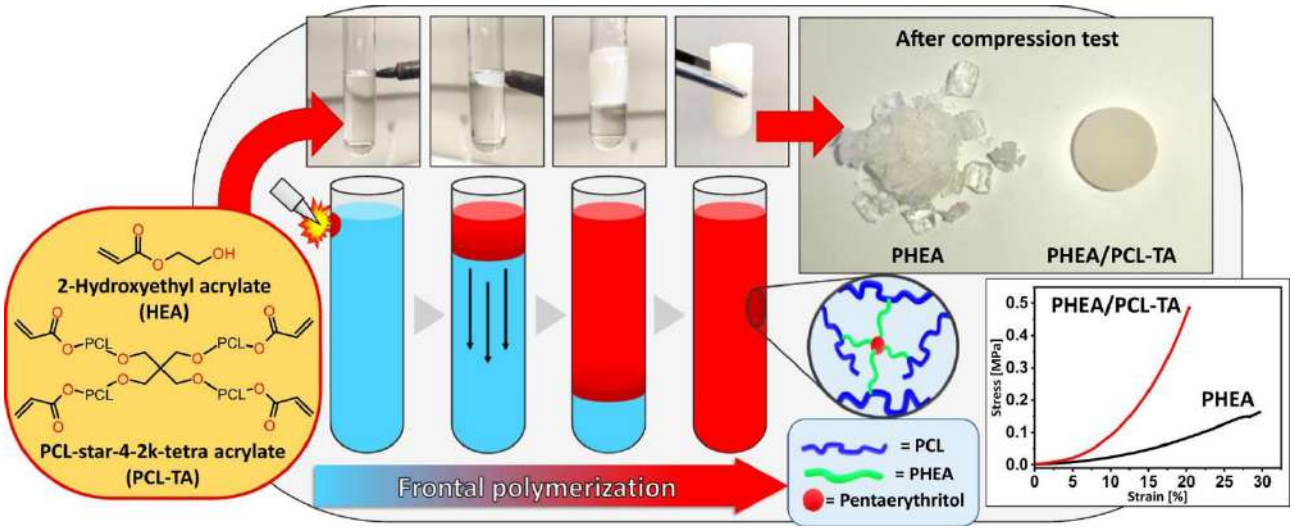

European Polymer Journal 171 (2022) 111226

Contents lists available at ScienceDirect

European Polymer Journal

journal homepage: www.elsevier.com/locate/europolj

On novel hydrogels based on poly(2-hydroxyethyl acrylate) and polycaprolactone with improved mechanical properties prepared by frontal polymerization

Giacomo Damonte [a], Lorenza Maddalena [b], Alberto Fina [b], Dario Cavallo [a], Alejandro J. Müller [c,d], Maria Rosaria Caputo [c,d], Alberto Mariani [e,*], Orietta Monticelli [a,*]

[a] Dipartimento di Chimica e Chimica Industriale, Università di Genova, Via Dodecaneso 31, 16146 Genova, Italy
[b] Dipartimento di Scienza Applicata e Tecnologia, Politecnico di Torino-Alessandria Campus, Viale Teresa Michel, 5, 15121 Alessandria, Italy
[c] POLYMAT and Department of Polymers and Advanced Materials: Physics, Chemistry and Technology, Faculty of Chemistry, University of the Basque Country UPV/EHU, Paseo Manuel de Lardizabal 3, 20018 Donostia-San Sebastián, Spain
[d] IKERBASQUE, Basque Foundation for Science, Plaza Euskadi 5, Bilbao 48009, Spain
[e] Dipartimento di Chimica e Farmacia, Università di Sassari, and INSTM, Via Vienna 2, 07100 Sassari, Italy

ARTICLE INFO

Keywords:
Frontal polymerization
Hydrogels
PCL
Mechanical properties

ABSTRACT

This work aimed to improve the mechanical properties of poly(2-hydroxyethyl acrylate) (PHEA)-based hydrogels by performing their polymerization in the presence of an *ad hoc* synthesized star-shaped polymer, whose arms are composed of a biopolymer, i.e., polycaprolactone (PCL) end-capped with acrylic units to act as a crosslinker for PHEA. Indeed, this system was designed to have (i) biocompatible, biodegradable, and mechanical strong arms as well as (ii) a star structure with acrylic functionalities to promote the crosslinking of the material. ^{1}H NMR, IR and TGA measurements confirmed the star PCL functionalization, which was carried out starting from a hydroxyl-terminated polymer. Hydrogels were prepared by varying the concentration of the synthesized star polymer, and the properties of the materials obtained by frontal (FP) and bulk polymerization (BP) were compared. Moreover, to evaluate the specific effect of PCL-star-4-2 k-tetraacrylate (PCL-TA) on the crosslinking of the systems, samples were also synthesized using a commercial acrylate crosslinker. For what concerns the frontal polymerization process, fronts were found to be stable in the presence of PCL-TA. The thermal characterization results showed a significant decrease in the PHEA glass transition temperature with increasing PCL-TA content, which was particularly evident in the samples prepared by FP. This result can be attributed to the partial miscibility of the two polymers, which become compatible during the polymerization process by forming a copolymer system. This was confirmed by analyzing the thermal behavior of hydrogels polymerized in the presence of a hydroxyl terminated PCL, i.e., a polymer without active functional end groups. The samples synthesized by FP with the star polymer and the commercial crosslinker, as well as neat PHEA, were subjected to mechanical tests. The mechanical behavior of PCL-based hydrogels was outstanding, exhibiting three time higher modulus than that of crosslinked PHEA, and were structurally stable even under high compression loadings. This remarkable property, combined with the fast and efficient polymerization method and the environmentally friendly properties of PCL, make the developed hydrogels promising systems for practical applications in various fields.

1. Introduction

Polymer-based hydrogels have gained increasing attention in both academia and industry due to their unique features, which can be tuned by modifying the starting materials as well as their synthesis method [1–3]. Indeed, due to their wide variety of properties, hydrogels find applications in various fields, such as tissue engineering [4], biomedicine [5,6], agriculture [7], and sensing [8,9]. Despite the increasing interest in hydrogels, their low mechanical strength, especially when large amounts of water are absorbed, tremendously limits their

* Corresponding authors.
E-mail addresses: mariani@uniss.it (A. Mariani), orietta.monticelli@unige.it (O. Monticelli).

https://doi.org/10.1016/j.eurpolymj.2022.111226
Received 22 February 2022; Received in revised form 11 April 2022; Accepted 20 April 2022
Available online 25 April 2022

applications.

Many attempts have been made to improve the mechanical behavior of hydrogels by reinforcing the polymer networks with suitable particles/nanoparticles [10–13] or by applying new methods of gelation [14,15]. Concerning the former approach, micro/nanoparticles can either crosslink the gel, be used to attach and adsorb polymer chains, or be physically dispersed within the network [15]. In particular, in the case of nanocomposite hydrogels, the combination of the polymer system with graphene-related materials such as graphene oxide, reduced graphene oxide, and graphite nanoplatelets represent the more recent evolution [16,17]. Although this approach seems to be effective, several aspects should be considered, mainly related to the dispersion of nanoparticles. On the one hand, it may be difficult for some systems to achieve nanoscale dispersion, and on the other, the nanofiller may strongly influence the final properties of the material, such as biocompatibility and degradability [18].

In the case of poly(2-hydroxyethyl acrylate) (PHEA), the issue related to its poor mechanical properties was addressed by introducing graphene oxide (GO) into the polymerization medium [19]. Indeed, in the composite hydrogels containing 2 wt% of GO, the modulus determined by tensile tests was increased by 100% compared to that of the neat PHEA [19]. In another work, the monomer, 2-hydroxyethyl acrylate (HEA), was polymerized by free radical polymerization in the presence of divinylbenzene as crosslinker and azobisisobutyronitrile as initiator with various comonomers such as N-vinylpyrrolidone, methacrylic acid, glycidyl methacrylate, and glycerol monomethacrylate to tune the mechanical properties of the system [20]. It was reported that the modulus increased with increasing the amount of crosslinker, which is probably due to the increment in crosslinking density, while among the prepared hydrogels, those based on glycidyl methacrylate exhibited the highest modulus [20]. It is worth mentioning that the cited research works do not report the compression behavior of the material in the swollen state, which is in fact an important property affecting the applicability of hydrogels.

In all the above-mentioned works, classical polymerization methods, such as in a batch reactor, were used, which in some cases also took many hours of prolonged heating. The novelty of the present work is related to two aspects: the use of an *ad hoc* synthesized polymer with a star structure capable of participating in the polymerization/crosslinking process, and the synthetic technique used. Regarding the first aspect, a star-shaped polymer was developed and exploited to increase the crosslinking of the system. The arms of the above compound were made of polycaprolactone (PCL), a biodegradable, biocompatible polymer with high mechanical strength [21]. In addition, frontal polymerization (FP) was the approach used to develop these particular hydrogels.

FP is an exothermic polymerization in which monomers are converted to polymers by propagating a localized reaction zone throughout the system [22,23]. Once FP is ignited, the heat released is sufficient to support the reaction to come, and no further energy is required. Unlike other polymerization techniques, FP is highlighted with several advantages, such as fast reaction rates, flexible operation, and lower energy requirements [24]. For these advantages, since the pioneering work [24], the above method has been widely used for the preparation of several systems, such as polyurethane materials, gradient materials, interpenetrating polymer networks and functional hydrogels [25–27].

Our work was organized by first performing the preliminary synthesis of the star-shaped polymer. Then, hydrogels were prepared by applying frontal polymerization, varying the concentration of the star polymer (Fig. 1). Front stability, temperature, and velocity as a function of star polymer or acrylate crosslinker concentration were then determined. The features of the PHEA/PCL samples prepared by frontal polymerization in terms of thermal, mechanical, and swelling properties were compared with those of neat PHEA and with those of PHEA crosslinked with a classical crosslinker, as well as with systems prepared by bulk polymerization.

2. Materials and methods

2.1. Materials

2-Hydroxyethylacrylate (HEA, purity ≥ 96%), N-methylpyrrolidone (NMP, purity = 99.5%), benzoyl peroxide (BPO, with 25% H_2O), caprolactone (ε-CL, purity ≥ 97%), pentaerythritol (purity = 99%), pentaerythritol tetra acrylate (PE-TA, with 350 ppm hydroquinone monomethyl ether), tin octoate ($Sn(Oct)_2$, purity ≥ 96%), methanol (99,9%), acryloyl chloride (purity ≥ 97%, with 400 ppm phenothiazine as stabilizer), potassium carbonate (purity ≥ 99%, anhydrous) and dichloromethane (DCM, purity ≥ 99.8%, stabilized with amylene) were purchased from Sigma Aldrich®. ε-caprolactone and DCM were purified prior to use by vacuum distillation over CaH_2 and stored under Argon

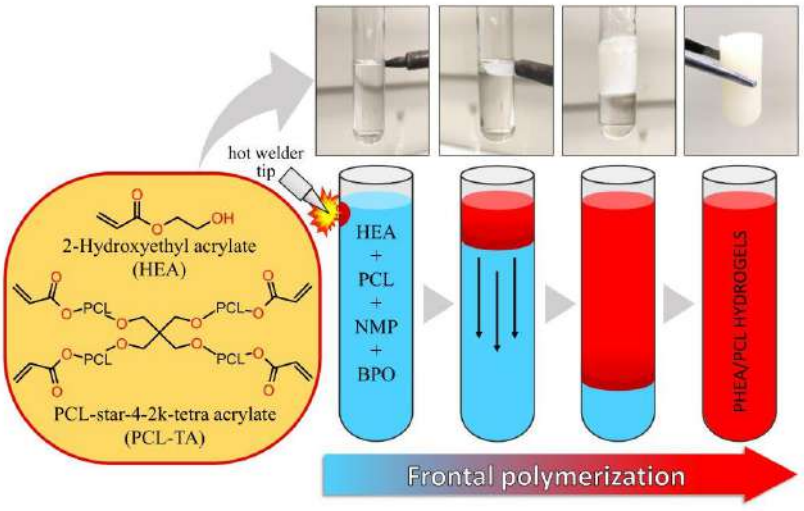

Fig. 1. Scheme of the hydrogel preparation by FP.

atmosphere. Pentaerythritol was dried in vacuum oven at 40 °C prior use. All the other reagents were of analytical grade and used without purification.

2.2. Synthesis of acrylated star PCL

The acrylated star PCL (referred to as PCL-TA in the sample code) was synthesized starting from a hydroxyl-terminated star PCL (referred to as PCL-OH in the sample code), prepared by ring opening polymerization (ROP) of ε-CL using pentaerythritol as initiator in the presence of $Sn(Oct)_2$ as reported elsewhere [21,28–32]. 5 g (0.61 mmol) of PCL-star-4-2k-OH and 15 mL of anhydrous DCM were placed in a 50 mL round bottom flask with two necks, which was purged with argon. After complete dissolution of the polymer, the flask was placed in an ice-water bath and 2.07 g (15 mmol) of anhydrous potassium carbonate was added, then 596 μL (7.4 mmol, 3 equivalents with respect to PCL hydroxyl groups) of acryloyl chloride was added dropwise under stirring. The reaction was carried out at room temperature for 48 h under argon. The reaction mixture was then filtered to remove the insoluble solids. The crude product was precipitated in 400 mL of cold methanol under vigorous stirring, filtered on Büchner funnel, washed several times with cold methanol, and dried under vacuum at 40 °C for 72 h.

2.3. Synthesis of neat PHEA hydrogels via frontal or bulk polymerization

In the case of the preparation of PHEA via frontal polymerization (FP), 8 mg of BPO (0.1 mol% respect to HEA) were dissolved in 1 mL of NMP into a glass tube (13 mm internal diameter and 100 mm lenght), then 4 mL of HEA (35 mmoles) were added. The reaction was initiated with a hand-held tin welder (tip temperature = 450 °C) placed directly in contact with the outer surface of the glass tube below the meniscus of the solution until the reaction started.

To perform bulk polymerization (BP), the samples were inserted in the glass tube described above which was placed in an 80 °C water bath for 1 h. Some hydrogels were also prepared using pentaerythritol tetraacrylate as crosslinker. For this purpose, different amounts of PE-TA ($3 \cdot 10^{-2}$, $6 \cdot 10^{-2}$, $12 \cdot 10^{-2}$ mmoles corresponding to 250, 500, 1000 mg) were added to the HEA/NMP/BPO mixture described previously. After complete dissolution under stirring, the mixture was polymerized by FP or BP under the conditions described above. The hydrogels were then recovered by carefully breaking the glass with a hammer. NMP was removed from the samples by immersion in milli-Q® water, replacing the water daily for 4 days. The samples were then vacuum dried at 30 °C until they reached a constant weight. The prepared samples were defined by specifying the amount of PE-TA used (11, 21, and 42 mg corresponding to $3 \cdot 10^{-2}$, $6 \cdot 10^{-2}$, $12 \cdot 10^{-2}$ mmoles) and by indicating the polymerization method used (frontal as (F) and bulk (B)) in the code. The example PHEA/PE-TA_6(F) denotes a hydrogel prepared by frontal polymerization starting from $6 \cdot 10^{-2}$ mmoles of PE-TA.

2.4. Preparation of hydrogels based on PCL-TA via frontal or bulk polymerization

For the polymerization of HEA in the presence of PCL-TA, the previously described HEA/NMP/BPO mixture was added to different amounts (250, 500, 1000 mg corresponding to $3 \cdot 10^{-2}$, $6 \cdot 10^{-2}$, $12 \cdot 10^{-2}$ mmoles) of the star polymer. After complete dissolution under stirring, FP or BP was initiated. Samples were then washed with milli-Q® water and dried as previously described. Some hydrogels were also prepared by adding the PCL-OH to the reaction mixture and applying the same procedures and amount used to synthesize the samples based on PCL-TA. Samples were defined by specifying the star-PCL used (PCL-TA or PCL-OH) and its molar content (3, 6, or $12 \cdot 10^{-2}$ mmoles) and by indicating the polymerization type (frontal as (F) and bulk (B)) in the code. The example PHEA/PCL-TA_6(F) denotes a hydrogel prepared by frontal polymerization starting from $6 \cdot 10^{-2}$ mmoles of PCL-star-4–2 k-tetraacrylate.

2.5. Characterization

FT-IR spectroscopy was performed on powdered samples using a Bruker "Vertex 70®" working in ATR mode, in the range 400–4000 cm^{-1}. ^1H NMR proton spectroscopy was accomplished with a Varian "Mercury 300", with a frequency of 300 MHz. The samples, priorly dissolved in $CDCl_3$ at a concentration of 30 mg/mL, were analyzed in 10 mm NMR tubes at room temperature. The thermal properties of synthesized polymers were measured by using a Mettler Toledo "DSC1 STAR^e System®" differential scanning calorimeter (DSC), in the temperature range from −80 to 100 °C, at a heating rate of 10 °C/min, under a nitrogen flow of 20 mL/min. The corresponding xerogels were obtained by drying hydrogel samples in vacuum at 30 °C until constant weight. The crystallinity degree (X_c) of PCL in the xerogels was calculated on the base of their contents, Φ_{PCL}, following Eq. (1):

$$X_c(\%) = \frac{\Delta H_m}{\Delta H_m^0 \times \varphi_{PCL}} \times 100\% \quad (1)$$

where ΔH_m = melting enthalpy (measured), Φ_{PCL} is the PCL content in the xerogels and ΔH_m^0 is the melting enthalpy of a 100% crystalline PCL, commonly found in the literature (139 J/g) [33]. The second heating scan was considered for the above calculation.

It should be noted that as PCL is not soluble in water, it is expected that the calorimetric behavior of the PCL phase (within the complex hydrogels prepared) will be the same if directly measured in the hydrogels or in dehydrated samples (xerogels). Measuring dehydrated samples by DSC is easier, as the entire sample mass is composed by the polymeric material, leading to higher resolution.

Thermogravimetric analysis (TGA) was performed with a Mettler Toledo "TGA/DSC1 STAR^e System®" in the range from 30 to 800 °C, under an 80 mL/min nitrogen flow, using a heating rate of 10 °C/min.

Swelling tests were performed by immersing a 4x4x4 mm^3 cube of a dried sample in Milli-Q at 20 °C and weighing the swollen sample directly at different times. The swelling ratio (SR%) of the prepared hydrogels was calculated by applying equation (2).

$$SR(\%) = \frac{M_s - M_i}{M_i} \times 100\% \quad (2)$$

The evaluation of SR% as a function of temperature was carried on the fully swollen cube-shaped samples (4x4x4 mm^3), increasing the temperature by 10 °C/day from 20 to 70 °C.

Wide-angle X-ray scattering (WAXS) at room temperature were collected. The experiments were carried out with a synchrotron radiation at beamline BL11-NDC in the ALBA Synchrotron in Barcelona (Spain). Samples were placed in aluminium pans and located in the beam path. To ensure an inert environment during the measurements, the chamber where the samples are placed was subjected to a continuous flow of nitrogen gas. The used X-ray energy amounted to 12.4 keV (λ = 1.03 Å) and the sample-detector distance was 132.6 mm and the tilt angle was 21.2°. For WAXS measurements, the detector was a Rayonix LX255-HS (Evanston, IL, USA), calibrated with chromium (III) oxide and with a resolution of 1920 × 5760 pixels and pixel size of 44 × 44 μm^2. Scattering curves were obtained, in which the intensity is plotted as a function of the scattering vector q ($q = 4\pi\sin\theta\lambda^{-1}$), where θ is the diffraction angle.

Mechanical properties of hydrogels were measured by compression tests performed on a DMA TA-Q-800 (TA instrument, New Castle, DE, USA). Compression stress/strain curves for all samples were collected between 0% and 30% strain at 25 °C, applying 5%/min strain rate. The 0% strain was determined by applying 0.05 N pre-load. Specimens of cylindrical shape (6 mm in diameter and 2 mm in height) were compressed between 13 mm diameter plates after gentle removal of water

excess using filter paper. Measurements were carried out in triplicate to provide representative averages and deviations. The compressive modulus was calculated as the slope of the linear region of stress–strain curve in the 19–20% strain range. This corresponds to the strain region representing "compact" material after the excess water is eliminated from the hydrogel [34].

3. Results and discussion

3.1. Preparation and characterization of PCL-TA

The work initially focused on the synthesis of acrylated PCL star (PCL-TA), which was prepared by direct esterification with acryloyl chloride using potassium carbonate as acid scavenger. The above reagent was chosen to overcome some disadvantages related to the use of other compounds, such as triethylamine [35], which might remain trapped in the polymer and lead to side reactions. To prove the chemical structure of the polymer, FT-IR and ^{1}H NMR measurements were performed.

Fig. 2 shows a comparison between the spectra of the hydroxyl-terminated starting polymer (PCL-OH) and PCL-TA. In both samples, the signals characteristic of PCL [36] are present at the wavenumbers of 2950 cm^{-1} and 2870 cm^{-1} (symmetric/unsymmetric stretching of Csp^3-H bonds in the methylene unit), 1728 cm^{-1} (carbonyl stretching), at 1296 cm^{-1} (C—O and C—C stretching), 1241 cm^{-1} and 1170 cm^{-1} (unsymmetric/symmetric C—O—C stretching). In the esterified acrylate product, two distinct new absorption bands appear at 1641 cm^{-1} (C=C stretching) and 814 cm^{-1} (Csp^2-H twisting), which can be assigned to acrylic double bonds [37], thus preliminarily confirming the occurrence of the polymer functionalization.

To further elucidate the chemical structure of the synthesized polymers and evaluate their average molecular weight, ^{1}H NMR characterization was also accomplished. The spectra of PCL-star-4-2k-OH and PCL-star-4-2k-tetraacrylate are shown in Fig. 3. For the starting material, PCL-star-4-2k-OH, it is possible to recognize signals typical of PCL backbone [38,39] at 4.05 (**5**, t), 3.63 (**5′**, t), 2.29 (**1**, m) 1.64 (**2** and **4**, m), 1.38 (**3**, m) ppm. The measured molecular mass, 2000 g mol^{-1}, calculated by the ratio of the areas of signal 1 and 5′, agreed with the theoretical average molecular weight calculated from the initiator concentration. In the acrylated product spectra, in addition to PCL signal previously described, a series of signals in the vinylic proton zone appeared at: **6** (dd, 5.81 ppm), **7** (dd, 6.11 ppm), **8** (dd, 6.39 ppm). Furthermore, the esterification reaction was demonstrated by the shift of the 5′ signal value from 3.65 to 4.15 ppm, typical of acrylic esters of aliphatic alcohols [40].

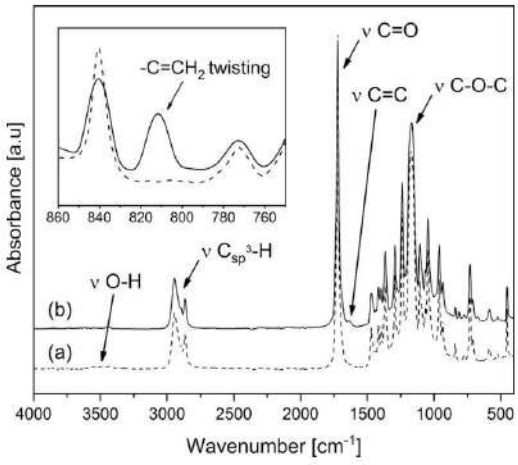

Fig. 2. FT-IR spectra of: (continuous line) PCL-TA and (dashed line) of PCL-OH.

The synthesized star polymers were also characterized by DSC and TGA measurements. The relevant plots are reported in the Supporting Information (Figs. S1 and S2), while the results are summarized in Table 1. The analysis of the crystallization temperature (T_c) and enthalpy (ΔH_c) as well as the crystallinity degree (χ_c) evidenced a negligible influence of the functional groups on the thermal behavior of PCL. Moreover, the values found agree with those reported for other types of star PCLs with similar molar masses [41].

It was found that the degradation behavior of the two studied polymers strongly depends on the nature of the end groups (Fig. S2). In particular, the onset of the degradation temperature (T_{onset}) was about 70 °C higher for the acrylate polymer than for the hydroxyl-terminated polymer (Table 1). Moreover, the temperature of the maximum degradation rate of PCL-TA increased by about 40 °C compared to PCL-OH. It is indeed possible to elucidate this phenomenon based on the degradation mechanisms of PCL. As reported in the literature [42], the polymer decomposition may be obtained by two possible mechanisms, namely the depolymerization, which occurs at lower temperature and requires a nucleophilic terminal chain group or the random chain scission by β-elimination, which needs at least one hydrogen atom on the β-carbon in the alcoholic side of the ester moiety. It can be deduced that the increase in thermal stability observed for the acrylate polymer might be due to the esterification of the end groups, which suppresses the mechanism of depolymerization by backbiting the hydroxyl chain ends to produce ε-caprolactone. Since the acrylate polymer can decompose only by statistic β-elimination, its thermostability is clearly improved compared to the hydroxyl-terminated polymer. These results, in turn, once again confirmed the occurrence of the functionalization reaction.

3.2. Preliminary experiments for the preparation of hydrogels via FP

The dynamics occurring in frontal polymerization processes, especially for those radical-initiated, is a complex and very important aspect to consider. In general, a constant front velocity is one of the most important features to prove the occurrence of pure FP without spontaneous polymerization [22,43–45]. Therefore, the formation of a stable front was verified in several preliminary experiments.

Fig. S3 shows the position of the front as a function of time for all prepared systems. The experimental data are well fitted by a straight line, showing that a constant velocity was achieved and pure FP occurred (i.e., without the simultaneous occurrence of any other chemical reaction). Fig. 4a and b show the effect of the crosslinker (PE-TA and PCL-TA) and the inert additive (PCL-OH) content on the front velocity (V_f) and the maximum front temperature (T_{max}) of the prepared compounds. It was found that, by increasing the star polymer content, both T_{max} and V_f decrease. In detail, by considering the sample containing no crosslinker or inert component - for which the values of T_{max} = 168 °C and V_f = 1.05 cm/min were found - as a reference, by adding PE-TA, which is characterized by a relatively low molecular weight/number of reactive groups ratio, the above parameters remain almost constant in all the concentration range studied.

On the other hand, the addition of PCL-TA resulted in a decrease of both parameters down to 146 °C and 0.75 cm/min, respectively. By comparison, when the PCL-OH was added, a further decrease of V_f was found (0.62 cm/min) as the above inert component concentration increased. Indeed, the presence of PCL chains, which are inert and absorb part of the heat released by the reaction, resulted in an expected decrease of V_f. In PCL-OH this effect is the largest since it does not contain any reactive group that may contribute to the overall exothermicity of the reaction. However, it is worth mentioning that in all cases a pure frontal polymerization was achieved.

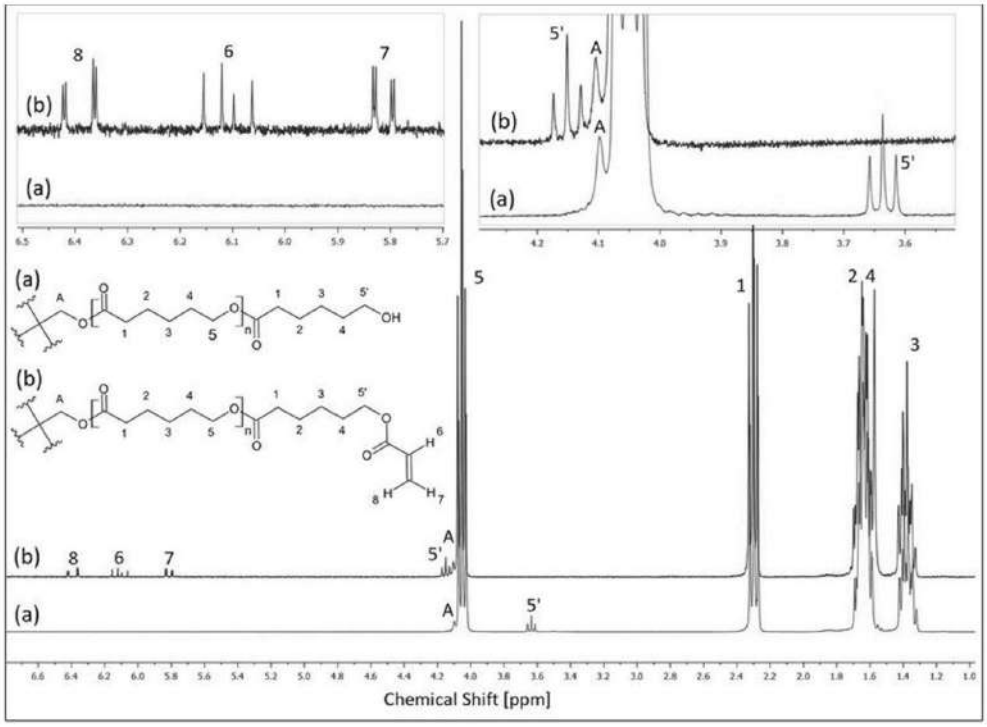

Fig. 3. ^{1}H NMR spectra of: (a) of PCL-OH and (b) PCL-TA.

Table 1
Thermal properties of the synthesized star PCL.

Sample code	T_c [°C]	ΔH_c [J/g]	T_m [°C]	ΔH_m [J/g]	χ_c [%]	T_{onset} [°C]	Tr_{max} [°C]
PCL-OH	32	−69	49	79	57	318	384
PCL-TA	28	−70	48	83	59	392	427

The subscript m and c indicate the values measured during melting and crystallization, respectively. χ_c is the degree of crystallinity calculated by assuming the ideal enthalpy of fusion as 139 J/g. T_{onset} and Tr_{max} indicate the onset of the degradation temperature at a weight loss of 5 % and the maximum rate of degradation temperature, respectively.

3.3. Xerogel thermal properties

DSC traces of neat PHEA and the xerogels crosslinked with PE-TA, prepared by FP are shown in Fig. S4, while the thermal data are provided in Table 2. The results obtained by using BP are similar (results not shown). Indeed, neat PHEA exhibits a glass transition temperature at about 13 °C, in agreement with the values reported in the literature [19,46]. Moreover, the addition of the crosslinker slightly increases the polymer T_g, a phenomenon which can be ascribed to the reduction of the macromolecular chain mobility.

Fig. 5 shows the DSC traces, recorded during cooling and second heating of the xerogels prepared by FP or BP. Considering the above results (Table 2), a significant decrease in the T_g of PHEA was observed. This phenomenon is likely due to a partial miscibility between the PCL and PHEA. Moreover, in the case of the systems based on PCL-TA, the formation of a copolymer during the polymerization, which can locate at the interface between the two polymer phases can increase their compatibility. To support this hypothesis, xerogels based on PCL-OH, i.e., the polymer without reactive groups, were prepared. The thermal results (Fig. S5 and Table S1) show a negligible dependence of PHEA T_g on the amount of PCL-OH added to the polymerization mixture, highlighting the influence of the polymer functionalization on the final properties of the material. Moreover, considering the trend of PCL χ_c given in Table 2, referred to the systems based on PCL-TA, all the samples turned out to be characterized by a significant decrease of χ_c compared to that of the neat polymer (Table 1). As reported in the literature [47], this phenomenon can be associated with the decrease in the mobility of the chains after crosslinking, proving once again the reactivity of the synthesized PCL-TA. The crosslinking of PCL was also demonstrated by the negligible amount of the polymer extracted from the xerogels when subjected to an intensive wash with a solvent capable of dissolving the polymer. Despite the decrease in the crystallinity of the system PHEA/PCL-TA, it is worth noting that PCL was still capable of undergoing crystallization, developing crystallization degrees in the range of 35–44%. This can be explained by the fact that PCL chains within the synthesized stars are not interrupted by chemical reactions, as crosslinking proceeds via the reaction of the acrylate terminal groups only.

Fig. S6 shows WAXS diffractograms measured on xerogel samples at room temperature. In the case of PHEA/PCL-TA-3(F), the material is completely amorphous. This is consistent with the results shown in Fig. 5A(b), i.e. sample does not crystallize if it is only cooled down to room temperature. In the case of this sample, the crystallization of PCL only occurs at much lower temperatures (about −50 °C) as a result of confinement as it will be explained below. On the other hand, the PHEA/PCL-TA-12(F) sample, which contains a larger amount of PCL chains, was able to crystallize when cooled to room temperature and exhibits a typical semicrystalline PCL WAXS trace shown in Fig. S6.

The examination of the crystallization behavior of the PCL

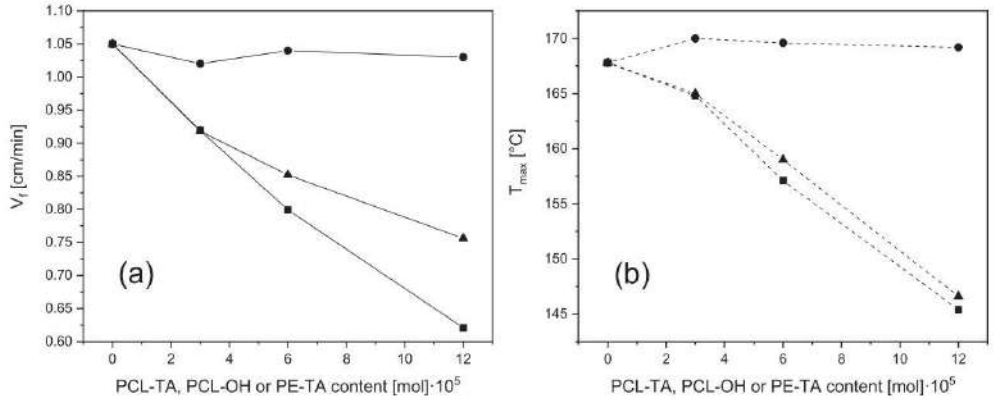

Fig. 4. (a) V_f and (b) T_{max} as function of crosslinker or additive content for: ● PHEA/PE-TA (F), ▲ PHEA/PCL-TA (F), ■ PHEA/PCL-OH (F).

Table 2
Thermal properties of the prepared xerogels.

Sample code	T_c [°C]	ΔH_c [J/g]	T_g [°C]	T_m [°C]	ΔH_m [J/g]	$\chi_{c\ CORR}$ [%]
PHEA(F)	–	–	15	–	–	–
PHEA/PE-TA_3 (F)	–	–	21	–	–	–
PHEA/PE-TA_6 (F)	–	–	21	–	–	–
PHEA/PE-TA_12(F)	–	–	23	–	–	–
PHEA/PCL-TA_3(F)	−50	1	13	50	3	35
PHEA/PCL-TA_6(F)	15	5	11	48	6	44
PHEA/PCL-TA_12(F)	14	9	−3	48	12	43
PHEA(B)	–	–	13	–	–	–
PHEA/PCL-TA_3(B)	−50	1	16	49	3	40
PHEA/PCL-TA_6(B)	17	1	11	48	6	38
PHEA/PCL-TA_12(B)	19	6	4	48	12	42

The subscript m and c indicate the values measured during melting and crystallization, respectively. χ_c is the degree of crystallinity calculated by assuming the ideal enthalpies of fusion as 139 J/g and considering the PCL content in the xerogel.

component in the xerogels prepared via frontal or bulk polymerization, leads to the following observations. As expected, the total enthalpy of crystallization generally decreases with decreasing PCL content in the system for both series of samples. Regarding the crystallization temperatures, the xerogels PHEA/PCL-TA_6 and PHEA/PCL-TA_12 have values between 19 and 14 °C, all distinctly lower than the pristine PCL-star-4-2k-tetra acrylate (28 °C, see Table 1). Notably, multiple (double) exothermic peaks can be observed in the bulk polymerized xerogels containing the highest amount of PCL. Finally, and most remarkably, the sample with the lowest content of PCL, i.e., PHEA/PCL-TA_3(F) and PHEA/PCL-TA_3(B), displays a single crystallization peak located at extremely low temperatures, close to the glass transition temperature of neat PCL. Moreover, we notice that, while the size of the melting peak is obviously dependent on PCL content, its temperature is not (Fig. 2b).

All the above observations are consistent with the occurrence of fractionated crystallization of the PCL phase [48]. Fractionated crystallization occurs when a semicrystalline polymer is subdivided into small micro/nano-domains that contain less or less active heterogeneities, so that nucleation and crystallization of the polymer can only happen at larger undercoolings. In the present case of the xerogels, it is thus deduced that partially mixed domains of PHEA and PCL finely dispersed within the xerogel must exist. When such domains have particularly small size, they might be clean of any nucleating impurities, therefore their crystallization is controlled by homogeneous nucleation and happens at the maximum possible undercooling, i.e., close to the glass transition temperature [48]. This is the situation for PHEA/PCL-TA_3(F) e PHEA/PCL-TA_3(B), but it has been previously reported for other systems, which all crystallize at temperatures of −40/−50 °C. For example, PCL crystallizes at these temperatures when it is segregated within nanosized spheres in block copolymers [49,50,51] or in the poly (lactide) interlamellar regions of partially miscible poly(lactide)-block-poly(caprolactone) copolymers [52].

3.4. Swelling capability of the prepared hydrogels

The trend of the swelling ratio (SR%) as a function of temperature for the samples based on neat PHEA and PCL-TA is given in Fig. 6. The data reported are SR% obtained after 24 h and represent equilibrium values. As an example, in Fig. S7 the swelling ratio as a function of time for the FP-samples based on PHEA is given. It is worth underlying that, as reported in the literature, although neat PHEA should be water soluble, it undergoes crosslinking due to the formation of a diester (ethylene glycol diacrylate) by transesterification reactions that take place during the polymerization process. It was found that SR% of PHEA decreases significantly with increasing temperature, dropping from ca. 110% at room temperature to ca. 90% at 70 °C.

The above behavior, previously reported for other PHEA-based hydrogels [53], was associated with an imbalance between hydrophilic and hydrophobic interactions inside the material, causing a decrease in the osmotic pressure difference. In addition, the crosslinked hydrogels were found to change their swelling behavior slightly, which is also independent of the type of polymerization, FP or BP. Considering the trend for the samples based on PCL-TA, it is evident that the swelling ratio was lower than for PHEA hydrogels (Fig. 6). This decrease, which was related to the amount of PCL, can be attributed to the hydrophobicity of the polymer. Nevertheless, even the hydrogel containing the highest amount of PCL (PHEA/PCL-TA_12(F)) maintained the ability to retain water, SR% being about 50%. Moreover, the swelling ratio was constant in the temperature range studied for the above hydrogels. To highlight the role of the star polymer functionality in this behavior, hydrogels based on PCL-OH were also studied. The curves reported in

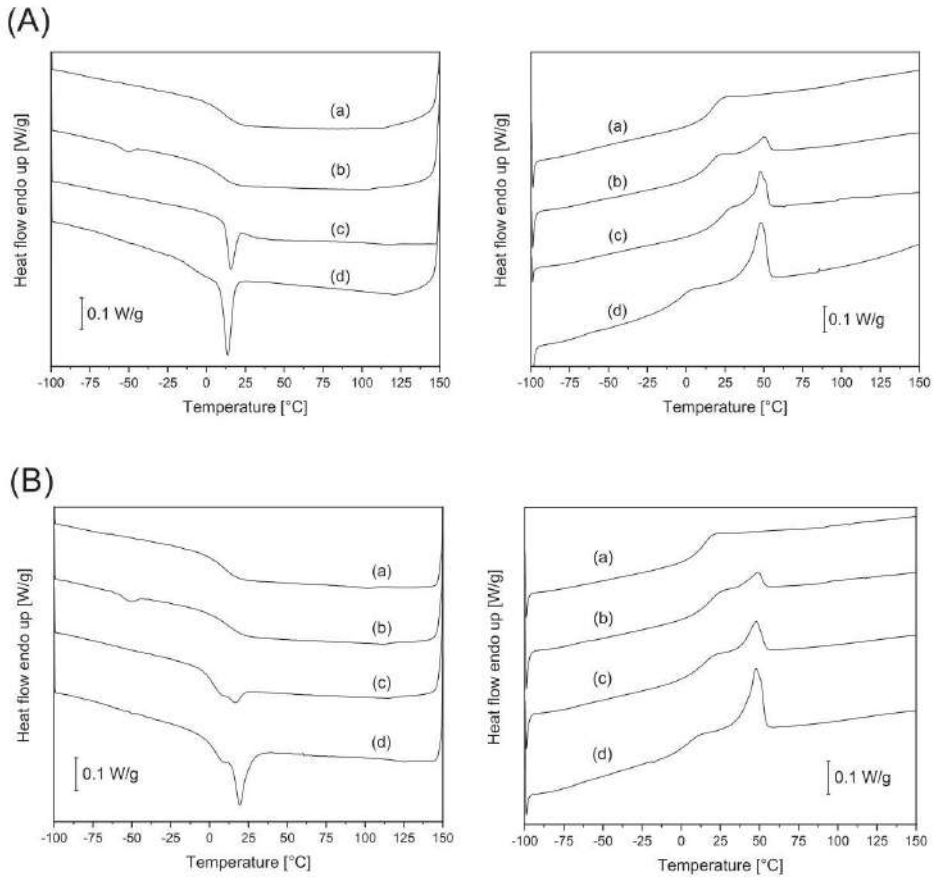

Fig. 5. (A) DSC traces on cooling and on heating of the xerogels prepared by FP: (a) PHEA(F), (b) PHEA/PCL-TA_3(F), (c) PHEA/PCL-TA_6(F) and (d) PHEA/PCL-TA_12(F). (B) DSC traces on cooling and on heating of the xerogels prepared by BP: (a) PHEA(B), (b) PHEA/PCL-TA_3(B), (c) PHEA/PCL-TA_6(B) and (d) PHEA/PCL-TA_12(B).

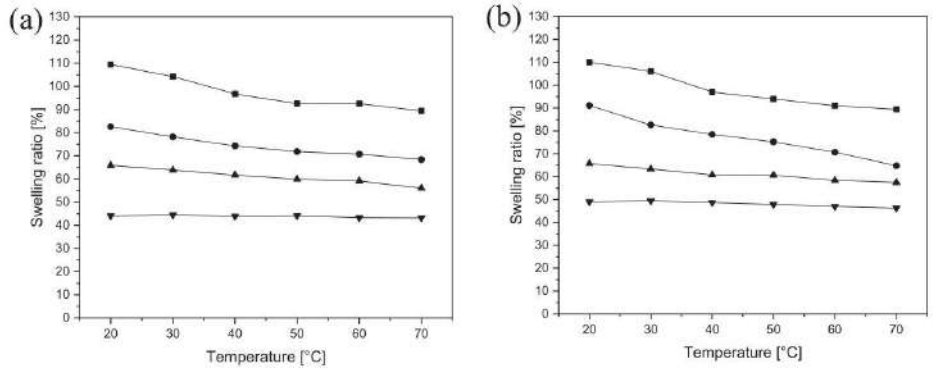

Fig. 6. Swelling ratio as a function of temperature of: (a) ■ PHEA(F), ● PHEA/PCL-TA_3(F), ▲ PHEA/PCL-TA_6(F) and ▼ PHEA/PCL-TA_12(F) and (b) ■ PHEA(B), ● PHEA/PCL-TA_3(B), ▲ PHEA/PCL-TA_6(B) and ▼ PHEA/PCL-TA_12(B).

Fig. S8 show that the hydrogels containing the star polymer bearing hydroxyl groups, which are not active in the polymerization process, exhibited a rapid SR% increase near the polymer melting temperature. This phenomenon could be related to the fact that the macromolecular chains are not blocked in the polymer network. Based on the described results, it can be concluded that the presence of PCL allows to tune and also stabilize SR%.

3.5. Mechanical properties of the prepared hydrogels

Mechanical properties of prepared hydrogels were tested in compression mode, and obtained results are reported in Fig. 7 and Table 3.

As it shown in Fig. 7, PHEA(F) exhibits the typical J shape stress–strain curves [54] of hydrogels reaching a compressive modulus of 0.77 ± 0.06 MPa and ultimate compressive strength at fracture of about 0.6 MPa at 28% strain.

The inclusion of PE-TA as crosslinker does not significantly affect the mechanical properties of the composites exhibiting comparable values of compressive modulus, as well as ultimate strain and resistance. By contrast, the presence of PCL-TA significantly increases the stiffness of hydrogel compared to PHEA(F). Indeed, the stiffness of the PCL containing hydrogels increases almost linearly with the PCL concentration as an effect of higher crosslinking density between PHEA chains, reaching the modulus of 2.76 ± 0.12 MPa and 5.32 ± 0.42 MPa for 6 and 12 PCL molar content, respectively. The comparison of obtained results for the two types of crosslinkers suggests a length-effect on the mechanical properties. This might be explained by a higher order in the hydrogel structure obtained with the longer crosslinker, as previously suggested for polyacrylamide hydrogels [55,56]. Moreover, hydrogels based on PCL-TA showed much higher resistance to compressive failure compared to the systems crosslinked with PE-TA. As an example, PHEA/PCL-TA_12(F) did not break during the compressive test, up to the maximum load applied, whereas the corresponding PHEA/PE-TA_12(F) failed at much lower compressive stress, as shown in Fig. S9.

4. Conclusions

In this work, frontal polymerization was efficiently applied to obtain new hydrogels based on PHEA and a PCL synthesized *ad hoc* and designed to have suitable features for this peculiar preparation method. The synthetic approach used allowed obtaining a star acrylated polymer (PCL-TA), with low molecular weight and acrylic functionalities, able to participate in the crosslinking/polymerization process. It was found that the presence of PCL-TA in the reaction mixture did not modify the polymerization, maintaining a pure frontal process, and it also allowed preparing a polymer system in which the two phases increased their compatibility.

It is of utmost relevance that the systems prepared, which showed much higher resistance to compressive failure and swelling stability, have a much higher modulus than hydrogels polymerized with a conventional crosslinker. The polymerization approach applied, which is fast and energy-efficient, as well as the properties imparted to the system by the bio-based polymer, make the developed materials promising and applicable in various fields.

CRediT authorship contribution statement

Giacomo Damonte: Investigation, Visualization, Writing – original draft. **Lorenza Maddalena:** Investigation, Visualization. **Alberto Fina:** Validation. **Dario Cavallo:** Validation. **Alejandro J. Müller:** Validation. **Maria Rosaria Caputo:** Investigation. **Alberto Mariani:** Conceptualization, Writing – review & editing. **Orietta Monticelli:** Conceptualization, Supervision, Writing – review & editing.

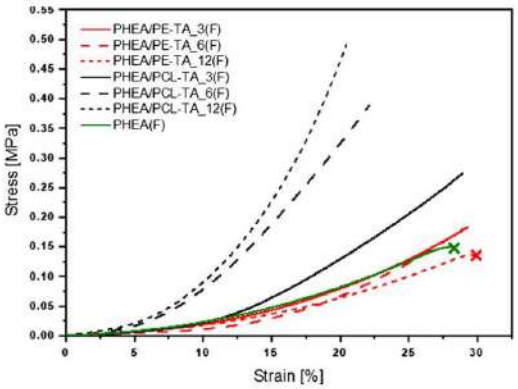

Fig. 7. Compression stress/strain of the hydrogels prepared by FP: (green) PHEA(F), (continuous, black) PHEA/PCL-TA_3(F), (dashed, black) PHEA/PCL-TA_6(F) and (short dashed line, black) PHEA/PCL-TA_12(F), (continuous, red) PHEA/PE-TA_3(F), (dashed, red) PHEA/PE-TA_6(F) and (short dashed, red) PHEA/PE-TA_12(F). (For interpretation of the references to colour in this figure legend, the reader is referred to the web version of this article.)

Table 3
Compression modulus of the hydrogels prepared by FP.

Sample code	E [MPa]
PHEA(F)	0.90 ± 0.04
PHEA/PE-TA_3(F)	0.96 ± 0.18
PHEA/PE-TA_6(F)	1.43 ± 0.14
PHEA/PE-TA_12(F)	0.78 ± 0.05
PHEA/PCL-TA_3(F)	1.71 ± 0.14
PHEA/PCL-TA_6(F)	2.85 ± 0.05
PHEA/PCL-TA_12(F)	5.44 ± 0.21

Declaration of Competing Interest

The authors declare that they have no known competing financial interests or personal relationships that could have appeared to influence the work reported in this paper.

Acknowledgement

AJM acknowledges funding from MICINN project PID2020-113045 GB-C21.

Appendix A. Supplementary material

Supplementary data to this article can be found online at https://doi.org/10.1016/j.eurpolymj.2022.111226.

References

[1] U.S.K. Madduma-Bandarage, S.V. Madihally, Synthetic hydrogels: synthesis, novel trends, and applications, J. Appl. Polym. Sci. 138 (19) (2021) 50376, https://doi.org/10.1002/app.50376.
[2] P. Nezhad-Mokhtari, M. Ghorbani, L. Roshangar, J. Soleimani Rad, A review on the construction of hydrogel scaffolds by various chemically techniques for tissue engineering, Eur. Polym. J. 117 (2019) 64–76, https://doi.org/10.1016/j.eurpolymj.2019.05.004.
[3] E.M. Ahmed, Hydrogel: Preparation, characterization, and applications: a review, J. Adv. Res. 6 (2) (2015) 105–121, https://doi.org/10.1016/j.jare.2013.07.006.
[4] S. Mantha, S. Pillai, P. Khayambashi, A. Upadhyay, Y. Zhang, O. Tao, H.M. Pham, S.D. Tran, Smart hydrogels in tissue engineering and regenerative medicine, Materials 12 (2019) 3323, https://doi.org/10.3390/ma12203323.

[5] E. Caló, V.V. Khutoryanskiy, Biomedical applications of hydrogels: a review of patents and commercial products, Eur. Polym. J. 65 (2015) 252–267, https://doi.org/10.1016/j.eurpolymj.2014.11.024.

[6] Q. Chai, Y. Jiao, X. Yu, Hydrogels for biomedical applications: their characteristics and the mechanisms behind them, Gels 3 (2017) 6, https://doi.org/10.3390/gels3010006.

[7] R. Vundavalli, S. Vundavalli, M. Nakka, D.S. Rao, Biodegradable nano-hydrogels in agricultural farming – alternative source for water resources, Proc. Mater. Sci. 10 (2015) 548–554, https://doi.org/10.1016/j.mspro.2015.06.005.

[8] D. Buenger, F. Topuz, J. Groll, Hydrogels in sensing applications, Prog. Polym. Sci. 37 (12) (2012) 1678–1719, https://doi.org/10.1016/j.progpolymsci.2012.09.001.

[9] A. Herrmann, R. Haag, U. Schedler, Hydrogels and their role in biosensing applications, Adv. Healthc. Mater. 10 (11) (2021) 2100062, https://doi.org/10.1002/adhm.202100062.

[10] K. Haraguchi, R. Farnworth, A. Ohbayashi, T. Takehisa, Compositional effects on mechanical properties of nanocomposite hydrogels composed of poly(N, N-dimethylacrylamide) and clay, Macromolecules 36 (15) (2003) 5732–5741, https://doi.org/10.1021/ma034366i.

[11] G. Gao, G. Du, Y. Sun, J. Fu, Self-healable, tough, and ultrastretchable nanocomposite hydrogels based on reversible polyacrylamide/montmorillonite adsorption, ACS Appl. Mater. Interf. 7 (8) (2015) 5029–5037, https://doi.org/10.1021/acsami.5b00704.

[12] M.I. Sujan, S.D. Sarkar, S. Sultana, L. Bushra, R. Tareq, C.K. Roy, M.S. Azam, Bi-functional silica nanoparticles for simultaneous enhancement of mechanical strength and swelling capacity of hydrogels, RSC Adv. 10 (11) (2020) 6213–6222.

[13] D.H. Lee, A. Tamura, Y. Arisaka, J.-H. Seo, N. Yui, Mechanically reinforced gelatin hydrogels by introducing slidable supramolecular crosslinkers, Polymers 11 (2019) 1787, https://doi.org/10.3390/polym11111787.

[14] G. Kaklamani, D. Cheneler, L.M. Grover, M.J. Adams, J. Bowen, Mechanical properties of alginate hydrogels manufactured using external gelation, J. Mech. Behav. Biomed. Mater. 36 (2014) 135–142, https://doi.org/10.1016/j.jmbbm.2014.04.013.

[15] X. Li, Q. Sun, Q. Li, N. Kawazoe, G. Chen, Functional hydrogels with tunable structures and properties for tissue engineering applications, Front. Chem. 6 (2018), https://doi.org/10.3389/fchem.2018.00499.

[16] P. Arnaldi, D. Di Lisa, L. Maddalena, F. Carosio, A. Fina, L. Pastorino, O. Monticelli, A facile approach for the development of high mechanical strength 3D neuronal network scaffold based on chitosan and graphite nanoplatelets, Carbohydr. Polym. 271 (2021) 118420, https://doi.org/10.1016/j.carbpol.2021.118420.

[17] R. Liu, S. Liang, X.-Z. Tang, D. Yan, X. Li, Z.-Z. Yu, Tough and highly stretchable graphene oxide/polyacrylamide nanocomposite hydrogels, J. Mater. Chem. 22 (28) (2012) 14160, https://doi.org/10.1039/c2jm32541a.

[18] A.K. Gaharwar, N.A. Peppas, A. Khademhosseini, Nanocomposite hydrogels for biomedical applications, Biotechnol. Bioeng. 111 (3) (2014) 441–453, https://doi.org/10.1002/bit.25160.

[19] F. Sánchez-Correa, C. Vidaurre-Agut, Á. Serrano-Aroca, A.J. Campillo-Fernández, Poly(2-hydroxyethyl acrylate) hydrogels reinforced with graphene oxide: remarkable improvement of water diffusion and mechanical properties, J. Appl. Polym. Sci. 135 (15) (2018) 46158, https://doi.org/10.1002/app.46158.

[20] E. Seo, S. Kumar, J. Lee, J. Jang, J.H. Park, M.C. Chang, I. Kwon, J.-S. Lee, Y.-i. Huh, Modified hydrogels based on poly(2-hydroxyethyl methacrylate) (pHEMA) with higher surface wettability and mechanical properties, Macromol. Res. 25 (7) (2017) 704–711, https://doi.org/10.1007/s13233-017-5068-y.

[21] M. Labet, W. Thielemans, Synthesis of polycaprolactone: a review, Chem. Soc. Rev. 38 (12) (2009) 3484, https://doi.org/10.1039/b820162p.

[22] J.A. Pojman, G. Curtis, V.M. Ilyashenko, Frontal polymerization in solution, J. Am. Chem. Soc. 118 (15) (1996) 3783–3784, https://doi.org/10.1021/ja9600688.

[23] I.D. Robertson, M. Yourdkhani, P.J. Centellas, J.E. Aw, D.G. Ivanoff, E. Goli, E. M. Lloyd, L.M. Dean, N.R. Sottos, P.H. Geubelle, J.S. Moore, S.R. White, Rapid energy-efficient manufacturing of polymers and composites via frontal polymerization, Nature 557 (7704) (2018) 223–227, https://doi.org/10.1038/s41586-018-0054-x.

[24] N.S. Chechilo, N.M. Khvilivitskii, R.J. Enikolopyan, On the phenomenon of polymerization reaction spreading, Dokl. Akad. Nauk. (1972) 1180–1181.

[25] D. Nuvoli, V. Alzari, J.A. Pojman, V. Sanna, A. Ruiu, D. Sanna, G. Malucelli, A. Mariani, Synthesis and characterization of functionally gradient materials obtained by frontal polymerization, ACS Appl. Mater. Interfaces. 7 (6) (2015) 3600–3606, https://doi.org/10.1021/am507725k.

[26] S. Fiori, A. Mariani, L. Ricco, S. Russo, First synthesis of a polyurethane by frontal polymerization, Macromolecules. 36 (8) (2003) 2674–2679, https://doi.org/10.1021/ma0211941.

[27] A. Mariani, S. Bidali, S. Fiori, G. Malucelli, E. Sanna, Synthesis and characterization of a polyurethane prepared by frontal polymerization, E-Polymers. 3 (2003), https://doi.org/10.1515/epoly.2003.3.1.587.

[28] P. Baheti, C. Bonneaud, C. Bouilhac, C. Joly-Duhamel, S.M. Howdle, P. Lacroix-Desmazes, Novel green route towards polyesters-based resin by photopolymerization of star polymers, Exp. Polym. Lett. 13 (12) (2019) 1104–1115, https://doi.org/10.3144/expresspolymlett.2019.95.

[29] T. Chen, T. Cai, Q. Jin, J. Ji, Design and fabrication of functional polycaprolactone, E-Polymers 15 (2015) 3–13, https://doi.org/10.1515/epoly-2014-0158.

[30] G. Damonte, A. Vallin, A. Fina, O. Monticelli, On the development of an effective method to produce conductive pcl film, Nanomaterials 11 (2021) 1385, https://doi.org/10.3390/nano11061385.

[31] G. Damonte, A. Vallin, D. Battegazzore, A. Fina, O. Monticelli, Synthesis and characterization of a novel star polycaprolactone to be applied in the development of graphite nanoplates-based nanopapers, React. Funct. Polym. 167 (2021) 105019, https://doi.org/10.1016/j.reactfunctpolym.2021.105019.

[32] E.R. Leone, L.S. Ferraraccio, G. Damonte, P. Lova, P. Bertoncello, O. Monticelli, On the development of electrochemical sensors coated with polycaprolactone, Electrochem. Commun. 129 (2021) 107089, https://doi.org/10.1016/j.elecom.2021.107089.

[33] M.A. Woodruff, D.W. Hutmacher, The return of a forgotten polymer - polycaprolactone in the 21st century, Prog. Polym. Sci. 35 (10) (2010) 1217–1256, https://doi.org/10.1016/j.progpolymsci.2010.04.002.

[34] L.J. Gibson, Cellular solids, MRS Bull. 28 (4) (2003) 270–274, https://doi.org/10.1557/mrs2003.79.

[35] S. Khoee, Y. Bagheri, A. Hashemi, Composition controlled synthesis of PCL–PEG janus nanoparticles: magnetite nanoparticles prepared from one-pot photo-click reaction, Nanoscale. 7 (9) (2015) 4134–4148, https://doi.org/10.1039/C4NR06590E.

[36] M. Biswas, J.A. Libera, S.B. Darling, J.W. Elam, Polycaprolactone: a promising addition to the sequential infiltration synthesis polymer family identified through in situ infrared spectroscopy, ACS Appl. Polym. Mater. 2 (12) (2020) 5501–5510, https://doi.org/10.1021/acsapm.0c00855l0.1021/acsapm.0c00855.s001.

[37] J.F. Jean-Pierre Fouassier, Rabek, Radiation curing in polymer science and technology - volume II, Springer. (1993), https://doi.org/10.1007/978-94-011-1876-7.

[38] K. Żółtowska, M. Sobczak, E. Olędzka, Novel zinc-catalytic systems for ring-opening polymerization of ε-caprolactone, Molecules 20 (2015) 2816–2827, https://doi.org/10.3390/molecules20022816.

[39] I. Kerman, L. Toppare, F. Yilmaz, Y. Yagci, Thiophene ended ε-caprolactone conducting copolymers and their electrochromic properties, J. Macromol. Sci. Part A. 42 (4) (2005) 509–520, https://doi.org/10.1081/MA-200054363.

[40] F. Pardal, V. Lapinte, J.-J. Robin, Kinetics of cotelomerization of 3-(trimethoxysilyl)propyl methacrylate and perfluorodecylacrylate, Eur. Polym. J. 45 (4) (2009) 1198–1207, https://doi.org/10.1016/j.eurpolymj.2008.12.035.

[41] J.-L. Wang, C.-M. Dong, Physical properties, crystallization kinetics, and spherulitic growth of well-defined poly(ε-caprolactone)s with different arms, Polymer 47 (9) (2006) 3218–3228, https://doi.org/10.1016/j.polymer.2006.02.047.

[42] M. Unger, C. Vogel, H.W. Siesler, Molecular weight dependence of the thermal degradation of poly(ε-caprolactone): a thermogravimetric differential thermal fourier transform infrared spectroscopy study, Appl. Spectrosc. 64 (7) (2010) 805–809, https://doi.org/10.1366/000370210791666309.

[43] S.P. Davtyan, A.O. Tonoyan, The frontal polymerization method in high technology applications, Rev. J. Chem. 9 (1) (2019) 71–94, https://doi.org/10.1134/S2079978018040039.

[44] V. Alzari, D. Nuvoli, S. Scognamillo, M. Piccinini, E. Gioffredi, G. Malucelli, S. Marceddu, M. Sechi, V. Sanna, A. Mariani, Graphene-containing thermoresponsive nanocomposite hydrogels of poly(N-isopropylacrylamide) prepared by frontal polymerization, J. Mater. Chem. 21 (24) (2011) 8727, https://doi.org/10.1039/c1jm11076d.

[45] G. Malucelli, J. Dore, D. Sanna, D. Nuvoli, M. Rassu, A. Mariani, V. Alzari, Sliding crosslinked thermoresponsive materials: polypseudorotaxanes made of poly(N-isopropylacrylamide) and acrylamide-γ-cyclodextrin, Front. Chem. 6 (2018) 1–8, https://doi.org/10.3389/fchem.2018.00585.

[46] E. Vargün, A. Usanmaz, Polymerization of 2-hydroxyethyl acrylate in bulk and solution by chemical initiator and by ATRP method, J. Polym. Sci. Part A Polym. Chem. 43 (17) (2005) 3957–3965, https://doi.org/10.1002/pola.20867.

[47] I. Sedov, T. Magsumov, A. Abdullin, E. Yarko, T. Mukhametzyanov, A. Klimovitsky, C. Schick, Influence of the cross-link density on the rate of crystallization of poly (ε-caprolactone), Polymers. 10 (2018) 902, https://doi.org/10.3390/polym10080902.

[48] L. Sangroniz, B. Wang, Y. Su, G. Liu, D. Cavallo, D. Wang, A.J. Müller, Fractionated crystallization in semicrystalline polymers, Prog. Polym. Sci. 115 (2021) 101376, https://doi.org/10.1016/j.progpolymsci.2021.101376.

[49] S. Nojima, M. Toei, S. Hara, S. Tanimoto, S. Sasaki, Size dependence of crystallization within spherical microdomain structures, Polymer 43 (14) (2002) 4087–4090, https://doi.org/10.1016/S0032-3861(02)00217-3.

[50] A.J. Müller, V. Balsamo, M.L. Arnal, T. Jakob, H. Schmalz, V. Abetz, Homogeneous nucleation and fractionated crystallization in block copolymers, Macromolecules. 35 (8) (2002) 3048–3058, https://doi.org/10.1021/ma012026w.

[51] A.J. Müller, V. Balsamo, M.L. Arnal, Nucleation and crystallization in diblock and triblock copolymers, Adv. Polym. Sci. 190 (2005), https://doi.org/10.1007/12_001.

[52] R.V. Castillo, A.J. Müller, J.-M. Raquez, P. Dubois, Crystallization kinetics and morphology of biodegradable double crystalline PLLA-b-PCL diblock copolymers, Macromolecules 43 (9) (2010) 4149–4160, https://doi.org/10.1021/ma100201g.

[53] G.A. Mun, B.B. Yermukhambetova, P.I. Urkimbayeva, R.B. Bakytbekov, G. S. Irmukhametova, R.A. Mangazbayeva, I.E. Suleimenov, Synthesis and characterization of water soluble and water swelling thermo-sensitive copolymers based on 2-hydroxyethylacrylate and 2-hydroxyethylmethacrylate, AASRI Proc. 3 (2012) 601–606, https://doi.org/10.1016/j.aasri.2012.11.095.

[54] Y.-W. Mai, A.G. Atkins, Further comments on J-shaped stress-strain curves and the crack resistance of biological materials, J. Phys. D. Appl. Phys. 22 (1) (1989) 48–54, https://doi.org/10.1088/0022-3727/22/1/007.
[55] K. Syverud, S.R. Pettersen, K. Draget, G. Chinga-Carrasco, Controlling the elastic modulus of cellulose nanofibril hydrogels—scaffolds with potential in tissue engineering, Cellulose 22 (1) (2015) 473–481, https://doi.org/10.1007/s10570-014-0470-5.
[56] J. Zaragoza, A. Chang, P. Asuri, Effect of crosslinker length on the elastic and compression modulus of poly(acrylamide) nanocomposite hydrogels, J. Phys. Conf. Ser. 790 (2017) 012037, https://doi.org/10.1088/1742-6596/790/1/012037.

Supporting Information - On novel hydrogels based on poly(2-hydroxyethyl acrylate) and polycaprolactone with improved mechanical properties prepared by frontal polymerization

Supporting Information

On novel hydrogels based on poly(2-hydroxyethyl acrylate) and polycaprolactone with improved mechanical properties prepared by frontal polymerization

Giacomo Damonte[1], Lorenza Maddalena[2], Alberto Fina[2], Dario Cavallo[1], Alejandro J. Müller[3,4], Maria Rosaria Caputo[3,4], Alberto Mariani[5], Orietta Monticelli[1*]*

[1]Dipartimento di Chimica e Chimica Industriale, Università di Genova, Via Dodecaneso 31, 16146 Genova, Italy

[2]Dipartimento di Scienza Applicata e Tecnologia, Politecnico di Torino-Alessandria campus, Viale Teresa Michel, 5, 15121 Alessandria, Italy

[3]POLYMAT and Department of Polymers and Advanced Materials: Physics, Chemistry and Technology, Faculty of Chemistry, University of the Basque Country UPV/EHU, Paseo Manuel de Lardizabal 3, 20018, Donostia-San Sebastián, Spain

[4]IKERBASQUE, Basque Foundation for Science, Bilbao, 48009, Spain

[5]Dipartimento di Chimica e Farmacia, Università di Sassari, and INST, Via Vienna 2, 07100 Sassari, Italy

*Corresponding authors: orietta.monticelli@unige.it; mariani@uniss.it

(a)

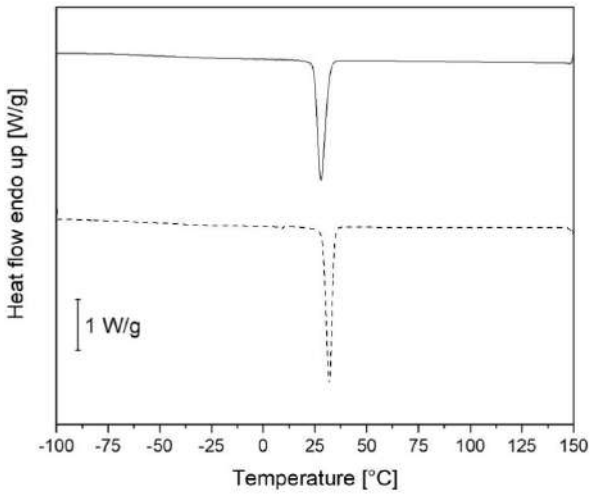

(b)

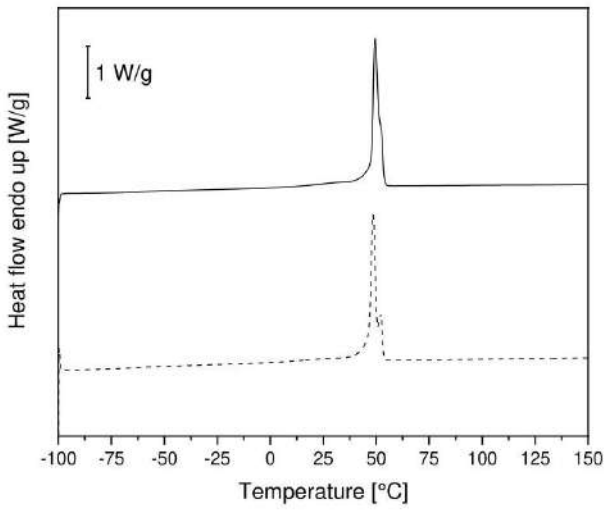

Fig. S1. DSC traces on (a) cooling and (b) on heating of: PCL-star-4-2k-OH (continuous line) and PCL-star-4-2k-tetra acrylate (dashed line).

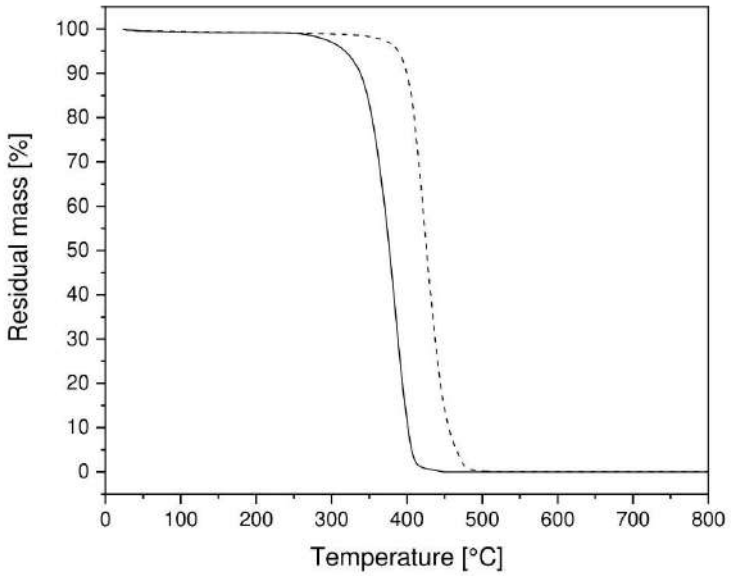

Figure S2. TGA curves of: PCL-star-4-2k-OH (continuous line) and PCL-star-4-2k-tetra acrylate (dashed line).

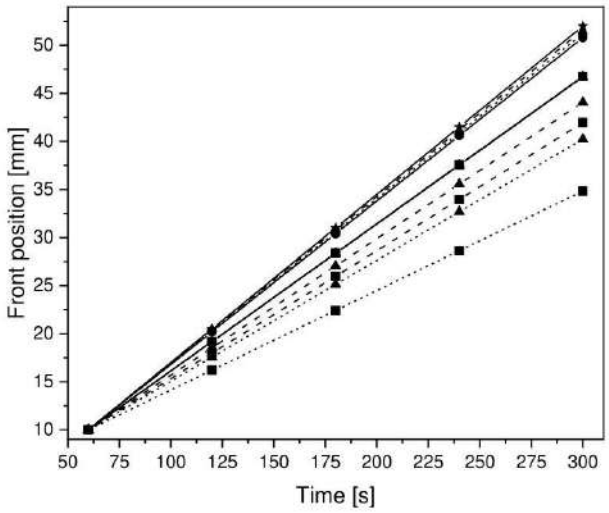

Figure S3. Front position as a function of time of: ★ PHEA(F) continuous line, ● PHEA/PE-TA_3(F) continuous line, ● PHEA/PE-TA_6(F) dashed line, ● PHEA/PE-TA_12(F) short dashed line, ▲ HEA/PCL-TA_3(F) continuous line, ▲ HEA/PCL-TA_6(F) dashed line, ▲ HEA/PCL-TA_12(F) short dashed line, ■ PHEA/PCL-OH_3(F) continuous line, ■ PHEA/PCL-OH_6(F) dashed line, ■ PHEA/PCL-OH_12(F) short dashed line.

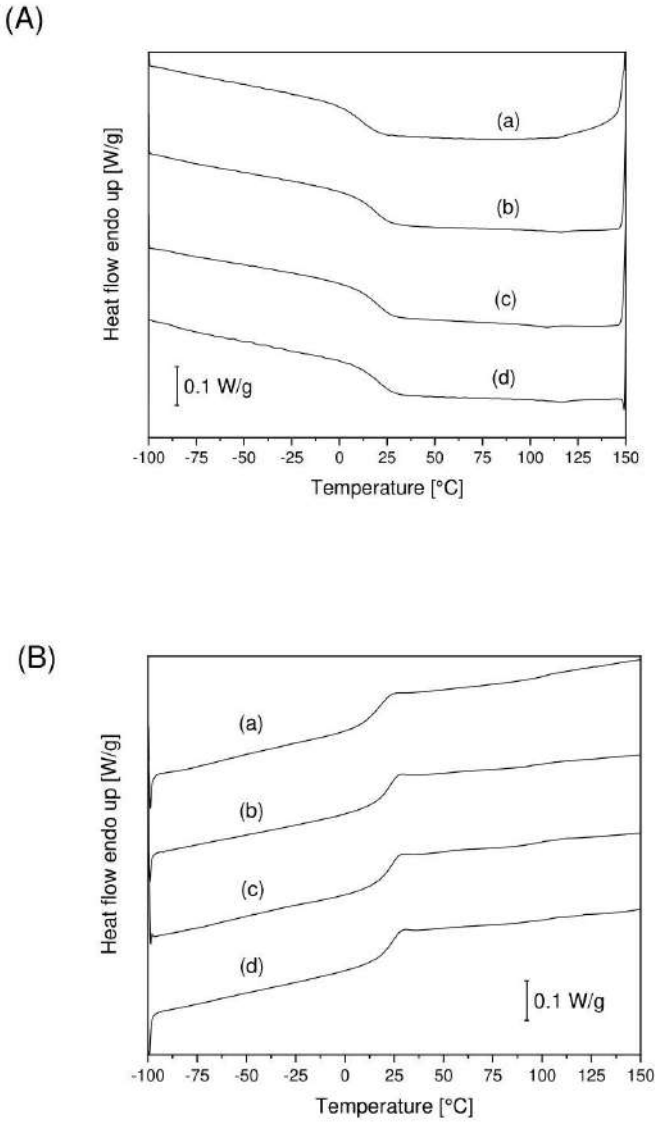

Figure S4. DSC traces on (A) cooling and (B) on heating of: (a) PHEA(F), (b) PHEA/PE-TA_3(F), (c) PHEA/PE-TA_6(F) and (d) PHEA/PE-TA_12(F).

(A)

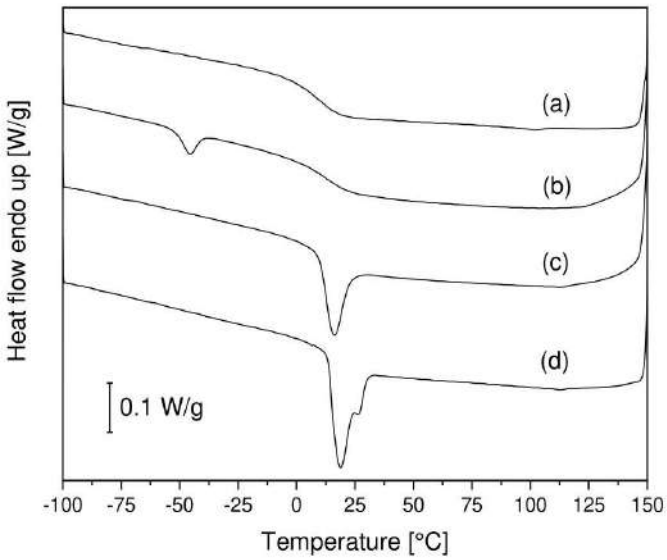

(B)

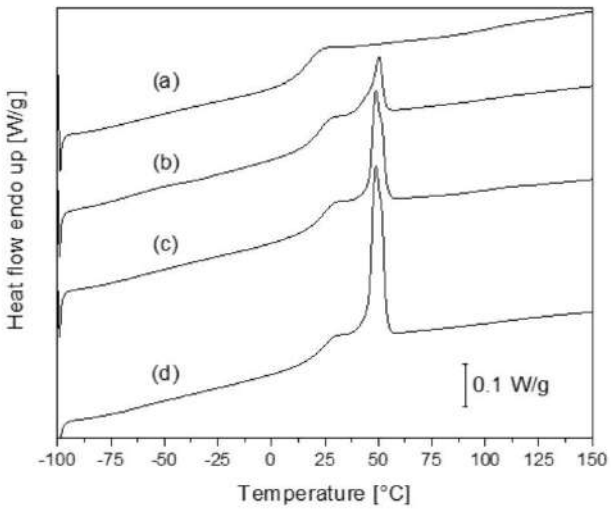

Figure S5. DSC traces on (A) cooling and (B) on heating of: (a) PHEA(F), (b) PHEA/PCL-OH_3(F), (c) PHEA/PCL-OH_6(F) and (d) PHEA/PCL-OH_12(F).

Table S1. Thermal properties of the neat PHEA and the xerogels based on PCL-star-4-2k-OH (PCL-OH)

Sample code	T_c [°C]	ΔH_c [J/g]	T_g [°C]	T_m [°C]	ΔH_m [J/g]	$\chi_{c\ CORR}$ [%]
PHEA(F)	-	-	15	-	-	-
PHEA/PCL-OH_3(F)	-45	-2	22	50	5	62
PHEA/PCL-OH_6(F)	19	-9	24	49	9	59
PHEA/PCL-OH_12(F)	19	-15	24	49	15	54

The subscript m and c indicate the values measured during melting and crystallization, respectively. χ_c is the degree of crystallinity calculated by assuming the ideal enthalpies of fusion as 139 J/g and considering PCL content in the xerogel.

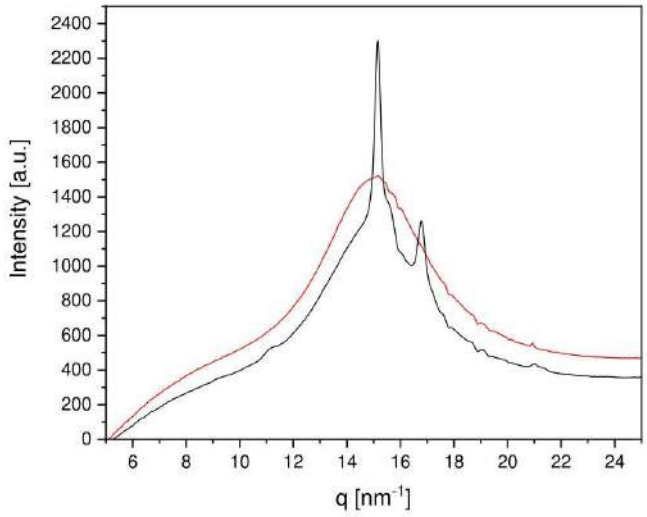

Figure S6. WAXD profile of: PHEA/PCL-TA_3(F) (red line) and PHEA/PCL-TA_12(F) (black line)

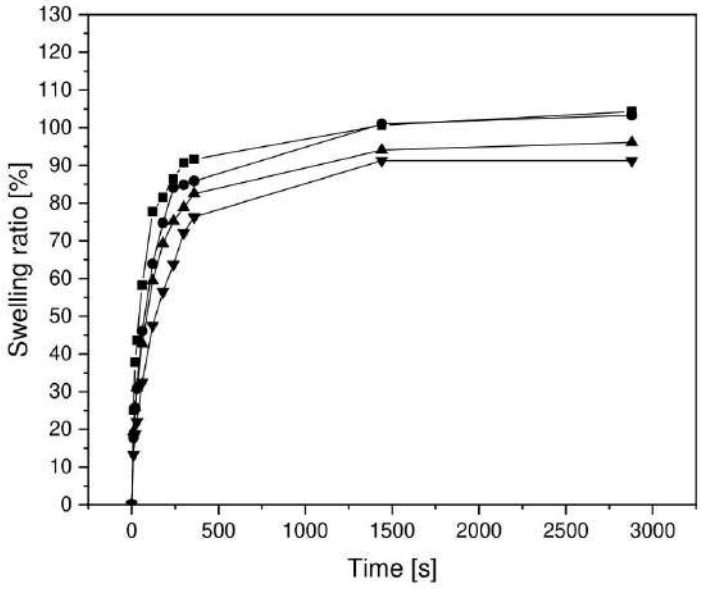

Figure S7. Swelling ratio as a function of time of: ■ PHEA(F), ● PHEA/PCL-TA_3(F), ▲ PHEA/PCL-TA_6(F) and ▼ PHEA/PCL-TA_12(F)

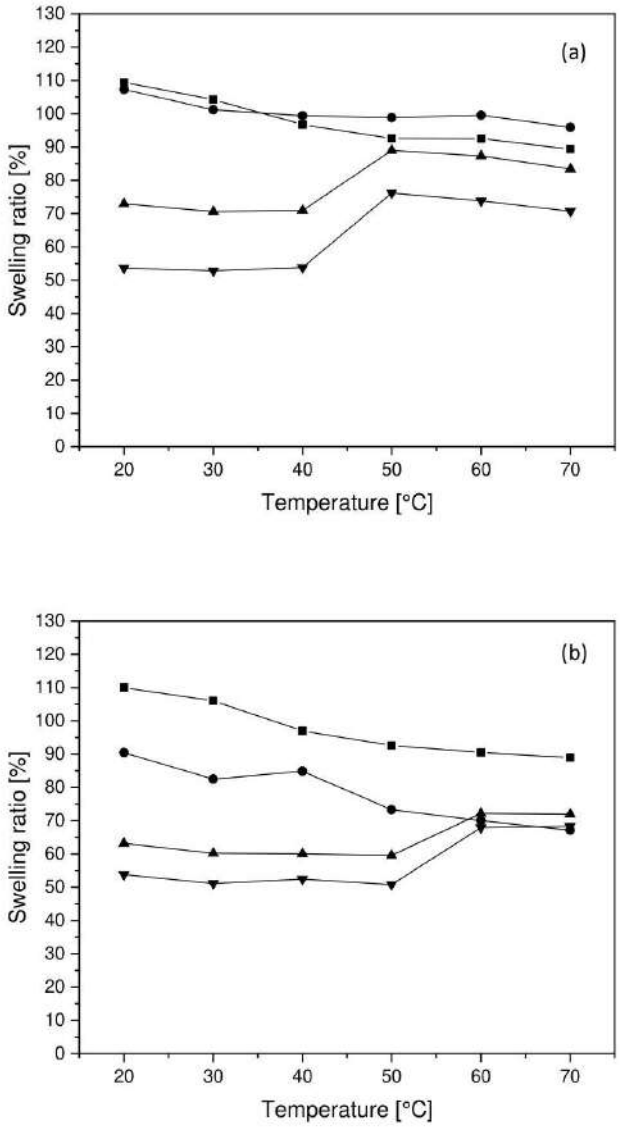

Figure S8. Swelling ratio as a function of temperature of: (a) ■ PHEA(F), ● PHEA/PCL-OH_3(F), ▲ PHEA/PCL-OH_6(F) and ▼ PHEA/PCL-OH_12(F) and (b) ■ PHEA(B), ● PHEA/PCL-OH_3(B), ▲ PHEA/PCL-OH_6(B) and ▼ PHEA/PCL-OH_12(B).

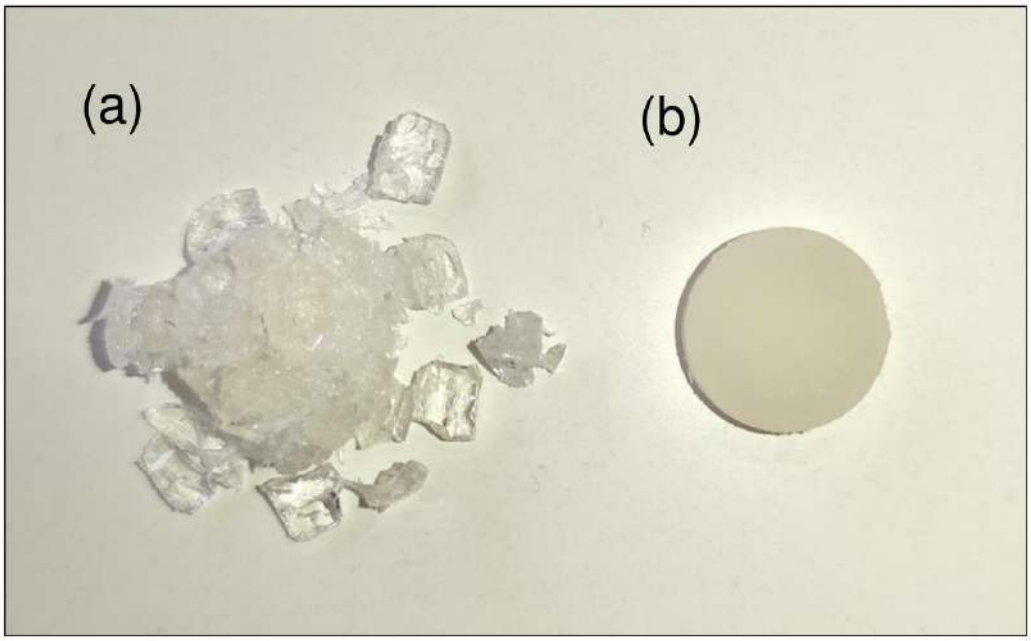

Figure S9. Photos of: (a) PHEA/PE-TA_12(F) and (b) PHEA/PCL-TA_12(F) after compression test.

Chapter 5: Multifunctional porous films based on polylactic acid/polycaprolactone blend and graphite nanoplatelets

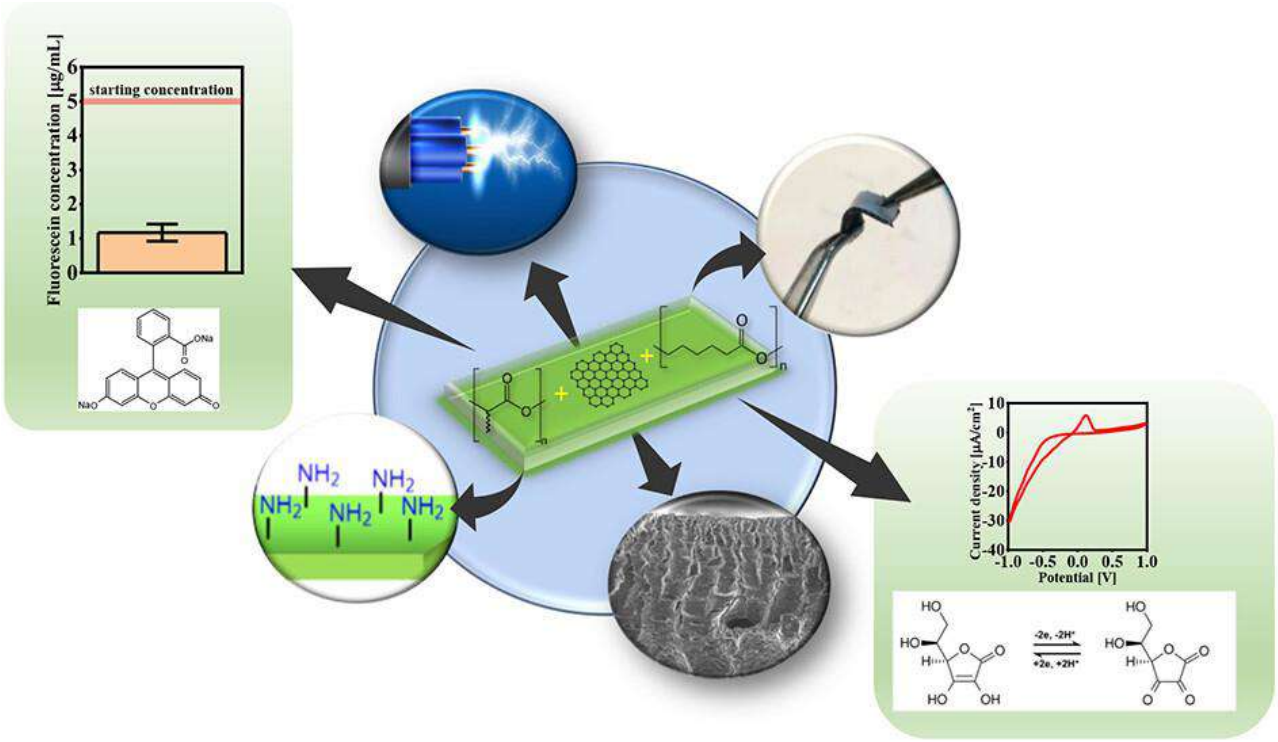

ACS APPLIED POLYMER MATERIALS

pubs.acs.org/acsapm Article

Multifunctional Porous Films Based on Polylactic Acid/ Polycaprolactone Blend and Graphite Nanoplateles

Giacomo Damonte, Roberto Spotorno, Daniela Di Fonzo, and Orietta Monticelli*

Cite This: *ACS Appl. Polym. Mater.* 2022, 4, 6521−6530 Read Online

ACCESS | Metrics & More | Article Recommendations | Supporting Information

ABSTRACT: The aim of this work was to develop polylactic acid (PLA) based porous films with suitable properties to be used as sensors and absorbers. The formulation was designed to make the films porous, ductile, and conductive and characterized by surface functionalization. The phase inversion method was used to impart porosity to the polymer film. Polycaprolactone (PCL) and graphite, in the form of graphite nanoplatelets (GNP), were added to increase the elongation at break of the polymer matrix and to make the systems conductive, respectively. To optimize the formulation, the effect of polymer concentration in the initial solution on the viscosity, porosity, and morphology was investigated. FE-SEM measurements showed that the phase inversion method allowed limiting the aggregation of both PCL domains and GNP, whose flakes were found to adhere well to the polymer matrix and to have a nucleating effect, as evidenced by DSC measurements. A simple aminolysis reaction was performed using a diamine, i.e., ethylenediamine, to generate surface amino functionalities. In particular, the extent of functionalization as a function of reaction time was investigated by using FT-IR spectroscopic measurements. By combining these results with the stability of the polymer film, which tends to lose its structural integrity due to the erosion caused by the aminolysis reaction, the optimal contact time with the aqueous solution of ethylenediamine was found. Mechanical measurements showed that the presence of PCL increased the elongation at break of films by 3 times compared to neat PLA. Finally, the films developed starting from the optimized formulations based on PLA/PCL blends, containing GNP and surface functionalized, proved to be effective electrodes for the voltammetric determination of ascorbic acid. In addition, it is of utmost relevance that both amino functionalization and GNP conferred high capacity to the films to retain fluorescein, a model dye.

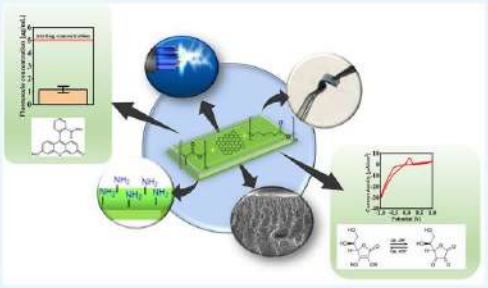

KEYWORDS: *PLA, porous film, blend, graphite, sensors, adsorption*

1. INTRODUCTION

The significant interest in bioplastics has led both academic and industrial researchers to find strategies to improve their features and to disclose different properties in order to expand their exploitation.[1−3] In the case of biopolymers, the design of innovative applications must take into account some of their drawbacks[3] and endow them with different properties by applying scalable approaches.[4,5] The aim of our work was to develop systems based on polylactic acid (PLA), one of the most promising bioplastics,[2,3] suitable for sensing applications and characterized by a high adsorption capacity, taking into account the aspects mentioned above. Indeed, films suitable for these uses should have specific properties such as (i) high porosity to favor the contact surface with the analyte or the component to be adsorbed, (ii) adequate mechanical properties, (iii) electrical conductivity in the case of sensing applications, and (iv) specific surface functionalities to interact with the analyte or component to be adsorbed.

In general, porous PLA films, used mainly in the biomedical field,[6,7] were prepared by dip precipitation, a process in which the polymer solution is poured onto a glass plate and then immersed in a coagulation bath. Indeed, when the polymer solution comes into contact with the nonsolvent during solidification, two phases (a polymer-rich phase and a polymer-poor phase) form rapidly due to the uneven exchange between the nonsolvent and the solvent.[8] Subsequently, pores form in the polymer-poor phase due to the loss of nonsolvent and solvent.[8] Even in the early works dealing with the preparation of porous films based on PLA,[7,9] it was reported that the exchange rate between the solvent and the nonsolvent affects the morphology of the membrane. In addition, the influence of the PLA concentration in the casting solution was demonstrated by Liu et al.,[7] who also studied the equilibrium phase

Received: June 1, 2022
Accepted: July 22, 2022
Published: August 11, 2022

https://doi.org/10.1021/acsapm.2c00923
ACS Appl. Polym. Mater. 2022, 4, 6521−6530

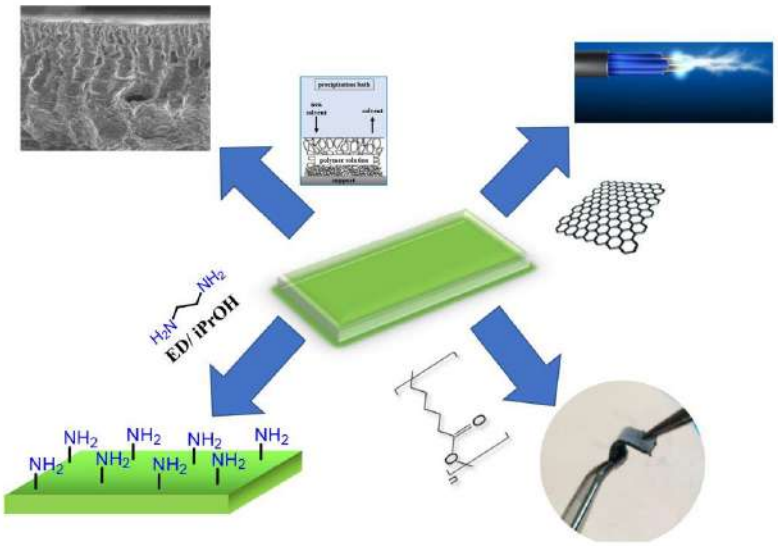

Figure 1. Scheme of the properties of the developed films.

diagram of PLA, methylene chloride, and ethanol. Van de Witte et al.[9] also investigated the relationship between the final porous structure and the polymer/solvent/nonsolvent phase diagram and found that the segregation process is the key factor affecting the evolution of the morphology. Using a coagulation bath of ethanol and water, Xing et al.[10] showed that as the water concentration increased the uniform spongelike structure was damaged.

More recently, Hu et al.[11] proposed a membrane preparation method based on the application of an ultrasonic atomizer, which changes the state of the nonsolvent from water to water droplets to control the exchange rate between the solvent and the nonsolvent. The application of the above approach resulted in a decrease in the phase inversion rate between solvent and water droplets, which prolonged the solidification time and affected the membrane morphology.

All these works were mainly focused on studying the influence of the preparation conditions on the final morphology of the membrane rather than its properties. Moreover, it is worth mentioning that the solvents used for the casting solutions were those generally applied to dissolve this polymer, such as chloroform and dichloromethane. In our work, PLA was combined with graphite nanoplateles (GNP) to make the membrane conductive and thus applicable in the sensing field, by using an unconventional solvent. Indeed, there are several works in the literature reporting the fabrication of dense films based on PLA and graphite,[12−14] but in this work, we attempted to develop a porous composite system for the first time. In order to favor the dispersion of the filler and thus the possibility of obtaining a percolating system, a solvent that promotes the dispersion of the graphite was used. Solvents with these properties are those characterized by a surface energy close to that of graphite, such as 1-methyl-2-pyrrolidinone, dimethylformamide, and *N*,*N*-dimethylacetamide.[15]

Considering the poor mechanical properties of PLA, especially in terms of elongation at break, it was decided to add a biobased polymer to the formulation that can increase the ductility of the polymer matrix, i.e., polycaprolactone (PCL).[16,17] As widely reported in the literature, the final properties of the PLA/PCL blend are influenced by the compatibility of the two polymers and, as recently highlighted, by the size of the PCL domains.[18] It is important to underline that the technique used to prepare the films can favor the dispersion of graphite, since the precipitation in the coagulation bath can freeze the distribution of the filler in the liquid medium and affect the size of the PCL domains.[19] Finally, the issue of limited functionality of the polymer was addressed by applying a simple aminolysis reaction to the formed membrane, which may promote the formation of amino groups on the polymer surface when a diamine is used.[20−22] The scheme shown in Figure 1 illustrates the properties of the developed films (conductivity, ductility, porosity, and functionalization) as a function of the selected formulation, i.e., GNP and PCL addition, preparation method, and surface aminolysis.

2. EXPERIMENTAL SECTION

2.1. Materials. Polylactic acid (PLA) Luminy LX175 (M_n = 163 000 g/mol, melt flow index (MFI) = 6.0 g/10 min) was purchased from Corbion (Amsterdam, Netherlands). Polycaprolactone (PCL) was obtained from Perstorp (Malmö, Sweden; CAPA 6500, M_n = 50 000 g/mol, MFI = 7 g/10 min). *N*,*N*-Dimethylformamide (DMF), ethylenediamine, 2-propanol (iPrOH), and ascorbic acid (AA) were purchased from Sigma-Aldrich and used as received. Graphite nanoplatelets (GNP) prepared by thermal reduction of graphene oxide (GO), with a BET surface area of 196 m^2/g, were supplied by Avanzare Innovacion Tecnologica (Navarrete, Spain).

2.2. Porous Film Preparation. PLA solutions were prepared by dissolving different amounts of polymer in 10 mL of DMF at 80 °C to obtain concentrations of 5, 10, 15, and 20% w/v (Table 1). Porous films were prepared by casting the PLA/DMF solutions onto a glass

https://doi.org/10.1021/acsapm.2c00923
ACS Appl. Polym. Mater. 2022, 4, 6521−6530

Table 1. Characteristics of the Prepared Films[a]

sample code	polymer concn [% w/v]	PLA	PCL	GNP
PLA_5	5	100	–	–
PLA_10	10	100	–	–
PLA_15	15	100	–	–
PLA_20	20	100	–	–
PLA_25	25	100	–	–
PCL_10	10	–	100	–
PLA_PCL_95_5	10	95	5	–
PLA_PCL_90_10	10	90	10	–
PLA_PCL_80_20	10	80	20	–
PLA_PCL_G_95_5_0.5	10	95	5	0.5
PLA_PCL_G_95_5_1	10	95	5	1.0

[a]Solvent, DMF; solution temperature, 80 °C; coagulation bath temperature, 25 °C.

plate and then immediately placing them in coagulation baths (25 °C), where they remained for 2 h. The films were washed by soaking them in water for 6 h, repeatedly exchanging the water. The as-prepared films were dried for 24 h at room temperature and then in a vacuum oven at 30 °C. A polymer concentration of 10% w/v was selected to prepare PLA/PCL blend films, since the above concentration allowed the development of films with the best rigidity−toughness−porosity balance. Different PLA/PCL ratios (95/5, 90/10, and 80/20) were introduced in the solution, and the films were prepared following the procedure previously described. The films were defined by indicating in the code the polymer concentration and the PLA/PCL ratio (as an example, PLA_PCL_80_20 indicates a film prepared with a polymer concentration of 10% w/v, namely the optimized formulation, and with a ratio PLA/PCL of 80/20).

2.3. Composite Film Preparation. GNP powder was sonicated in a sonication bath at 40 kHz for 120 min in 10 mL of DMF at 80 °C to obtain a homogeneous suspension. The amount of GNP was adjusted to obtain concentrations of 0.5 and 1 wt % in the polymer film. Then, 3 mL of a 10% (w/v) PLA/PCL polymer solution (with a PLA/PCL ratio of 95/5) in DMF was added to the GNP dispersion and sonicated for 2 h at 80 °C. Finally, the phase inversion method described above was used to obtain the porous composite film.

2.4. Film Functionalization. Aminolysis reaction conditions were established with porous PLA films (10 × 20 mm^2) prepared from 10% w/v polymer solutions. The films were prewetted in 5 mL of isopropanol for 5 min. After this time, an equal volume of a 10% v/v ethylenediamine solution in isopropanol was added to reach a final amine concentration of 5 wt %, and the reaction was run for different reaction times (15, 30, 60, 120, 180 min) at 30 °C. At the end of the reaction, the film sections were removed from the reaction mixture, carefully dried on a paper towel to remove the excess absorbed amine solution, and soaked in 5 mL of fresh isopropanol for 5 min. After this time, the isopropanol was replaced with a fresh amount of 5 mL, and washing was continued for another hour. The wet sections were then removed, air-dried until the excess alcohol was removed, and placed in a vacuum oven at 30 °C for 2 days. The same procedure was used for the functionalization of PLA_PCL_95_5 and PLA_PCL_G_95_5_1 films based on the optimized formulations, maintaining a contact time with ethylenediamine solution of 30 min. The aminolyzed samples were identified by adding an "A" to their code (PLA_10A, PLA_PCL_95_5A, and PLA_PCL_G_95_5_1A).

2.5. Characterization. A Zeiss Supra 40 VP field emission scanning electron microscope equipped with a backscattered electron detector was exploited to examine the prepared film morphologies. The specimens were submerged in liquid nitrogen for 30 min and fractured cryogenically. All samples were thinly sputter coated with carbon by using a Polaron E5100 sputter coater.

The FT-IR spectroscopic analysis was carried out with a Bruker Vertex 70 operating in ATR mode in the range 400−4000 cm^{-1}.

Differential scanning calorimetric analysis was performed under a continuous nitrogen purge on a Mettler calorimetric apparatus, model DSC1 STAR^e System. Both calibrations of heat flow and temperature were based on a run in which one standard sample (indium) was heated through its melting point. The neat PLA films, having a mass between 2.5 and 6 mg, were heated from room temperature to 200 °C, then cooled to room temperature, and finally heated to 200 °C again. A scan rate of 10 °C/min was used both on heating and cooling. In the case of the films containing PCL, the investigated temperature range was from −100 to 200 °C.

The degree of crystallinity (X_c) of PCL was calculated by considering their real contents, Φ_{PCL}, following eq 1:

$$X_c\ (\%) = \frac{\Delta H_m}{\Delta H_m^\circ \Phi_{PCL}} \times 100\% \quad (1)$$

where ΔH_m is the measured heat of fusion and ΔH_m° is the melting enthalpy of the 100% crystalline PCL (139 J/g).[23]

Thermal gravimetrical analysis (TGA) was performed with a STAR^e System Mettler thermobalance under a flow of nitrogen of 80 mL/min. The weight losses of the samples (having initial masses of ca. 10 mg) were measured from room temperature to 800 °C at a heating rate of 10 °C/min.

The tensile properties of the prepared films were determined at room temperature by an Instron mechanical tester (Instron 5565) at a crosshead speed of 1 mm/min by using rectangular specimens with dimensions of 10 × 25 mm^3. The reported property values represent an average of the results for tests run on six specimens, along with their experimental deviations.

The viscosities of the polymer solutions and of the treated samples with the prepared enzyme-based systems were analyzed at 80 °C by using a viscosimeter Brookfield model DV-II+.

2.6. Conductivity Measurements. Conductivity tests were performed on film specimens with a size of 5.5 × 8 × 0.5 mm. For the measurements, a potential difference of 150 V cm^3 was applied to the samples and the current was evaluated by employing a picoammeter (Keithley Instruments, Solon, OH, USA).

2.7. Adsorption Tests. Dye absorption tests were performed by placing three film disks (6 mm diameter) in a 1.5 mL Eppendorf centrifuge tube followed by 1 mL of a 5 μM solution of sodium fluoresceinate in Milli-Q water. The films were then soaked in the dye solution for 24 h under stirring on a rotating mixer (speed = 10 rpm, tilt angle = 80°). The samples were then removed and the solution was centrifuged for 10 min at 8000 rpm with an Eppendorf minispin minicentrifuge to remove all suspended polymer particles. The clean surnatants were then analyzed with a Shimadzu UV−vis UV-1800 spectrophotometer with a quartz cell (b = 1 cm, scan speed, very slow) in the range 300−600 nm. The concentration of fluorescein was determined by its absorption at λ_{max} = 465 nm. A calibration curve in the linearity range (0, 0.5, 1, 2, 5, 10 μg/mL) was constructed for the quantification of the dye and is shown in eq 2.

$$\text{absorbance (AU)} = 0.08799 \cdot \text{concentration } (\mu g/mL) - 0.01213 \quad (R^2 = 0.99574) \quad (2)$$

2.8. Electrochemical Detection of Ascorbic Acid. Electrochemical characterization was carried out by cyclic voltammetry (CV) using an EmStat3 potentiostat (PalmSens BV, Houten, Netherlands) and a three-electrode cell. In this setup, the porous films were mounted on a Ta clip as working electrodes to provide mechanical support and electrical connection to the potentiostat; an Ag/AgCl electrode, saturated with KCl, formed the reference electrode; a platinum wire was used as the counter electrode. Measurements were performed after 5 min of immersion in a 5 mM solution of ascorbic acid. Cyclic voltammograms were recorded in the potential range −1.0 to 1.0 V vs Ag/AgCl at scan rates of 10, 20, and 50 mV/s.

3. RESULTS AND DISCUSSION

3.1. Film Porosity Evaluation. The porous films were prepared by a phase inversion process, keeping the method as

https://doi.org/10.1021/acsapm.2c00923
ACS Appl. Polym. Mater. 2022, 4, 6521−6530

simple as possible. It is worth mentioning that the choice of the solvent used, namely DMF, was related to favoring graphite exfoliation, which in turn may also affect its dispersion in the polymer matrix. As described in the literature, the dispersion/exfoliation of graphite is promoted by specific interactions between the solvent and the graphene flakes. In particular, it was reported that the exfoliation of graphite occurs in solvents whose surface energy is equivalent to that of graphene.[15,24] Indeed, DMF, which possesses the above property, proved to be one of the most effective compounds capable of exfoliating graphite to a high extent.

To optimize the formulation, the viscosities of solutions with different PLA concentrations were analyzed and these measurements were correlated with the porosity of the obtained membranes, which was calculated using eq 3:[25,26]

$$\text{porosity}\ (\%) = \frac{V_m - V_p}{V_m} \times 100 \quad (3)$$

where V_m is the sample volume, which is determined from the area (A) and thickness of the sample; the polymer volume inside the membrane (V_p) is calculated using the formula W_f/ρ_p (ρ_p is the PLA density, which is equal to 1.24 g/cm^3, and W_f is the film weight).

It is difficult to compare the data obtained with those reported in the literature, which generally refer to other types of solvents and at room temperature.[7,9−11,25,26] Considering the viscosities shown in Table 2, an exponential trend can be observed (Figure S1), with extremely high values for the solutions prepared using polymer concentrations of 20 and 25% w/v. Indeed, for the above polymer concentrations, the high viscosities make it difficult to cast the solutions on the glass plate and obtain uniform films.

Table 2. Characteristics of the Casting Solutions and of the Prepared Films

sample code	viscosity [mPa·s]	porosity [%]
PLA_5	6	92
PLA_10	26	85
PLA_15	52	81
PLA_20	145	80
PLA_25	350	75

The porosities calculated from eq 3 and presented in Table 2 proved to be higher than the values reported in the literature for porous PLA films prepared from dioxane-based solutions and using mixtures of water and ethanol of different compositions as nonsolvents.[25] For these latter systems, the porosity value found when using pure water as a nonsolvent was 50%. It was reported that this value could be increased only by introducing ethanol into the precipitation mixture. Comparing these results with those obtained in our measurements, it is possible to highlight a fundamental role of the type of solvent in the formation of the porous structure, since in our systems it was possible to obtain a high porosity (above 70%) without changing the polymer precipitation medium, which was pure water for all the prepared films. However, it is clear that the porosity decreased with increasing polymer concentration from 92% in the films prepared with a concentration of 5% w/v to 75% in those prepared with a concentration of 25% w/v. This phenomenon can be related to the more difficult diffusion of the nonsolvent in systems characterized by a higher polymer concentration.

In order to better elucidate the process of film formation, cloud point measurements were performed, and the results are summarized in the ternary phase diagram shown in Figure S2. Indeed, the cloud points separate the homogeneous region, where all components are miscible, from a region that represents a liquid−liquid demixing gap, where the system separates into polymer-rich and polymer-poor phases.[27] Considering the ternary phase diagram of the PLA/DMF/water system, it is clear that the homogeneous region is very limited. As a result, DMF is rapidly exchanged with water to reach the thermodynamic equilibrium state, which would promote the formation of irregular pores in PLA films. It is worth underlining that a similar behavior was also found in films based on other polymers, such as PU.[28]

3.2. Film Morphologies. The morphologies of the PLA films were evaluated as a function of polymer concentration, keeping the temperature of the coagulation bath and that of the solution constant. Even at a macroscopic level, the prepared films showed significant differences. As shown in the photos in Figure S3, the films prepared with a low PLA concentration (PLA_5) are inhomogeneous and very thin (500 μm), while those prepared from the most concentrated solution (PLA_25) are thick (800 μm) and extremely brittle. FE-SEM measurements allowed the analysis in detail the cross sections of the PLA films. The micrographs of the samples prepared from different polymer concentrations (Figure 2) show that the films were characterized by an asymmetric structure including spongy and fingerlike regions. Thus, these morphological observations confirm the cloud point measurements previously discussed.

Moreover, as reported in the literature,[27] this peculiar morphology, characterized by a predominance of fingerlike pores, is typical of systems coagulated in water. This phenomenon was ascribed to the variation of the exchange rate between solvent and nonsolvent at different locations of the cross sections or the hydrodynamic flow of the nonsolvent as the pores are generated and grow along the flow direction. Indeed, a pure spongelike structure can be obtained when a water/ethanol coagulation bath with a water concentration of less than 60% or only ethanol is used.[10] In this context, it is worth underlining that, in the case of PLA, the contact with ethanol can promote ethanolysis,[29] a process that may modify

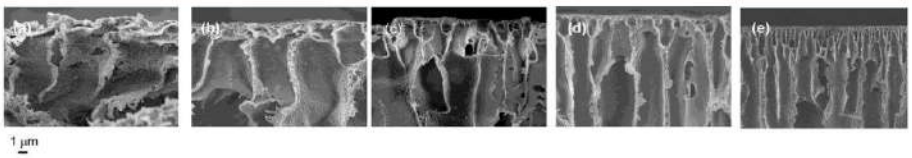

Figure 2. FE-SEM micrographs of (a) PLA_5, (b) PLA_10, (c) PLA_15, (d) PLA_20, and (e) PLA_25.

https://doi.org/10.1021/acsapm.2c00923
ACS Appl. Polym. Mater. 2022, 4, 6521−6530

ACS Applied Polymer Materials pubs.acs.org/acsapm Article

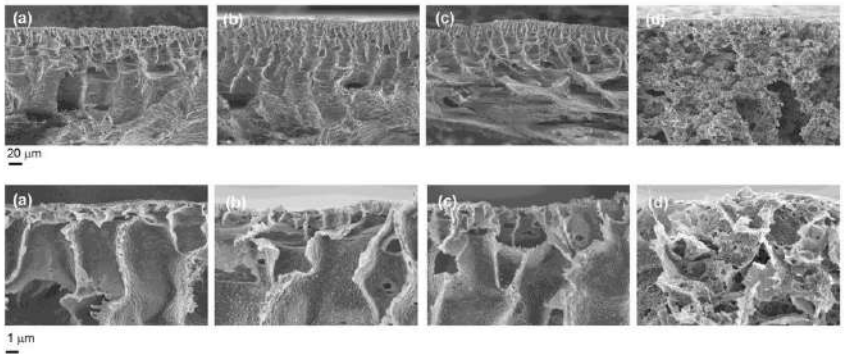

Figure 3. FE-SEM micrographs of: (a) PLA_10, (b) PLA_PCL_90_10, (c) PLA_PCL_95_5, and (d) PLA_PCL_G_95_5_1.

the chemical structure of the polymer surface in an uncontrolled way. From this point of view, it is more preferable to use water as a nonsolvent in the production of porous films based on PLA. In addition, the asymmetric porous structure, which can be obtained under the applied conditions, may be of interest for certain applications, for example in the field of filtration. On the basis of the morphological observations, the porosity measurements, and the structural homogeneity, the optimal concentration was set at 10% w/v, and this condition was chosen for the preparation of blend films based on a PLA/PCL blend. Indeed, different PLA/PCL ratios were used, namely 95/5, 90/10, and 80/20. In the sample with the highest percentage of PCL, segregation of the two polymer phases was observed during film formation while the neat PCL film, obtained by applying the same conditions used for the PLA films, was not uniform (Figure S4). On this basis, films with PLA/PCL ratios of 90/10 and 95/5 were analyzed by FE-SEM, i.e., those characterized by structural uniformity. Analysis of the micrographs, shown in Figure 3, indicates that the presence of PCL does not affect the morphology of the sections, which was characterized by a prevalence of fingers as in the neat PLA films. It is important to note that no PCL aggregates are visible, a phenomenon that can be attributed to both the low PCL concentration and the mechanism of the film formation, which could limit the segregation of the polymer within the polymer matrix due to the rapid precipitation of the polymer blend in a nonsolvent.

Despite the similar morphological structures of the films prepared from the PLA/PCL blends, the porosity calculated using eq 3 and considering the composition of the system and the density of the two polymers (ρ = 1.24 and 1.15 g/cm^3 for PLA and PCL, respectively) is higher than that of the PLA films. In fact, the porosity of the PLA/PCL films was found to be ca. 90%, while that of the neat PLA-based films (PLA_10) was 85%.

For other systems, such as PLA and PU, the porosity of blend-based films was also found to be higher than that of pure polymer films, a phenomenon that can be attributed to the efficient nucleation of the polymer-lean phase at the interface between the dispersed domains and the polymer matrix.[28]

As previously reported, graphite nanoplatelets (GNP) were introduced into the blend films to make them conductive. On the basis of the morphological results and in order to avoid segregation of the two components of the blend as much as possible, it was decided to focus on the composition with a PLA/PCL ratio of 95/5, maintaining the polymer concentration at 10% w/v, and introducing different amounts of GNP into the solvent, i.e., 0.5 and 1 wt % relative to the polymer system. The micrographs in Figure 3d show the cross section of the PLA_PCL_G_95_5_1 film containing 1 wt % GNP as indicated in Table 1. Similar results were obtained in the analysis of the PLA_PCL_G_95_5_0.5 film (results not shown). It is evident that the presence of GNP changed the morphology of the film compared to the neat film, as the composite system appears more porous and the fingerlike region is less distinct. This result could be related to the effect of GNP, which can influence the precipitation of the polymer system in the nonsolvent and thus the thermodynamics of the film formation. As for the GNP dispersion, a homogeneous distribution of the filler was found in PLA_PCL_G_95_5_1, whose micrographs also prove the strong adhesion of GNP with the polymer matrix. It is relevant to underline that it is generally necessary to add compatibilizers to increase the dispersion of graphite in dense films.[30] Indeed, in the case of PCL-based films containing GNP concentrations comparable to those of our formulations, high dispersion is achieved only by using an ad hoc synthesized polymer ending with a pyrene group that can interact with the graphite layers.[31]

In addition, other works report that the dispersion of graphite in the polymer matrix is promoted by removing through sedimentation/centrifugation the portion of the filler that does not exfoliate in the solvent in which the polymer is dissolved.[32]

Thus, on this basis, it is possible to hypothesize that the method used to produce the porous film favors the dispersion of GNP. As previously mentioned, the precipitation of the polymer system in the nonsolvent could limit GNP aggregation and maintain the dispersion present in the solvent−polymer system.

3.3. Film Thermal Properties. The thermal properties of neat PLA films prepared by using different polymer concentrations were studied by means of DSC. The DSC traces from the second heating (Figure S5) and the thermal data summarized in Table S1 show that all the films prepared were characterized by cold crystallization and a melting peak. Indeed, the melting enthalpy (ΔH_m) and the cold crystallization enthalpy (ΔH_{cc}) were comparable, indicating that the systems were amorphous. It was also found that the initial

https://doi.org/10.1021/acsapm.2c00923
ACS Appl. Polym. Mater. 2022, 4, 6521−6530

Table 3. Thermal Properties of the Prepared Films[a]

sample code	T_c [°C]	ΔH_c [J/g]	T_g [°C]	ΔH_{cc} [J/g]	T_{cc} [°C]	T_m [°C]	ΔH_m [J/g]
PLA_10	–	–	59	12	125	155	13
PCL_10	30	63	–	–	–	–	–
PLA_PCL_95_5							
PCL	26	12	–	–	–	–	–
PLA	–	–	56	8	126	153	8
PLA_PCL_90_10							
PCL	32	28	–	–	–	–	–
PLA	–	–	58	13	127	153	13
PLA_PCL_G_95_5_0.5							
PCL	44	19	–	–	–	–	–
PLA	–	–	–	9	127	153	9
PLA_PCL_G_95_5_1							
PCL	45	–	–	–	–	–	–
PLA	–	–	–	10	121	152	11

[a]The subscripts "m" and "cc" indicate the values measured during melting and cold crystallization, respectively.

polymer concentration did not significantly affect the thermal behavior.

Figure S6 displays the characteristic DSC scans upon cooling and heating of neat PLA and PCL films as well as the films based on their blends, while the thermal properties for all the samples are collected in Table 3.

The different crystallizabilities of the two neat polymer films PLA_10 and PCL_10 can be noticed. Indeed, PCL crystallizes with a large and relatively narrow peak at around 30 °C, while the crystallization of PLA, as previously described, occurs only upon subsequent heating above the glass transition, at ca. 120 °C.

A significant effect of the blending process on the crystallization/melting of the two phases can be observed. Upon cooling, it can be seen that crystallization of the PCL phase at high temperature is hindered and this effect is more evident by decreasing the PCL content in the blend. This phenomenon can be ascribed to the extremely limited size of the PCL domains, which are not resolvable by FE-SEM. As a consequence, a very small number of nucleating impurities are present in the PCL domains, decreasing the crystallization kinetics. Moreover, it is difficult to evaluate the melting enthalpy of PCL, since the peak is partially overlapped with the PLA enthalpic relaxation. On the other hand, the increase in the melting enthalpy of PLA can be ascribed to a nucleating effect of PCL domains, which is particularly evident in PLA_PCL_80_20. It is worth underlining that a similar behavior has already been observed in other PLA/PCL systems.[33,34] Despite the kinetic effect on crystallization, the melting temperature of PLA is not affected by the blending process (T_m of PCL is difficult to determine because it is superimposed by the enthalpic relaxation of PLA). In particular, no evident melting point depression was detected, indicating thermodynamic immiscibility between the polymers, although the morphology evidenced a fine dispersion of the PCL domains in the polymer matrix.

In the composite systems, the addition of GNP led to a significant increase in the crystallization temperature of the PCL, which increased from 26 °C for PLA_PCL_95_5 to about 45 °C for PLA_PCL_G_95_5_0.5 and PLA_PCL_G_95_5_1. This result can be attributed to the well-known nucleation effect of graphite,[31] which tends to saturate with increasing its content, as already reported.[31]

3.4. Study of Film Surface Functionalization. The functionalization of the film surface was carried out by an aminolysis reaction with an ethylenediamine solution. In particular, the effect of reaction time on film properties was studied, while the other parameters, namely temperature, diamine concentration, and film size/reagent ratio, were kept constant. Aminolysis occurs at the interface between the diamine solution and the polymer film, adding amino and hydroxyl groups to the polyester surface.[20−22] Due to the specific mechanism of the above reaction, erosion of the polymer surface inevitably occurs, accompanied by penetration of the reagent to a certain depth of the polyester surface.[20−22] On this basis, it was necessary to determine the optimal conditions that would allow surface functionalization without significant change in the film structure.

Functionalization was studied with FT-IR spectroscopy using a PLA film prepared under the optimized conditions, namely PLA_10. Figure 4 compares the IR spectrum of the neat PLA film with those of the same film treated for 15, 30, 60, 90, and 180 min. In the former sample, strong bands were observed at 1760 cm^{-1}, which can be assigned to the carbonyl stretching mode, and at 2900 and 1200 cm^{-1} corresponding to

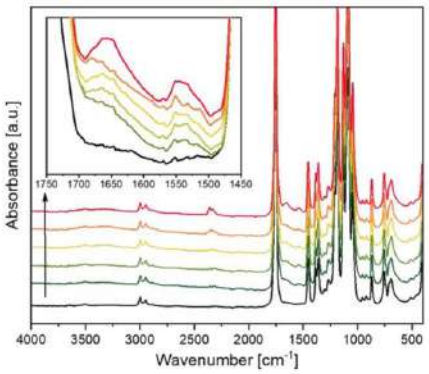

Figure 4. FT-IR spectra of PLA_10 (black —) and films treated with diamine solution for different contact times: 15 (cyan —), 30 (green —), 60 (yellow —), 120 (orange —), and 180 min (red —) (increasing time in the direction of the arrow).

https://doi.org/10.1021/acsapm.2c00923
ACS Appl. Polym. Mater. 2022, 4, 6521−6530

Table 4. Film Mechanical and Conductivity Measurement Results

sample code	E [MPa]	σ_{max} [MPa]	ε_{break} [%]	conductivity [S/m]
PLA_10	49 ± 2	1.06 ± 0.08	3 ± 0.3	$<10^{-12}$
PLA_PCL_95_5	22 ± 1	0.85 ± 0.05	10 ± 2	$<10^{-12}$
PLA_PCL_G_95_5_0.5	6 ± 1	0.36 ± 0.02	9 ± 2	$<10^{-12}$
PLA_PCL_G_95_5_1	4 ± 1	0.48 ± 0.09	11 ± 2	1.4×10^{-9}

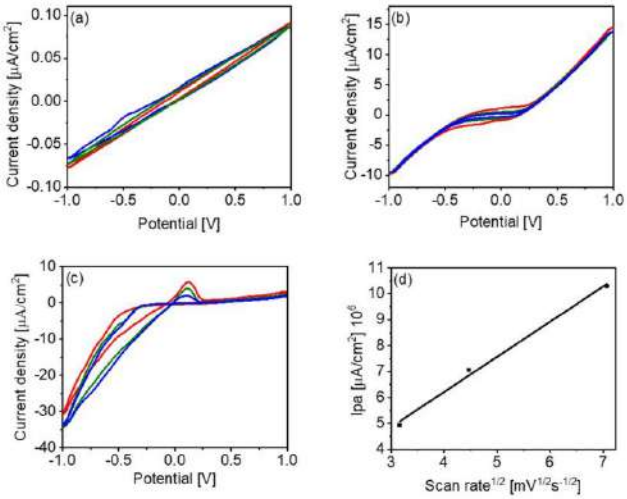

Figure 5. (a) Voltammograms of PLA_10 at scan rates of 50 (red —), 20 (green —), and 10 mV/s (blue —). (b) Voltammograms of PLA_PCL_G_95_5_1 at scan rates of 50 (red —), 20 (green —), and 10 mV/s (blue —). (c) Voltammograms of PLA_PCL_G_95_5_1_A at scan rates of 50 (red —), 20 (green —), and 10 mV/s (blue —). (d) Peak anodic current (I_{pa}) versus square root of scan rate.

C−H and C−C stretching, respectively.[35] In the treated films, in addition to the characteristic signals of PLA, bands were detected at about 1660 and 1530 cm^{-1}, which can be assigned to the amide group[20,22] and whose intensity increases with increasing reaction time. On the basis of the above spectra, it is clear that surface functionalization already occurs at low contact time.

The macroscopic morphology of the treated films was also analyzed because, as mentioned above, the aminolysis reaction can damage the structure through a phenomenon of surface erosion. Figure S7 compares a photograph of the neat PLA film (PLA_10) with those of the same sample exposed to the diamine-containing solution for different lengths of time.

It is clear that the structure is preserved only in the films treated at low contact times, i.e., 15 and 30 min. For this reason, and considering that at these times a certain degree of functionalization is already achieved, it was decided to set 30 min as the contact time of the film with the amine solution, which is the maximum time to avoid degradation of the polymer. It is important to underline that under this condition the porosity of the polymer film increases from 85 to 92%, a phenomenon that may be related to the erosion caused by the aminolysis reaction. To better highlight the effects of this reaction on the properties of the polymer films, FE-SEM measurements were performed. The cross sections and the surfaces (dense and porous) of the PLA_10 film and the same sample aminolyzed for 30 min (PLA_10A) are shown in Figure S8.

The comparison of the micrographs evidences that the two films had a similar morphological structure of the section, while the two surfaces significantly increased their porosity, which is in agreement with the theoretical calculation. This result demonstrates that the erosion effect of the aminolysis reaction was limited only to the polymer surface, at least at this contact time. Moreover, it is worth underlining that the increase in porosity may be functional for the application of films in sensors and as absorbers to favor the contact area of analytes with the polymer film.

In order to further verify the influence of the aminolysis reaction on the film thermal stability, TGA measurements were performed, analyzing both samples PLA_10 and PLA_10A. The thermograms of the films, shown in Figure S9, exhibited very similar profiles, with the maximum temperature degradation rate (T_{max}) for both analyzed samples being around 380 °C. This result shows that the aminolysis reaction, which involves a decrease in molecular weight and should therefore lead to a decrease in T_{max}, since it is confined only to the surface of the polymer film, does not affect the thermal stability of the polymer bulk.

3.5. Film Mechanical and Conductivity Properties. In Table 4, the mechanical properties of the films prepared with the optimized conditions are summarized. PLA is well-known to be a glassy polymer at room temperature, showing a relatively high modulus, and associated with a low deformation at break.[35]

Due to the porosity created by the phase inversion, neat PLA film (PLA_10) was characterized by a lower modulus

https://doi.org/10.1021/acsapm.2c00923
ACS Appl. Polym. Mater. 2022, 4, 6521−6530

than that generally reported for dense films, that is 800−1000 MPa.[2,3,35] Nevertheless, the film retained an acceptable modulus and appeared extremely fragile. It is interesting to note that the addition of PCL to the formulation lowers the modulus but triples the elongation at break, which increased from 3% for PLA_10 to 10% in the case of the PLA_PCL-95_5 blend film, thus highlighting an effective effect of PCL on film ductility.

Indeed, in the preparation of blends based on PLA/PCL by melt blending or casting, the poor compatibility of the two polymer systems, which limits the final properties of the material, such as elongation at break, is generally improved by the addition of suitable compatibilizers, such as copolymers and fillers/nanofillers[4,18,34] that reduce the size of the PCL domains and promote interactions at the interface of the two polymer systems. In the case of our formulation, as mentioned above, it is possible to hypothesize that the phase inversion technique limits the segregation of PCL domains and favors their dispersion in the polymer matrix, leading to an increase in elongation even at low concentrations. The lower modulus values of the GNP-based films, which were 6 and 4 MPa for PLA_PCL_G_95_5_0.5 and PLA_PCL_G_95_5_1, respectively, can be attributed to the different morphological structures, as shown by FE-SEM measurements. However, the samples are still easy to handle and retain a high elongation at break (ca. 10%). Similar results were obtained when the aminolyzed samples were examined.

As for the conductivity measurements, the films based on the neat polymers were found to be electrically insulating, with conductivities in the range of 10^{-12} S/m. The addition of 1 wt % GNP resulted in a significant improvement in conductivity, which increased from 10^{-12} to 10^{-9} S/m. Although it may be difficult to achieve a graphite percolation network in a porous material, these results demonstrate the effective function of GNP in improving the electrical properties of the film.

3.6. Cyclic Voltammetry Measurements. Cyclic voltammetry (CV) measurements were performed on the neat PLA films (PLA_10) and on the films prepared by the optimized formulations based on 1 wt % GNP, namely PLA_PCL_G_95_5_1 and PLA_PCL_G_95_5_1A. Measurements were carried out using a 5 mM solution of ascorbic acid (AA) in water as a negative redox mediator (pH 4.5) to evaluate the oxidation reaction to dehydroascorbic acid.

The PLA_10 sample, tested at three different scan rates, resulted in the formation of overlapping voltammograms, shown in Figure 5a, with no significant hysteresis, typical of nonpolarizable systems. The slope of the voltammograms allowed calculation of the interfacial resistance of the electrode, which was found to be 1.2×10^{7} Ω·cm^2, thus indicating an insulating behavior of the PLA_10 film.

The curves of the blend film PLA_PCL_G_95_5_1, which was not subjected to aminolysis treatment, are shown in Figure 5b. In this case, higher currents were measured, suggesting the beneficial effect of GNP in increasing the conductivity at the electrode−electrolyte interface. The voltammograms showed also an hysteresis phenomenon, connected to the polarization at the electrode interface.[36] The shape of the hysteresis and the increases in current, proportional to the scan rate, suggest the presence of a pseudocapacitive behavior.[37] The measured capacitance resulted was 1.52×10^{-7} F·cm^{-2}, 2 orders of magnitude lower than typical double layer values. Despite the improved electrochemical properties of this film, the voltammograms did not show any signal related to the oxidation of AA, a phenomenon that can be attributed to the poor interaction of the material with the analyte. In this context, it is worth underlining that both the polymeric matrix and GNP are weakly acid substrates. Considering this peculiarity of the material consisting of the PLA/GNP system, it is possible to assume a limited interaction of the analyte with the surface of the film.

On the contrary, in the voltammograms of the aminolyzed sample PLA_PCL_G_95_5_1A, shown in Figure 5c, a peak associated with the oxidation of AA to dehydroascorbic acid at potentials of 100, 108, and 127 mV vs Ag/AgCl can be observed. These results demonstrate the effectiveness of surface functionalization of the film in developing electrodes capable of detecting the presence of an acidic analyte. The oxidation peaks resulted at less positive potential compared to other studies,[38,39] thus suggesting the requirement of lower energy to oxidize the electroactive species on the surface of the electrode.[40] This could be due to the effect of the pH value of the electrolyte that in acid conditions favors the deprotonation of the AA. In the voltammogram, there is no trace of reduction peaks as is common for irreversible reactions. This phenomenon, previously reported in the literature,[38,39] can be attributed to the formation of dehydroascorbic acid, derived from the oxidation of ascorbic acid, which tends to dimerize at a faster reaction rate than reduction. In addition, an increase in the peak anodic current (I_{pa}) with sweep rate is observed, accompanied by a slight shift of the peak to higher potential values. The current value linearly correlates with the square root of the scan rate (Figure 5d), indicating a diffusion-controlled electrochemical reaction.[41]

Although these are preliminary results, it is possible to hypothesize that the amino functionalities formed on the surface of the porous film as a result of the aminolysis reaction allow electrostatic interactions with the acidic analyte. This phenomenon could therefore favor the concentration of ascorbic acid on the surface of the film, leading to an increase in the oxidation peak current.

3.7. Adsorption Tests. To assess the ability of the developed materials to adsorb negatively charged molecules, the films were immersed for 24 h in a solution of sodium fluorescein, a molecule commonly used as a model compound for drugs and pollutants.[42] After the above contact time, the dye concentration in the solution was quantified by UV−vis measurements and the results are shown in Figure 6. The neat films, PLA_PCL_95_5, are characterized by low dye adsorption, as the concentration of fluorescein remained almost unchanged after the test. For the GNP-containing sample, PLA_PCL_95_5_G1, an increase in retention of about 30% was observed compared to the neat polymer films. To clarify the specific effect of the filler on the retention capacity of the film, an equal amount of GNP as in the above film was dispersed in the fluorescein solution.

As shown in Figure 6, GNP turned out to be characterized by an elevated capacity to adsorb the molecule, with the retention of the fluorescein being almost complete. This property, as previously reported, can be ascribed to the high GNP surface area.[43] Clearly, the possibility to support the adsorber on a film represents a relevant advantage for a practical exploitation of the material, as the recovery of the adsorber can be done easier than the powder form.

The behavior of the film PLA_PCL_G_95_5_1A, based on the optimized formulation, containing GNP and aminolyzed on the surface, deserves a special comment. For the above

https://doi.org/10.1021/acsapm.2c00923
ACS Appl. Polym. Mater. 2022, 4, 6521−6530

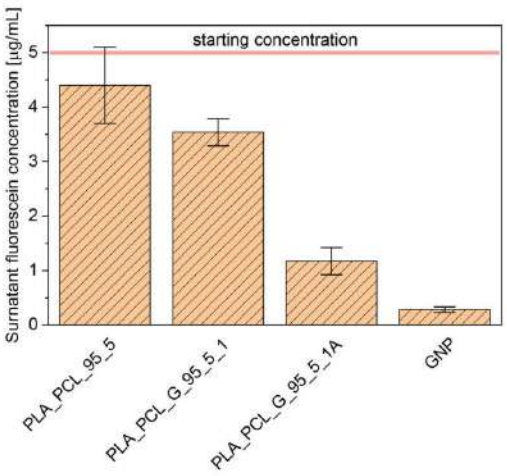

Figure 6. Surnatant fluorescein concentration of the solution contacted for 24 h with the developed films and with GNP powders.

sample, the decrease in the dye concentration is about 70%, i.e., 40% more than for the same formulation not treated with diamine. From these results it can be concluded that both the presence of GNP and the surface functionalization contribute to increase the ability of the material to retain the dye, thus expanding the possibilities for the application of the developed films.

4. CONCLUSIONS

In this work, PLA-based porous films were developed to be used in sensing and as absorbers. The designed and optimized film formulation consisted of a composite system prepared by combining PLA with PCL and GNP and surface functionalized by a simple aminolysis reaction. The easily scalable method of film preparation, i.e., phase inversion, not only allowed the formation of films with asymmetric porous structure but also favored the dispersion of PCL and GNP in the polymer matrix. Thus, the films prepared with the optimized composition were characterized by higher elongation at break and electrical conductivity than the neat PLA films.

Indeed, the developed materials were effectively applied as absorbers for negatively charged molecules and in the voltammetric determination of ascorbic acid. The above properties, together with the "green" nature of the constituents as well as the easy and sustainable preparation procedure, make the developed films attractive for various applications.

■ ASSOCIATED CONTENT

Supporting Information

The Supporting Information is available free of charge at https://pubs.acs.org/doi/10.1021/acsapm.2c00923.

PLA film porosity as a function of polymer solution concentration; phase diagram of PLA/DMF/water; photographs of PLA and PLA/PCL based films; thermal properties of PLA based films; DSC thermograms of produced films; photographs of neat PLA film and films treated with diamine solutions for different times; FE-SEM micrographs of surface and cross section of neat PLA film and film treated with diamine solution; TGA thermograms of neat PLA film and film treated with diamine solution (PDF)

■ AUTHOR INFORMATION

Corresponding Author

Orietta Monticelli − *Dipartimento di Chimica e Chimica Industriale, Università di Genova, 16146 Genova, Italy;* orcid.org/0000-0003-4999-3069; Email: orietta.monticelli@unige.it

Authors

Giacomo Damonte − *Dipartimento di Chimica e Chimica Industriale, Università di Genova, 16146 Genova, Italy*

Roberto Spotorno − *Dipartimento di Chimica e Chimica Industriale, Università di Genova, 16146 Genova, Italy*

Daniela Di Fonzo − *Dipartimento di Chimica e Chimica Industriale, Università di Genova, 16146 Genova, Italy*

Complete contact information is available at: https://pubs.acs.org/10.1021/acsapm.2c00923

Author Contributions

The manuscript was written through contributions of all authors. All authors have given approval to the final version of the manuscript.

Notes

The authors declare no competing financial interest.

■ REFERENCES

(1) *Handbook of Biopolymers and Biodegradable Plastics*; Ebnesajjad, S., Ed.; Elsevier: 2013.

(2) Lim, L.-T.; Auras, R.; Rubino, M. Processing Technologies for Poly(lactic acid). *Prog. Polym. Sci.* **2008**, *33*, 820−852.

(3) Nagarajan, V.; Mohanty, A. K.; Misra, M. Perspective on Polylactic Acid (PLA) Based Sustainable Materials for Durable Applications: Focus on Toughness and Heat Resistance. *ACS Sustainable Chem. Eng.* **2016**, *4*, 2899−2916.

(4) Forouharshad, M.; Gardella, L.; Furfaro, D.; Galimberti, M.; Monticelli, O. A Low-Environmental-Impact Approach for Novel Bio-Composites Based on PLA/PCL Blends and High Surface Area Graphite. *Eur. Polym. J.* **2015**, *70*, 28−36.

(5) Gardella, L.; Furfaro, D.; Galimberti, M.; Monticelli, O. On the Development of a Facile Approach Based on the Use of Ionic Liquids: Preparation of PLA (Sc-PLA)/High Surface Area Nano-Graphite Systems. *Green Chem.* **2015**, *17*, 4082−4088.

(6) Saini, P.; Arora, M.; Ravi Kumar, M. N. V. Poly(Lactic Acid) Blends in Biomedical Applications. *Adv. Drug Delivery Rev.* **2016**, *107*, 47−59.

(7) Liu, H.-C.; Lee, I.-C.; Wang, J.-H.; Yang, S.-H.; Young, T.-H. Preparation of PLA Membranes with Different Morphologies for Culture of MG-63 Cells. *Biomaterials* **2004**, *25*, 4047−4056.

(8) Guillen, G. R.; Pan, Y.; Li, M.; Hoek, E. M. V. Preparation and Characterization of Membranes Formed by Nonsolvent Induced Phase Separation: A Review. *Ind. Eng. Chem. Res.* **2011**, *50*, 3798−3817.

(9) van de Witte, P.; Esselbrugge, H.; Dijkstra, P. J.; van den Berg, J. W. A.; Feijen, J. Phase Transitions During Membrane Formation of Polylactides. I. A Morphological Study of Membranes Obtained from the System Polylactide-Chloroform-Methanol. *J. Membr. Sci.* **1996**, *113*, 223−236.

(10) Xing, Q.; Dong, X.; Li, R.; Yang, H.; Han, C. C.; Wang, D. Morphology and Performance Control of PLA-Based Porous Membranes by Phase Separation. *Polymer* **2013**, *54*, 5965−5973.

(11) Hu, R.; Pi, Y.; Wang, N.; Zhang, Q.; Feng, J.; Xu, W.; Dong, X.; Wang, D.; Yang, H. The Formation of the S-Shaped Edge-On Lamellae on the thin Porous Polylactic Acid Membrane via Phase

https://doi.org/10.1021/acsapm.2c00923
ACS Appl. Polym. Mater. 2022, 4, 6521−6530

Separation Induced by Water Microdroplets. *J. Appl. Polym. Sci.* **2016**, *133*, 43355.
(12) Li, K.; Fina, A.; Marrè, D.; Carosio, F.; Monticelli, O. Graphite Oxide Nanocoatings as a Sustainable Route to Extend the Applicability of Biopolymer-Based Film. *Appl. Surf. Sci.* **2020**, *522*, 146471.
(13) Jellett, C.; Ghosh, K.; Browne, M. P.; Urbanová, V.; Pumera, M. Flexible Graphite−Poly(Lactic Acid) Composite Films as Large-Area Conductive Electrodes for Energy Applications. *ACS Appl. Energy Mater.* **2021**, *4*, 6975−6981.
(14) Gardella, L.; Colonna, S.; Fina, A.; Monticelli, O. A Novel Electrostimulated Drug Delivery System Based on PLA Composites Exploiting the Multiple Functions of Graphite Nanoplatelets. *ACS Appl. Mater. Interfaces* **2016**, *8*, 24909−24917.
(15) Hernandez, Y.; Nicolosi, V.; Lotya, M.; Blighe, F. M.; Sun, Z.; De, S.; McGovern, I. T.; Holland, B.; Byrne, M.; Gun'Ko, Y. K.; Boland, J. J.; Niraj, P.; Duesberg, G.; Krishnamurthy, S.; Goodhue, R.; Hutchison, J.; Scardaci, V.; Ferrari, A. C.; Coleman, J. N. High-Yield Production of Graphene by Liquid-Phase Exfoliation of Graphite. *Nat. Nanotechnol.* **2008**, *3*, 563−568.
(16) Labet, M.; Thielemans, W. Synthesis of Polycaprolactone: a Review. *Chem. Soc. Rev.* **2009**, *38*, 3484−3504.
(17) Malikmammadov, E.; Tanir, T. E.; Kiziltay, A.; Hasirci, V.; Hasirci, N. PCL and PCL-Based Materials in Biomedical Applications. *J. Biomater. Sci., Polym. Ed.* **2018**, *29*, 863−893.
(18) Fortelny, I.; Ujcic, A.; Fambri, L.; Slouf, M. Phase Structure, Compatibility, and Toughness of PLA/PCL Blends: a Review. *Front. Mater.* **2019**, *6*, 206.
(19) Hołda, A. K.; Vankelecom, I. F. J. Understanding and Guiding the Phase Inversion Process for Synthesis of Solvent Resistant Nanofiltration Membranes. *J. Appl. Polym. Sci.* **2015**, *132*, 42130.
(20) Blangiardo, A.; Lagomarsino, G.; Basso, A.; Canepa, P.; Cavalleri, O.; Rossi, S.; Monticelli, O. Preparation, Application and Recycling of a Catalytic Microflow Reactor Based on Polylactic Acid. *Appl. Surf. Sci.* **2021**, *569*, 151019.
(21) Zhu, Y.; Mao, Z.; Gao, C. Aminolysis-Based Surface Modification of Polyesters for Biomedical Applications. *RSC Adv.* **2013**, *3*, 2509−2519.
(22) Boi, S.; Dellacasa, E.; Bianchini, P.; Petrini, P.; Pastorino, L.; Monticelli, O. Encapsulated Functionalized Stereocomplex PLA Particles: an Effective System to Support Mucolytic Enzymes. *Colloids Surf., B* **2019**, *179*, 190−198.
(23) Crescenzi, V.; Manzini, G.; Calzolari, G.; Borri, C. Thermodynamics of Fusion of Poly-β-Propiolactone and Poly-ϵ Caprolactone. Comparative Analysis of the Melting of Aliphatic Polylactone and Polyester Chains. *Eur. Polym. J.* **1972**, *8*, 449−463.
(24) Johnson, D. W.; Dobson, B. P.; Coleman, K. S. A Manufacturing Perspective on Graphene Dispersions. *Curr. Opin. Colloid Interface Sci.* **2015**, *20*, 367−382.
(25) Wang, H.; Wang, L.; Liu, C.; Xu, Y.; Zhuang, Y.; Zhou, Y.; Gu, S.; Xu, W.; Yang, H. Effect of Temperature on the Morphology of Poly(Lactic Acid) Porous Membrane Prepared via Phase Inversion Induced by Water Droplets. *Int. J. Biol. Macromol.* **2019**, *133*, 902−910.
(26) Chinyerenwa, A. C.; Wang, H.; Zhang, Q.; Zhuang, Y.; Munna, K. H.; Ying, C.; Yang, H.; Xu, W. Structure and Thermal Properties of Porous Polylactic Acid Membranes Prepared via Phase Inversion Induced by Hot Water Droplets. *Polymer* **2018**, *141*, 62−69.
(27) Wijmans, J. G.; Kant, J.; Mulder, M. H. V.; Smolders, C. A. Phase Separation Phenomena in Solutions of Polysulfone in Mixtures of a Solvent and a Nonsolvent: Relationship with Membrane Formation. *Polymer* **1985**, *26*, 1539−1545.
(28) Khorasani, M. T.; Shorgashti, S. Fabrication of Microporous Thermoplastic Polyurethane for Use as Small-Diameter Vascular Graft Material. I. Phase-Inversion Method. *J. Biomed. Mater. Res.* **2006**, *76B*, 41−48.
(29) Iñiguez-Franco, F.; Auras, R.; Dolan, K.; Selke, S.; Holmes, D.; Rubino, M.; Soto-Valdez, H. Chemical Recycling of Poly(Lactic Acid) by Water-Ethanol Solutions. *Polym. Degrad. Stab.* **2018**, *149*, 28−38.
(30) Sengupta, R.; Bhattacharya, M.; Bandyopadhyay, S.; Bhowmick, A. K. A Review on the Mechanical and Electrical Properties of Graphite and Modified Graphite Reinforced Polymer Composites. *Prog. Polym. Sci.* **2011**, *36*, 638−670.
(31) Damonte, G.; Vallin, A.; Fina, A.; Monticelli, O. On the Development of an Effective Method to Produce Conductive PCL Film. *Nanomaterials* **2021**, *11*, 1385.
(32) Alzari, V.; Nuvoli, D.; Scognamillo, S.; Piccinini, M.; Gioffredi, E.; Malucelli, G.; Marceddu, S.; Sechi, M.; Sanna, V.; Mariani, A. Graphene-Containing Thermoresponsive Nanocomposite Hydrogels of Poly(N-Isopropylacrylamide) Prepared by Frontal Polymerization. *J. Mater. Chem.* **2011**, *21*, 8727−8733.
(33) Rizzuto, M.; Marinetti, L.; Caretti, D.; Mugica, A.; Zubitur, M.; Müller, A. J. Can Poly(ε-Caprolactone) Crystals Nucleate Glassy Polylactide? *CrystEngComm* **2017**, *19*, 3178−3191.
(34) Monticelli, O.; Calabrese, M.; Gardella, L.; Fina, A.; Gioffredi, E. Silsesquioxanes: Novel Compatibilizing Agents for Tuning the Microstructure and Properties of PLA/PCL Immiscible Blends. *Eur. Polym. J.* **2014**, *58*, 69−78.
(35) Madhavan Nampoothiri, K.; Nair, N. R.; John, R. P. An Overview of the Recent Developments in Polylactide (PLA) Research. *Bioresour. Technol.* **2010**, *101*, 8493−8501.
(36) Aryal, K. P.; Jeong, H. K. Carbon Nanofiber Modified with Reduced Graphite Oxide for Detection of Ascorbic Acid, Dopamine, and Uric Acid. *Chem. Phys. Lett.* **2020**, *739*, 136969.
(37) Gharbi, O.; Tran, M. T. T.; Tribollet, B.; Turmine, M.; Vivier, V. Revisiting Cyclic Voltammetry and Electrochemical Impedance Spectroscopy Analysis for Capacitance Measurements. *Electrochim. Acta* **2020**, *343*, 136109.
(38) Ngai, K. S.; Tan, W. T.; Zainal, Z.; Zawawi, R. b. M.; Zidan, M. Electrochemical Oxidation of Ascorbic Acid Mediated by Single-Walled Carbon Nanotube/Tungsten Oxide Nanoparticles Modified Glassy Carbon Electrode. *Int. J. Electrochem. Sci.* **2012**, *7*, 4210−4222.
(39) Bilal, S.; Akbar, A.; Shah, A. H. A. Highly Selective and Reproducible Electrochemical Sensing of Ascorbic Acid Through a Conductive Polymer Coated Electrode. *Polymers* **2019**, *11*, 1346.
(40) Rees, M.; Wright, A. G.; Holdcroft, S.; Bertoncello, P. Voltammetry at Hexamethyl-P-Terphenyl Poly(Benzimidazolium) (HMT-PMBI)-Coated Glassy Carbon Electrodes: Charge Transport Properties and Detection of Uric and Ascorbic Acid. *Sensors. Sensors* **2020**, *20*, 443.
(41) Bard, A. J.; Faulkner, L. R. *Electrochemical Methods: Fundamentals and Applications*, 2nd ed.; John Wiley & Sons: New York, 2000.
(42) Fisher, K. A.; Huddersman, K. D.; Taylor, M. J. Comparison of Micro-and Mesoporous Inorganic Materials in the Uptake and Release of the Drug Model Fluorescein and its Analogues. *Chem.—Eur. J.* **2003**, *9*, 5873−5878.
(43) Xu, C.; Jiao, C.; Yao, R.; Lin, A.; Jiao, W. Adsorption and Regeneration of Expanded Graphite Modified by CTAB-KBr/H_3PO_4 for Marine Oil Pollution. *Environ. Pollut.* **2018**, *233*, 194−200.

https://doi.org/10.1021/acsapm.2c00923
ACS Appl. Polym. Mater. 2022, 4, 6521−6530

Supporting Information - Multifunctional porous films based on polylactic acid/polycaprolactone blend and graphite nanoplatelets

Supporting information

Multifunctional porous films based on polylactic acid/polycaprolactone blend and graphite nanoplateles

*Giacomo Damonte[1], Roberto Spotorno[1], Daniela Di Fonzo[1], Orietta Monticelli[1]**

[1]Dipartimento di Chimica e Chimica Industriale, Università di Genova, Via Dodecaneso 31, 16146

Genova, Italy

**Corresponding author: orietta.monticelli@unige.it*

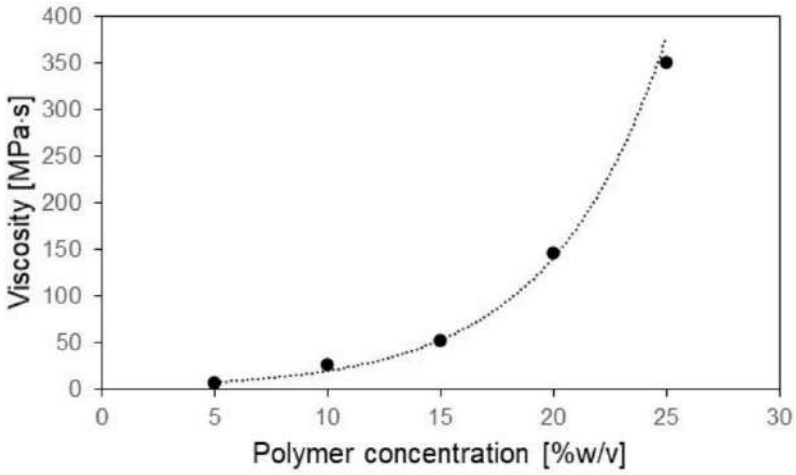

Figure S1. PLA film porosity as a function of the polymer solution concentration.

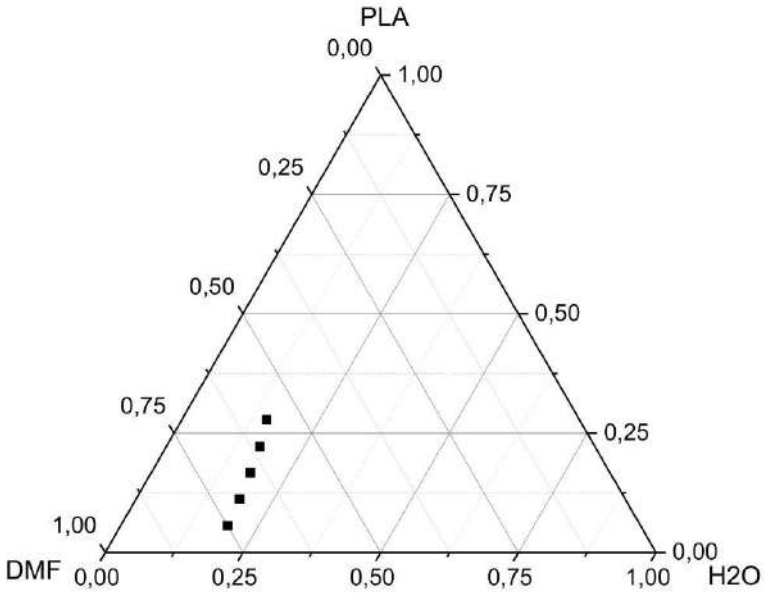

Figure S2. Phase diagram of PLA/DMF/water.

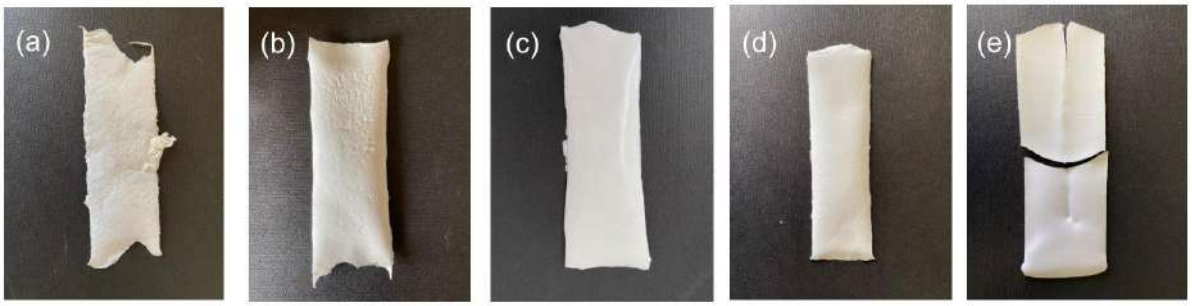

Figure S3. Photos of: (a) PLA_5, (b) PLA_10, (c) PLA_15, (d) PLA_20, (e) PLA_20 and (f) PLA-25.

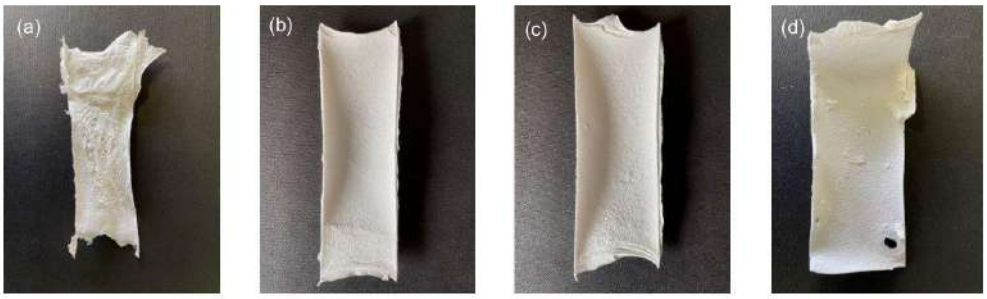

Figure S4. Photos of PCL_10, (b) PLA_PCL_95_5, (c) PLA_PCL_90_10 and (d) PLA_PCL_80_20.

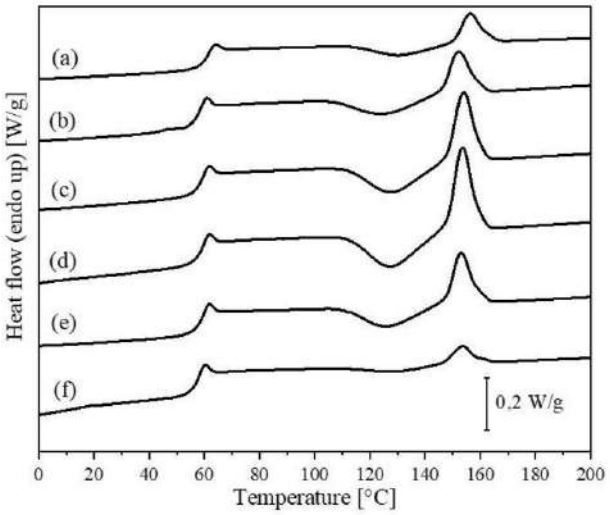

Figure S5. DSC traces on heating of: (a) PLA, (b) PLA_5, (c) PLA_10, (d) PLA_15, (e) PLA_20 and (f) PLA_25.

Table S1. Thermal properties of the neat PLA and PLA-based films.

Sample code	T_g [°C]	ΔH_{cc} [J/g]	T_{cc} [°C]	ΔH_m [J/g]	T_m [°C]
PLA	59	-12.3	125	13.8	155
PLA_5	57	-8.6	125	8.5	152
PLA_10	58	-13.1	128	12.3	154
PLA_15	58	-14.6	128	14.5	153
PLA_20	58	-9.0	126	9.4	153
PLA_25	57	-10.1	129	10.2	154

The subscripts m and cc indicate the values measured during melting and cold-crystallization, respectively.

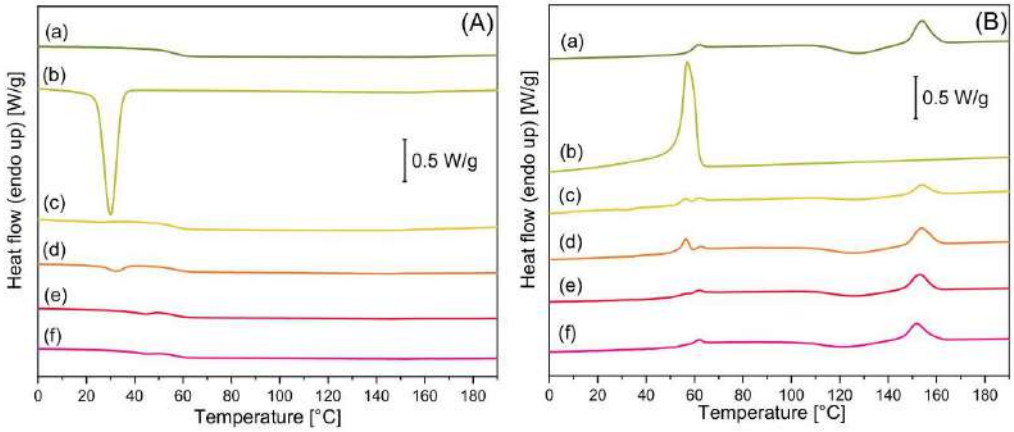

Figure S6. DSC thermograms, cooling (A) and second heating (B), of: (a) PLA_10 (—), (b) PCL_10 (—), (c) PLA_PCL_95_5 (—), (d) PLA_PCL_90_10 (—), (e) PLA_PCL_G_95_5_0.5 (—), (f) PLA_PCL_G_95_5_1 (—).

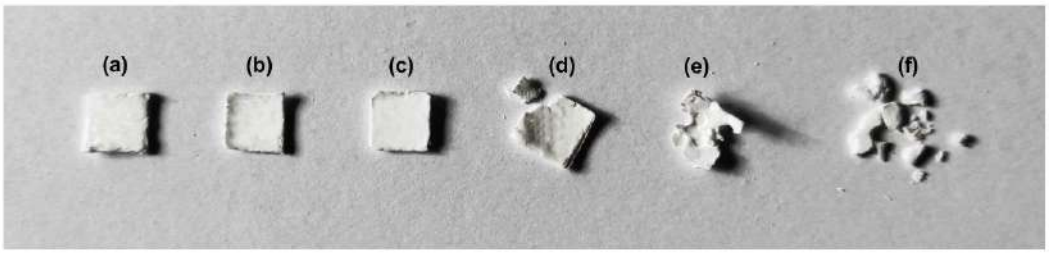

Figure S7. Photos of: (a) neat PLA film (PLA_10) and PLA_10 treated with diamine solution for (b) 15 min, (c) 30 min, (d) 60 min, (e) 120 min and (e) 180 min.

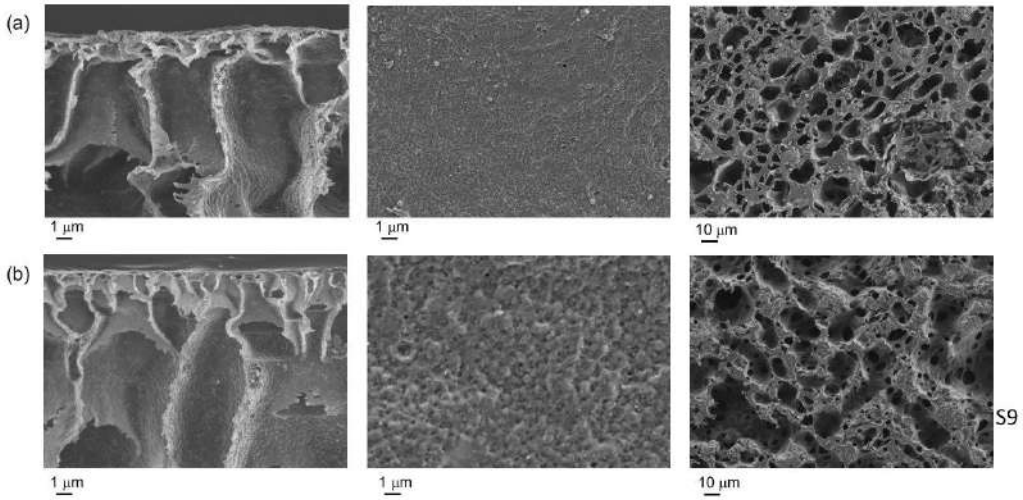

S9

Figure S8. FE-SEM micrographs of the surfaces (dense and porous) and cross sections of: (a) PLA_10 and (b) PLA_10 treated for 30 min with the diamine solution (PLA_10A).

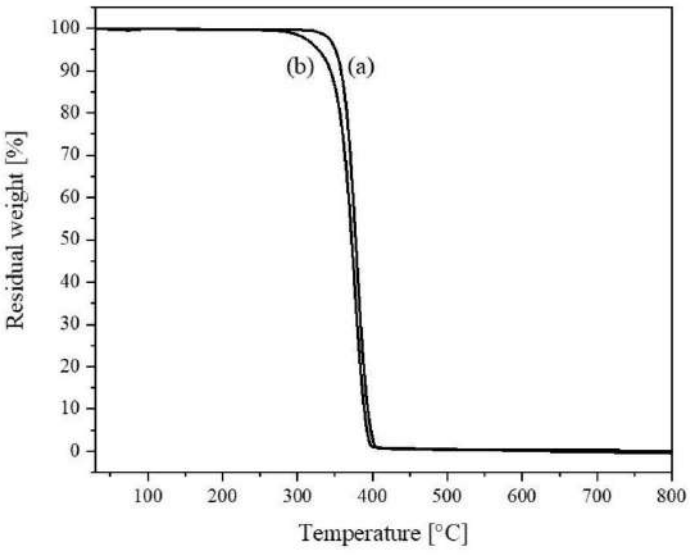

S10

Figure S9. TGA thermograms of (a) PLA_10 and (b) PLA_10A.

Chapter 6: On the effective application of star-shaped polycaprolactones with different end functionalities to improve the properties of polylactic acid blend films

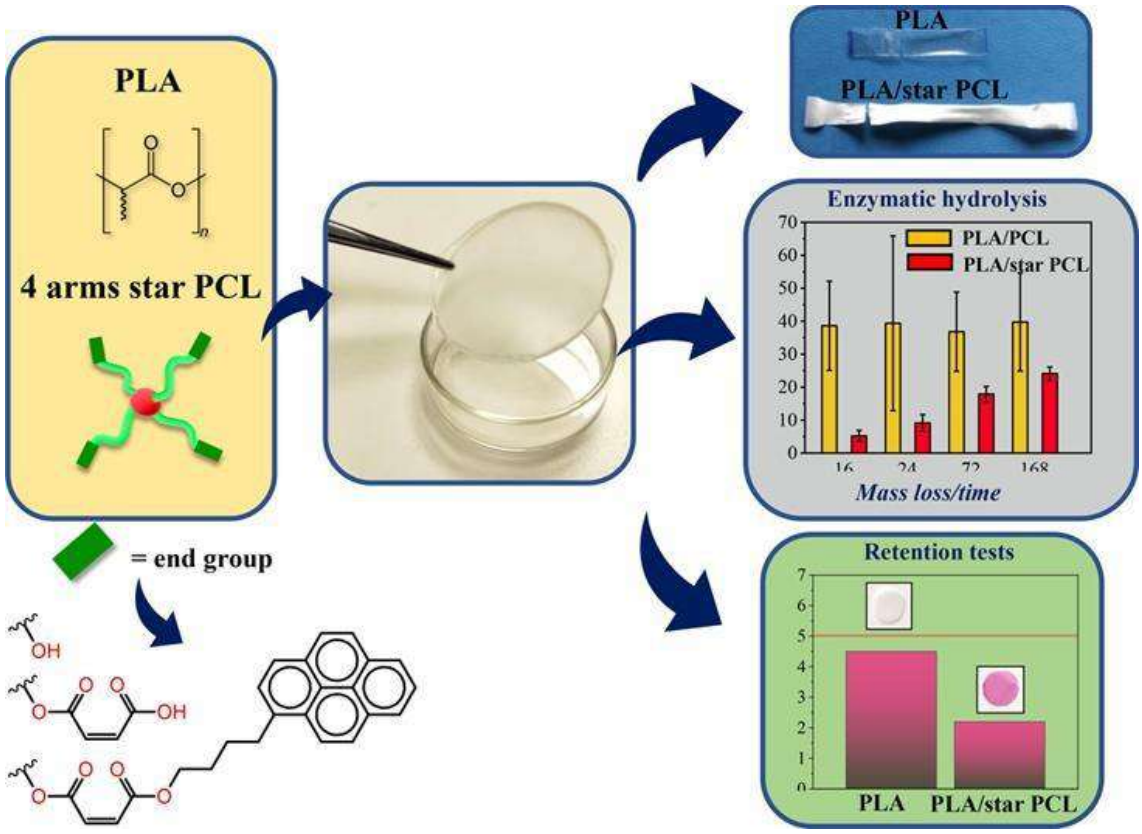

European Polymer Journal 176 (2022) 111402

Contents lists available at ScienceDirect

European Polymer Journal

journal homepage: www.elsevier.com/locate/europolj

On the effective application of star-shaped polycaprolactones with different end functionalities to improve the properties of polylactic acid blend films

Giacomo Damonte [a], Beatrice Barsanti [a], Alessandro Pellis [a], Georg M. Guebitz [b,c], Orietta Monticelli [a,*]

[a] Dipartimento di Chimica e Chimica Industriale, Università di Genova, Via Dodecaneso 31, 16146 Genova, Italy
[b] Department of Agrobiotechnology, IFA-Tulln, Institute of Environmental Biotechnology, University of Natural Resources and Life Sciences Vienna BOKU, Konrad-Lorenz-Strasse 20, 3430 Tulln an der Donau, Austria
[c] Austrian Centre of Industrial Biotechnology, Konrad-Lorenz-Strasse 20, 3430 Tulln an der Donau, Austria

ARTICLE INFO

Keywords:
PLA
PCL
Star polymer
Blend
Enzymatic hydrolysis

ABSTRACT

The aim of this work was to improve and disclose novel properties of polylactic acid (PLA)-based films, using *ad-hoc* synthesized star-shaped polymers characterized by short polycaprolactone (PCL) arms having the same length but different end functionalities, namely: hydroxyl (coded as PCL-OH), carboxyl (coded as PCL-COOH) and pyrenyl (PCL-Pyr) groups. The properties of the films prepared by adding the synthesized PCLs to the polymer matrix were compared with those of films based on PLA and a commercial linear PCL (coded as PCL-L), which is commonly used in the development of PLA/PCL blends. The comparison of film morphology, evaluated by Field Emission Scanning Electron Microscopy (FE-SEM) measurements, showed that the dimensions of the PCL domains in the systems containing the star-shaped PCLs were smaller and adhered better to the polymer matrix than those of the films prepared from the commercial linear PCL. Moreover, it was found that the specific characteristics of the PCL domains, as well as the thermal properties of the films, depended on the nature of the end functionalities of the synthesized PCL. The peculiar dispersion of PCL domains in the films containing star-shaped PCLs resulted in a better elongation at break (ca. 40%) than the PLA/PCL-L films (8%), while maintaining an acceptable stiffness. Contact angle measurements performed on the developed films showed an influence of the PCL functionalities also on their wettability, with the PLA/PCL-COOH systems exhibiting the highest hydrophilicity (contact angle of 71.9). To assess the effect of the star-shaped PCLs on the adsorption capacity of amino-functionalized compounds, the films were contacted with a solution containing pararosaniline, an amino dye. Interestingly, the films based on PCL-COOH showed the highest tendency to retain the cationic dye. This indicates that the functionalities conferred to the polymer system by the functionalized PCL allowed interactions with positively charged molecules. The enzymatic hydrolysis behaviour was studied by applying a cutinase, a well-known enzyme hydrolysing various polyesters. It is of outmost relevance to underline that films containing star-shaped PCLs exhibited slower and more controlled hydrolysis kinetics when compared to PLA/PCL systems and that this property could be tuned by changing the PCL end functionality.

1. Introduction

The main challenge related to the widespread use of bioplastics is the development of strategies to improve their characteristics and introduce novel properties. Particularly, in the case of polylactic acid (PLA), the drawbacks that must be overcome for it to compete with fossil polymers are related to its high brittleness, lack of functional groups, and difficulties in tuning its degradation. An efficient approach to improve the toughness of a brittle polymer is in general the blending with ductile polymers. The combination of PLA with polycaprolactone (PCL), a biocompatible and biodegradable semi-crystalline polyester with a rubbery amorphous phase at room temperature, seems to be an effective approach. PLA/PCL blends exhibit higher impact strength than pure PLA, while maintaining the biocompatibility and biodegradability of the formulation [1]. Several works have focused on the morphology and the mechanical properties of PLA/PCL blends [1–4]. Most of these studies

* Corresponding author.
E-mail address: orietta.monticelli@unige.it (O. Monticelli).

https://doi.org/10.1016/j.eurpolymj.2022.111402
Received 1 June 2022; Received in revised form 29 June 2022; Accepted 6 July 2022
Available online 8 July 2022

concluded that PLA and PCL are incompatible polymers since their large interfacial tension leads to coarse morphologies and poorer mechanical properties. Therefore, compatibilization is considered necessary for the preparation of PLA/PCL blends with high toughness. Indeed, the compatibilization of PLA/PCL blends with various prefabricated PLA-PCL block copolymers has been well studied for many decades [2,4–7]. In one of the pioneering works, Dell'Erba et al. showed that the addition of PLLA-b-PCL-b-PLLA triblock copolymers to PLLA/PCL blends significantly reduced the size of PCL particles [8]. In a more recent and detailed work, Xiang et al. studied the compatibilization efficiency of PLLA-b-PCL block copolymers having various compositions and molecular weights for PLLA/PCL blends prepared in a batch mixer [9]. Addition of 5 wt-% of these copolymers caused reduction of the PCL particle size and substantially enhanced elongation at break. The reactive compatibilization of PLA/PCL blends has been investigated quite intensively by different authors for compositions containing PCL in the range of 15–30 wt% [10–12]. Another strategy to improve the compatibility and therefore the toughness was to add nanofillers such as layered silicate [13,14], POSS [15,16], carbon nanotubes [17,18] and graphite [19–23]. In addition, it was reported that the average size of the PCL domains could also affect the mechanical properties of the blends, with data on impact strength generally studied and reported [1]. However, it is relevant to underline that not all the works dealing with the above-mentioned material properties included a statistical analysis of the PCL domain dimensions, but focused mainly on the morphology of the two phases and, in particular, on their adhesion.

In all the previously cited papers, polymers having a high molecular weight and linear structure were considered, therefore an advancement compared to the known literature would be the analysis of the properties of blends based on star-shaped PCL having low molecular masses and different end groups. Indeed, the modification of PCL functionalities might allow studying also the effect of the polymer functionalization on the material final properties. PCL with the above specific architecture, used in combination with PLA, could: i) lead to the formation of aggregates with dimensions different from those of linear polymers, ii) have high compatibility with the PLA matrix thanks to the high number of end groups, iii) make the system functional and able to interact with certain molecules, because of the increased functionalities [24] and iv) modify the system degradation kinetic [25]. Along with the above benefits, the formulation would retain its "green" properties because the arms of the star structure would be made of PCL, a biocompatible and biodegradable polymer. It is worth underling that PCL-based star systems, generally prepared by the ring-opening polymerization of ε-caprolactone using various types of initiators, until now, were mainly applied in the biomedical field [26,27]. Considering the potential of these polymers in the development of formulations consisting of their combination with PLA, in this work, for the first time and in a systematic way, the properties of blends based on PLA and *ad-hoc* synthesized star PCL with four arms characterized by the same length but different end functionalities, namely hydroxyl (coded as PCL-OH), carboxyl (coded as PCL-COOH) and pyrenyl (coded PCL-Pyr) groups, were studied (Fig. 1). The influence of the star structure and end functionalities on the final properties of the blends was analysed by comparing the characteristics of films based on the synthesized PCL with those of films prepared starting from the same PLA and a high molecular weight commercial PCL.

2. Experimental

2.1. Materials

High molecular weight PCL (referred to as PCL-L), CAPA® 6500 (M_w = 50 kg/mol), was purchased from Perstorp. High molecular weight PLA, Luminy® LX 175 (stereochemical purity: 96% L-isomer, M_w = 245 kg/mol), was purchased from Corbion. ε-caprolactone (purity ≥ 97%), pentaerythritol (purity ≥ 99%), dipentaerythritol (purity 99%), 1-pyrenebutanol (purity ≥ 99%), tin(II) 2-ethylhexanoate ($Sn(Oct)_2$) (purity ≥ 96%), toluene (anhydrous, purity 99,7%), dichloromethane (stabilized with 0,002% 2-methyl-2-butene), chloroform (≥99,5%, 100–200 ppm amylenes as stabilizer), methanol (99,9%), pararosaniline hydrochloride (≥85%), maleic anhydride (≥99%) N,N'-Dicyclohexylcarbodiimide (DCC), 4-Dimethylaminopyridine (DMAP) and PBS buffer tablet (pH 7.2–7.6, 1 tablet/200 mL) were purchased from Sigma Aldrich®. ε-caprolactone and DCM were purified/dried prior to use by vacuum distillation over CaH_2. Novozym ® 51,032 (product code: 06–3135) was purchased from STREM Chemicals. All the other reagents were of analytical grade and used without purification.

Fig. 1. Scheme of blend film preparation.

2.2. Synthesis of PCL-star-4–2 k-OH (PCL-OH)

The synthesis of the four-armed, star-shaped, hydroxyl-terminated PCL (PCL-star-4–2 k-OH, referred to as PCL-OH) was performed exploiting the ring opening polymerization (ROP) of ε-caprolactone using pentaerythritol as initiator and tin 2-ethylhexanoate as catalyst, following the previously procedure described [28–32]. Briefly, the monomer was added to a 50-mL two-neck round-bottomed flask using an argon atmosphere, followed by the initiator, whose quantity was adjusted to obtain the desired molecular weight. Subsequently, the system was gently heated to 80 °C to favour the dissolution of the initiator. The temperature was then raised to 120 °C under stirring and a calculated amount of $Sn(Oct)_2$ was added as a 100 mg/mL solution in anhydrous toluene to maintain the [ε-CL]/[$Sn(Oct)_2$] ratio = 5000. After 24 h, the mixture was cooled, and the crude polymer was dissolved in a small amount of DCM. The product was then precipitated from ice cold methanol under vigorous stirring (50 mL/g PCL), filtered through a Büchner funnel, washed several times with small portions of ice-cold methanol, and dried under vacuum at 30 °C for 72 h.

^{1}H NMR chemical shifts of PCL-OH (Fig. S1a): 4.09 ppm (–CH_2- pentaerythritol, s); 4.05 ppm (–CH_2-, t); 3.63 ppm (–CH_2-OH PCL chain terminal, t); 2.29 ppm (–CH_2-, t); 1.64 (–CH_2-, m); 1.38 (ppm –CH_2-, m).

IR signals of PCL-OH (Fig. S2a): 2945 cm^{-1} (asymmetric –CH_2- stretching); 2870 cm^{-1} (symmetric –CH_2- stretching); 1725 cm^{-1} (symmetric > **C** = **O** stretching); 1297 cm^{-1} (-**C-O-** and -**C-C-** stretching); 1242 cm^{-1} (asymmetric -**C-O-C-** stretching); 1179 cm^{-1} (symmetric -**C-O-C-** stretching).

2.3. Synthesis of PCL-star-4–2 k-COOH (PCL-COOH)

The synthesis of the four-armed, star-shaped, carboxyl-terminated polymer (PCL-star-4–2 k-COOH, referred to as PCL-COOH) was carried

out by esterification of PCL-OH with maleic anhydride. 3 g of PCL-OH was added to a 50-mL round bottom flask under argon, followed by 4 equivalents of maleic anhydride with respect to the terminal hydroxyl groups. Successively, 3 mL/g PCL of anhydrous toluene were added under stirring, and the reaction was carried out at 80 °C for 24 h. The crude product was obtained by precipitation in ice cold methanol (50 mL/g PCL), followed by Büchner filtration and washed several times with small portions of cold methanol. The polymer was then vacuum dried at 30 °C for 72 h.

^{1}H NMR chemical shifts of PCL-COOH (Fig. S1b): 4.09 ppm (–**CH$_2$**-pentaerythritol, s); 4.05 ppm (–**CH$_2$**-, t); 3.63 ppm (–**CH$_2$**-OH PCL chain terminal, t); 2.29 ppm (–**CH$_2$**-, t); 1.64 (–**CH$_2$**-, m); 1.38 (ppm –**CH$_2$**-, m). Along with PCL characteristic chain signal, two additive signals were observed in the vinylic proton zone, respectively at 6.42 (R-OOC-**CH** = **CH**-COOH, d) and 6.31 ppm (R-OOC-**CH** = CH-COOH, d), generated by the maleic proton system. In addition, the signal of the terminal protons of PCL chains (–**CH$_2$**-OOC-, t) shifted to a value of 4.28 ppm, typical of maleic esters [33].

IR peaks (cm^{-1}) of PCL-COOH (Fig. S2b): 2945 cm^{-1} (asymmetric –**CH$_2$**- stretching); 2870 cm^{-1} (symmetric –**CH$_2$**- stretching); 1725 cm^{-1} (symmetric > **C = O** stretching); 1297 cm^{-1} (-**C**-**O**- and -**C**-**C**- stretching); 1242 cm^{-1} (asymmetric -**C**-**O**-**C**- stretching); 1179 cm^{-1} (symmetric -**C**-**O**-**C**- stretching). In addition to the signals of PCL-OH, additive peaks at 1640 cm^{-1} (-**C** = **C**- stretching, maleic unit) and 822 cm^{-1} (-**Csp^2**-**H** bending, maleic unit) are present.

2.4. Synthesis of PCL-star-4–2 k-Pyr (PCL-Pyr)

The pyrenyl-terminated polymer (PCL-star-4–2 k-Pyr, referred to as PCL-Pyr) was prepared by esterification of carboxyl-terminated PCL with 1-pyrenebutanol under the mild conditions of Steglich esterification [34].

Briefly, the desired amount of carboxyl-terminated PCL (typically 2–3 g) was added to a 50 mL round bottomed flask under argon, followed by 1.1 eq. (with respect to –COOH groups) of DCC, 10 % mol DMAP (with respect to DCC), and 1.07 eq. (with respect to –COOH) of 1-pyrenebutanol. Successively, 3 mL/g PCL of anhydrous toluene was added, and the reaction was performed at 80 °C for 24 h under stirring. The crude product was then obtained by precipitation in cold methanol (50 mL/g PCL) followed by Büchner filtration, washing the material several times with small amopunts of cold methanol. The polymer was then vacuum dried at 30 °C until constant weight.

^{1}H NMR chemical shifts of PCL-Pyr (Fig. S1c): in addition to the characteristic PCL chain signals previously reported for –COOH-terminated polymers, additional peaks were detected in the 8 ppm range caused by the presence of pyrenic units. In the vinyl proton zone, a signal related to the vinyl protons of the maleic acid ester was observed at 6.42 ppm (R-OOC-**CH** = **CH**-COOR', s). This is originated by an equal shielding of the vinylic protons introduced by the esterification of the free carboxylic group. Finally, at 4.16 ppm (–COO-**CH$_2$**-, t), 3.37 ppm (–**CH$_2$**-, t), 1.92 ppm (–**CH$_2$**-, quint), 1.80 ppm (–**CH$_2$**-, quint) ppm four butylic chain signals are clearly visible. The value reached by the α-protons confirm complete esterification of the alcohol during the reaction.

IR peaks of PCL- Pyr (Figure S2c): 2945 cm^{-1} (asymmetric –**CH$_2$**- stretching); 2870 cm^{-1} (symmetric –**CH$_2$**- stretching); 1725 cm^{-1} (symmetric > **C = O** stretching); 1297 cm^{-1} (-**C**-**O**- and -**C**-**C**- stretching); 1242 cm^{-1} (asymmetric -**C**-**O**-**C**- stretching); 1179 cm^{-1} (symmetric -**C**-**O**-**C**- stretching) 1640 cm^{-1} (-**C** = **C**- stretching, maleic unit) and 822 cm^{-1} (-**Csp^2**-**H** bending, maleic unit). In addition, it is possible to recognize additive peaks in the fingerprint zone related to complex vibrational motions of the pyrenic unit at 896 cm^{-1}, 848 cm^{-1}, 764 cm^{-1}, 686 cm^{-1}, 623 cm^{-1} and 439 cm^{-1}.

2.5. Preparation of polymer films

Polymer films were prepared by the solvent casting method by pouring 10 mL of a 200 mg/10 mL polymer solution in DCM into a Petri dish with an inner diameter of 54 mm. The PLA/PCL ratio was 80/20 by weight. The solvent was then evaporated overnight at 30 °C and the films were then placed in a vacuum oven for 24 h at 30 °C.

2.6. Dye retention tests

Dye retention tests were performed by placing 5 small film disks (each 5 mm in diameter) in 1 mL of a 5 μg/mL solution of pararosaniline hydrochloride for 24 h. The disks were then removed, and the solution was analysed using a Shimadzu® UV 1800 UV–Vis spectrometer at the absorbance value of 540 nm. Quantification of the dye concentration in the supernatant was carried out preparing a calibration curve using pararosaniline standard solutions in Milli-Q® water (concentrations: 0.5, 1, 2, 5, and 10 μg/mL), which is shown in Equation (1).

$$Absorbance\ (a.u.) = 0.21758 \cdot Concentration\ (\mu g/mL) + 0.02848\ (r^2 = 0.99769) \quad (1)$$

2.7. Enzymatic hydrolysis experiments

Enzymatic hydrolysis of polymers was performed by placing a single film disk (5 mm diameter, n = 4) in a 1 mL eppendorf together with 1 mL of a 5 μM solution of cutinase (Novozym®) 51,032 in 0.1 M PBS buffer, pH 7.4. Samples were incubated for 16, 24, 72 and 168 h at 50 °C. At the desired time point, the polymer sample was removed from the enzyme solution, washed three times in ultrapure water and then dried at 30 °C overnight before gravimetric measurement of the weight loss (±0.0001 g).

2.8. Materials characterization

FT-IR spectra were recorded with a Bruker mod. "Vertex 70®" in ATR mode in the 400 to 4000 cm^{-1} range on powdered samples.

^{1}H NMR spectra were recorded using a Varian "Mercury 300®", at a frequency of 300 MHz with polymer samples dissolved in $CDCl_3$ (concentration of 30 mg/mL).

Differential Scanning Calorimeter (DSC) thermograms were measured using a Mettler Toledo "DSC1 STAR^e System®" in the temperature range from −100 to 150 °C at a heating/cooling rate of ± 10 °C/min, with a nitrogen flow of 20 mL/min.

The crystallinity degree (X_c) of PCL in the blend was calculated on the base of their contents, Φ_{PCL}, following the equation (2):

$$X_c(\%) = \frac{\Delta H_m}{H_m^0 \times \phi_{PCL}} \times 100\% \quad (2)$$

where ΔH_m = melting enthalpy (measured), ϕ_{PCL} is the PCL content in the blend and H_m^0 is the melting enthalpy of a 100% crystalline PCL, commonly found in the literature (139 J/g) [35]. The second heating scan was considered for the above calculation.

Thermogravimetric analysis (TGA) was performed using a Mettler Toledo "TGA/DSC1 STAR^e System®" in the temperature range from 30 to 800 °C using a heating rate of 10 °C/min, under a 80 mL/min nitrogen flow.

Field emission scanning electron microscopy (FE-SEM) was performed with a Zeiss "Supra 40 VP". All specimens were graphite coated with a Polaron "E5100" prior to analysis. The PCL domain dimensions were evaluated by applying the software ImageJ.

Strain tests were performed by an Instron Mechanical Tester (Instron 5565) (speed 1 mm/min, initial gage length l_0 = 20 mm) on 30x5x0.4 mm^3 specimens cut from films previously dried in a vacuum oven at 30 °C.

Contact angle measurements were carried out at room temperature with an Attension® contact angle meter using pure distilled water as probe liquid on the surface of the films that was in contact with the Petri dish. The average static contact angles were determined by measuring at least three drops on each film sample.

3. Results and discussion

3.1. FE-SEM characterization

FE-SEM micrographs at various magnifications of the prepared film cross-section are shown in Fig. 2. A sea-island morphology typical of PLA/PCL blend systems was observed in all analysed samples [36,37]. A comparison of the morphology of the PLA/PCL-L film (Fig. 2a) with that of the films based on the star-shaped PCL blends (Fig. 2b-2d) showed a difference in the size of the PCL domains, which went from 1.2 ± 0.5 μm for PLA/PCL to 0.8 ± 0.1 μm for PLA/PCL-Pyr. Moreover, voids between the PCL domains and the PLA matrix as well as exposed PCL domains are easily visible in the PLA/PCL-L sample (Fig. 2a), indicating poor adhesion between the two phases. In contrast, the blends based on PCL-OH and PCL-COOH showed better phase adhesion, although they had larger PCL domains than the PLA/PCL-Pyr sample (1.9 ± 0.3 and 2.7 ± 0.3 μm, respectively). In fact, PLA/PCL-Pyr system was characterised by smaller PCL clusters protruding from the studied surface, similar to PLA/PCL-L. Based on the above results, it can be hypothesized that the effect of PCL domain reduction is less effective than adhesion to the polymer matrix.

These results, which cannot be related to the different viscosity of the star-shaped PCL since they are characterized by the same molecular weight, demonstrate that the application of the synthesized polymers in the blend formulation improves the compatibility of PCL with the polymer matrix. Indeed, this phenomenon can be attributed to the peculiar star-shaped geometry, the lower molecular weight, and the higher concentrations of terminal functionalities of the star polymers compared to the standard commercial PCL. In addition, it is worth underling that other star-shaped PCLs were applied in the development of PLA-based blends, which also used a compatibilizer to improve the morphology of the material [25]. On this basis, one of the advantages of our system is that the improvement of the material properties was achieved without the addition of compounds other than the star-shaped PCL, but by the proper choice of their end groups.

3.2. Thermal characterization

DSC traces of the neat polymers and the prepared films are shown in Fig. 3, while the thermal data are summarized in Table 1. It can be seen that the commercial PLA and PCL-L were characterized by different thermal behaviours. While PCL showed a typical behaviour of a semi-crystalline polymer, PLA was amorphous and could not crystallize under the applied cooling conditions. For the synthesized star-shaped polymers, especially for the samples PCL-COOH and PCL-Pyr, a decrease in the crystallinity (χ_c) and crystallization temperature (T_c) was observed compared to the linear PCL-L. In particular, the drastic decrease in the above parameters observed for PCL-Pyr could be related to the formation of physical crosslinking resulting from π-π-stacking interactions among the pyrenic units [32]. These results show that not only the geometry but also the nature of the end functionalities of the polymer can strongly influence its thermal properties [32,38].

As for the blend systems, a slight increase in T_c and a relevant decrease in crystallinity for the PCL fraction were observed for the PLA/PCL-L film. As previously reported, this phenomenon can be attributed to the presence of PLA, which partially hinders the structuring of PCL chains during the crystallization process [39]. At the same time, an increase in cold crystallization enthalpy (ΔH_{cc}) and melting enthalpy (ΔH_m) of the PLA fraction indicated an enhancement of the crystallization process promoted by PCL. This observation, previously reported by Zhang et al. [40], clearly indicates a higher chain mobility of PLA in the blend ascribable to a reduction in the overall viscosity of the system.

The same trend of increasing T_c and decreasing χ_c compared to the neat star-shaped PCL was observed in the PCL fraction of the corresponding blends, with the largest gap found in the systems containing PCL-Pyr. Moreover, an increase in ΔH_{cc} and ΔH_m of the PLA fraction was also observed in the above-mentioned blends.

The study of the thermal properties of the neat polymers and of the blends was completed with TGA measurements (Table S1). It is important to underline that, although the star polymers are characterized by a lower degradation temperature compared to neat PLA, the corresponding blends showed a similar thermal degradation behaviour as the polymer matrix. Thus, this result indicates that the addition of the low molecular weight star molecules does not reduce the thermal stability of the blend.

3.3. Mechanical properties

Table 2 shows the mechanical properties of the starting polymers, PLA and PCL-L, and of the blends based on the star-shaped PCL

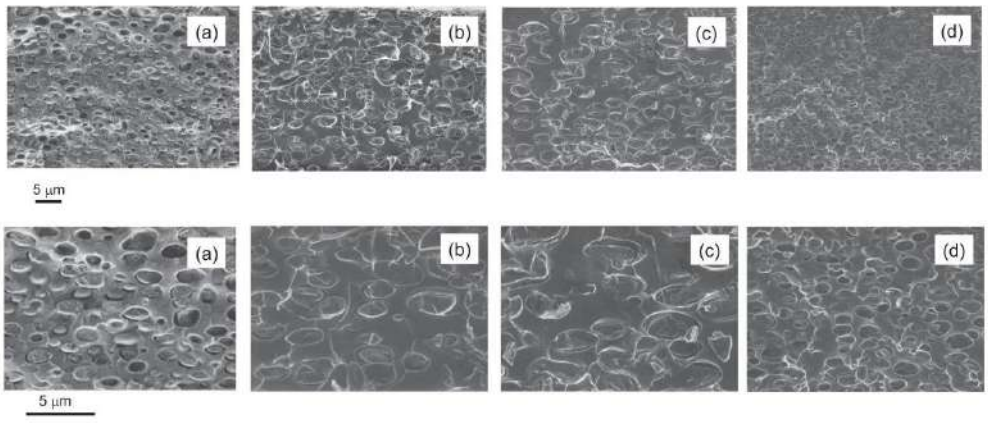

Fig. 2. FE-SEM micrographs of blend film cross-sections at different magnifications: (a) PLA/PCL-L, (b) PLA/PCL-OH, (c) PLA/PCL- COOH, (d) PLA/PCL-Pyr.

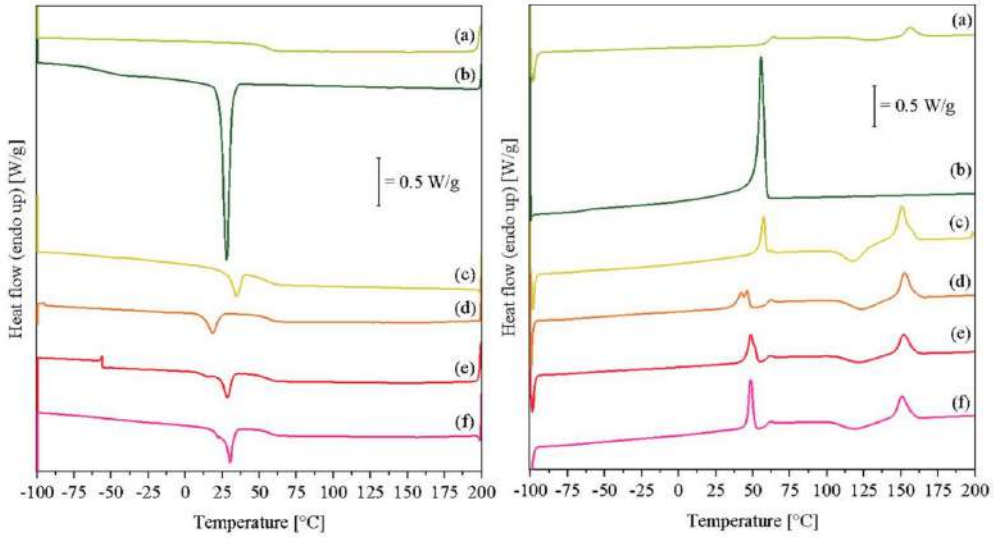

Fig. 3. DSC thermograms, cooling (left) and second heating (right) for: (a) PLA, (b) PCL-L, (c) PLA/PCL, (d) PLA/PCL-Pyr, (e) PLA/PCL-COOH, (f) PLA/PCL-OH.

Table 1
Thermal properties from DSC analysis of neat polymers and respective films.

	PCL fraction					PLA fraction			
Sample code	ΔH_c [J/g]	T_c [°C]	ΔH_m [J/g]	T_m [°C]	χ_c [%]	T_g [°C]	ΔH_{cc} [J/g]	ΔH_m [J/g]	T_m [°C]
PLA	–	–	–	–	–	55	−4	5	156
PCL-L	−65	30	69	57	50	–	–	–	–
PLA/PCL-L	−50	35	45	57	34	54	−23	25	151
PCL-OH	−70	28	69	49	50	–	–	–	–
PLA/PCL-OH	−45	30	65	49	46	57	−13	16	151
PCL-COOH	−62	22	60	44	43	–	–	–	–
PLA/PCL-COOH	−50	28	50	49	37	55	−13	16	152
PCL-Pyr	−56	8	53	45	38	–	–	–	–
PLA/PCL-Pyr	−50	19	45	46	34	57	−16	19	153

ΔH_c = crystallization enthalpy, T_c = crystallization temperature, ΔH_m = melting enthalpy, T_m = melting temperature, χ_c = crystallinity percentage, T_g = glass transition temperature, ΔH_{cc} = cold crystallization enthalpy.

Table 2
Mechanical properties of the prepared films.

Sample code	Young modulus [MPa]	Elongation at break [%]	Yield strength [MPa]
PLA	2150 ± 174	4 ± 0.14	44 ± 3
PCL-L	279 ± 18	102 ± 6	14 ± 1
PLA/PCL-L	1421 ± 83	8 ± 0.95	27 ± 2
PLA/PCL-OH	1512 ± 23	47 ± 14	24 ± 1
PLA/PCL-COOH	1766 ± 203	37 ± 11	29 ± 4
PLA/PCL-Pyr	1888 ± 63	8 ± 3	30 ± 2

materials. PLA was characterized by a relatively high modulus (2150 MPa) and maximum strength (44 MPa), combined with a low deformation at break (ε_{break}) of about 4 %. PCL, on the other hand, had much lower stiffness (279 MPa) and strength (14 MPa), but exhibited a very a high ε_{break} (about 102%), values consistent with the results found in the literature [1,36,37,41–43]. For the blend PLA/PCL-L, both the modulus and the strength are between those of the neat polymers. On the contrary, the elongation at break was not significantly changed compared to that of PLA, proving that the presence of PCL-L had no toughening effect, thus confirming the very low interaction at the interface of the two polymers. In the case of films based on the star-shaped polymers, the decrease in modulus was lower than for the PLA/PCL-L blend, while the strength showed similar values. One property that deserves detailed analysis is the elongation at break, which was found to be strictly dependent on the type of star-shaped polymer in the blend system. In particular, ε_{break} was 47%, 37% and 8% for PLA/PCL-OH, PLA/PCL-COOH and PLA/PCL-Pyr, respectively. Indeed, in order to explain this behaviour, it is necessary to consider the effects of the end functionalities on the specific interactions of star-shaped PCL with the PLA matrix. In particular, in the case of the blend based on PCL-Pyr, it is possible to hypothesize that the intermolecular π-π-stacking interactions caused by the pyrenyl functionalities limit the interaction with PLA at the interface, reducing the interfacial adhesion of the polymer phase, as shown by the results of the FE-SEM measurements, and causing poor load transfer in the resulting blend. Remarkably, the elongation at break of the systems based on PCL-OH and PCL-COOH, respectively, was 6 and 5 times higher than that of the blend with the commercial polymers. Indeed, the lower ε_{break} measured for the system with the carboxyl-terminated PCL could again be due to intermolecular interactions caused by the chain ends, which, similar to the pyrenic polymer, could limit the interactions with the PLA matrix in the interphase.

However, the high elongation at break values as well as the maintenance of acceptable stiffness of the systems based on PCL-OH and PCL-

COOH demonstrate the effectiveness of the developed approach. It is relevant to underline that, unlike linear high molecular weight PCL, the use of the star polymer does not require the addition of components that promote the compatibility of the two polymer phases, such as copolymers or fillers [2,6,13–15]. Indeed, the simplicity and scalability of the star-shaped polymer synthesis and their potential ability to modify other properties of the matrix, such as its functionality, make these systems promising additives for the development of PLA-based films.

3.4. Wettability tests

To evaluate the effect of the star-shaped PCLs on wetting properties of PLA/PCL films, contact angle (ϑ) measurements were carried out on the neat PLA and PCL-L, on the blend PLA/PCL-L and on the films containing the synthesized polymers (Fig. 4). In particular, neat PCL-L exhibited a higher ϑ than neat PLA, with contact angles of 77.5° and 70.8° for PCL-L and PLA, respectively. The above values, which are in agreement with those reported in the literature, demonstrate a higher hydrophobicity of the PCL film [44–46]. Interestingly, the PLA/PCL-L film showed a similar contact angle to that of the neat PCL-L, indicating a predominant effect of this polymer over that of PLA. The films based on the star-shaped polymers exhibited a lower contact angle than the PLA/PCL-L sample, with ϑ of PLA/PCL-COOH, PLA/PCL-OH and PLA/PCL-Pyr being 71.9, 73.6 and 76.5, respectively. Thus, it is worth underling that this decrease depends on the nature of the functional end groups of the star-shaped polymer. This indicates the possibility of tuning the material wettability by changing the chemical structure of the synthesized PCL. Moreover, these results show that the functionalities created by the introduction of the star-shaped PCL into the polymer film are exposed on the surface and therefore can potentially interact with chemical species and also modulate the material degradability. With regard to the wettability of the blend components, the improvement of hydrophilicity is an important issue in PCL-based systems, especially for the application of the aforementioned polymer in the biomedical field. To this end, Solovieva et al. treated electrospun PCL fibers with $Ar/CO_2/C_2H_2$ plasma to functionalize the surface with –COOH groups and produce a scaffold with enhanced cell adhesion and proliferation [47]. In a recent work, Permyakova et al. showed improved wettability for the same system compared to untreated electrospun PCL [48].

Also with regard to PLA, the modification of the surface wettability was obtained by air atmospheric plasma treatment, with the formation of oxygen-based polar species [49]. Other approaches were based on the incorporation of proper fillers, such as layered silicates [50], into the polymer matrix and on the application of the Layer-by-Layer method [51]. The use of the synthesized star-shaped PCLs is indeed an innovative approach to tune the wettability of PLA.

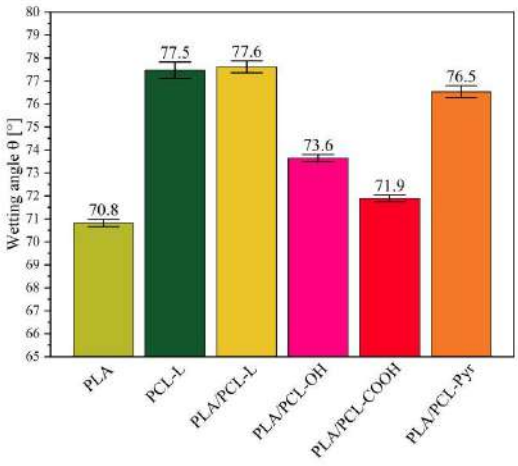

Fig. 4. Contact angle of the films based on neat PLA, PCL-L and on the blends.

3.5. Dye retention tests

To evaluate the retention capacity of the developed materials, dye adsorption tests were performed by immersing the films directly in a pararosaniline hydrochloride solution for 24 h and then analysing the remaining dye concentration in the supernatant. A triarylmethane compound, containing amino groups, was chosen to mimic the behaviour of positively charged amine-containing molecules such as drugs, pollutants, enzymes, and biogenic amines [52]. In particular, pararosaniline was selected as a model molecule because it is stable in solution over a long period of time and can be easily detected even at low concentrations. Fig. 5 shows the concentration of the dye in the medium that came into contact with the polymer film, as determined by spectrophotometric measurements, together with the photographs of the film after contact.

The limited capacity of the blend PLA/PCL-L to retain the amino dye can be related to the properties of the two components of the system. Although the polymer matrix of PLA is characterized by carboxyl end groups, the low concentration of these functionalities limits its ability to interact with positively charged molecules. To improve the retention properties of PLA, different approaches were investigated, such as surface functionalization [53–55], dispersion of fillers/nano-fillers or specific components [56]. When analysing the behaviour of the other films developed, it is interesting to note that the films based on PCL-OH and PCL-Pyr showed similar behaviour to the PLA/PCL-L blend. Conversely, the PLA/PCL-COOH sample had about twice the retention capacity for the dye as the other systems studied. This phenomenon is also evident in the final coloration of the PLA/PCL-COOH film exposed to a pararosaniline hydrochloride solution. This significant result can be attributed to the carboxyl functionalities of the star-shaped PCL, which not only increase the hydrophilicity of the film but also allow specific interactions with positively charged molecule.

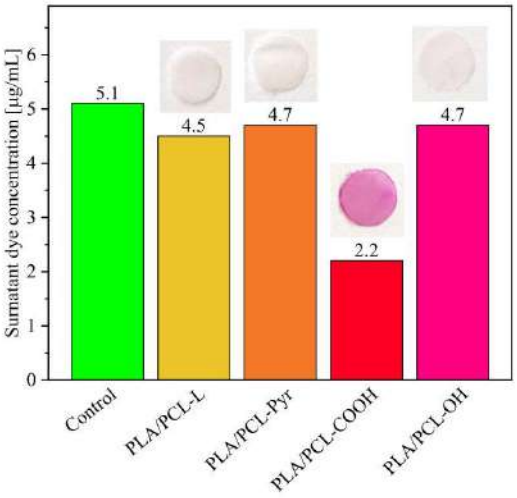

Fig. 5. Concentration of pararosaniline hydrochloride in the solutions after contact with the prepared films for 24 h (photos of the films after the contact time).

3.6. Enzymatic hydrolysis of blended films

Enzymatic hydrolysis of the developed polymer films was carried out by using a cutinase reported previously to hydrolyse various polyesters [57–59]. For high molecular weight PCL samples (PCL-L, dark green bars), it was possible to observe a complete hydrolysis of the film after only 4 h of reaction. On the other hand, the neat PLA samples (light green bars) exhibited a slower hydrolysis profile characterized by a latency period during the first 24 h followed by an increase in the hydrolysis rate until a mass loss of 22% was reached after 7 days.

In addition, the recovery of the film at the end of the test suggested that hydrolysis occurred by superficial erosive process, as reported in previous works on commercial PLA films [57]. The different hydrolysis profiles of PLA and PCL were most likely due to several factors, including different enzymatic affinity for the substrate [58], surface tension and physical state and structure of the polymers.

Moreover, this difference in hydrolysis behaviour is in agreement with the results of another work carried out under similar conditions, employing a cutinase-like enzyme [59]. The samples prepared with PLA/PCL-L blends showed significant differences in % mass loss when examined during a time course reaction (Fig. 6, yellow bars). After a reaction time of 16 h, some of the PLA/PCL-L films were almost completely degraded and could no longer be weighted while other samples could be easily recovered like the neat PLA films. This phenomenon may be related to the limited dispersion of PCL-L domains in PLA, which hardly adhere to the polymer matrix and are easily degraded, causing the film losing its integrity.

Conversely, for the samples prepared using the synthesized star-shaped PCLs, a significantly lower % mass loss, (from 3 to 5%) in comparison with the one measured for the PLA/PCL-L blend film (38%), was observed. This is a clear proof that the low molecular weight star-shaped PCL polymers are better dispersed in the PLA matrix therefore leading to a more homogeneous material.

At the same time, it was possible to highlight a slight influence of terminal functionalities of the star-shaped PCLs on the hydrolysis kinetics. The mass loss observed after one week for the three systems was in the order PLA/PCL-Pyr < PLA/PCL-OH < PLA/PCL-COOH with a % mass loss of 18, 21 and 24%, respectively. The presence of free carboxyl end groups may in fact have triggered a slight phenomenon of a self-catalyzed hydrolysis of the polymer matrix that therefore accelerated the enzymatic hydrolysis process [60].

However, the absence of the above-mentioned self-catalysed hydrolysis effect in the samples containing -PCL-OH and PCL-Pyr did not have a major impact on the overall hydrolytic stability of the polymers, yielding similar results to those observed for PLA. Interestingly, a FE-SEM comparison between PLA and PLA/PCL-COOH after 72 h of enzyme exposure (Fig. 7a and 7b) showed that the cutinase preferentially eroded PCL domains, leaving holes and cavities in the PLA matrix therefore confirming once more the fast PCL and slow PLA hydrolysis kinetics.

4. Conclusions

In this work, blended films based on PLA and star-shaped PCLs were developed with better and novel properties than those of PLA matrix and blends prepared from a commercial linear PCL (PCL-L). In particular, the influence of the functionalities of the *ad-hoc* synthesized star-shaped PCLs with the same molecular weight but different end groups, i.e., pyrenyl (PCL-Pyr), carboxyl (PCL-COOH) and alcoholic (PCL-OH), on the final properties of the material was demonstrated. The films based on PCL-OH and PCL-COOH, characterized by PCL domains with high adhesion to the polymer matrix, showed elongation at break up to six times higher than the PLA/PCL-L blends, while exhibiting acceptable stiffness. Moreover, it was found that the acid functionalities conferred to the blend by the star-shaped PCL ending with COOH groups gave the blend the highest wettability and a relevant ability to interact/retain amino-functionalized compounds. Moreover, films based on the star-shaped PCLs exhibited slower and more controlled enzymatic hydrolysis kinetics compared to PLA/PCL systems, and it was found that this property can be adjusted by changing the PCL end functionality.

Based on the above properties, the developed blends based on the star-shaped PCLs, whose synthesis is easily scalable, represent promising materials that could find new and attractive applications.

CRediT authorship contribution statement

Giacomo Damonte: Investigation, Visualization, Writing – original draft. **Beatrice Barsanti:** Investigation, Visualization. **Alessandro**

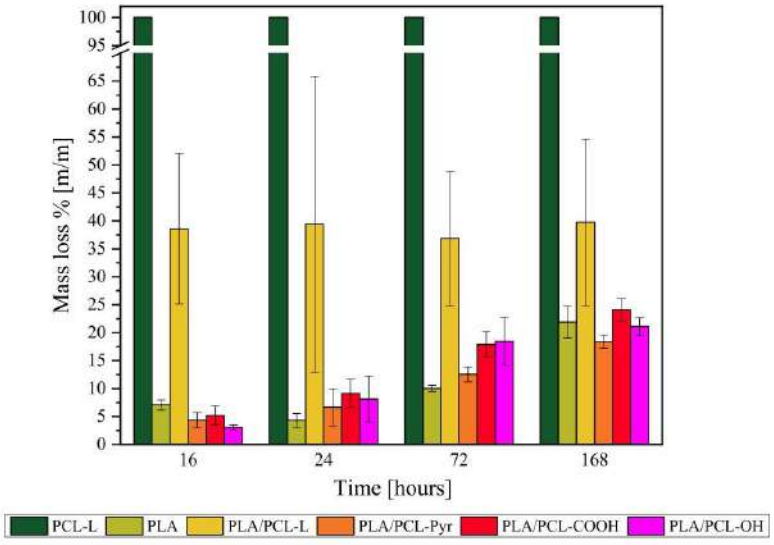

Fig. 6. Enzymatic hydrolysis of neat and blended polymer films.

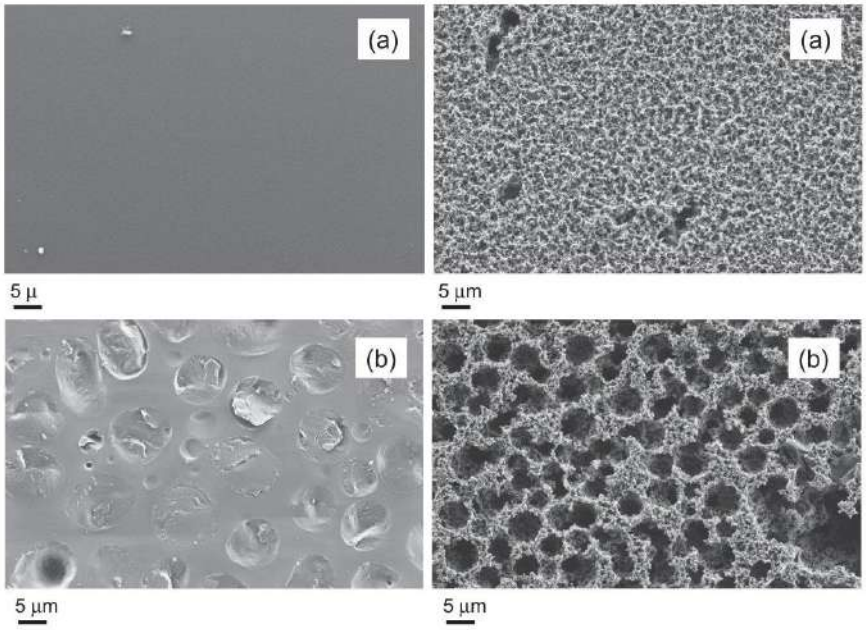

Fig. 7. Film surface FE-SEM micrographs of: (a) PLA, (b) PLA/PCL-COOH, before (left) and after (right) 72 h of contact with enzyme solution.

Pellis: Conceptualization, Writing – review & editing. **Georg M. Guebitz:** Validation. **Orietta Monticelli:** Conceptualization, Supervision, Writing – review & editing.

Declaration of Competing Interest

The authors declare that they have no known competing financial interests or personal relationships that could have appeared to influence the work reported in this paper.

Data availability

Data will be made available on request.

References

[1] I. Fortelny, A. Ujcic, L. Fambri, M. Slouf, Phase structure, compatibility, and toughness of PLA/PCL blends: a review, Front. Mater. 6 (2019), https://doi.org/10.3389/fmats.2019.00206.

[2] X. Xiao, V.S. Chevali, P. Song, B. Yu, Y. Yang, H. Wang, Enhanced toughness of PLLA/PCL blends using poly(d-lactide)-poly(ε-caprolactone)-poly(d-lactide) as compatibilizer, Compos. Commun. 21 (2020), 100385, https://doi.org/10.1016/j.coco.2020.100385.

[3] S. Wachirahuttapong, C. Thongpin, N. Sombatsompop, Effect of PCL and compatibility contents on the morphology, crystallization and mechanical properties of PLA/PCL blends, Energy Procedia 89 (2016) 198–206, https://doi.org/10.1016/J.EGYPRO.2016.05.026.

[4] H. Tsuji, T. Yamada, M. Suzuki, S. Itsuno, Effects of poly(L-lactide-co-ε-caprolactone) on morphology, structure, crystallization, and physical properties of blends of poly(L-lactide) and poly(ε-caprolactone), Polym. Int. 52 (2003) 269–275, https://doi.org/10.1002/pi.1093.

[5] L. Calandrelli, A. Calarco, P. Laurienzo, M. Malinconico, O. Petillo, G. Peluso, Compatibilized polymer blends based on PDLLA and PCL for application in bioartificial liver, Biomacromolecules 9 (2008) 1527–1534, https://doi.org/10.1021/bm7013087.

[6] N.-S. Choi, C.-H. Kim, K.Y. Cho, J.-K. Park, Morphology and hydrolysis of PCL/PLLA blends compatibilized with P(LLA-co-PCL) or P(LLA-b-PCL), J. Appl. Polym. Sci. 86 (2002) 1892–1898, https://doi.org/10.1002/app.11134.

[7] G. Maglio, A. Migliozzi, R. Palumbo, B. Immirzi, M.G. Volpe, Compatibilized poly (ε-caprolactone)/poly(L-lactide) blends for biomedical uses, Macromol. Rapid Commun. 20 (1999) 236–238, https://doi.org/10.1002/(SICI)1521-3927(19990401)20:4<236::AID-MARC236>3.0.CO;2-V.

[8] R. Dell'Erba, G. Groeninckx, G. Maglio, M. Malinconico, A. Migliozzi, Immiscible polymer blends of semicrystalline biocompatible components: thermal properties and phase morphology analysis of PLLA/PCL blends, Polymer 42 (2001) 7831–7840, https://doi.org/10.1016/S0032-3861(01)00269-5.

[9] S. Xiang, L. Feng, X. Bian, B. Zhang, B. Sun, Y. Liu, G. Li, X. Chen, Toughening modification of PLLA with PCL in the presence of PCL-b-PLLA diblock copolymers as compatibilizer, Polym. Adv. Technol. 30 (2019) 963–972, https://doi.org/10.1002/pat.4530.

[10] M. Przybysz-Romatowska, J. Haponiuk, K. Formela, Poly(ε-caprolactone)/poly (lactic acid) blends compatibilized by peroxide initiators: comparison of two strategies, Polymers 12 (2020) 228, https://doi.org/10.3390/polym12010228.

[11] M. Harada, K. Iida, K. Okamoto, H. Hayashi, K. Hirano, Reactive compatibilization of biodegradable poly(lactic acid)/poly(ε-caprolactone) blends with reactive processing agents, Polym. Eng. Sci. 48 (2008) 1359–1368, https://doi.org/10.1002/pen.21088.

[12] J.S. Jeon, D.H. Han, B.Y. Shin, Improvements in the rheological properties, impact strength, and the biodegradability of PLA/PCL blend compatibilized by electron-beam irradiation in the presence of a reactive agent, Adv. Mater. Sci. Eng. 2018 (2018) 1–8, https://doi.org/10.1155/2018/5316175.

[13] R. Umamaheswara Rao, B. Venkatanarayana, K.N. Suman, Enhancement of mechanical properties of PLA/PCL (80/20) blend by reinforcing with MMT nanoclay, Mater. Today Proc. 18 (2019) 85–97, https://doi.org/10.1016/j.matpr.2019.06.280.

[14] I. Kelnar, I. Fortelný, L. Kaprálková, J. Kratochvíl, B. Angelov, M. Nevoralová, Effect of layered silicates on fibril formation and properties of PCL/PLA microfibrillar composites, J. Appl. Polym. Sci. 133 (2016) 1–9, https://doi.org/10.1002/app.43061.

[15] O. Monticelli, M. Calabrese, L. Gardella, A. Fina, E. Gioffredi, Silsesquioxanes: novel compatibilizing agents for tuning the microstructure and properties of PLA/PCL immiscible blends, Eur. Polym. J. 58 (2014) 69–78, https://doi.org/10.1016/j.eurpolymj.2014.06.021.

[16] M.D. Doganci, F. Aynali, E. Doganci, G. Ozkoc, Mechanical, thermal and morphological properties of poly(lactic acid) by using star-shaped poly (ε-caprolactone) with POSS core, Eur. Polym. J. 121 (2019), 109316, https://doi.org/10.1016/j.eurpolymj.2019.109316.

[17] D. Wu, Y. Zhang, M. Zhang, W. Yu, Selective localization of multiwalled carbon nanotubes in poly(ε-caprolactone)/polylactide blend, Biomacromolecules 10 (2009) 417–424, https://doi.org/10.1021/bm801183f.

[18] Y. Liu, H. He, G. Tian, Y. Wang, J. Gao, C. Wang, L. Xu, H. Zhang, Morphology evolution to form double percolation polylactide/polycaprolactone/MWCNTs nanocomposites with ultralow percolation threshold and excellent EMI shielding, Compos. Sci. Technol. 214 (2021), 108956, https://doi.org/10.1016/J.COMPSCITECH.2021.108956.

[19] I. Kelnar, J. Kratochvíl, L. Kaprálková, A. Zhigunov, M. Nevoralová, Graphite nanoplatelets-modified PLA/PCL: effect of blend ratio and nanofiller localization on structure and properties, J. Mech. Behav. Biomed. Mater. 71 (2017) 271–278, https://doi.org/10.1016/j.jmbbm.2017.03.028.

[20] A.S. Luyt, I. Kelnar, Effect of blend ratio and nanofiller localization on the thermal degradation of graphite nanoplatelets-modified PLA/PCL, J. Therm. Anal. Calorim. 136 (2019) 2373–2382, https://doi.org/10.1007/s10973-018-7870-y.

[21] I. Kelnar, J. Kratochvíl, I. Fortelný, L. Kaprálková, A. Zhigunov, M. Nevoralová, Effect of graphite nanoplatelets on melt drawing and properties of PCL/PLA microfibrillar composites, Polym. Compos. 39 (2018) 3147–3156, https://doi.org/10.1002/pc.24322.

[22] I. Kelnar, Unique role of graphite nanoplatelets in upgrading biodegradable polymer systems, 2018 IEEE 8th Int. Conf. Nanomater. Appl. Prop. (2018) 1–4. https://doi.org/10.1109/NAP.2018.8914990.

[23] M. Forouharshad, L. Gardella, D. Furfaro, M. Galimberti, O. Monticelli, A low-environmental-impact approach for novel bio-composites based on PLLA/PCL blends and high surface area graphite, Eur. Polym. J. 70 (2015) 28–36, https://doi.org/10.1016/j.eurpolymj.2015.06.016.

[24] O. Monticelli, S. Russo, R. Campagna, B. Voit, Preparation and characterisation of blends based on polyamide 6 and hyperbranched aramids as palladium nanoparticle supports, Polymer 46 (2005) 3597–3606, https://doi.org/10.1016/j.polymer.2005.03.029.

[25] M.D. Doganci, Effects of star-shaped PCL having different numbers of arms on the mechanical, morphological, and thermal properties of PLA/PCL blends, J. Polym. Res. 28 (2021) 11, https://doi.org/10.1007/s10965-020-02380-2.

[26] A.M. Bhayo, R. Abdul-Karim, S.G. Musharraf, M.I. Malik, Synthesis and characterization of 4-arm star-shaped amphiphilic block copolymers consisting of poly(ethylene oxide) and poly(ε-caprolactone), RSC Adv. 8 (2018) 28569–28580, https://doi.org/10.1039/c8ra05000g.

[27] C. Mota, D. Puppi, D. Dinucci, M. Gazzarri, F. Chiellini, Additive manufacturing of star poly(ε-caprolactone) wet-spun scaffolds for bone tissue engineering applications, J. Bioact. Compat. Polym. 28 (2013) 320–340, https://doi.org/10.1177/0883911513490341.

[28] M. Labet, W. Thielemans, Synthesis of polycaprolactone: a review, Chem. Soc. Rev. 38 (2009) 3484, https://doi.org/10.1039/b820162p.

[29] M. Sobczak, Ring-opening polymerization of cyclic esters in the presence of choline/$SnOct_2$ catalytic system, Polym. Bull. 68 (2012) 2219–2228, https://doi.org/10.1007/s00289-011-0676-8.

[30] E.R. Leone, L.S. Ferraraccio, G. Damonte, P. Lova, P. Bertoncello, O. Monticelli, On the development of electrochemical sensors coated with polycaprolactone, Electrochem. Commun. 129 (2021), 107089, https://doi.org/10.1016/j.elecom.2021.107089.

[31] G. Damonte, A. Vallin, A. Fina, O. Monticelli, On the development of an effective method to produce conductive pcl film, Nanomaterials 11 (2021) 1385, https://doi.org/10.3390/nano11061385.

[32] G. Damonte, A. Vallin, D. Battegazzore, A. Fina, O. Monticelli, Synthesis and characterization of a novel star polycaprolactone to be applied in the development of graphite nanoplates-based nanopapers, React. Funct. Polym. 167 (2021), 105019, https://doi.org/10.1016/j.reactfunctpolym.2021.105019.

[33] G.M. De Oca-Ramirez, L. Rios-Guerrero, J.-A. Trejo-O'Reilly, G. Flores-Rosete, A. Guyot, J. Guillot, E. Bourgeat-Lami, Synthesis and characterization of monoalkyl maleates and their use in emulsion polymerization of vinyl acetate, Macromol. Symp. 150 (2000) 161–169. https://doi.org/10.1002/1521-3900(200002)150:1<161::AID-MASY161>3.0.CO;2-H.

[34] B. Neises, W. Steglich, Simple method for the esterification of carboxylic acids, Angew. Chemie Int. Ed. English. 17 (1978) 522–524, https://doi.org/10.1002/anie.197805221.

[35] M.A. Woodruff, D.W. Hutmacher, The return of a forgotten polymer - polycaprolactone in the 21st century, Prog. Polym. Sci. 35 (2010) 1217–1256, https://doi.org/10.1016/j.progpolymsci.2010.04.002.

[36] M. Rizzuto, L. Marinetti, D. Caretti, A. Mugica, M. Zubitur, A.J. Müller, Can poly (ε-caprolactone) crystals nucleate glassy polylactide? CrystEngComm. 19 (2017) 3178–3191, https://doi.org/10.1039/C7CE00578D.

[37] L. Gardella, M. Calabrese, O. Monticelli, PLA maleation: an easy and effective method to modify the properties of PLA/PCL immiscible blends, Colloid Polym. Sci. 292 (2014) 2391–2398, https://doi.org/10.1007/s00396-014-3328-3.

[38] T.T. Truong, S.H. Thai, H.T. Nguyen, V.D. Vuong, L.T.T. Nguyen, Synthesis of allyl end-block functionalized poly(ε-caprolactone)s and their facile post-functionalization via thiol-ene reaction, J. Polym. Sci. Part A Polym. Chem. 55 (2017) 928–939, https://doi.org/10.1002/pola.28454.

[39] G. Giacobazzi, M. Rizzuto, M. Zubitur, A. Mugica, D. Caretti, A.J. Müller, Crystallization kinetics as a sensitive tool to detect degradation in poly(lactide)/poly(ε-caprolactone)/PCL-co-PC copolymers blends, Polym. Degrad. Stab. 168 (2019), 108939, https://doi.org/10.1016/j.polymdegradstab.2019.108939.

[40] C. Zhang, Q. Lan, T. Zhai, S. Nie, J. Luo, W. Yan, Melt crystallization behavior and crystalline morphology of polylactide/poly(ε-caprolactone) blends compatibilized by lactide-caprolactone copolymer, Polymers 10 (2018) 1181, https://doi.org/10.3390/polym10111181.

[41] J. Urquijo, G. Guerrica-Echevarría, J.I. Eguiazábal, Melt processed PLA/PCL blends: effect of processing method on phase structure, morphology, and mechanical properties, J. Appl. Polym. Sci. 132 (2015) 1–9, https://doi.org/10.1002/app.42641.

[42] A. Granado, J.I. Eguiazábal, J. Nazábal, Structure and mechanical properties of blends of poly(ε-caprolactone) with a poly(amino ether), J. Appl. Polym. Sci. 109 (2008) 3892–3899, https://doi.org/10.1002/app.28615.

[43] F. Carrasco, P. Pagès, J. Gámez-Pérez, O.O. Santana, M.L. Maspoch, Processing of poly(lactic acid): characterization of chemical structure, thermal stability and mechanical properties, Polym. Degrad. Stab. 95 (2010) 116–125, https://doi.org/10.1016/j.polymdegradstab.2009.11.045.

[44] S. Kumar, S. Bose, K. Chatterjee, Amine-functionalized multiwall carbon nanotubes impart osteoinductive and bactericidal properties in poly(ε-caprolactone) composites, RSC Adv. 4 (2014) 19086–19098, https://doi.org/10.1039/C4RA00875H.

[45] R. Khalifehzadeh, B.D. Ratner, Trifluoromethyl-functionalized poly(lactic acid): a fluoropolyester designed for blood contact applications, Biomater. Sci. 7 (2019) 3764–3778, https://doi.org/10.1039/C9BM00353C.

[46] L. Magazzini, S. Grilli, S.E. Fenni, A. Donetti, D. Cavallo, O. Monticelli, The blending of poly(glycolic acid) with polycaprolactone and poly(l-lactide): promising combinations, Polymers 13 (2021) 2780, https://doi.org/10.3390/polym13162780.

[47] A. Solovieva, S. Miroshnichenko, A. Kovalskii, E. Permyakova, Z. Popov, E. Dvořáková, P. Kiryukhantsev-Korneev, A. Obrosov, J. Polčak, L. Zajíčková, D. Shtansky, A. Manakhov, Immobilization of platelet-rich plasma onto COOH plasma-coated PCL nanofibers boost viability and proliferation of human mesenchymal stem cells, Polymers 9 (2017) 736, https://doi.org/10.3390/polym9120736.

[48] E.S. Permyakova, P.V. Kiryukhantsev-Korneev, K.Y. Gudz, A.S. Konopatsky, J. Polčak, I.Y. Zhitnyak, N.A. Gloushankova, D.V. Shtansky, A.M. Manakhov, Comparison of different approaches to surface functionalization of biodegradable polycaprolactone scaffolds, Nanomaterials 9 (2019) 1769, https://doi.org/10.3390/nano9121769.

[49] A. Jordá-Vilaplana, V. Fombuena, D. García-García, M.D. Samper, L. Sánchez-Nácher, Surface modification of polylactic acid (PLA) by air atmospheric plasma treatment, Eur. Polym. J. 58 (2014) 23–33.

[50] O. Monticelli, S. Bocchini, L. Gardella, D. Cavallo, P. Cebe, G. Germelli, Impact of synthetic talc on PLLA electrospun fibers, Eur. Polym. J. 49 (9) (2013) 2572–2583.

[51] K. Li, A. Fina, D. Marrè, F. Carosio, O. Monticelli, Graphite oxide nanocoatings as a sustainable route to extend the applicability of biopolymer-based film, Appl. Surf. Sci. 522 (2020), 146471, https://doi.org/10.1016/j.apsusc.2020.146471.

[52] D.A. Gopakumar, V. Arumukhan, R.V. Gelamo, D. Pasquini, L.C. de Morais, S. Rizal, D. Hermawan, A. Nzihou, H.P.A. Khalil, Carbon dioxide plasma treated PVDF electrospun membrane for the removal of crystal violet dyes and iron oxide nanoparticles from water, Nano-Struct. Nano-Objects. 18 (2019), 100268, https://doi.org/10.1016/j.nanoso.2019.100268.

[53] A. Pellis, L. Silvestrini, D. Scaini, J.M. Coburn, L. Gardossi, D.L. Kaplan, E.H. Acero, G.M. Guebitz, Enzyme-catalyzed functionalization of poly(L-lactic acid) for drug delivery applications, Process Biochem. 59 (2017) 77–83, https://doi.org/10.1016/j.procbio.2016.10.014.

[54] A. Blangiardo, G. Lagomarsino, A. Basso, P. Canepa, O. Cavalleri, S. Rossi, O. Monticelli, Preparation, application and recycling of a catalytic microflow reactor based on polylactic acid, Appl. Surf. Sci. 569 (2021), 151019, https://doi.org/10.1016/j.apsusc.2021.151019.

[55] S. Boi, E. Dellacasa, P. Bianchini, P. Petrini, L. Pastorino, O. Monticelli, Encapsulated functionalized stereocomplex PLA particles: An effective system to support mucolytic enzymes, Colloids Surf. B 179 (2019) 190–198, https://doi.org/10.1016/j.colsurfb.2019.03.071.

[56] R. Schneider, M.H.M. Facure, A.D. Alvarenga, P.A.M. Chagas, D.M. dos Santos, D. S. Correa, Dye adsorption capacity of MoS2 nanoflakes immobilized on poly(lactic acid) fibrous membranes, ACS Appl. Nano Mater. 4 (2021) 4881–4894, https://doi.org/10.1021/acsanm.1c00442.

[57] A. Pellis, E.H. Acero, H. Weber, M. Obersriebnig, R. Breinbauer, E. Srebotnik, G. M. Guebitz, Biocatalyzed approach for the surface functionalization of poly(L-lactic acid) films using hydrolytic enzymes, Biotechnol. J. 10 (2015) 1739–1749, https://doi.org/10.1002/biot.201500074.

[58] A. Gricajeva, A.K. Nadda, R. Gudiukaite, Insights into polyester plastic biodegradation by carboxyl ester hydrolases, J. Chem. Technol. Biotechnol. 97 (2022) 359–380, https://doi.org/10.1002/jctb.6745.

[59] K. Masaki, N.R. Kamini, H. Ikeda, H. Iefuji, Cutinase-like enzyme from the yeast cryptococcus sp. strain S-2 hydrolyzes polylactic acid and other biodegradable plastics, Appl. Environ. Microbiol. 71 (2005) 7548–7550, https://doi.org/10.1128/AEM.71.11.7548-7550.2005.

[60] S. Teixeira, K.M. Eblagon, F. Miranda, M.F.R. Pereira, J.L. Figueiredo, Towards controlled degradation of poly(lactic) acid in technical applications, C-Journal of Carbon Research 7 (2021) 42, https://doi.org/10.3390/c7020042.

Chapter 7: Star-shaped furoate-PCL: An effective compound for the development of graphite nanoplatelets-based films

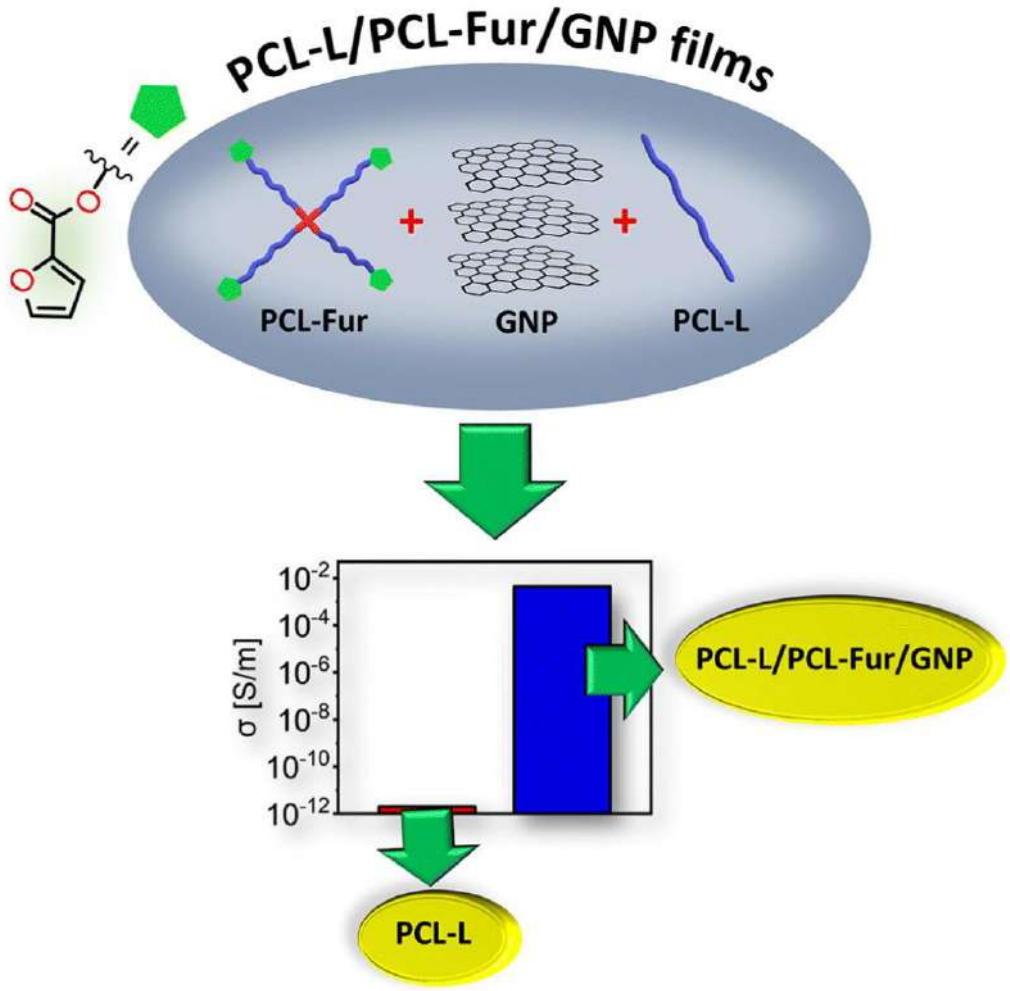

Reactive and Functional Polymers 184 (2023) 105515

Contents lists available at ScienceDirect

Reactive and Functional Polymers

journal homepage: www.elsevier.com/locate/react

Star-shaped furoate-PCL: An effective compound for the development of graphite nanoplatelets-based films

Giacomo Damonte [a], Francesco Cantamessa [b], Alberto Fina [b], Orietta Monticelli [a,*]

[a] Dipartimento di Chimica e Chimica Industriale, Università degli studi di Genova, Via Dodecaneso 31, 16146 Genoa, Italy
[b] Dipartimento di Scienza Applicata e Tecnologia, Politecnico di Torino-sede di Alessandria, Viale Teresa Michel, 5, 15121 Alessandria, Italy

ARTICLE INFO

Keywords:
Star-shaped PCL
Furoate-PCL
GNP
Composite films
Electrically conductive films

ABSTRACT

The aim of this study was to improve the dispersibility of graphite nanoplatelets (GNP) in films based on poly (ε-caprolactone) (PCL). To this end, a star-shaped PCL with furoate-like end groups (PCL-Fur), potentially capable of interacting/reacting with the surface of the graphene layers through Diels-Alder reactions, was synthesized by enzymatic catalysis. PCL-Fur was applied for film development by blending it with a commercial high molecular weight PCL (PCL-L) and GNP. The reactivity of GNP with respect to furoate groups was demonstrated by studying the thermal behavior of the GNP/methyl 2-furoate system, while the dispersibility of graphite in the solution containing PCL-Fur was studied by UV–Vis measurements. GNP proved to be well dispersed and adhered to the polymer matrix in the PCL-L/PCL-Fur/GNP composite films prepared by casting, in contrast to the films based on the neat PCL-L. This fine GNP dispersion resulted in films characterized by high electrical conductivity.

1. Introduction

The dispersion of graphene-related materials (GRM) in polymers represents an important and widely studied aspect for the production of high performance systems [1]. Indeed, although the exploitation of such fillers/nanofillers, such as graphite nanoplatelets (GNP), can improve the mechanical and thermal properties and, most importantly, increase the electrical and thermal conductivity of the polymer, these performances are closely related to the GRM dispersion in the matrix. In the case of biopolymers, the improvement of their properties is an even more important issue that is being studied in order to make these systems competitive with those from fossil sources and not biodegradable. Among the various biopolymers of academic and industrial interest, poly(ε-caprolactone) (PCL) was considered in this work for its wide range of applications [2]. Indeed, its biocompatibility properties make it a polymer that can be used in the biomedical field [3], while its elongation and biodegradation allow it to be applied alone or in combination with other polymers in the packaging field [4]. Concerning the formation of polymer/GRM systems, the dispersion of GRM can be promoted by modifying the structure of the nanofiller [5] or that of the polymer [6]. In the first case, the surface of graphite can generally be oxidized, making the resulting graphite oxide or graphene oxide (GO) much more compatible with polar polymers [7]. In addition, GO can be further functionalized to improve its compatibility with the polymer matrix [8–10]. For example, the above approach was described for polypropylene (PP)-based systems in which GO reacted with 4,4-diphenylmethane diisocyanate (MDI) and then stearic acid to form functionalized sheets, which exhibited strong interfacial adhesion with PP [8] and promoted the orientation of PP crystallites [10].

In the case of PCL, there are several examples dealing with the combination of this polymer with GO, especially in the context of the formation of nanofibers made by electrospinning [11]. Despite the easy dispersibility of GO, oxidation is naturally associated with a reduction of electrical and thermal conductivity, which can be restored by the use of strong chemical reducing agents [12] and/or high temperatures [13]. Therefore, modifying the polymer structure to increase the affinity of the polymer with the nanofiller surface seems to be a promising route. Indeed, star-shaped or linear PCLs ending with pyrene groups, able to interact with the graphite surface through π-stacking-like interactions have been recently synthesized [14,15]. The resulting PCL/GNP systems, characterized by a fine nanofiller dispersion, exhibited high thermal and electrical conductivity. In this work, we extended the application of PCL, by moving from a polymer with functionalities which promote the dispersion of GNP through specific interactions to a

* Corresponding author.
E-mail address: orietta.monticelli@unige.it (O. Monticelli).

https://doi.org/10.1016/j.reactfunctpolym.2023.105515
Received 26 September 2022; Received in revised form 20 January 2023; Accepted 22 January 2023
Available online 25 January 2023

PCL with groups capable not only of interacting with graphene layers but also of reacting with them. Thus, a star-shaped PCL ending with furan-type functional groups (PCL-Fur) which can act as a diene in Diels-Alder (DA) reactions with edges [16,17] and defects, normally present on the surface of graphite nanoplates, was synthesized [16–18] (Fig. 1). The material was specifically designed for the preparation of dense films. To this end, PCL-Fur, characterized by a star-shaped architecture and low molecular weight to maximize end functionalities, prepared from a hydroxyl-terminated polymer, the synthesis of which was previously reported by the authors [15,19], was mixed with a high molecular weight linear commercial polymer suitable for film development.

Indeed, as described in literature, blends consisting of branched polymers with arms of the same type as the main polymer are fully miscible [20]. To obtain a high efficiency and sustainable functionalization, the furoate polymer was synthesized by enzymatic catalysis. The films, consisting of a linear high molecular weight commercial PCL (PCL-L), PCL-Fur and GNP, were prepared by solvent casting and characterized to evaluate their thermal, and electrical conductivity properties (Fig. 1). In addition, the properties of the developed systems were compared with those of films made of PCL-L, PCL-Fur and the composite with GNP dispersed in PCL-L.

2. Materials and methods

2.1. Materials

ε-caprolactone, methanol, tin octanoate ($Sn(Oct)_2$), dichloromethane (DCM), methyl-2-furoate, acetonitrile, anhydrous toluene, calcium hydride, deuterated chloroform ($CDCl_3$), acetone were purchased by Sigma-Aldrich. High molecular weight (M_w = 50,000 g/mol) PCL CAPA 6500® (hereafter referred to as PCL-L) was obtained from Perstorp (Sweden). Immobilized Candida Antarctica Lipase B (CALB) Novozyme 435® was purchased by Novozymes®. Graphite nanoplatelets (GNP), with BET surface area of 196 m^2/g, were supplied by Avanzare Innovacion Tecnologica (Navarrete, Spain). ε-caprolactone was distilled over CaH_2 under reduced pressure. All the other reagents were used directly as received without purification.

2.2. Synthesis of furoate-PCL (PCL-Fur)

The furoate PCL (hereafter referred to as PCL-Fur) was synthesized starting from a star-shaped hydroxyl-terminated PCL (hereafter referred to as PCL-OH), prepared by ring opening polymerization (ROP) of ε-caprolactone in bulk, using pentaerythritol as initiator and $Sn(Oct)_2$ as catalyst, according to a procedure reported in the literature [21]. Specifically, ε-caprolactone was added to a 50-mL two-neck round bottom flask purged with argon gas, followed by the proper amount of initiator to achieve the desired molecular weight of 2000 g/mol per arm. The system was then gently heated to 80 °C with stirring to dissolve the initiator in the monomer and produce a homogeneous solution. When the mixture was clear, the temperature was increased to 120 °C with stirring and $Sn(Oct)_2$ was added as a 100 mg/mL solution in anhydrous toluene to maintain the ratio $[\varepsilon\text{-CL}]/[Sn(Oct)_2] = 5000$. After 24 h, the warm crude polymer was dissolved in an equal amount of DCM. The purified product was obtained as a fine powder by slowly dropping the solution into a large volume of ice-cold methanol with vigorous stirring (50 mL/g PCL). This was filtered through a Büchner funnel, washed several times with small volumes of fresh methanol, and dried in vacuum at 30 °C for 72 h.

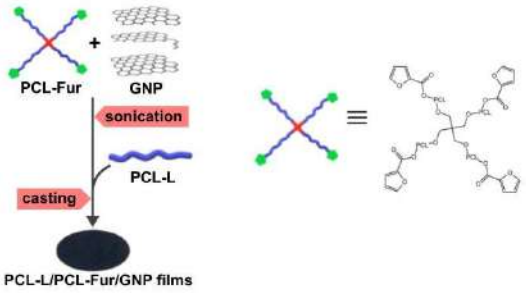

Fig. 1. Scheme of PCL-L/PCL-Fur/GNP film preparation procedure.

IR signals of PCL-OH: 2945 cm^{-1} (asymmetric -CH_2- stretching); 2870 cm^{-1} (symmetric -CH_2- stretching); 1725 cm^{-1} (symmetric >C=O stretching); 1297 cm^{-1} (-C-O- and -C-C- stretching); 1242 cm^{-1} (asymmetric -C-O-C- stretching); 1179 cm^{-1} (symmetric -C-O-C- stretching).

^{1}H NMR chemical shifts of PCL-OH: 4.09 ppm (-CH_2- pentaerythritol, s); 4.05 ppm (-CH_2-, t); 3.63 ppm (-CH_2-OH PCL chain terminal, t); 2.31 ppm (-CH_2-, t); 1.65 (-CH_2-, m); 1.38 (ppm -CH_2-, m).

PCL-Fur was synthesized by enzimatic esterification of the synthesized PCL-OH with CALB, as previously reported [22] (Fig. 2). To a two-necked round bottomed flask equipped with a stir bar and flowed with argon, 1 g PCL-OH (1 eq.), 78.8 μL methyl 2-furoate (6 eq.), 78.8 mg CALB (equal quantity as methyl 2-furoate) and 3 mL anhydrous toluene were added. The system was then stirred at 60 °C for 72 h. At the end of the reaction, the solution was filtered to remove the enzyme on the acrylic resin beads. The polymer was then precipitated from cold methanol (50 mL/g), filtered through a Büchner funnel, and washed several times with small portions of ice-cold methanol. The polymer was dried in a vacuum oven at 30 °C for 72 h.

2.3. Film preparation procedure

Polymer films were prepared from DCM solution by solvent casting. Specifically, 10 mL of DCM containing 200 mg of the neat PCL-L or the mixture PCL-L/PCL-Fur with a ratio 80/20, was poured into a Petri dish with an inner diameter of 54 mm. To prepare the GNP-containing films, the appropriate amount of GNP (1 or 2 wt% based on the total polymer content) was dispersed in the solvent together with PCL-Fur by sonication in a sonication bath at 40 kHz for two h. After the sonication phase, the high molecular weight PCL-L was added with stirring to obtain a homogeneous dispersion of GNP, maintaining the PCL-L/PCL-Fur ratio at 80/20. The films were then prepared by slowly evaporating the solvent for 24 h at 30 °C in an oven. To remove the remaining solvent, the films were then released from the Petri dishes and placed in vacuum oven for additional 48 h at 30 °C. The films were defined by indicating in the code GNP concentration (as an example: PCL-L/PCL-Fur/G1 indicates a film prepared with a GNP concentration of 1 wt% and with a ratio PCL-L/PCL-Fur of 80/20).

2.4. Characterization

FT-IR analysis was performed on polymer films using a Bruker "Vertex 70®" in ATR mode in the range 400–4000 cm^{-1}. ^{1}H NMR spectroscopy was performed with a JEOL ECZ400R/S3 at a frequency of 400 MHz using 10 mm NMR tubes and $CDCl_3$ as solvent at r.t. DSC analysis of the films was performed using a Mettler Toledo "DSC1 STARe System®" in the temperature range of −100 to 150 °C at a heating rate of 10 °C/min and a nitrogen flow of 20 mL/min. The degree of crystallinity (Xc) of PCL in the films was then calculated using Eq. (1)

$$X_c = \frac{\Delta H_m}{\Delta H_m^0} 100 \quad (1)$$

where ΔH_m = fusion enthalpy (measured in the second heating scan) and ΔH_m^0 = fusion enthalpy of a 100% crystalline PCL, a value found in the literature (139 J/g) [23].

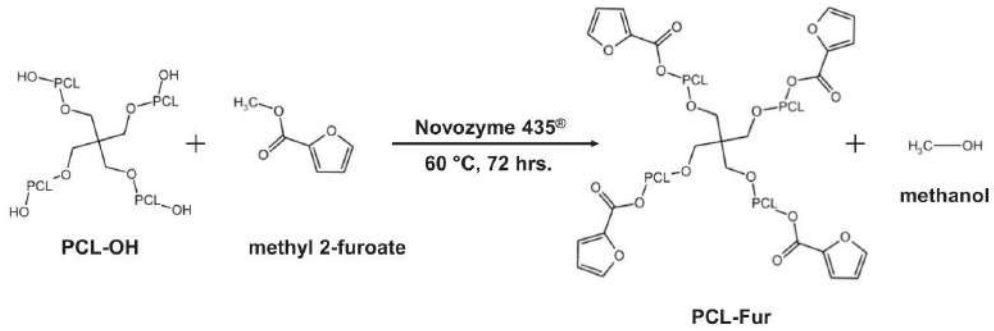

Fig. 2. Reaction scheme of the enzymatic furoylation reaction of PCL-OH.

To study the Diels-Alder (DA) reaction between GNP and the furoate-type functionalities, 35 mg of GNP was sonicated in 4 mL of methyl 2-furoate for one h. The mixture was then allowed to react at 30 °C for 72 h, the same time and temperature as for the film preparation. The modified GNP was then obtained by centrifugation (three times at 6000g for 5 min, washing the material each time with fresh acetone) and dried at room temperature. The retro DA was evaluated by DSC analysis in a single heating scan from 0 to 150 °C at a heating rate of 10 °C/min and a nitrogen flow of 20 mL/min.

TGA was performed using a Mettler Toledo "TGA/DSC1 STARe System®" from 30 °C to 800 °C with a heating rate of 10 °C/min under a nitrogen atmosphere of 80 mL/min. UV–Vis spectra were recorded with a Shimadzu® UV 1800 UV–Vis spectrometer in the 200–400 nm range using quartz cells in acetonitrile solution.

Conductivity measurements were performed at room temperature on rectangular films (dimensions: length 30 mm, width 5 mm, thickness approximately 0.08 mm) connected with flat copper clamps (10 mm wide to ensure full contact over the entire sample width), at a distance of 20 mm and connected to a current generator set to 150 V cc. The current flow through the sample was measured using a picoammeter (Keithley Instruments, Solon, OH, USA) and then the material conductivity was calculated by applying Ohm's laws.

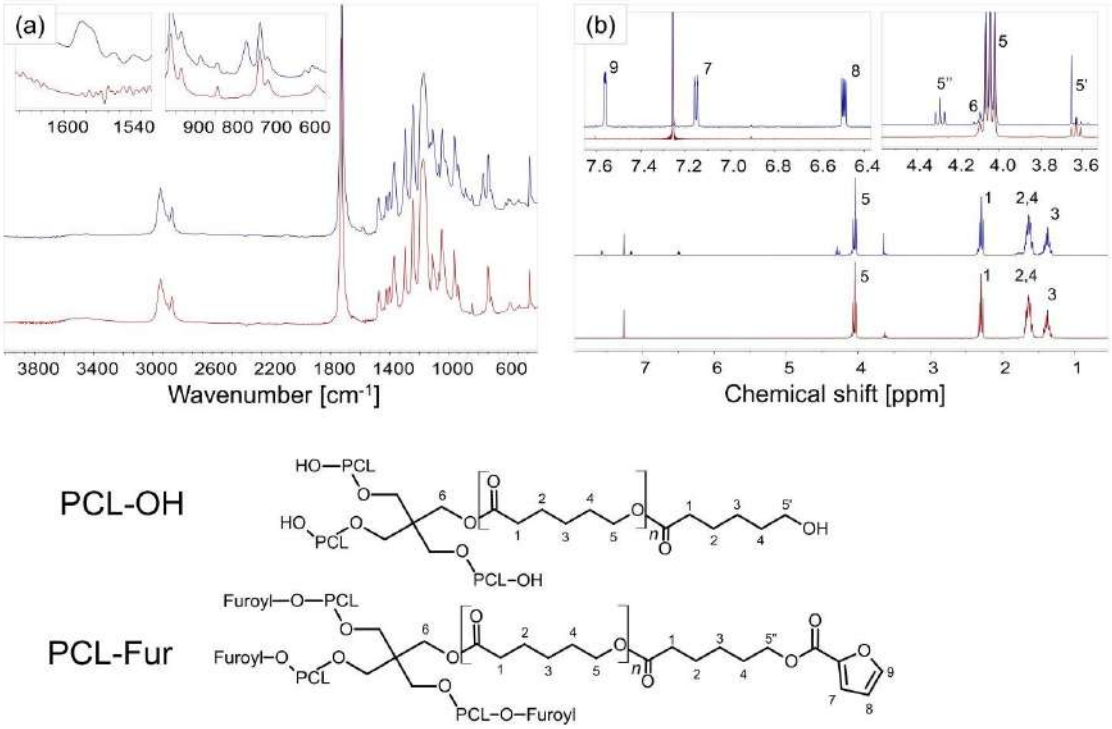

Fig. 3. FT-IR (a) and ^{1}H NMR (b) spectra of: PCL-OH (red) and PCL-Fur (blue). The polymer structures are indicated below with proton numbering for the sake of clarity. (For interpretation of the references to colour in this figure legend, the reader is referred to the web version of this article.)

3. Results and discussion

3.1. PCL-Fur characterization

To confirm the functionalization of the star-shaped PCL-OH, its FT-IR spectrum was compared with that of PCL-Fur (Fig. 3a). For both the synthesized polymers, all signals typical of PCL [24] can be detected at 2945 cm^{-1} (asymmetric -CH_2- stretching); 2870 cm^{-1} (symmetric -CH_2- stretching); 1725 cm^{-1} (symmetric >C=O stretching); 1297 cm^{-1} (-C-O- and -C-C- stretching); 1242 cm^{-1} (asymmetric -C-O-C- stretching); 1179 cm^{-1} (symmetric -C-O-C- stretching). Additional signals were observed in the spectrum of PCL-Fur at 1580 cm^{-1} (C=C stretching furan) and 886 cm^{-1}, 768 cm^{-1}, 616 cm^{-1} (furan ring vibrational motions), which can be attributed to 2-furoate unit [25]. This finding preliminarily corroborated the functionalization of the polymer after the esterification reaction.

^{1}H NMR spectra of PCL-OH and PCL-Fur are reported in Fig. 3b. For both polymers, typical signals of PCL can be observed [26] at 4.09 ppm (6, -CH_2- pentaerythritol, s); 4.05 ppm (5, -CH_2-, t); 2.31 ppm (1, -CH_2-, t); 1.65 pp. (2 and 4, -CH_2-, m); 1.38 ppm (3, -CH_2-, m). In the spectrum of PCL-OH, the presence of a signal at 3.65 ppm (5′, -CH_2-OH PCL chain terminal, t) indicates the presence of hydroxyl groups. In contrast, in PCL-Fur spectrum, the occurrence of the esterification was proven by the presence of the furan proton signals at 7.58 ppm (9, furan -CH-, dd); 7.17 ppm (7, furan -CH-, dd); 6.50 ppm (8, furan -CH-, dd); and by the formation of a new signal at 4.30 ppm (5″, -CH_2-O-furoyl PCL chain terminal, t), demonstrating the esterification of hydroxyl end groups of PCL-OH [15,27].

From the evaluation of M_{nNMR}, calculated from the ratio between the areas of the signals of terminals and chain protons ($A_{5'}/A_1$ for PCL-OH and $A_{5''+5'}/A_1$ for PCL-Fur), a decrease in the molecular weight of the star-shaped PCL was observed after the enzymatic esterification reaction. Indeed, the M_{nNMR} value went from 2000 g/mol per arm for the PCL-OH to about 1400 g/mol in PCL-Fur. The above decrease in molecular weight was probably caused by a depolymerization process due to the effect of CALB on the PCL ester bonds. Nevertheless, the polymer obtained is suitable for the intended purpose due to the high degree of functionalization (ca. 80%).

To verify the effects of functionalization on the thermal properties of the *star*-shaped polymer, both PCL-OH and PCL-Fur were characterized by DSC and TGA measurements (Fig. S1 and Table S1). In particular, PCL-OH showed values of crystallization temperature (T_c), melting temperature (T_m) and degree of crystallinity (χ_c) in perfect agreement with those reported in the literature for four-arm PCL with similar molecular weight [15,28]. It was found that esterification does not significantly change the thermal properties of the polymer, since only a slight change in the crystallization and melting temperature (T_c from 28 °C for PCL-OH to 25 °C for PCL-Fur, T_m from 49 °C for PCL-OH to 46 °C for PCL-Fur) was observed. In the case of PCL-Fur, the double peak in the heating curve can be ascribed to the crystal lamellae thickness distribution produced during crystallization [14], which is possibly affected by the presence of furoate end groups.

As for the TGA analysis, the values of the onset of degradation temperature (T_{onset}) and the maximum rate of degradation temperature (T_{max}) of PCL-OH, which are consistent with those previously reported for polymers with similar features [15], are related to an unzipping-type degradation mechanism, as a consequence of the hydroxyl end groups of the *star*-shaped polymer. Interestingly, the esterified polymer exhibited higher T_{onset} and T_{max} with respect to PCL-OH. This phenomenon can be explained by the fact that the esterification of the hydroxyl end groups in PCL-Fur suppresses the unzipping mechanism and thus favors β-elimination, a mechanism typical of high molecular weight PCL [15,29]. Indeed, this finding provides further support for the esterification of PCL-OH hydroxyl end groups.

3.2. Study of interactions/reactions of furoate functionalities with GNP and GNP dispersibility

To verify the interactions/reactions of the furoate group with the graphene layers, the thermal behavior of the mixture of GNP and methyl 2-furoate was investigated treating it at the same temperature and time of the film preparation process, as reported in the Experimental Section. It is worth underling that the analysis of the DSC trace can provide information about the reaction between the above compound and GNP, since the direct Diels-Alder (DA) reaction, which can occur between the furoate functionalities, acting as diene, and the graphene layers defects, acting as dienophile, is exothermic and reversible [30]. Therefore, once the bond is formed, it may be possible to reverse the reaction (retro DA) and then break the formed bond by simple heating. Methyl-2-furoate was chosen as a probe molecule to maximize the extent of functionalization and thus the signal obtained, taking into account of the relatively low concentration of the furoate as terminal groups in the star shaped PCL. In addition, since PCL melts at about 60 °C, its endothermic melting peak may mask the endothermic peak associated with DA transitions. Indeed, in order to focus on the above reaction, a heating scan was performed in the range 0 °C - 150 °C. From the thermogram in Fig. 4a, it can be seen that the curve of neat GNP is completely flat in the studied temperature range, clearly indicating the absence of a thermal transition. On the other hand, the methyl 2-furoate/GNP sample showed a broad peak at about 80 °C, which can be attributed to the process of retro DA, as described in the literature for other furan-based systems [31]. This observation brings evidence the ability of furan derivatives to serve as a source of reversible networks in graphene-containing materials. Based on these findings, the same furoate-GNP interaction is expected between the star-shaped PCL end groups and the GNP surface, which can be exploited to promote dispersion of graphite in the polymer matrix.

To investigate the effect of PCL-Fur on the dispersibility of GNP, different solutions containing a fixed amount of this polymer in acetonitrile were sonicated together with different quantities of GNP (1, 2 and 5 mg) and allowed to sediment for one week. In Fig. 4b, the UV–Vis spectra of the leftover surnatant of dispersions remaining after the sedimentation time are reported. A peak at 250 nm was observed in all the analyzed samples, which can be attributed to the absorption of the furoate group [32]. It is relevant to underline that the intensity of the above peak decreased with increasing GNP content in the system. This finding indicates a direct decrease in the PCL-Fur content in the solution and, especially for the system with the highest GNP concentration (5 mg), the ability of GNP to interact with the polymer, causing its adsorption and consequently its concentration decrease in the solution. Moreover, in the sample containing 2 mg of GNP, a shoulder was visible at about 290 nm, which, as previously reported [14,33], can be related to the absorption caused by the dispersed graphite.

3.3. Characterization of blend and composite films

The prepared composite films were preliminarily characterized from a morphological point of view. Fig. 5 compares the photo and Fig. S2 the optical microscopy image of PCL-L/PCL-Fur/G2 film containing 2 wt% of GNP with a film prepared by adding the same amount of nanofiller to the neat PCL (PCL-L/G2).

It is evident that PCL/G2 film is extremely inhomogeneous with visible aggregates. In contrast, PCL/PCL-Fur/G2 film, prepared under the same conditions as the previous one, is characterized by a homogeneous graphite dispersion, which is evident by the absence of visible GNP agglomerates. FE-SEM measurements, carried out only on the sample which showed visible homogeneity, allowed to study in detail the dispersion of GNP in the cross-section of the polymer films. The micrographs shown in Fig. 5c refer to PCL-L/PCL-Fur/G2, the morphology of the sample with 2 wt% graphite, PCL-L/PCL-Fur/G1 being very similar. The analysis of these micrographs reveals that the

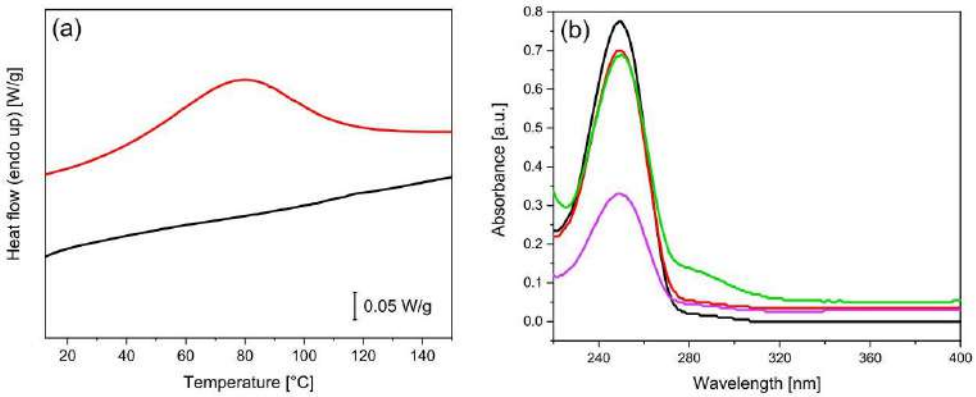

Fig. 4. (a) DSC trace of methyl 2-furoate/GNP mixture (red curve) and pristine GNP (black curve). (b) Comparison between the UV–Vis spectra of the dispersions of PCL-Fur (black curve) with different concentrations of graphite in acetonitrile (1 mg red, 2 mg green, 5 mg violet curve). (For interpretation of the references to colour in this figure legend, the reader is referred to the web version of this article.)

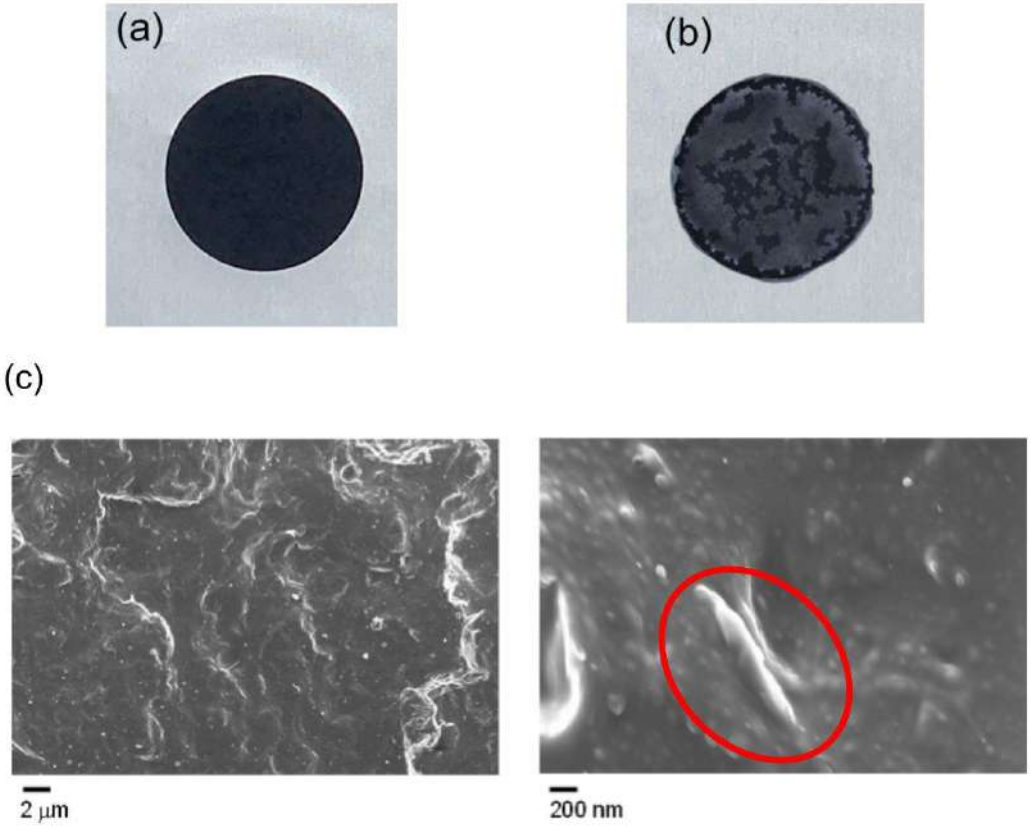

Fig. 5. Photos of: (a) PCL-L/PCL-Fur/G2 and (b) PCL-L /G2. (c) FE-SEM micrographs of PCL-L/PCL-Fur/G2 at different magnifications.

GNP was well distributed in the cross-section of the film, and higher magnification in particular shows that they also adhered well to the polymer (see GNP highlighted within the red circle). This result can be attributed to the specific interactions/reactions that can occur between GNP and the furoate groups of PCL-Fur, which is rich in functionalities thanks to its star-shaped architecture. The above system indeed proved

to be homogeneously dispersed in the PCL matrix, since it is characterized by arms of the same chemical nature and its interactions with the graphite ensure a similarly good dispersion.

The thermal properties of the neat films based on PCL-L and the blend PCL-L/PCL-Fur were compared with those of the composite films containing 1 wt% and 2 wt% GNP (PCL-L/PCL-Fur/G1 and PCL-L/PCL-Fur/G2). The DSC traces are shown in Fig. 6, while the results are summarized in Table 1. The crystallization temperature (T_c), melting temperature (T_m) and crystallinity (X_c) of the PCL-L-based film are in agreement with the values reported in the literature [34,35]. The film obtained by mixing the two polymers (PCL-L/PCL-Fur) exhibited a slightly higher crystallinity than PCL-L, with X_c increasing from 50% for PCL-L to 57% for PCL-L/PCL-Fur, a phenomenon probably due to the presence of the furoate polymer in the mixture, which is characterized a higher crystallinity because of its lower molecular weight. It worth underlining that only one melting temperature appeared in the thermogram of the blend system, indicating the complete miscibility between PCL-L and PCL-Fur. An increase in crystallization temperature for the GNP-containing samples was found, with T_c increasing from 30 °C for the neat samples to 37 °C and 38 °C in the presence of 1 or 2% wt. GNP, respectively. As described in the literature [14,15], this result can be attributed to the nucleating effect of GNP. Regarding the thermal decomposition, all the prepared films showed similar T_{onset} and T_{max}. Indeed, the weight loss decomposition step occurred in the range between 400 and 450 °C, indicating a decomposition that follows a β-elimination mechanism as described in the literature [36].

The effect of GNP on the electrical properties of the prepared films was evaluated by comparing the conductivity (σ) of the neat PCL-L and PCL-L/PCL-Fur films with those of the GNP-based films (Fig. 7). As can be seen from the histogram, both PCL-L and the PCL-L/PCL-Fur blend were found to be insulating materials with σ in the range of 10^{-12} S·m^{-1}. However, the presence of GNP resulted in a significant increase in the measured current flow and thus in the conductivity of the films. In particular, the addition of 1 wt% GNP in PCL-L/PCL-Fur/G1 led to an increase in conductivity to a value of $1.1 \cdot 10^{-10}$ S·m^{-1}, while PCL-L/PCL-Fur/G2, containing 2 wt% of GNP reached a value of $4.3 \cdot 10^{-3}$ S·m^{-1}, namely seven orders of magnitude higher than PCL-L/PCL-Fur/G1 and nine higher than PCL-L and PCL-L/PCL-Fur. It is worth underling that the conductivity found for PCL-L/PCL-Fur/G2 is among the highest values reported for PCL/GRM systems, characterized by the same filler content [14,37]. This result can be attributed to the formation of an efficient percolative network within the polymer matrix [38]. The conversion point from insulator to conductor is observed here between 1 and 2% wt., confirming the fine GNP dispersion, which may be ascribed

Table 1
Thermal properties of the prepared films.

Sample code	ΔH_c [J/g]	T_c [°C]	ΔH_m [J/g]	T_m [°C]	X_c [%]	T_{onset} [°C]	T_{max} [°C]
PCL-L	−56	30	69	57	50	388	426
PCL-L/PCL-Fur	−78	30	80	54	57	382	428
PCL-L/PCL-Fur/G1	−65	37	78	56	57	389	428
PCL-L/PCL-Fur/G2	−82	38	84	55	62	388	428

The subscript m and c indicate the values measured during melting and crystallization, respectively. X_c is the degree of crystallinity calculated by assuming the ideal enthalpies of fusion as 139 J/g. T_{onset} and T_{max} indicate the onset of the degradation temperature at a weight loss of 5% and the maximum rate of degradation temperature, respectively.

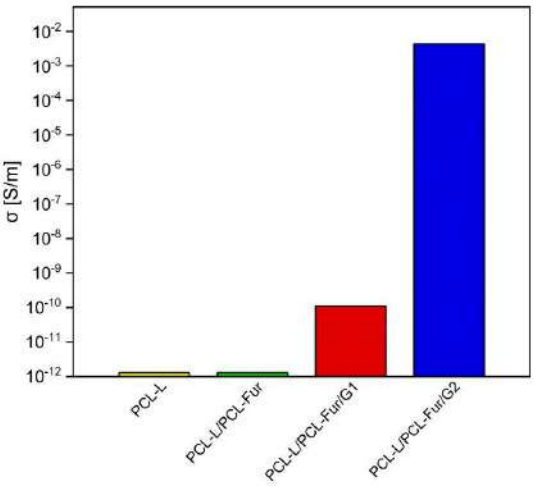

Fig. 7. Conductivity of neat PCL-L and PCL-L/PCL-Fur films and the films based on GNP.

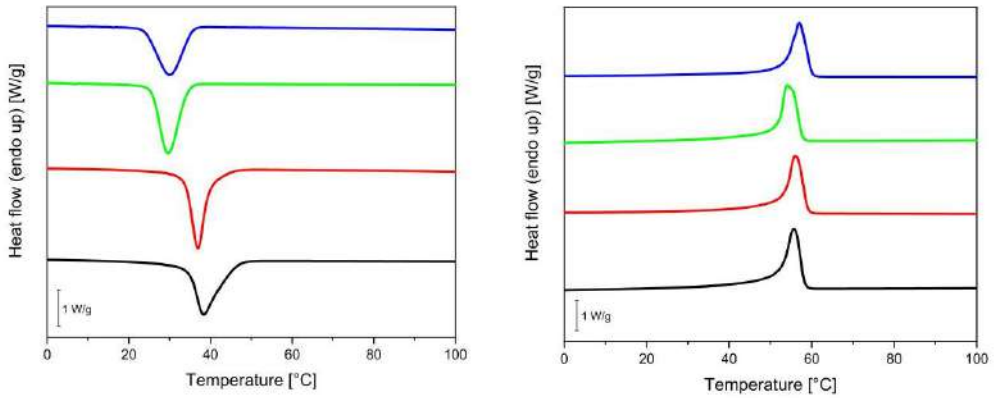

Fig. 6. DSC thermograms, second heating (left) and cooling (right) of: PCL-L (blue curve), PCL-L/PCL-Fur (green curve), PCL-L/PCL-Fur/G1 (red curve) and PCL-L/PCL-Fur/G2 (black curve). (For interpretation of the references to colour in this figure legend, the reader is referred to the web version of this article.)

to the interactions/reactions between the *star*-shaped furoate polymer and GNP.

4. Conclusions

In this work, a strategy was developed to render films based on PCL electrically conductive. The approach is based not only on the addition of GNP to the polymer matrix, but also on the blending a high molecular weight PCL (PCL-L) with a star-shaped PCL (PCL-Fur) synthesized ad-hoc by an environmentally friendly enzymatic functionalization process. The arms of the *star*-shaped polymer, being of the same nature as the matrix, ensured a good miscibility in the system, while the furoate-like end groups, capable of reacting via Diels-Alder reaction with the surface of the graphene layers, promoted GNP dispersion. Consequently, PCL-L/PCL-Fur/G2 composite film based on 2 wt% GNP exhibited a surface conductivity among the highest found in the literature for this type of system. The "green" nature of the polymer matrix, as well as the final properties of the material and its simple preparation procedure, make the developed system attractive for application in various fields. In the biomedical field, for example, one can imagine the development of scaffolds containing drugs that can be released by electrical stimulation, while in the field of packaging, ductile conductive films can be used for electronic components.

CRediT authorship contribution statement

Giacomo Damonte: Investigation, Validation, Data curation. **Francesco Cantamessa:** Investigation, Data curation. **Alberto Fina:** Conceptualization, Supervision, Writing – review & editing. **Orietta Monticelli:** Conceptualization, Supervision, Writing – original draft, Writing – review & editing.

Declaration of Competing Interest

The authors declare that they have no known competing financial interests or personal relationships that could have appeared to influence the work reported in this paper.

Data availability

Data will be made available on request.

Appendix A. Supplementary data

Supplementary data to this article can be found online at https://doi.org/10.1016/j.reactfunctpolym.2023.105515.

References

[1] S. Perumal, R. Atchudan, I.W. Cheong, Recent studies on dispersion of graphene–polymer composites, Polymers 13 (2021) 2375, https://doi.org/10.3390/polym13142375.

[2] M. Labeta, W. Thielemans, Synthesis of polycaprolactone: a review, Chem. Soc. Rev. 38 (2009) 3484–3504, https://doi.org/10.1039/b820162p.

[3] E. Malikmammadov, T.E. Tanir, A. Kiziltay, V. Hasirci, N. Hasirci, PCL and PCL-based materials in biomedical applications, J. Biomater. Sci. Polym. Ed. 29 (2018) 863–893, https://doi.org/10.1080/09205063.2017.1394711.

[4] J.S. Lyu, J.-S. Lee, J. Han, Development of a biodegradable polycaprolactone film incorporated with an antimicrobial agent via an extrusion process, Sci. Rep. 9 (2019) 20236, https://doi.org/10.1038/s41598-019-56757-5.

[5] D. Razzaghi, M. Rezaei, A. Babaie, The effect of incorporating graphene and polycaprolactone-grafted graphene oxide nanosheets on thermal and physico-mechanical properties, microstructure and biocompatibility of electrospun polyurethane nanocomposite mats, Compos. Part B Eng. 224 (2021), 109210, https://doi.org/10.1016/j.compositesb.2021.109210.

[6] A. Fina, S. Colonna, L. Maddalena, M. Tortello, O. Monticelli, Facile and low environmental impact approach to prepare thermally conductive nanocomposites based on polylactide and graphite nanoplatelets, ACS Sustain. Chem. Eng. 6 (2018) 14340–14347, https://doi.org/10.1021/acssuschemeng.8b03013.

[7] M. Sabzevari, D.E. Cree, L.D. Wilson, Graphene oxide-chitosan composite material for treatment of a model dye effluent, ACS Omega 3 (2018) 13045–13054, https://doi.org/10.1021/acsomega.8b01871.

[8] F. Qiu, Y. Hao, X. Li, B. Wang, M. Wang, Functionalized graphene sheets filled isotactic polypropylene nanocomposites, Compos. Part B Eng. 71 (2015) 175–183, https://doi.org/10.1016/j.compositesb.2014.11.027.

[9] L. Gan, F. Qiu, Y.-B. Hao, K. Zhang, Z.-Y. Zhou, J.-B. Zeng, M. Wang, Shear-induced orientation of functional graphene oxide sheets in isotactic polypropylene, J. Mater. Sci. 51 (2016) 5185–5195, https://doi.org/10.1007/s10853-016-9820-z.

[10] S. Pu, Y.-B. Hao, X.-X. Dai, P.-P. Zhang, J.-B. Zeng, M. Wang, Morphological, rheological, crystalline and mechanical properties of ethylene-vinyl acetate copolymer/linear low-density polyethylene/amphiphilic graphene oxide nanocomposites, Polym. Test. 63 (2017) 289–297, https://doi.org/10.1016/j.polymertesting.2017.08.028.

[11] J. Song, H. Gao, G. Zhu, X. Cao, X. Shi, Y. Wang, The preparation and characterization of polycaprolactone/graphene oxide biocomposite nanofiber scaffolds and their application for directing cell behaviors, Carbon 95 (2015) 1039–1050, https://doi.org/10.1016/j.carbon.2015.09.011.

[12] S. Pei, H.M. Cheng, The reduction of graphene oxide, Carbon 50 (2012) 3210–3228, https://doi.org/10.1016/j.carbon.2011.11.010.

[13] M.M. Bernal, M. Tortello, S. Colonna, G. Saracco, A. Fina, Thermally and electrically conductive nanopapers from reduced graphene oxide: effect of nanoflakes thermal annealing on the film structure and properties, Nanomaterials 7 (2017) 2–8, https://doi.org/10.3390/nano7120428.

[14] G. Damonte, A. Vallin, A. Fina, O. Monticelli, On the development of an effective method to produce conductive PCL film, Nanomaterials 11 (2021) 1385, https://doi.org/10.3390/nano11061385.

[15] G. Damonte, A. Vallin, D. Battegazzore, A. Fina, O. Monticelli, Synthesis and characterization of a novel star polycaprolactone to be applied in the development of graphite nanoplates-based nanopapers, React. Funct. Polym. 167 (2021), 105019, https://doi.org/10.1016/j.reactfunctpolym.2021.105019.

[16] Y. Cao, S. Osuna, Y. Liang, R.C. Haddon, K.N. Houk, Diels-alder reactions of graphene: computational predictions of products and sites of reaction, J. Am. Chem. Soc. 135 (2013) 17643–17649, https://doi.org/10.1021/ja410225u.

[17] P.A. Denis, Organic chemistry of graphene: the diels-alder reaction, Chem. Eur. J. 19 (2013) 15719–15725, https://doi.org/10.1002/chem.201302622.

[18] C.-R. Oh, S.-H. Lee, J.-H. Park, D.-S. Lee, Thermally self-healing graphene-nanoplate/polyurethane nanocomposites via diels-alder reaction through a one-shot process, Nanomaterials 9 (2019) 434, https://doi.org/10.3390/nano9030434.

[19] E.R. Leone, L.S. Ferraraccio, G. Damonte, P. Lova, P. Bertoncello, O. Monticelli, On the development of electrochemical sensors coated with polycaprolactone, Electrochem. Commun. 129 (2021), 107089, https://doi.org/10.1016/j.elecom.2021.107089.

[20] O. Monticelli, D. Oliva, S. Russo, C. Clausnitzer, P. Pötschke, B. Voit, On blends of polyamide 6 and a hyperbranched aramid, Macromol. Mater. Eng. 288 (2003) 318–325, https://doi.org/10.1002/mame.200390033.

[21] A.M. Bhayo, R. Abdul-Karim, S.G. Musharraf, M.I. Malik, Synthesis and characterization of 4-arm star-shaped amphiphilic block copolymers consisting of poly(ethylene oxide) and poly(ε-caprolactone), RSC Adv. 8 (2018) 28569–28580, https://doi.org/10.1039/c8ra05000g.

[22] W. Farhat, A. Biundo, A. Stamm, E. Malmström, P. Syrén, Lactone monomers obtained by enzyme catalysis and their use in reversible thermoresponsive networks, J. Appl. Polym. Sci. 137 (2020) 48949, https://doi.org/10.1002/app.48949.

[23] N. Gokalp, C. Ulker, Y.A. Guvenilir, Synthesis of polycaprolactone via ring opening polymerization catalyzed by candida antarctica lipase b immobilized onto an amorphous silica support, J. Polym. Mater. 33 (2016) 87–100.

[24] M. Azizi, M. Azimzadeh, M. Afzali, M. Alafzadeh, S.H. Mirhosseini, Characterization and optimization of using calendula officinalis extract in the fabrication of polycaprolactone/gelatin electrospun nanofibers for wound dressing applications, J. Adv. Mater. Process. 6 (2018) 34–46.

[25] A.H.J. Cross, S.G.E. Stevens, T.H.E. Watts, Some characteristic infra-red absorption frequencies of furan compounds. I, J. Appl. Chem. 7 (2007) 562–565, https://doi.org/10.1002/jctb.5010071008.

[26] M. Sobczak, Ring-opening polymerization of cyclic esters in the presence of choline/$SnOct_2$ catalytic system, Polym. Bull. 68 (2012) 2219–2228, https://doi.org/10.1007/s00289-011-0676-8.

[27] T. Defize, R. Riva, J.-M. Raquez, P. Dubois, C. Jérôme, M. Alexandre, Thermoreversibly crosslinked poly(ε-caprolactone) as recyclable shape-memory polymer network, Macromol. Rapid Commun. 32 (2011) 1264–1269, https://doi.org/10.1002/marc.201100250.

[28] J.-L. Wang, C.-M. Dong, Physical properties, crystallization kinetics, and spherulitic growth of well-defined poly(ε-caprolactone)s with different arms, Polymer 47 (2006) 3218–3228, https://doi.org/10.1016/j.polymer.2006.02.047.

[29] G. Damonte, L. Maddalena, A. Fina, D. Cavallo, A.J. Müller, M.R. Caputo, A. Mariani, O. Monticelli, On novel hydrogels based on poly(2-hydroxyethyl acrylate) and polycaprolactone with improved mechanical properties prepared by frontal polymerization, Eur. Polym. J. 171 (2022), 111226, https://doi.org/10.1016/j.eurpolymj.2022.111226.

[30] K. Ramesh, D.S.B. Anugrah, A.K. Mishra, B.-H. Ahn, Y.-S. Gal, K.T. Lim, Green and sono synthetic approach for direct-functionalization of reduced graphene oxide with poly(styrene-alt-maleic anhydride) by diels alder "click" reaction, Appl. Surf. Sci. 504 (2020), 144482, https://doi.org/10.1016/j.apsusc.2019.144482.

[31] C. Cai, Y. Zhang, M. Li, Y. Chen, R. Zhang, X. Wang, Q. Wu, T. Chen, P. Sun, Multiple-responsive shape memory polyacrylonitrile/graphene nanocomposites

with rapid self-healing and recycling properties, RSC Adv. 8 (2018) 1225–1231, https://doi.org/10.1039/c7ra11484b.
[32] D.G. Manly, E.D. Amstutz, Ultraviolet spectra of 2-substituted furans and 5-substituted methyl furoates, J. Organomet. Chem. 22 (1957), https://doi.org/10.1021/jo01354a601.
[33] Y. Xu, J. Geng, X. Zheng, K.D. Dearn, X. Hu, Friction-induced transformation from graphite dispersed in esterified bio-oil to graphene, Tribol. Lett. 63 (2016), https://doi.org/10.1007/s11249-016-0708-5.
[34] Q. Ma, K. Shi, T. Su, Z. Wang, Biodegradation of polycaprolactone (pcl) with different molecular weights by candida antarctica lipase, J. Polym. Environ. 28 (2020) 2947–2955, https://doi.org/10.1007/s10924-020-01826-4.
[35] G. Damonte, B. Barsanti, A. Pellis, G.M. Guebitz, O. Monticelli, On the effective application of star-shaped polycaprolactones with different end functionalities to improve the properties of polylactic acid blend films, Eur. Polym. J. 176 (2022), 111402, https://doi.org/10.1016/j.eurpolymj.2022.111402.
[36] M. Unger, C. Vogel, H.W. Siesler, Molecular weight dependence of the thermal degradation of poly(ε-caprolactone): a thermogravimetric differential thermal fourier transform infrared spectroscopy study, Appl. Spectrosc. 64 (2010) 805–809, https://doi.org/10.1366/000370210791666309.
[37] E. Correa, M.E. Moncada, O.D. Gutiérrez, C.A. Vargas, V.H. Zapata, Characterization of polycaprolactone/rgo nanocomposite scaffolds obtained by electrospinning, Mater. Sci. Eng. C 103 (2019), 109773, https://doi.org/10.1016/j.msec.2019.109773.
[38] Y.-D. Shi, J. Li, Y.-J. Tan, Y.-F. Chen, M. Wang, Percolation behavior of electromagnetic interference shielding in polymer/multi-walled carbon nanotube nanocomposites, Compos. Sci. Technol. 170 (2019) 70–76, https://doi.org/10.1016/j.compscitech.2018.11.033.

Chapter 8: Mechanically-reinforced biocompatible hydrogels based on poly(N-isopropylacrylamide) and star-shaped polycaprolactones

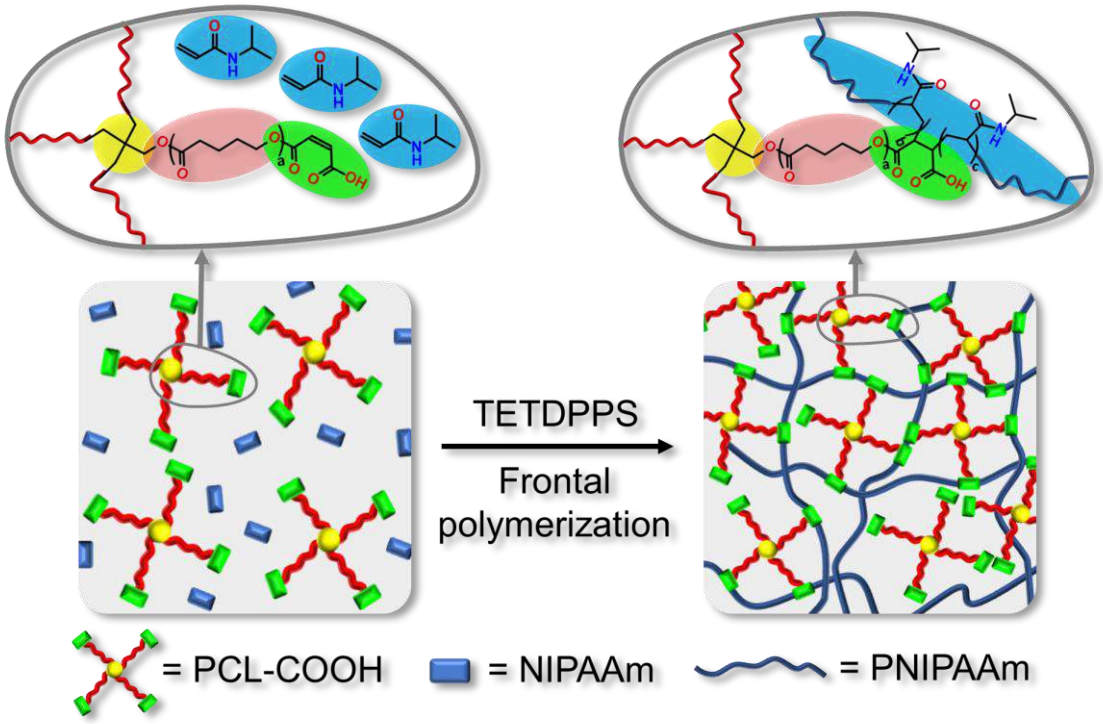

European Polymer Journal 195 (2023) 112239

Contents lists available at ScienceDirect

European Polymer Journal

journal homepage: www.elsevier.com/locate/europolj

Mechanically-reinforced biocompatible hydrogels based on poly (N-isopropylacrylamide) and star-shaped polycaprolactones

Giacomo Damonte [a], Martina Cozzani [a], Donatella Di Lisa [b], Laura Pastorino [b], Alberto Mariani [c], Orietta Monticelli [a,*]

[a] Dipartimento di Chimica e Chimica Industriale, Università di Genova, Via Dodecaneso 31, 16146 Genova, Italy
[b] Dipartimento di Informatica, Bioingegneria, Robotica e Ingegneria dei Sistemi, Università di Genova, Via All'Opera Pia 13, 16145 Genova, Italy
[c] Dipartimento di Chimica e Farmacia, Università di Sassari, and INSTM, Via Vienna 2, 07100 Sassari, Italy

ARTICLE INFO

Keywords:
poly(N-isopropylacrylamide)
Polycaprolactone
Star-shaped polymers
Hydrogels
Frontal polymerization
Drug delivery

ABSTRACT

The aim of this work was to improve the properties of hydrogels based on poly(N-isopropyl acrylamide) (PNIPAAm) in terms of mechanical features and functionality by combining the polymer with a star-shaped tetrafunctional polycaprolactone (PCL), which was synthesized *ad-hoc* and introduced into the reaction mixture. The synthesized PCL (coded as PCL-COOH), selected to maintain the biocompatibility of the final material, was designed with a star structure characterized by four strong arms ending with maleic groups to increase the functionalization potential capable of participating in the radical polymerization and adding acid groups to the system. Specifically, various hydrogels were prepared by partially replacing pentaerytritol tetraacrylate (PE-TA), a commercial crosslinker, with increasing concentrations of PCL-COOH in the presence of trihexyl(tetradecyl) phosphonium persulfate (TETDPPS) as non-gas-releasing radical initiator. In addition, frontal polymerization (FP) was employed, a fast and energy efficient technique, potentially capable of promoting the dispersibility of PCL in the polymer matrix.

The influence of the star-shaped PCL on the polymerization process as well as on the hydrogel properties in terms of chemical structure, swelling behaviour, thermal and mechanical features was investigated. Indeed, it was found that the presence of PCL allowed the formation of a stable polymerization front up to a concentration of 25 wt%. FT-IR measurements allowed to evaluate the fraction of PCL effectively bonded to the hydrogel structure, while the morphological analysis performed by FE-SEM characterization revealed that the hydrogel pore size tended to decrease as the amount of PCL in the system increased. In addition, the star-shaped PCL was found to affect the material swelling properties, by reducing the swelling ratio without affecting the thermoresponsive behavior. Mechanical tests performed on the neat PNIPAAm hydrogels and on PCL-containing hydrogels, showed a relevant increase in the material stiffness due to the PCL-COOH addition. The DSC characterization results showed a decrease in the glass transition temperature with increasing PCL-COOH content, indicating a partial miscibility of the two polymers likely due to a compatibilization effect of a copolymer formed during the polymerization process. To demonstrate the capability of the hydrogels to retain positively charged molecules, the prepared systems were contacted with solutions containing pararosaniline hydrochloride. The retention capacity as well as the kinetic release were investigated. The measurements evidenced a higher retaining capacity and a lower release rate in the PCL-containing hydrogels. Finally, the biocompatibility and the low citoxicity of the PNIPAAm/PCL hydrogels were confirmed by a cell viability assay using the SH-SY5Y cell line.

1. Introduction

Poly(N-isopropylacrylamide) represents one of the most promising polymers applied for the preparation of hydrogels. Indeed, PNIPAAm is a thermoresponsive biocompatible polymer used for the development of smart materials with potential biomedical applications, such as controlled scaffolds for tissue engineering, wound dressings, and drug delivery systems [1,2]. However, despite the appealing properties of

* Corresponding author.
E-mail address: orietta.monticelli@unige.it (O. Monticelli).

https://doi.org/10.1016/j.eurpolymj.2023.112239
Received 12 May 2023; Received in revised form 7 June 2023; Accepted 17 June 2023
Available online 19 June 2023

PNIPAAm-based hydrogels, they have drawbacks, particularly in terms of mechanical and retention properties. Regarding the latter, the chemical structure of PNIPAAm is devoid of functional chain groups, which limits both ionic and covalent interactions required for binding with target molecules. In particular, the lack of functionality was found to make the incorporation of hydrophobic drugs very difficult especially below the lower critical solution temperature (LCST) [3]. At the same time, PNIPAAm-based hydrogels lack mechanical strength, due to high water uptake and the resulting low density of polymer chains in the swollen hydrogel, limits their use for structural applications [4,5]. To address the above drawback, various approaches were explored by adding one or more components to NIPAAm in the form of monomers, polymers, or fillers [4]. Indeed, it is worth underlining that a direct comparison among the values of the mechanical parameters of the different studied systems is difficult because the mechanical behaviour is influenced by several variables, such as the degree of swelling, the applied temperature, the measuring method, etc. Nevertheless, among the various proposed approaches, some resulted to be the most effective. In particular, PNIPAAm-based interpenetrated networks (IPN) hydrogels, developed mainly to modify swelling behaviour, showed improvement in mechanical properties [4]. For example, Petrusic et al. prepared thermoresponsive IPN hydrogels that achieved a modulus of 120 KPa by reinforcing a PNIPAAm network with calcium alginate [6]. It was found that another approach to improve the mechanical properties of PNIPAAm-based hydrogels is based on double networks (DN), *i.e.*, a type of IPN in which the degree of crosslinking between the two polymeric networks is asymmetric [7–9]. In this case, in order to improve the mechanical properties, the first network should be able to swell sufficiently in the second and consequently be less crosslinked. Using this strategy, Fei et al. prepared P(NIPAAm-*co*-2-acrylamido-2-methylpropane sulfonic acid)/PNIPAAm DN hydrogels that achieved a compressive modulus of 340 KPa [8].

In addition, the incorporation of fillers/nanofillers, such as graphene oxide (GO) [9,10], silica [11,12], Fe_2O_3 [13], Au nanoparticles [14], TiO_2 [15] and clay [16,17] was found to play a role in the improvement of the mechanical behaviour of hydrogels. In this case, the compatibility of the fillers and the non-simple dispersion have to be considered [18]. These works, demonstrating the interest in developing methods to modify the properties of PNIPAAm-based hydrogels, generally focused on improving a single property. The development of an approach to overcome the various drawbacks associated with these materials is therefore of great interest.

In the field of coupling polymers with monomers and polymers - a method essentially used to functionalize the matrix and modify its LCST - few works focused on polycaprolactone (PCL), namely the polymer objective of the work. Indeed, as far as we know in all the works published so far, PCL was combined with PNIPAAm in the form of a copolymer. In particular, in NIPAAM/PCL-based block copolymer hydrogels, various forms of PCL have been used as crosslinkers. However, they all had a linear structure. Indeed, it was introduced in the form of PCL-diacrylate [19], PCL-methacrylate [20] or PCL-hydroxyethylmethacrylate macromonomer [21] with the main purpose of introducing a hydrolysable degradable fraction in PNIPAAm, rather than improving its mechanical properties.

In our work, a new formulation was developed by polymerizing NIPAAm with an *ad-hoc* developed polymer potentially capable of improving some of the properties of the matrix without changing its biocompatibility. A star-shaped tetrafunctional PCL, characterized by maleic end groups (PCL-COOH) and thus capable of participating in radical polymerization and conferring acid functionalities to the system, was synthesized and added to the polymerization mixture at different concentrations (Fig. 1). The decision to use a star-shaped polymer, which is a novelty in the current literature, is related to the fact that the synthesized polymer contains a greater number of functionals groups compared to a linear system with the same molecular weight. This property can significantly affect the ability of the macromolecule to be covalently inserted into the hydrogel system, thanks to the reactivity of the double bond, and promoting the network crosslinking, thanks to the tetrafunctional structure. In addition, the high number of the carboxyl end groups of the star-shaped polymer, always compared to a linear structure, can significantly increase the material ability to interact with positively charged molecules.

Moreover, frontal polymerization, a fast and energy-efficient method, was applied to promote PCL dispersion in PNIPAAm matrix, by "freezing" the homogeneity of the polymerization mixture [22].

Frontal polymerization can indeed be considered an "energy-efficient" approach, since the only external energy required for frontal polymerization is an initial thermal stimulus that ignites the reaction locally. It is the exothermicity of the reaction that provides local heating, and the transfer of this thermal energy to adjacent monomers in the reaction medium results in a self-sustaining reaction zone that produces fully cured thermosets and thermoplastics. The propagation of this

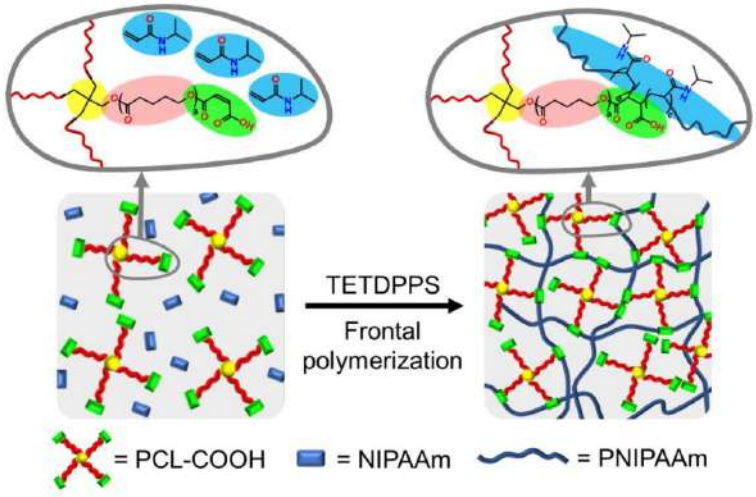

Fig. 1. Scheme of the developed PNIPAAm/PCL hydrogels.

polymerization front continues through the unreacted monomer medium until either all reactants are consumed or sufficient heat loss stops further reaction [22].

The prepared hydrogels were fully characterized by IR, DSC, TGA, FE-SEM, swelling and mechanical measurements. Dye retention and release tests were performed to assess the binding capacity of hydrogels towards PR (pararosaniline hydrochloride), a triarylmethane cationic dye. Cell viability tests were performed using SH-SY5Y cell line to prove the biocompatibility of the material.

2. Materials and methods

2.1. Materials

N-isopropylacrylamide (NIPAAm, purity ≥ 97%), ε-caprolactone (ε-CL, purity = 97%), dimetylsulfoxide (DMSO, purity ≥ 99%), aliquat 336 chloride (AQC, purity ≥ 98%), ammonium persulphate (APS, purity ≥ 98 %), pentaerythritol (purity = 99%), pentaerythritol tetraacrylate (PE-TA, with 350 ppm hydroquinone monomethyl ether), tin octoate (Sn $(Oct)_2$, purity ≥ 96%), methanol (99.9%), maleic anhydride (purity ≥ 99%), diethyl ether (purity 99 %, stabilized with BHT), toluene (purity = 99.8%, anhydrous), pararosaniline hydrochloride (PR, purity ≥ 85 %), N-methyl pyrrolidone (NMP, purity ≥ 99.5 %, anhydrous), 2,2′-azobis(2-methylpropionitrile) (AIBN, purity ≥ 98.0 %), benzoyl peroxide (BPO, with 25 % water, for synthesis) and dichloromethane (DCM, purity ≥ 99.8%, stabilized with amylene) were purchased from Sigma Aldrich®. Trihexyl tetradecyl phosphonium chloride (TETDPC, purity ≥ 97%) was purchased from TCI chemicals. ε-caprolactone and DCM were purified prior to use by vacuum distillation over CaH_2 and stored under Ar atmosphere. Diethyl ether was purified by distillation to remove inhibitor prior to use. Pentaerythritol was dried in vacuum oven at 40 °C prior use. BPO was dried before use. All the other reagents were of analytical grade and used without further purification.

2.2. Synthesis of maleated star-shaped PCL (PCL-COOH) and initiators

The tetrafunctional maleated star PCL (PCL-COOH) was prepared by esterification of an hydroxyl-terminated star tetrafunctional PCL (PCL-OH) with molecular weight ($M_{n,NMR}$) of 2000 g/mol per arm, following a procedure already reported in the literature [23–26]. FT-IR and ^{1}H NMR signals for PCL-OH and PCL-COOH, are reported in the Table S1 of the Supporting Information. Aliquat persulphate (AQPS) was prepared according to a previous procedure reported by Masere et al. by metathesis reaction between APS and AQC [27], whereas for the synthesis of trihexyl tetradecyl phosphonium persulphate (TETDPPS), the procedure reported by Mariani et al. by metathesis reaction between TETDPC and APS was used [28].

2.3. Preparation of poly(NIPAAm)/PCL-COOH hydrogels

The polymerization process was studied preliminarly by determining the type of solvent and the minimum concentration for the solubilization of NIPAAm and PCL-COOH. Indeed, NMP and DMSO were tested by contacting the solvents with 1 g of NIPAAm (Table S2). To determine the minimum amount of solvent required to dissolve a mixture of 1 g of NIPAAm and 0.5 g PCL-COOH, different amounts of DMSO, which was found to be the optimal solvent, were added to the above mixture. In order to carry out the frontal polymerization in the optimized conditions, 5 g of NIPAAm were dissolved in 3 mL of DMSO inside a glass test tube (13 mm internal diameter and 100 mm length), with mechanical stirring, followed by the appropriate amount of crosslinker (PETA or a mixture of PETA and PCL-COOH as reported in Table 1 for sake of convinience). After complete dissolution of the solids, 150 mg (0.5 mol% respect to NIPAAm) of TETDPPS were added and stirred for an additional 30 s. FP of the samples was then initiated by heating the outer wall of the upper part of the test tube with the tip of a tin welder (450 °C).

Table 1
Characteristics of the prepared NIPAAm-based hydrogels.

Sample code	PETA/ PCL ratio[1]	PCL content[2] [m/m%]	PCL content[2] [mol%]	PETA[3] [mg]	PCL[3] [mg]
PNIP_F	100/0	0	0	100	0
PNIP_PCL_10_F	80/20	10	0.132	80	500
PNIP_PCL_20_F	60/40	20	0.264	60	1000
PNIP_PCL_25_F	50/50	25	0.33	50	1250

Crosslinker content, expressed as the sum of PETA and PCL-COOH respect NIPAAm moles, was 0.66 mol%. [1]PETA/PCL indicates the composition of the crosslinking fraction added to NIPAAm expressed as mol/mol ratio respect the total amount of crosslinker. [2]PCL content is calculated respect NIPAAm. [3]PETA and PCL are expressed as the quantity required for 5 g of NIPAAm.

After polymerization, the hydrogels were carefully removed by breaking the tube, sliced in the desired shape, and immersed in milliQ water for 5 days, changing the water every day to remove DMSO and other water-soluble contaminants.

2.4. Characterization

^{1}H NMR proton spectroscopy was performed with a Jeol ECZ400R/S3 400 MHz by using 10 mm NMR test tubes and $CDCl_3$ as solvent. The samples, priorly dissolved in $CDCl_3$ at a concentration of 30 mg/mL, were analyzed at room temperature.

FT-IR spectra of the xerogels were recorded in ATR from 400 to 4000 cm^{-1} using a Bruker "Vertex 70®". To estimate the quantity of covalently bound PCL in the structure, the samples were subjected to an extraction process performed by soaking the materials for 24 h in an excess of DCM, a good solvent for PCL. After extraction, the samples were dried in a vacuum oven for several days at room temperature and analysed. The PCL content was then determined by plotting the areas for the C=O stretching peak of PCL at 1725 cm^{-1} vs. the PCL content of dried, unwashed xerogels to obtain a calibration curve for PCL. The concentration of PCL-COOH in the extracted samples was then calculated by measuring the area in the same way and inserting it into the calibration curve.

Thermal analysis of the samples was performed on xerogels with a Mettler Toledo differential scanning calorimeter (DSC1 STAR^e System®), between −100 and 150 °C, at a heating/cooling rate of ± 10 °C/min and an N_2 flow of 20 mL/min. The crystallinity degree (X_c) of PCL in the xerogels was calculated based on their PCL contents, Φ_{PCL}, following the Eq. (1). Thermogravimetric analysis (TGA) was performed in the range 30–800 °C under inert atmosphere with an N_2 flow of 80 mL/min.

$$X_c(\%) = \frac{\Delta H_m}{\Delta H_m^0 \times \varphi_{PCL}} \times 100\% \quad (1)$$

where ΔH_m = measured melting enthalpy, Φ_{PCL} = PCL weight fraction in the xerogel and ΔH_m^0 is the melting enthalpy of a 100% crystalline PCL, considered as 139 J/g [29].

For the above calculation, the second heating scan was considered. The temperature of the front during FP was measured using a K-type thermocouple inserted into the reaction mixture at 2 cm from the bottom of the test tube. The temperature change was then monitored by a digital thermometer. The polymerized samples were obtained by carefully breaking the test tube, cut into pieces, and washed in milliQ water for 5 days, changing water every 24 h. After washing, the samples were dried in a vacuum oven at room temperature, until constant weight. Swelling ratio was measured from 20 to 70 °C on small hydrogel disks (5 mm diameter, 3 mm of thickness) using milliQ water as solvent and increasing the water bath temperature by 5 °C/day (2 °C/day between 30 and 40 °C for improved LCST resolution). The swelling ratio % (SR%) was then obtained by applying Eq. (2).

$$SR\% = \frac{M_s - M_i}{M_i} \cdot 100 \quad (2)$$

Where M_s and M_i are the weight of the swollen hydrogel and dried xerogel respectively.

Field emission scanning electron microscopy (FE-SEM) was performed with a Zeiss Supra 40 VP equipped with a backscattered electron detector. The freeze-dried samples were immersed in liquid nitrogen, cryogenically fractured and thinly sputter-coated with carbon using a Polaron E5100 sputter coater prior to analysis. Statistical analysis of pore size in xerogels was performed by using ImageJ software.

Mechanical tests were performed using a Zwick/Roell Z0.5 electromechanical testing machine (Standards EN 2562–EN 2746) equipped with a planar support. For this characterization, swollen samples were prepared punching out into a small round slice with a hole puncher (Ø = 5 mm in diameter and h = 2 mm); the tests were run at a rate of 1 mm/min. The modulus of hydrogels was obtained by compressing the samples at a strain rate of 20–25%. Moreover, indentation tests were performed using a prototype DMA apparatus, consisting of a mini-shaker operating in a range between 1 Hz and 10 KHz with maximum force of 1.5 N, a laser vibrometer to measure the displacement, set at 80 μm/V and a force transducer. All tests were run on swollen cylindrical samples (Ø = 5 mm in diameter and h = 1 mm) at 22 °C. The samples were place on a plate connected with the shaker, a cylindrical indenter of 5 mm in diameter was approached until touching the upper surface of the sample and then 20% pre-strain has been applied. The test was run with an oscillation between 2 Hz and 100 Hz and the sinusoidal signal of the displacement and of the force, respectively response and stimulus, was elaborated by the software producing a spectrum containing the storage modulus and the loss modulus vs. the frequency. Both mechanical tests were performed at room temperature.

2.5. Dye absorption and release tests

Xerogel disks prepared by cutting hydrogel pieces 5 mm in diameter and 2 mm thick were individually immersed in 5 mL of pararosaniline dye solution (5 μg/mL) for 24 h, in the dark at 22 °C. After this time, the concentration in the surnatant was analyzed by means of UV–Vis spectrometry. The corrected concentration was determined by considering the amount of water retained by the dried hydrogels during the absorption time, based on their weight change from the dry to the swollen state in swelling test, and then applying the following Eqs. (3) and (4):

$$C_{CORR} = \frac{C_1 V_1}{V_2} \tag{3}$$

$$\text{Dye absorbed} = \frac{(C_i - C_{CORR}) \cdot V_2}{m_{dry}} \tag{4}$$

Where C_1 is the measured concentration, V_1 is 5 mL – X mL of water absorbed by the xerogel during the swelling phase, C_{CORR} is the corrected concentration and V_2 = 5 mL. C_i = initial concentration, m_{dry} = initial mass of the dried xerogel disk.

All the concentrations were expressed in μg/mL. The quantity of dye absorbed by the materials was expressed as μg/g of dried xerogel. The dye release tests were performed in the same manner as the dye adsorption tests, but a more concentrated solutions (100 μg/mL) was used. The hydrogel disks were then removed, externally dried by gently tapping with a paper towel, and immersed in 5 mL of milliQ water at 22 °C. Dye release was followed by means of UV–Vis spectrometry until a plateau was reached in the measured absorbance.

2.6. Cell culture conditions and viability evaluation

The human neuroblastoma cell line SH-SY5Y was grown in 75 cm^2 tissue culture flasks in complete Dulbecco's modified Eagle's medium (DMEM (4.5 g/L)) supplemented with 10% fetal bovine serum (FBS), 1% penicillin–streptomycin and 1% glutamax, at 37 °C in 5% CO_2. The day before plating, the samples were sterilized in 70% ethanol for 40 min, then washed three times in H_2O and normalized overnight in culture medium. For all experiments, cells were plated in 6-well plates at a density of $2{\cdot}10^5$ cells/well in 2 mL of culture medium. After 24 h, the samples were placed in 40 μm cell strainers and then in 6-well plates for 48 h, to evaluate the cytotoxic effect of substances leaching from the samples. Cells were observed before and after the exposition to the samples and every 24 h, acquiring contrast phase images by an inverted IX-51 Olympus microscope equipped with a DP70 digital camera. The survival rate of cells was observed after 48 h of culture. Cell viability was assessed using a standard live/dead™ assay (calcein AM/ethidium homodimer) according to the manufacturer's instructions. To perform the assay, 1 mL of the staining solution containing 0.50 μL of calcein AM and 2 μL of ethidium homodimer in DPBS was used to replace the cell culture medium, followed by incubation in the dark at 37 °C for 20 min. Live and dead cells were imaged using Olympus BX-51 upright microscope equipped with a Hamamatsu Orca ER II digital cooled CCD camera driven by Image ProPlus software (Media Cybernetic) at excitation/emission wavelengths of 494/515 nm for calcein (green, live cells) and 528/617 nm for ethidium homodimer-1 (red, dead cells). NIH ImageJ software was used to quantify the cell viability based on the ratio of the live cell number to the total number of cells.

3. Results and discussion

3.1. Optimization of the polymerization conditions

This work preliminarily focused on the optimization of the polymerization process, including the type of solvent and initiator as well as the monomer concentration. Regarding the solvent, some properties were considered, namely the water solubility and the ability to dissolve both the system components, namely NIPAAm and the star-shaped PCL. Indeed, it is worth underling that in order to perform the FP process, the solutions should be sufficiently concentrated to generate an appropriate thermal output and allowing for the propagation front to self-sustain. The behavior of NMP and DMSO was evaluated by carrying out a preliminary solubility test with NIPAAm. From the results shown in Table S2, it results that the use of DMSO allowed the preparation of NIPAAM solutions characterized by a higher concentration than those prepared using NMP. Based on the above results, DMSO was chosen, and the minimum amount of solvent required to solubilize a system consisting of NIPAAm and PCL-COOH was determined. The polymerization condition assessment also considered the selection of the most suitable radical initiator. Indeed, by using some classical radical initiators such as BPO and AIBN, particularly at high concentration, the formation of bubbles and defects within the gel during FP was observed, which might affect the mechanical properties of the material as well as the maintenance of a stable polymerization front during the FP process [30]. Moreover, the compounds generally used to obtain polymers based on NIPAAm are initiators that do not release gas, such as potassium [31,32] or ammonium [33,34] persulphates, which being soluble in highly polar media, cannot be used in our system. As such in this work, we considered the exploitation of persulphates soluble in organic solvents, such as AQPS [27] or TETDPPS [28]. Among the above two compounds, TETDPPS was chosen as it allowed to obtain a stable polymerization front.

The FP process was studied by evaluating the front position as a function of time (Fig. S1). Fig. S1 shows, as an example, the position of the front as a function of time for the sample with the highest amount of PCL-COOH, namely PNIP_PCL_25_F. A very similar trend was observed for all the other synthesized systems. Indeed, the experimental data fitted by a straight line demonstrated that the polymerization proceeds at a constant velocity and thus that a pure FP occurs. Moreover, it is relevant to underline that the presence of PCL-COOH did not negatively affect the frontal polymerization process, at least at the concentrations used.

The front velocity (V_f) as well as the front temperature (T_f) for all the

prepared systems are given in Table S3. The above results indicate that the addition of the star-shaped polymer to the reaction mixture decreased both the above parameters, with V_f going from 0.47 cm·min^{-1} for PNIP_F to 0.20 cm·min^{-1} for PNIP_PCL_25_F, while T_f, which was 135 °C for the neat PNIPAAm hydrogel, was reduced to 93 °C for the sample with the highest PCL content, PNIP_PCL_25_F. This finding may be attributed to a "diluting" effect of PCL-COOH, which, although characterized by double bonds and thus capable of participating in the polymerization process, is characterized by a low content of reacting groups as compared to its total mass, thus acting as heat sink much more than what NIPAAm does. Since frontal polymerization requires a certain amount of energy to propagate, it can be hypothesized that PCL-COOH limits the front formation at a certain concentration. Indeed, it was found that at a concentration of more than 25 wt% of the star-shaped polymer with respect to the monomer, a self-sustaining reaction front could not be achieved after initiation, likely due to the limited thermal output. Therefore, the above concentration was the highest used to develop the hydrogel by frontal polymerization.

3.2. FT-IR measurements

FT-IR spectra of the PNIPAAm-based xerogels are showed in Fig. 2. In PNIP_F, the sample prepared by using neat NIPAAm as monomer, the presence of signals clearly attributable to PNIPAAm was observed at: 3410 cm^{-1} (υ O–H, water), 3283 cm^{-1} (υ N–H), 2973 cm^{-1} (υ C–H asymmetric/symmetric), 2877 cm^{-1} (υ C–H asymmetric/symmetric isopropyl group), 1626 cm^{-1} (amide I band) and 1541 cm^{-1} (amide II band). The above bands are consistent with those previously reported by other authors [35]. In contrast, the analysis of the samples containing the star-shaped polymer showed additional peaks attributed to PCL chains at: 2950 cm^{-1} and 2870 cm^{-1} (υ Csp3- H methyleneic unit), 1725 cm^{-1} (υ C = O), at 1295 cm^{-1} (υ C–O and C–C), 1242 cm^{-1} and 1171 cm^{-1} (υ C–O–C asymmetric/symmetric), which are in good agreement with the results of previous studies [36,37]. In particular, the area of the peak belonging to υ C=O of PCL, at 1725 cm^{-1}, showed a good correlation with the PCL concentration in the sample, increasing with the PCL content. At the same time, the intensity of the PNIPAAm signals decreased, which can be attributed to a decrease in the PNIPAAm content in the xerogels. This trend was also reflected in the intensity of the O–H stretching at 3410 cm^{-1} caused by the water retained by the PNIPAAm backbone. This signal, which partially overlapped with N–H stretching of PNIPAAm, was reduced by the presence of PCL. These findings suggest that the addition of a hydrophobic polyester such as PCL can alter and reduce the water uptake of the xerogels structure. It can be deduced that the incorporation of PCL in the gel structure can lead to a change in the properties of the resulting materials, including their water affinity.

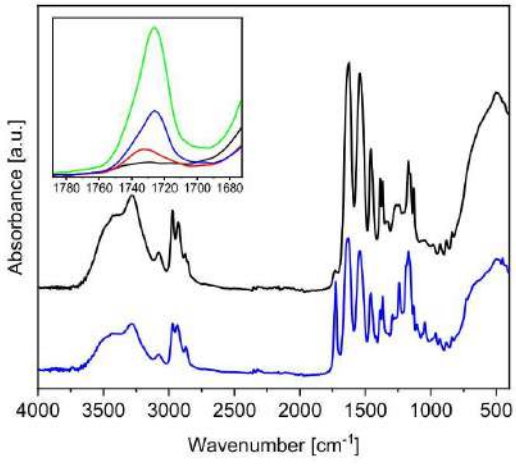

Fig. 2. FT-IR spectra of PNIP_F (black), PNIP_PCL_10_F (red), PNIP_PCL_20_F (blue), PNIP_PCL_25_F (green). (For interpretation of the references to colour in this figure legend, the reader is referred to the web version of this article.)

The conversion with respect to the monomer was calculated by weighing the gels before and after washing with water, taking into account the mass loss associated with DMSO removal (Table 2). The results reported in Table 2 indicate that a conversion of about 80% could be achieved with the frontal polymerization, a value that does not seem not to change significantly with the addition of the star-shaped polymer to the reaction mixture.

In order to estimate the fraction of PCL-COOH involved in the polymerization reaction to form star-block copolymers, the areas of the C=O peak of PCL at 1725 cm^{-1} were compared before and after the extraction of the xerogels with DCM, a good solvent for the star-shaped polymer. It is worth mentioning that the studied samples were previously washed with water. Therefore, the calculated amount of star-shaped polymer refers to PNIPAAm, i.e., to the system from which the monomer was removed. The concentration of PCL-COOH was then calculated and the percentages of bonded/unbonded PCL-COOH in the samples are reported in Table 2. This analysis provided valuable information on the efficiency of the reaction and the degree of incorporation of the polyester in the copolymer structure. Based on the results obtained, it was found that an increase in the concentration of PCL-COOH in the starting mixture led to an increase in the fraction of the polymer involved in the formation of the copolymer with NIPAAm. This increase is probably due to the fact that the probability that the maleic terminals (*i.e.*, the functional groups in PCL-COOH, which can react with NIPAAm) to participate in the radical polymerization reaction increases with increasing the concentration of PCL-COOH. This, in turn, results in a greater amount of polymer being bound to the gel matrix. Overall, this observation suggests that the concentration of PCL-COOH in the starting mixture may be a crucial factor in determining the properties of the resulting copolymer, such as its structure, composition, and mechanical properties. Further experiments may be required to further investigate the relationship between the concentration of PCL-COOH and the properties of the copolymer.

3.3. Xerogels thermal properties

The thermal behavior of xerogels was studied by DSC measurements. The DSC traces from the cooling and second heating are given in Fig. 3, while the thermal data are summarized in Table 3. For comparison, also DSC data from PCL-COOH are shown in the same table. In agreement with previous reports, neat PNIPAAm xerogels exhibited a glass transition temperature at about 140 °C [38]. It is relevant to underline that the PCL-based samples showed a relevant decrease of T_g, although it was found that the value depended on the content of the star-shaped polymer in the blend. Indeed, the T_g decreases from 140 °C in the case of PNIP_F

Table 2
PCL-COOH content after DCM extraction calculated by FT-IR measurements.

Sample	Monomer conversion[1] [%]	PCL-COOH before washing [m/m%]	PCL-COOH after washing [m/m%]	PCL-COOH bonded fraction [%]
PNIP_F	82	0	0	0
PNIP_PCL_10_F	80	10	2	20
PNIP_PCL_20_F	75	20	5	25
PNIP_PCL_25_F	78	25	7.5	30

[1] monomer conversion refers to NIPAAm and was calculated gravimetrically by weighing the gels before and after washing with water, taking into account the mass loss associated with DMSO removal.

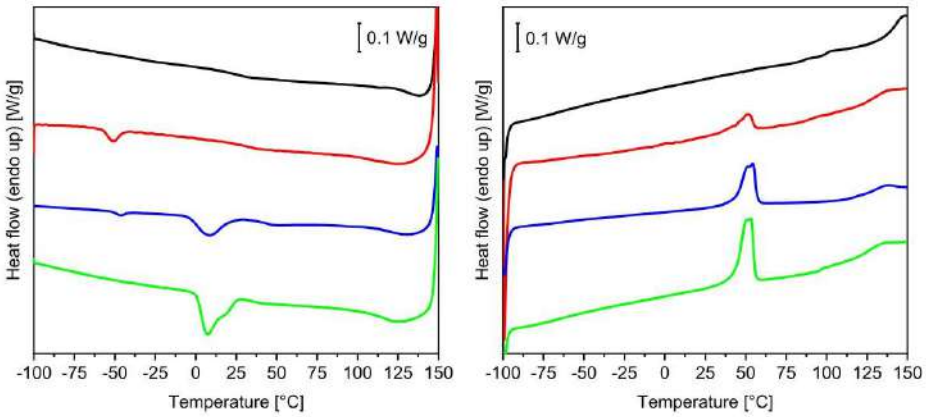

Fig. 3. DSC thermograms, cooling (left) and second heating (right), of: PNIP_F (black), PNIP_PCL_10_F (red), PNIP_PCL_20_F (blue), PNIP_PCL_25_F (green). (For interpretation of the references to colour in this figure legend, the reader is referred to the web version of this article.)

Table 3
Results from DSC analysis of PNIPAAm-based xerogels.

Sample code	T_c [°C]	$\Delta H_{c\ CORR}$ [J/g]	T_g [°C]	T_m [°C]	$\Delta H_{m\ CORR}$ [J/g]	$\chi_{c\ CORR}$ [%]
PCL-COOH	25	−71*	−60	47	70*	50*
PNIP_F	–	–	140	–	–	–
PNIP_PCL_10_F	−51	−20	135	44	51	31
PNIP_PCL_20_F	−45/8	−30	121	46	54	33
PNIP_PCL_25_F	7	−45	115	52	53	38

The subscript m and c indicate the values measured during melting and crystallization, respectively. χ_c is the degree of crystallinity calculated by assuming the ideal enthalpies of fusion as 139 J/g and considering the PCL content in the xerogel. *: the values reported for PCL-COOH were not subjected to corrections.

to 115 °C for PNIP_PCL_25_F, indicating a partial miscibility between the two polymer phases. To explain this phenomenon, as previously shown, it is necessary to consider the formation of a copolymer during the polymerization process, which can settle at the interface between the two polymer phases and increase their compatibility. Moreover, considering the PCL crystallization behavior, it is interesting to note that the crystallinity (χ_c) of PCL tended to decrease in the blend compared to the neat polymer. A slight difference was observed when the star-shaped polymer content was increased, χ_c ranging from 31% in the case of PNIP_PCL_10_F to 38% for the xerogel with the highest PCL content, PNIP_PCL_25_F. Again, these results can be explained considering that part of the PCL added to the reaction mixture is covalently bound and has a lower chain mobility, so that it can participate in the crystallization process only to a limited extent, while another part, which is mixed, can structuring. Looking at the cooling traces, we can see a very different behavior of the samples depending on the PCL content. In particular, for PNIP_PCL_10_F, a single crystallization peak was observed at a T_c of −51 °C, which was much lower than that of the neat PCL-COOH (T_c of about 25 °C). In the case of PNIP_PCL_20_F, two peaks are observed at 45 °C and 8 °C, while PNIP_PCL_25_is characterized by only one peak at 7 °C. As previously reported for other blended xerogel, e.g. based on PCL end-capped with acrylic units and poly(2-hydroxyethyl acrylate) (PHEA), the above results can be attributed to a fractioned crystallization of the PCL phase [39]. This phenomenon, which generally occurs when a semicrystalline polymer is subdivided into small domains containing less or less active heterogeneities so that nucleation and crystallization of the polymer can occur only at larger undercoolings, can be associated with the finely distributed domains of PCL in the xerogel. Indeed, the crystallization of the above domains, which could be free of nucleating impurities, may be controlled by homogeneous nucleation occurring at the maximum possible undercooling, i.e., near the glass transition temperature [40]. Of course, the phenomenon described above depends not only on the PCL content, but also on the size of the domains, which explains the different behavior of the samples. It is worth underling that PCL crystallizes at low temperatures when segregated in nanosized spheres in block copolymers [41–43] or in the interlamellar poly(lactide) regions of partially miscible poly(lactide)-block-poly(caprolactone) copolymers [44].

The thermal stability of xerogels was tested by TGA/DTG measurements, and the results are given in Fig. 4 and Table 4. An initial weight loss, $T_{onset5\%}$, below 200 °C was observed for all the samples tested, which was associated with the water molecules bound to the PNIPAAM structure by hydrogen bonds [45]. As expected, the amount of water loss in this step, which was also observed in other PNIPAAm-based systems [46–48], namely Δ_{m1}, was inversely correlated with the PCL content, and followed the trend PNIP_F > PNIP_PCL_10_F > PNIP_PCL_20_F > PNIP_PCL_25_F. Indeed, the presence of PCL, a hydrophobic and semicrystalline polymer, led to a decrease in the amount of water bound to the xerogel structure. At higher temperatures, all the samples showed similar TGA curves with a single degradation step mainly due to the statistical C–C backbone break of PNIPAAm. In the neat PNIPAAm xerogel, PNIP_F, the T_{max} measured for this step was 435 °C, in good agreement with the temperature of 420 °C reported by Schild et al. for a linear high molecular weight PNIPAAm sample [49]. For the PCL-containing samples, only a minor effect of PCL on the reduction of T_{max} was detected, which was accounted to a partial overlap between the statistical β-scission degradation step of PCL, which normally occurs at ca. 425 °C [50], and PNIPAAm degradation. Overall, these results suggest that the presence of PCL does not affect the thermal stability of the xerogels.

3.4. Swelling and thermoresponsive properties of hydrogels

Fig. 5 shows the swelling ratio % (SR%) of PNIPAAm-based hydrogels as a function of temperature. At 20 °C, the SR% of neat PNIPAAm hydrogels was in agreement with the values reported in the literature [51,52]. Indeed, the presence of PCL in the system led to a significant decrease in the swelling ratio, which ranged from about 1000% in the case of PNIP_F to 320% for the sample characterized by the highest PCL content, i.e., PNIP_PCL_25_F. As previously reported, the above phenomenon can be attributed to the intrinsic hydrophobicity of the polyester as well as to its semicrystalline structure, which is partially preserved in the blend hydrogels and appears to limit the ability of the

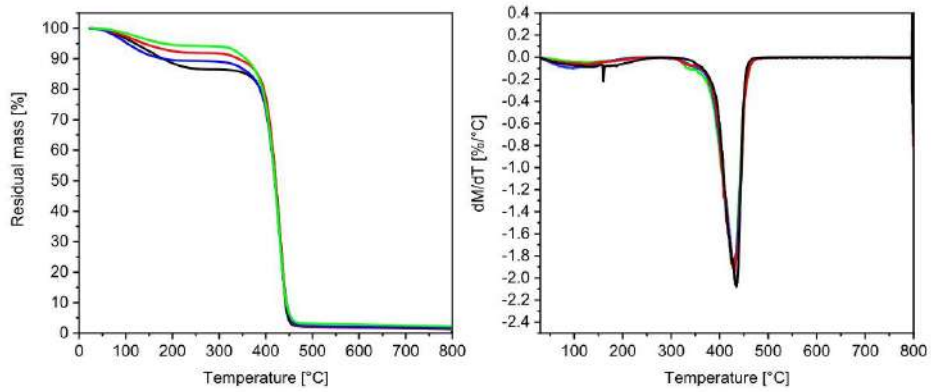

Fig. 4. TGA (left) and DTG curves (right) of: PNIP_F (black), PNIP_PCL_10_F (red), PNIP_PCL_20_F (blue), PNIP_PCL_25_F (green). (For interpretation of the references to colour in this figure legend, the reader is referred to the web version of this article.)

Table 4
Results from TGA analysis of PNIPAAm-based xerogels.

Sample code	$T_{onset5\%}$ [°C]	T_{max1}* [°C]	Δ_{m1} [%]	T_{max2}* [°C]
PCL-COOH	253	387	10	428
PNIP	80	160	13.5	435
PNIP_PCL_10_F	88	121	11.0	430
PNIP_PCL_20_F	71	106	8.2	431
PNIP_PCL_25_F	107	128	6.0	426

*:T_{max1} and T_{max2} values are extrapolated from DTG curves.

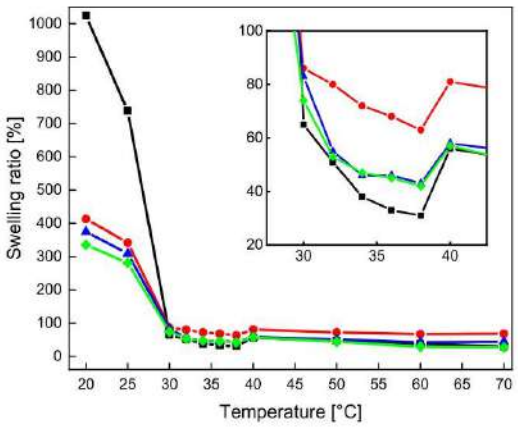

Fig. 5. Equilibrium SR% in function of temperature for PNIP_F (black), PNIP_PCL_10_F (red), PNIP_PCL_20_F (blue), PNIP_PCL_25_F (green). (For interpretation of the references to colour in this figure legend, the reader is referred to the web version of this article.)

system to retain water. Nevertheless, the values of the swelling ratio of the hydrogels containing PCL are significantly high to be used in areas where it is necessary to modify the material dimension by changing the environment [53]. In addition, it is worth underling that SR% tended to decrease when the amount of PCL in the hydrogel increased, but this variation was limited since the swelling ratio of PCL-based hydrogels ranged between 350 and 400 %. Considering the SR% of the neat PNIPAAm as a function of temperature, it showed a significant reduction with increasing temperature, demonstrating its well-established thermoresponsive behavior with a lower critical solution temperature (LCST) of ca. 32 °C [4,54]. Indeed, it was reported that when the temperature is increased, the hydrogen bonding, involving the hydrophilic amide group, is weakened and consequently, the interactions among the hydrophobic groups (–CH(CH_3)$_2$) become strong [4]. This phenomenon leads to the release of water from the structure and at the same time to the collapse of polymer chains. Considering the SR% of PCL-based samples as a function of temperature, a similar trend as the neat hydrogel was found, with a LCST, namely the temperature where the swelling ratio is the lowest and is the same for the samples, of ca. 32 °C. This result shows that the presence of the star-shaped polymer in the system affects its ability to retain water, but it is not responsible for the change in chain structure and interactions with the environment, i.e., it does not lead to a change in LCST. It is known that the modification of LCST in PNIPAAm-based hydrogels can be achieved only by forming proper random copolymers, such as those prepared e.g., from acrylic acid [55] or HEMA [56]. In our case, as previously reported, PCL forms a certain amount of copolymer, reacting with the monomer, responsible for the compatibilization of the mixed phases, but remains mainly dispersed in the PNIPAAm phase. Nevertheless, it is worth underling that the main aim of our work was indeed not to change the chemical structure of PNIPAAm, but to find a strategy to improve its features, such as mechanical properties and its ability to interact with certain types of chemicals.

3.5. Morphological analysis

The morphology of the neat PNIPAAm xerogel was compared with that of the systems containing the star-shaped PCL. Fig. 6 shows the FE-SEM micrographs of the cross-section of the synthesized freeze-dried samples, namely PNIP_F (Fig. 6a), PNIP_PCL_10_F (Fig. 6b), PNIP_PCL_20_F (Fig. 6c) and PNIP_PCL_25_F (Fig. 6d).

Although all the above samples showed a typical hydrogel sponge structure [57,58], some differences can be noted. Indeed, the size of pore diameter tended to decrease with increasing PCL content in the system. Indeed, in the case of PNIP_F, the mean pore size was of 4.02 ± 1.28 μm and decreased after PCL inclusion to 2.56 ± 0.77 μm in PNIP_PCL_10_F, 2.303 ± 0.67 μm in PNIP_PCL_20_F and 1.348 ± 0.408 μm in PNIP_PCL_25_F. From FE-SEM observations, it can be concluded that, in addition to the aforementioned properties of the hydrogels related to the hydrophobicity and crystallinity of PCL, the morphology of the PCL-based hydrogels must also be taken into account to explain their different swelling behavior compared to that of the neat PNIPAAm sample. Similar results were reported for other PNIPAAm-based systems,

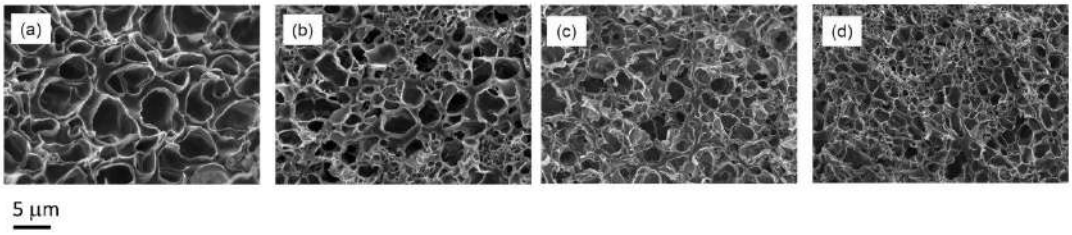

Fig. 6. FE-SEM micrographs: (a) PNIP_F, (b) PNIP_PCL_10_F, (c) PNIP_PCL_20_F and (d) PNIP_PCL_25_F.

such as in poly(-aminoester) (PBAE) crosslinked gels [59] and in semi-IPN structures [60] where the pore size was directly correlated with the degree of crosslinking and the material stiffness. In addition, it is relevant to underline that no PCL aggregates are visible, indicating a fine dispersion of the polyesters in the PNIPAAm phase and supporting the results of the DSC measurements.

3.6. Mechanical characterization of hydrogels

In the present work, the elastic modulus was characterized by two different techniques, namely static and dynamic mechanical analysis. Both types of measurements were performed to validate the developed hydrogels for different applications. In particular, dynamic characterization is important with respect to tissue engineering applications, since biological tissue is subjected to mechecanical stimuli.

The compressive modulus of the neat PNIPAAm hydrogel was compared with that of the PCL-based samples to evidence the influence of the star-shaped polymer on the mechanical behaviour of the developed materials (Fig. 7). In particular, the force–deformation curves of the prepared samples, shown in Fig. 7a, indicate that all the prepared systems exhibited an hyperelastic behavior, typical of hydrogel materials [61,62]. As for the compressive modulus (E_0), PNIP_F showed an E_0 of ca. 100 kPa, a value in agreement with those previously reported in the literature for PNIPAAm hydrogels [8] (Fig. 7b). The presence of PCL led to a relevant increase of E_0, which increased with increasing the star-shaped polymer content in the hydrogels. In particular, it is relevant to underline that in the sample with the highest concentration of PCL-COOH, *i.e.*, PNIP_PCL_25, E_0 was four times higher than in the neat PNIPAAm hydrogel.

This behavior was also confirmed by the results of the DMA used to measure the stiffness of the hydrogel in terms of elastic moduli (E_{20}) as a function of the frequency of the applied compressive load, with a pre-strain of 20% (Fig. S2). Specifically, neat PNIP_F showed an elastic modulus of about 37 kPa, while the samples based on PCL-COOH (10, 20, and 25 wt%), exhibited a drastic and linear increase in elastic moduli: 137.54 ± 23.07 kPa, 185.88 ± 30.59 kPa and 213.57 ± 16.76 kPa, respectively. Overall, the results indicated that the presence of the star shaped polymer contributes to the improvement of mechanical strenght of the PNIPAAm hydrogels. Although, as previously mentioned, it is difficult to make a comparison with data reported in the literature, since the mechanical properties of PNIPAAm-based hydrogels are highly dependent on a number of parameters, the moduli found make the developed material suitable for tissue engineering applications [4].

3.7. Cell viability evaluation

To determine the cytoxicity of the hydrogels on SH-SY5Y cultures, cells were exposed for 48 h to the two extreme conditions: sample without PCL (PNIP_F) and samples with the maximum amount of PCL (PNIP_PCL_25_F). First, SH-SY5Y cells were observed by optical microscopy before the exposition to the different samples (Fig. 8a) and after each 24 h to 48 h. Qualitatively, no differences were observed in both conditions during the time in culture. The live/dead assay showed that PNIP_PCL_25_F did not induce any toxic effect on the cultures of human neuroblastoma cells SH -SY5Y (Fig. 8b). This qualitative observation was confirmed by cell viability quantification shown in Fig. 8c, which was measured by normalizing the number of live cells with the total cell number. Under both conditions, comparable and high viability indexes were observed after 48 h. In particular, cell viability of SH-SY5Y exposed to PNIP_PCL_25_F samples showed a slightly decrease, but the result was not statistically different from that the control.

3.8. Dye absorption and release tests

To evaluate the effect of the addition of PCL-COOH to PNIPAAM on the retention capacity of the system, the prepared xerogels were contacted with a pararosaniline (PR) solution, a cationic dye. The results reported in the in Fig. 9 show the amount of PR absorbed by the hydrogels in their swollen state at 22 °C after 24 h. From the histogram, it can be seen that the amount of PR, retained by PNIP_F was negligible and difficult to estimate precisely due to the very small concentration differences of PR in solution. On the other hand, the quantity of PR

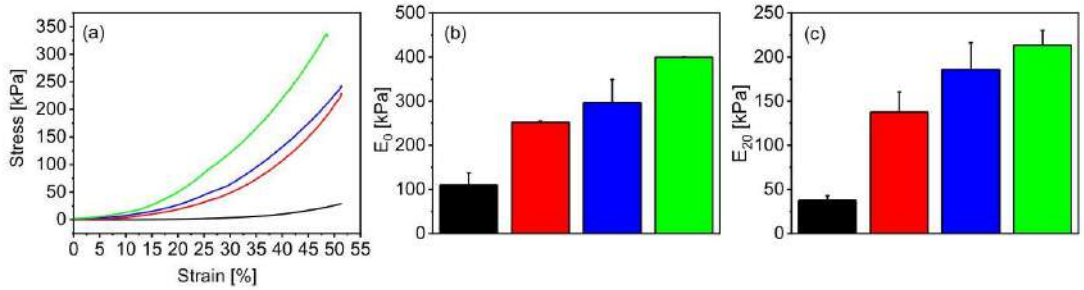

Fig. 7. (a) Force-deformation curve, (b) compressive modulus of PNIP samples from compressive static test, (c) elastic moduli of PNIP samples with and without PCL from DMA.

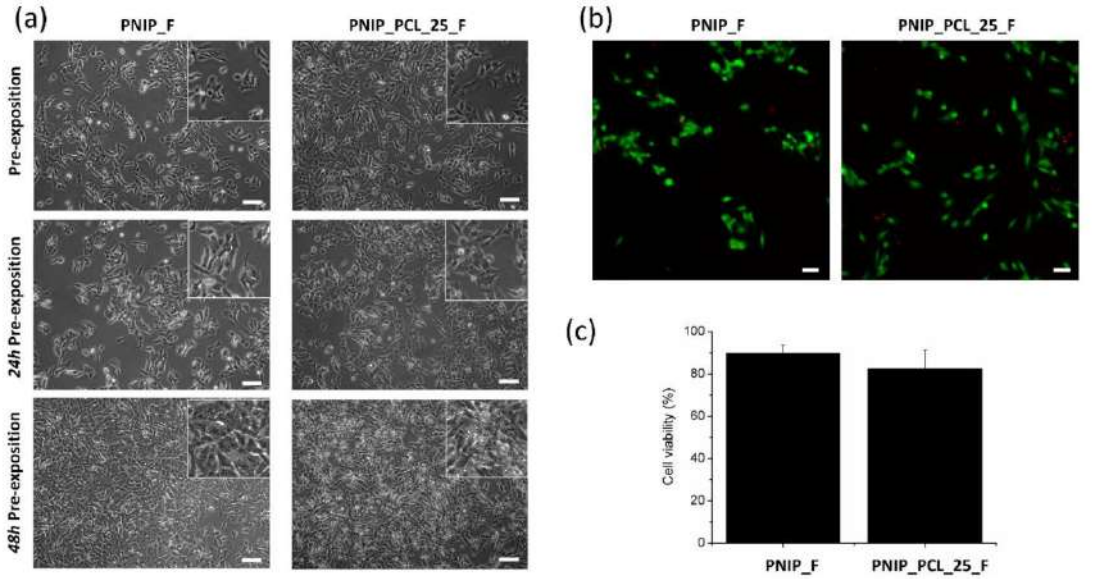

Fig. 8. Cell viability evaluation by (a) Optical contrast phase images of 2D SH-SY5Y cell culture before and 24–48 h after the exposition to PNIP_F an PNIP_PCL_25_F. Scale bars are 50 μm. (b) Live/dead staining with Calcein-AM (green) and EthD-1 (red); scale bars are 50 μm. (c) Percentage of cell viability, defined as the number of live cells divided by the total cell number. (For interpretation of the references to colour in this figure legend, the reader is referred to the web version of this article.)

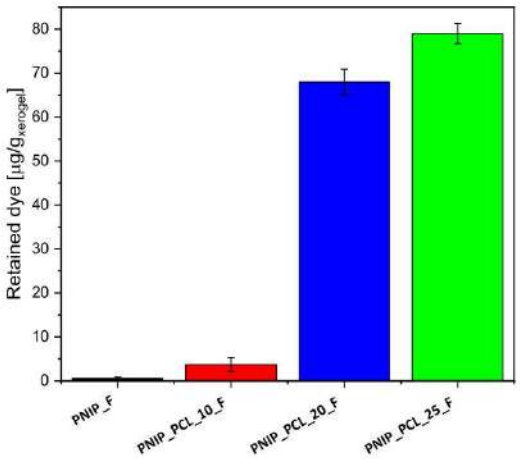

Fig. 9. PR retention at equilibrium at 22 °C, for PNIP_F (black), PNIP_PCL_10_F (red), PNIP_PCL_20_F (blue), PNIP_PCL_25_F (green). (For interpretation of the references to colour in this figure legend, the reader is referred to the web version of this article.)

absorbed by the materials increased steeply with PCL-COOH content and was mainly attributed to the presence of ionized carboxylic moieties, which are capable of interacting with the ionized amino group of PR through non-specific ionic interactions. In this regard, it is worth underling that as the pH of the solution used was 5.4 and the pK_a of PR and maleic end groups in PCL-COOH were 8.8 [63] and 1.9 [64], respectively, it can be concluded that both the amino groups of PR and the carboxy groups of PCL-COOH were present in their ionized form.

Indeed, as previously reported, the presence of the above ionized carboxyl groups ($-COO^-$) is essential for the adsorption of cationic species, such as drugs [65] or pollutants [6&] through the above-mentioned interactions. For example, Yang et al. prepared NIPAAM/acrylic acid/MoS_2 composite copolymer hydrogels by photopolymerization that were able to absorb methylene blue, potentially applicable in wastewater treatment [67]. Similarly, Mahida et al. developed nanohydrogels, by emulsion copolymerization of NIPAAM in combination with acrylic acid and N-allylisatin, capable of adsorbing hazardous cationic dyes [66]. The above works demonstrate the applicability of PNIPAAm-based systems as adsorbents and the need to combine the polymer matrix with suitable materials to make it functional. As for the specific adsorption capacity, the variability of the values found in the literature can be related to both the nature of the substances to be adsorbed as well as to the properties of the adsorbents in terms of concentration of functionalities, porosity, crystallinity, etc.

Dye release was studied by loading the hydrogels with PR and following the amount released over time (Fig. S3). It is worth underling that the lack of controlled release of neat PNIPAAm hydrogels is a significant aspect that could limit their potential application as drug carriers [68].

From the trend of Fig. S2, it can be seen that the release kinetics of the hydrogels were strongly influenced by the sample composition, with curves characterized by an initial burst phase followed by a decrease in the release rate until an equilibrium plateau was reached. In particular, as showed in Fig. S4, the release in the first phase followed a first-order kinetic with an initial release rate (RR_i), reported in Table S4, that was inversely proportional to the PCL amount. Indeed, the introduction of PCL-COOH affected the time required to reach the plateau concentration C_{max}, which increased from 9 h, measured for PNIP_F and PNIP_PCL_10_F, to ca. 30 h, for PNIP_PCL_20_F and PNIP_PCL_25_F samples. Considering the behavior of our PCL-based hydrogels, this may be related to several aspects, such as the specific interactions which occur between the PCL functionalities and the dye as well as the physical properties of the hydrogel, which are modified by the presence of the star-shaped polymer. Regarding the latter feature, the diffusion of the

dye in the hydrogels could also be reduced by the crystallinity imparted to the system by the presence of PCL-COOH and by the lower porosity of the PCL-based systems compared that of the neat PNIPAAm hydrogels.

4. Conclusions

In this work, novel PNIPAAm-based hydrogels were developed with high mechanical strength, ability to interact with positively charged molecules with tunable kinetic release and swelling ratio, biocompatibility, and thermoresponsiveness. Indeed, the above properties were achieved by adding to the reaction mixture a star-shaped PCL, synthesized *ad-hoc* using an environmentally friendly method, ending with maleic groups (PCL-COOH) that enable the polymer to participate in the polymerization process and impart active functionalities. In addition, the effectiveness of the frontal polymerization in the development of PNIPAAm/PCL-COOH hydrogels was demonstrated, which is a fast and efficient polymerization method, capable to guarantee a fine dispersion of the star-shaped polymer in the PNIPAAm matrix.

CRediT authorship contribution statement

Giacomo Damonte: Investigation, Visualization, Writing – original draft. **Martina Cozzani:** Investigation, Visualization. **Donatella Di Lisa:** Investigation, Visualization. **Laura Pastorino:** Investigation, Visualization. **Alberto Mariani:** Conceptualization, Writing – review & editing. **Orietta Monticelli:** Conceptualization, Supervision, Writing – review & editing.

Declaration of Competing Interest

The authors declare that they have no known competing financial interests or personal relationships that could have appeared to influence the work reported in this paper.

Data availability

Data will be made available on request.

Appendix A. Supplementary data

Supplementary data to this article can be found online at https://doi.org/10.1016/j.eurpolymj.2023.112239.

References

[1] S. Ziane, S. Schlaubitz, S. Miraux, A. Patwa, C. Lalande, I. Bilem, S. Lepreux, B. Rousseau, J.-F. Le Meins, L. Latxague, O.C. Barthélémy, A thermosensitive low molecular weight hydrogel as scaffold for tissue engineering, Eur. Cells Mater. 23 (2012) 147–160. https://doi.org/10.22203/eCM.v023a11.

[2] Y. Zhao, C. Shi, X. Yang, B. Shen, Y. Sun, Y. Chen, X. Xu, H. Sun, K. Yu, B. Yang, Q. Lin, pH- and Temperature-Sensitive hydrogel nanoparticles with dual photoluminescence for bioprobes, ACS Nano. 10 (2016) 5856–5863, https://doi.org/10.1021/acsnano.6b00770.

[3] L. Nie, J. Li, G. Lu, X. Wei, Y. Deng, S. Liu, S. Zhong, Q. Shi, R. Hou, Y. Sun, C. Politis, L. Fan, O.V. Okoro, A. Shavandi, Temperature responsive hydrogel for cells encapsulation based on graphene oxide reinforced poly(N-isopropylacrylamide)/hydroxyethyl-chitosan, Mater. Today Commun. 31 (2022), 103697, https://doi.org/10.1016/j.mtcomm.2022.103697.

[4] M.A. Haq, Y. Su, D. Wang, Mechanical properties of pnipam based hydrogels: a review, Mater. Sci. Eng. C. 70 (2017) 842–855, https://doi.org/10.1016/j.msec.2016.09.081.

[5] E. Ho, A. Lowman, M. Marcolongo, Synthesis and characterization of an injectable hydrogel with tunable mechanical properties for soft tissue repair, Biomacromolecules 7 (2006) 3223–3228, https://doi.org/10.1021/bm0602536.

[6] S. Petrusic, M. Lewandowski, S. Giraud, P. Jovancic, B. Bugarski, S. Ostojic, V. Koncar, Development and characterization of thermosensitive hydrogels based on poly(N-isopropylacrylamide) and calcium alginate, J. Appl. Polym. Sci. 124 (2012) 890–903, https://doi.org/10.1002/app.35122.

[7] R. Fei, J.T. George, J. Park, M.A. Grunlan, Thermoresponsive nanocomposite double network hydrogels, Soft Matter. 8 (2012) 481–487, https://doi.org/10.1039/C1SM06105D.

[8] R. Fei, J.T. George, J. Park, A.K. Means, M.A. Grunlan, Ultra-strong thermoresponsive double network hydrogels, Soft Matter. 9 (2013) 2912, https://doi.org/10.1039/c3sm27226e.

[9] Z. Li, J. Shen, H. Ma, X. Lu, M. Shi, N. Li, M. Ye, Preparation and characterization of ph- and temperature-responsive nanocomposite double network hydrogels, Mater. Sci. Eng. C. 33 (2013) 1951–1957, https://doi.org/10.1016/j.msec.2013.01.004.

[10] X. Ma, Y. Li, W. Wang, Q. Ji, Y. Xia, Temperature-sensitive poly(N-isopropylacrylamide)/graphene oxide nanocomposite hydrogels by in situ polymerization with improved swelling capability and mechanical behavior, Eur. Polym. J. 49 (2013) 389–396, https://doi.org/10.1016/j.eurpolymj.2012.10.034.

[11] K. Van Durme, B. Van Mele, W. Loos, F.E. Du Prez, Introduction of silica into thermo-responsive poly(N-isopropyl acrylamide) hydrogels: a novel approach to improve response rates, Polymer 46 (2005) 9851–9862, https://doi.org/10.1016/j.polymer.2005.08.032.

[12] B. Strachotová, A. Strachota, M. Uchman, M. Šlouf, J. Brus, J. Pleštil, L. Matějka, Super porous organic–inorganic poly(N-isopropylacrylamide)-based hydrogel with a very fast temperature response, Polymer 48 (2007) 1471–1482, https://doi.org/10.1016/j.polymer.2007.01.042.

[13] S.B. Campbell, M. Patenaude, T. Hoare, Injectable superparamagnets: highly elastic and degradable Poly(N-isopropylacrylamide)–superparamagnetic iron oxide nanoparticle (spion) composite hydrogels, Biomacromolecules 14 (2013) 644–653, https://doi.org/10.1021/bm301703x.

[14] G. Marcelo, M. López-González, F. Mendicuti, M.P. Tarazona, M. Valiente, Poly(N-isopropylacrylamide)/gold hybrid hydrogels prepared by catechol redox chemistry. characterization and smart tunable catalytic activity, Macromolecules 47 (2014) 6028–6036, https://doi.org/10.1021/ma501214k.

[15] G. Huerta-Angeles, K. Hishchak, A. Strachota, B. Strachota, M. Šlouf, L. Matějka, Super-porous nanocomposite pnipam hydrogels reinforced with titania nanoparticles, displaying a very fast temperature response as well as ph-sensitivity, Eur. Polym. J. 59 (2014) 341–352, https://doi.org/10.1016/j.eurpolymj.2014.07.033.

[16] Q. Zhang, T. Zhang, T. He, L. Chen, Removal of crystal violet by clay/pnipam nanocomposite hydrogels with various clay contents, Appl. Clay Sci. 90 (2014) 1–5, https://doi.org/10.1016/j.clay.2014.01.003.

[17] T. Huang, P(nipam-co-aa)/clay nanocomposite hydrogels exhibiting high swelling ratio accompanied by excellent mechanical strength, Appl. Phys. A Mater. Sci. Process. 107 (2012) 905–909, https://doi.org/10.1007/s00339-012-6817-6.

[18] K. Haraguchi, R. Farnworth, A. Ohbayashi, T. Takehisa, Compositional effects on mechanical properties of nanocomposite hydrogels composed of poly(N, N-dimethylacrylamide) and clay, Macromolecules 36 (2003) 5732–5741, https://doi.org/10.1021/ma034366i.

[19] W.-F. Lee, T.-S. Cheng, Studies on preparation and properties of porous biodegradable poly(nipaam) hydrogels, J. Appl. Polym. Sci. 109 (2008) 1982–1992, https://doi.org/10.1002/app.28370.

[20] R. París, I. Quijada-Garrido, Swelling and hydrolytic degradation behaviour of ph-responsive hydrogels of poly[(N-isopropylacrylamide)-co-(methacrylic acid)] crosslinked by biodegradable polycaprolactone chains, Polym. Int. 58 (2009) 362–367, https://doi.org/10.1002/pi.2539.

[21] G.T. Chao, Z.Y. Qian, M.J. Huang, B. Kan, Y.C. Gu, C.Y. Gong, J.L. Yang, K. Wang, M. Dai, X.Y. Li, M.L. Gou, M.J. Tu, Y.Q. Wei, Synthesis, characterization, and hydrolytic degradation behavior of a novel biodegradable pH-sensitive hydrogel based on polycaprolactone, methacrylic acid, and poly(ethylene glycol), J. Biomed. Mater. Res. Part A 85A (2008) 36–46, https://doi.org/10.1002/jbm.a.31362.

[22] B.A. Suslick, J. Hemmer, B.R. Groce, K.J. Stawiasz, P.H. Geubelle, G. Malucelli, A. Mariani, J.S. Moore, J.A. Pojman, N.R. Sottos, Frontal polymerizations: from chemical perspectives to macroscopic properties and applications, Chem. Rev. 123 (2023) 3237–3298, https://doi.org/10.1021/acs.chemrev.2c00686.

[23] G. Damonte, B. Barsanti, A. Pellis, G.M. Guebitz, O. Monticelli, On the effective application of star-shaped polycaprolactones with different end functionalities to improve the properties of polylactic acid blend films, Eur. Polym. J. 176 (2022), 111402, https://doi.org/10.1016/j.eurpolymj.2022.111402.

[24] G. Damonte, A. Vallin, D. Battegazzore, A. Fina, O. Monticelli, Synthesis and characterization of a novel star polycaprolactone to be applied in the development of graphite nanoplates-based nanopapers, React. Funct. Polym. 167 (2021), 105019, https://doi.org/10.1016/j.reactfunctpolym.2021.105019.

[25] G. Damonte, F. Cantamessa, A. Fina, O. Monticelli, Star-shaped furoate-pcl: an effective compound for the development of graphite nanoplatelets-based films, React. Funct. Polym. 184 (2023), 105515, https://doi.org/10.1016/j.reactfunctpolym.2023.105515.

[26] E.R. Leone, L.S. Ferraraccio, G. Damonte, P. Lova, P. Bertoncello, O. Monticelli, On the development of electrochemical sensors coated with polycaprolactone, Electrochem. Commun. 129 (2021), 107089, https://doi.org/10.1016/j.elecom.2021.107089.

[27] J. Masere, Y. Chekanov, J.R. Warren, F.D. Stewart, R. Al-Kaysi, J.K. Rasmussen, J. A. Pojman, Gas-free initiators for high-temperature free-radical polymerization, J. Polym. Sci. Part A Polym. Chem. 38 (2000) 3984–3990, https://doi.org/10.1002/1099-0518(20001101)38:21<3984::AID-POLA160>3.0.CO;2-Z.

[28] A. Mariani, D. Nuvoli, V. Alzari, M. Pini, Phosphonium-based ionic liquids as a new class of radical initiators and their use in gas-free frontal polymerization, Macromolecules 41 (2008) 5191–5196, https://doi.org/10.1021/ma800610g.

[29] M.A. Woodruff, D.W. Hutmacher, The return of a forgotten polymer - polycaprolactone in the 21st century, Prog. Polym. Sci. 35 (2010) 1217–1256, https://doi.org/10.1016/j.progpolymsci.2010.04.002.

[30] J.A. Pojman, G. Curtis, V.M. Ilyashenko, Frontal polymerization in solution, J. Am. Chem. Soc. 118 (1996) 3783–3784, https://doi.org/10.1021/ja9600688.

[31] N. do Nascimento Marques, P.S. Curti, A.M. da Silva Maia, R.d.C. Balaban, Temperature and ph effects on the stability and rheological behavior of the aqueous suspensions of smart polymers based on N-isopropylacrylamide, chitosan, and acrylic acid, J. Appl. Polym. Sci. 129 (1) (2013) 334–345.

[32] C. Erbil, Y. Yıldız, N. Uyanık, Effects of synthesis-solvent composition and initiator concentration on the swelling behaviour of poly(N-isopropylacrylamide) p (nipaam), poly(nipaam-co-dimethyl itaconate), and poly(nipaam-co-itaconic acid) gels, Polym. Int. 49 (2000) 795–800, https://doi.org/10.1002/1097-0126(200007)49:7<795::AID-PI457>3.0.CO;2-9.

[33] W. Liu, B. Zhang, W.W. Lu, X. Li, D. Zhu, K. De Yao, Q. Wang, C. Zhao, C. Wang, A rapid temperature-responsive sol-gel reversible poly(N-isopropylacrylamide)-g-methylcellulose copolymer hydrogel, Biomaterials 25 (2004) 3005–3012, https://doi.org/10.1016/j.biomaterials.2003.09.077.

[34] X. Hu, Z. Tong, L.A. Lyon, Control of poly(N-isopropylacrylamide) microgel network structure by precipitation polymerization near the lower critical solution temperature, Langmuir 27 (2011) 4142–4148, https://doi.org/10.1021/la200114s.

[35] N. Milašinović, Z. Knežević-Jugović, N. Milosavljević, M. Lučić Škorić, J. Filipović, M., Kalagasidis Krušić, Stimuli-sensitive hydrogel based on n-isopropylacrylamide and itaconic acid for entrapment and controlled release of candida rugosa lipase under mild conditions, Biomed Res. Int. (2014 (2014)) 1–9, https://doi.org/10.1155/2014/364930.

[36] A. Vallin, D. Battegazzore, G. Damonte, A. Fina, O. Monticelli, On the development of nanocomposite covalent associative networks based on polycaprolactone and reduced graphite oxide, Nanomaterials 12 (2022) 3744, https://doi.org/10.3390/nano12213744.

[37] M. Biswas, J.A. Libera, S.B. Darling, J.W. Elam, Polycaprolactone: a promising addition to the sequential infiltration synthesis polymer family identified through in situ infrared spectroscopy, ACS Appl. Polym. Mater. 2 (2020) 5501–5510, https://doi.org/10.1021/acsapm.0c00855.

[38] R.G. Sousa, W.F. Magalhães, R.F.S. Freitas, Glass transition and thermal stability of poly(N-isopropylacrylamide) gels and some of their copolymers with acrylamide, Polym. Degrad. Stab. 61 (1998) 275–281, https://doi.org/10.1016/S0141-3910(97)00209-7.

[39] G. Damonte, L. Maddalena, A. Fina, D. Cavallo, A.J. Müller, M.R. Caputo, A. Mariani, O. Monticelli, On novel hydrogels based on poly(2-hydroxyethyl acrylate) and polycaprolactone with improved mechanical properties prepared by frontal polymerization, Eur. Polym. J. 171 (2022), 111226, https://doi.org/10.1016/j.eurpolymj.2022.111226.

[40] L. Sangroniz, B. Wang, Y. Su, G. Liu, D. Cavallo, D. Wang, A.J. Müller, Fractionated crystallization in semicrystalline polymers, Prog. Polym. Sci. 115 (2021), 101376, https://doi.org/10.1016/j.progpolymsci.2021.101376.

[41] S. Nojima, M. Toei, S. Hara, S. Tanimoto, S. Sasaki, Size dependence of crystallization within spherical microdomain structures, Polymer 43 (2002) 4087–4090, https://doi.org/10.1016/S0032-3861(02)00217-3.

[42] A.J. Müller, V. Balsamo, M.L. Arnal, T. Jakob, H. Schmalz, V. Abetz, Homogeneous nucleation and fractionated crystallization in block copolymers, Macromolecules 35 (2002) 3048–3058, https://doi.org/10.1021/ma012026w.

[43] A.J. Müller, V. Balsamo, M.L. Arnal, in: Nucleation and Crystallization in Diblock and Triblock Copolymers, Springer-Verlag, Berlin/Heidelberg, 2005, pp. 1–63, https://doi.org/10.1007/12_001.

[44] R.V. Castillo, A.J. Müller, J.-M. Raquez, P. Dubois, Crystallization kinetics and morphology of biodegradable double crystalline plla-b-pcl diblock copolymers, Macromolecules 43 (2010) 4149–4160, https://doi.org/10.1021/ma100201g.

[45] L. Tavagnacco, E. Zaccarelli, E. Chiessi, On the molecular origin of the cooperative coil-to-globule transition of poly(N-isopropylacrylamide) in water, Phys. Chem. Chem. Phys. 20 (2018) 9997–10010, https://doi.org/10.1039/C8CP00537K.

[46] M. Zhang, Y. Li, Q. Yang, L. Huang, L. Chen, H. Xiao, Adsorption of methyl violet using pH- and temperature-sensitive cellulose filament/poly(nipam-co-aac) hybrid hydrogels, J. Mater. Sci. 53 (2018) 11837–11854, https://doi.org/10.1007/s10853-018-2342-0.

[47] A. Sosnik, J.C. Imperiale, B. Vázquez-González, M.M. Raskin, F. Muñoz-Muñoz, G. Burillo, G. Cedillo, E. Bucio, Mucoadhesive thermo-responsive chitosan-g-poly (N-isopropylacrylamide) polymeric micelles via a one-pot gamma-radiation-assisted pathway, Colloids Surfaces B Biointerfaces 136 (2015) 900–907, https://doi.org/10.1016/j.colsurfb.2015.10.036.

[48] A.S. Patil, A.P. Gadad, R.D. Hiremath, P.M. Dandagi, Exploration of the effect of chitosan and crosslinking agent concentration on the properties of dual responsive chitosan-g-poly(N-isopropylacrylamide) co-polymeric Particles, J. Polym. Environ. 26 (2018) 596–606, https://doi.org/10.1007/s10924-017-0971-z.

[49] H.G. Schild, Thermal decomposition of pnipaam: tga-ftir analysis, J. Polym. Sci. Part A Polym. Chem. 34 (1996) 2259–2262, https://doi.org/10.1002/(SICI)1099-0518(199608)34:11<2259::AID-POLA21>3.0.CO;2-D.

[50] M. Unger, C. Vogel, H.W. Siesler, Molecular weight dependence of the thermal degradation of poly(ε-caprolactone): a thermogravimetric differential thermal fourier transform infrared spectroscopy study, Appl. Spectrosc. 64 (2010) 805–809, https://doi.org/10.1366/000370210791666309.

[51] S. Li, X. Liu, Synthesis, characterization, and evaluation of enzymatically degradable poly(N-isopropylacrylamide-co-acrylic acid) hydrogels for colon-specific drug delivery, Polym. Adv. Technol. 19 (2008) 1536–1542, https://doi.org/10.1002/pat.1162.

[52] C.S. Biswas, V.K. Patel, N.K. Vishwakarma, A.K. Mishra, R. Bhimireddi, R. Rai, B. Ray, Synthesis, characterization, and drug release properties of poly(N-isopropylacrylamide) gels prepared in methanol-water cononsolvent medium, J. Appl. Polym. Sci. 125 (2012) 2000–2009, https://doi.org/10.1002/app.36318.

[53] C. Yu, Z. Duan, P. Yuan, Y. Li, Y. Su, X. Zhang, Y. Pan, L.L. Dai, R.G. Nuzzo, Y. Huang, H. Jiang, J.A. Rogers, Electronically programmable, reversible shape change in two- and three-dimensional hydrogel structures, Adv. Mater. 25 (2013) 1541–1546, https://doi.org/10.1002/adma.201204180.

[54] I. Bischofberger, V. Trappe, New aspects in the phase behaviour of poly-N-isopropyl acrylamide: systematic temperature dependent shrinking of pnipam assemblies well beyond the LCST, Sci. Rep. 5 (2015) 15520, https://doi.org/10.1038/srep15520.

[55] S.J. Lue, C.-H. Chen, C.-M. Shih, Tuning of lower critical solution temperature (lcst) of poly(N-isopropylacrylamide-co-acrylic acid) hydrogels, J. Macromol. Sci. Part B. 50 (2011) 563–579, https://doi.org/10.1080/00222341003784550.

[56] M. Kubo, M. Higuchi, T. Koshimura, E. Shoji, T. Tsukada, Control of the temperature responsiveness of poly(N-isopropylacrylamide-co-2-hydroxyethyl methacrylate) copolymer using ultrasonic irradiation, Ultrason. Sonochem. 79 (2021), 105752, https://doi.org/10.1016/j.ultsonch.2021.105752.

[57] K. Son, J. Lee, Synthesis and characterization of poly(ethylene glycol) based thermo-responsive hydrogels for cell sheet engineering, Materials 9 (2016) 854, https://doi.org/10.3390/ma9100854.

[58] J. Su, Y. Yang, Z. Chen, J. Zhou, X. Liu, Y. Fang, Y. Cui, Preparation and performance of thermosensitive poly(N-isopropylacrylamide) hydrogels by frontal photopolymerization, Polym. Int. 68 (2019) 1673–1680, https://doi.org/10.1002/pi.5868.

[59] Y. Balçık Tamer, A new design of poly(N-isopropylacrylamide) hydrogels using biodegradable poly(beta-aminoester) crosslinkers as fertilizer reservoirs for agricultural applications, Gels 9 (2023) 127. https://doi.org/10.3390/gels9020127.

[60] S.-P. Rwei, H. Tuan, W.-Y. Chiang, T.-F. Way, Synthesis and characterization of ph and thermo dual-responsive hydrogels with a semi-ipn structure based on n-isopropylacrylamide and itaconamic acid, Materials 11 (2018) 696, https://doi.org/10.3390/ma11050696.

[61] A. Sasson, S. Patchornik, R. Eliasy, D. Robinson, R. Haj-Ali, Hyperelastic mechanical behavior of chitosan hydrogels for nucleus pulposus replacement - experimental testing and constitutive modeling, J. Mech. Behav. Biomed. Mater. 8 (2012) 143–153, https://doi.org/10.1016/J.JMBBM.2011.12.008.

[62] J. Gan, X.X. Guan, J. Zheng, H. Guo, K. Wu, L. Liang, M. Lu, Biodegradable, thermoresponsive pnipam-based hydrogel scaffolds for the sustained release of levofloxacin, RSC Adv. 6 (2016) 32967–32978, https://doi.org/10.1039/c6ra03045a.

[63] H. Da Silva Junior, G.R.S. De Freitas, D.R.F. Néri, F.R.D.S. Pereira, R.F. De Farias, F.C. Pereira, Monitoramento do corante pararosanilina em amostras biológicas, Eclética Química J. 35 (2018) 147. https://doi.org/10.26850/1678-4618eqj.v35.3.2010.p147-156.

[64] F.R. Trull, S. Boiadjiev, D.A. Lightner, A.F. McDonagh, Aqueous dissociation constants of bile pigments and sparingly soluble carboxylic acids by ^{13}C NMR in aqueous dimethyl sulfoxide: effects of hydrogen bonding, J. Lipid Res. 38 (1997) 1178–1188, https://doi.org/10.1016/S0022-2275(20)37200-X.

[65] R.L. Bartlett, M.R. Medow, A. Panitch, B. Seal, Hemocompatible poly(nipam-mba-amps) colloidal nanoparticles as carriers of anti-inflammatory cell penetrating peptides, Biomacromolecules 13 (4) (2012) 1204–1211.

[66] V.P. Mahida, M.P. Patel, Removal of some most hazardous cationic dyes using novel poly (nipaam/aa/N-allylisatin) nanohydrogel, Arab. J. Chem. 9 (2016) 430–442, https://doi.org/10.1016/j.arabjc.2014.05.016.

[67] J. Yang, K. Wang, Z. Lv, W. Li, K. Luo, Z. Cao, facile preparation and dye adsorption performance of poly(N-isopropylacrylamide-co-acrylic acid)/molybdenum disulfide composite hydrogels, ACS Omega 6 (2021) 28285–28296, https://doi.org/10.1021/acsomega.1c04433.

[68] M.J. Ansari, R.R. Rajendran, S. Mohanto, U. Agarwal, K. Panda, K. Dhotre, R. Manne, A. Deepak, A. Zafar, M. Yasir, S. Pramanik, Poly(N-isopropylacrylamide)-based hydrogels for biomedical applications: a review of the state-of-the-art, Gels 8 (2022) 454, https://doi.org/10.3390/gels8070454.

Supporting Information - Mechanically-reinforced biocompatible hydrogels based on poly(N-isopropylacrylamide) and star-shaped polycaprolactones

Mechanically-reinforced biocompatible hydrogels based on poly(N-isopropylacrylamide) and star-shaped polycaprolactones

Giacomo Damonte[1], Martina Cozzani[1], Donatella Di Lisa[2], Laura Pastorino[2], Alberto Mariani[3], Orietta Monticelli[1]*

[1]Dipartimento di Chimica e Chimica Industriale, Università di Genova, Via Dodecaneso 31, 16146 Genova, Italy

[2]Dipartimento di Informatica, Bioingegneria, Robotica e Ingegneria dei Sistemi, Università di Genova, Via All'Opera Pia 13, 16145, Genoa, Italy

[3]Dipartimento di Chimica e Farmacia, Università di Sassari, and INSTM, Via Vienna 2, 07100 Sassari, Italy

Table S1. FT-IR and ^{1}H-NMR signals of PCL-COOH.

FT-IR
2945 cm^{-1} (υ CH_2 asymmetric); 2870 cm^{-1} (υ CH_2 symmetric); 1725 cm^{-1} (υ C=O symmetric); 1297 cm^{-1} (υ C-O and C-C); 1242 cm^{-1} (υ C-O-C asymmetric); 1179 cm^{-1} (υ C-O-C symmetric); 1640 cm^{-1} (υ C=C, maleic unit) and 822 cm^{-1} (out of plane deformation for carboxyl groups of maleic unit).
^{1}H-NMR
6.42 ppm (R-OOC-CH=C<u>H</u>-COOH maleic unit, d); 6.31 ppm (R-OOC-C<u>H</u>=CH-COOH maleic unit, d); 4.28 ppm (-C<u>H_2</u>-OOC-, t); 4.09 ppm (-C<u>H_2</u>- pentaerythritol, s); 4.05 ppm (-C<u>H_2</u>- PCL, t) 2.29 ppm (-C<u>H_2</u>- PCL, t); 1.64 (-C<u>H_2</u>- PCL, m); 1.38 (ppm -C<u>H_2</u>- PCL, m).

Table S2. Saturation concentration limit of NIPAAm in DMSO and NMP at 20 °C.

V_{DMSO} [mL]	Solubility	V_{NMP} [mL]	Solubility
0.30	-	0.5	-
0.35	-	1.0	-
0.40	-	1.2	-
0.45	-	1.5	-
0.50	+	2.0	+

The (-) sign indicates biphasic system while (+) sign indicates a monophasic system.

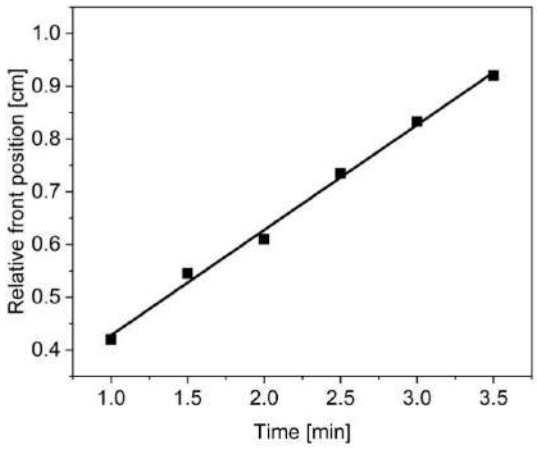

Figure S1. Front position vs. time for PNIP_PCL_25_F.

Table S3. Front velocity (V_f) and temperature (T_{max}) for the prepared samples.

Sample	V_f [cm/min]	T_{max} [°C]
PNIP(F)	0.47	135
PNIP_PCL_10_F	0.40	133
PNIP_PCL_20_F	0.32	132
PNIP_PCL_25_F	0.20	93

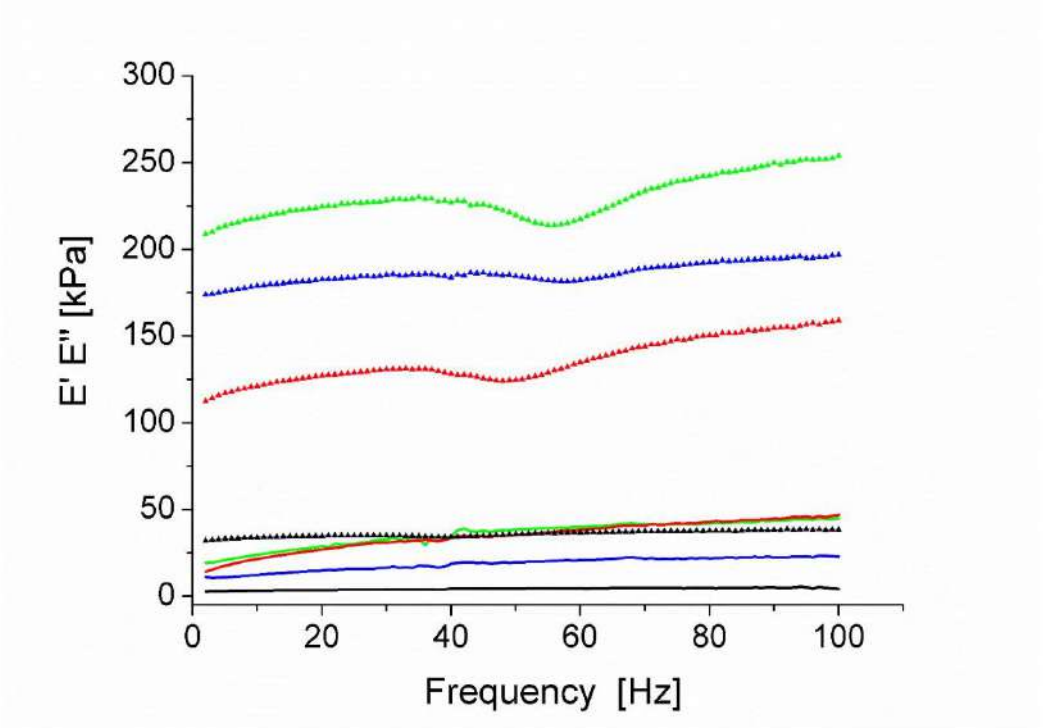

Figure S2. Results of DMA tests performed at 20% of pre-strain: storage modulus (E', ▲) and loss modulus (E'', ▬) vs Frequency. (—) PNIP_F, (—) PNIP_PCL_10_F, (—) PNIP_PCL_20_F and (—) PNIP_PCL_25_F.

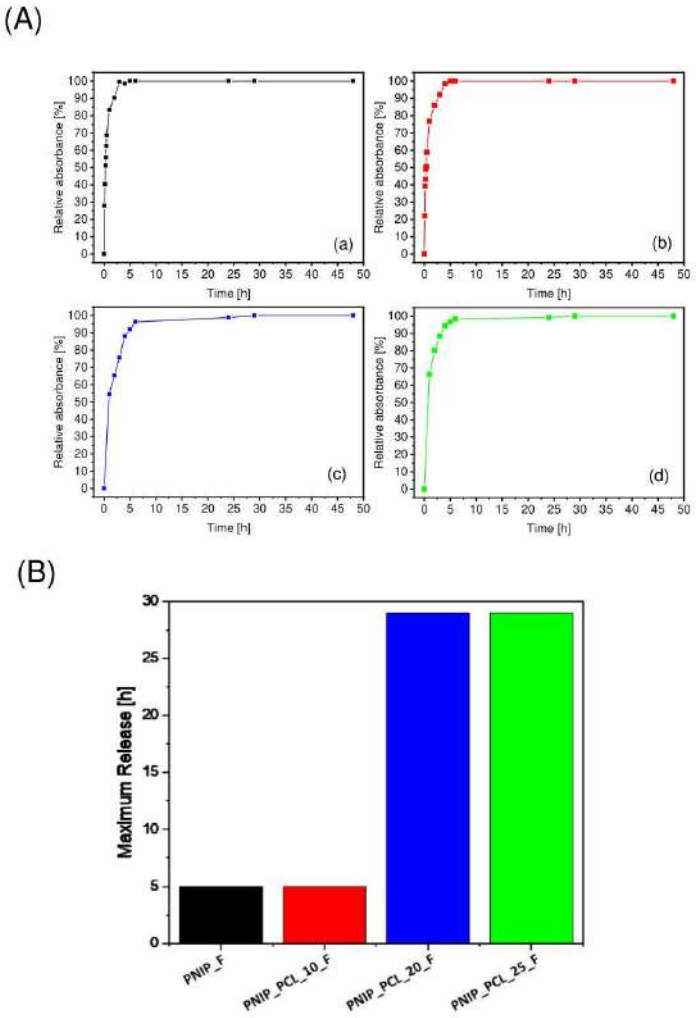

Figure S3. (A) Dye release over time of: (a) PNIP_F, (b) PNIP_PCL_10_F, (c) PNIP_PCL_20_F, (d) PNIP_PCL_25_F. (B) Maximum release time for PNIP_F, PNIP_PCL_10_F, PNIP_PCL_20_F and PNIP_PCL_25_F.

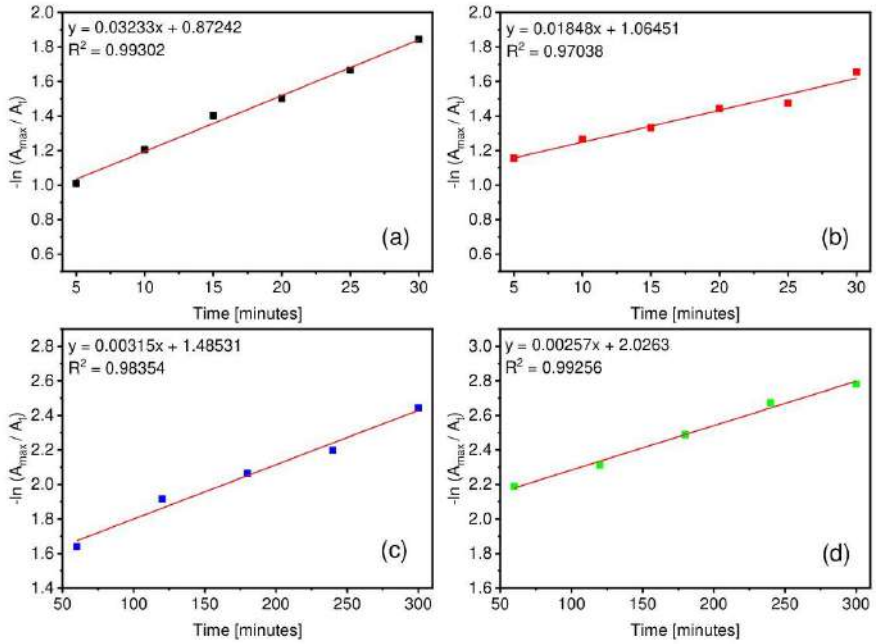

Figure S4. Plots of the ratio between the maximum amount released and the amount released at a given time as a function of time for: (a) PNIP_F, (b) PNIP_PCL_10_F, (c) PNIP_PCL_20_F, (d) PNIP_PCL_25_F.

Table S4. Initial release rate (RR_i) measured for the different hydrogels.

Sample	RR_i [µg/mL·min]
PNIP_F	0.0281
PNIP_PCL_10_F	0.0173
PNIP_PCL_20_F	0.0027
PNIP_PCL_25_F	0.0019

Chapter 9: On novel sustainable vitrimers based on polycaprolactones

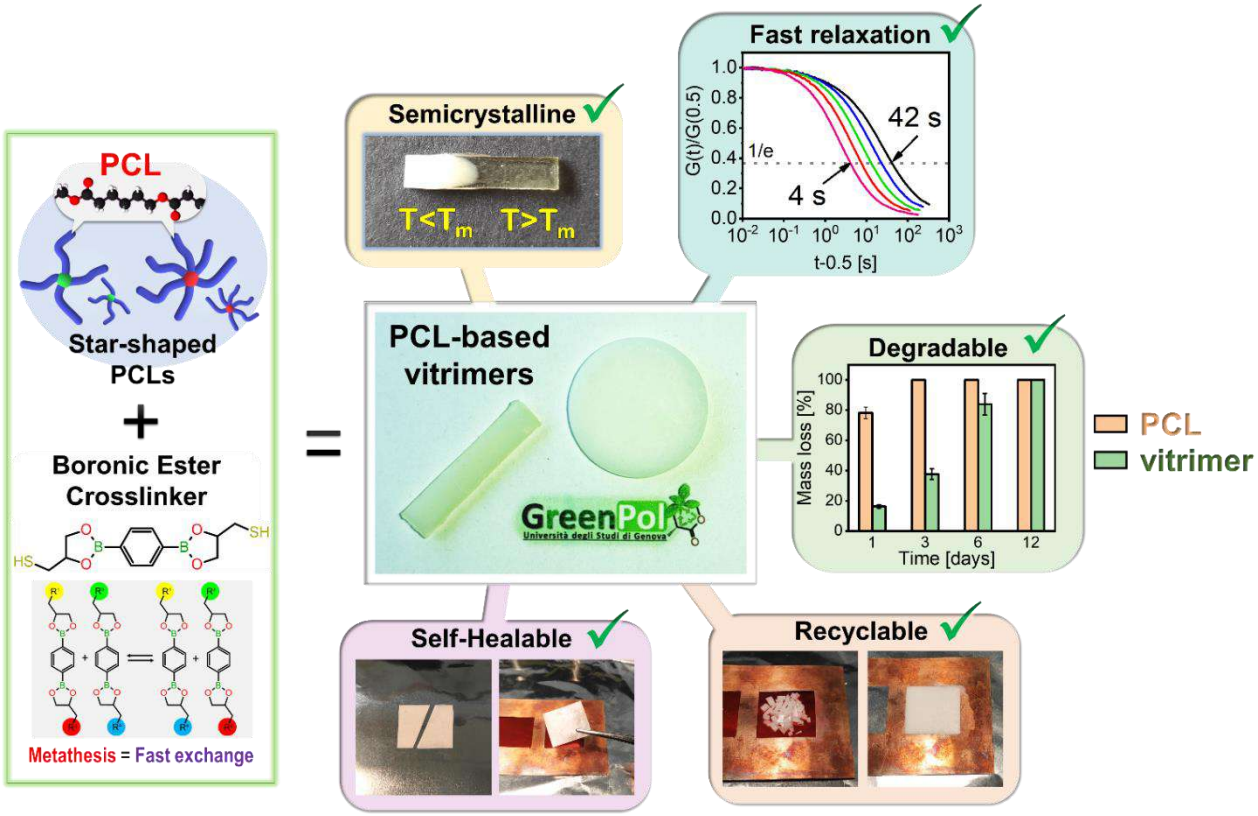

9.1 Abstract

Vitrimers represent an environmentally friendly class of novel materials, which behave like thermosets at room temperature but exhibit thermoplastic flow behaviour when heated, making them processable and recyclable, thus extending material life and reducing waste. However, to fully meet the current demand for a sustainable economy and close the loop, biodegradability at the end of the material life should also be considered, a property that not all vitrimers possess. Based on the above issues, this work aimed to develop novel biodegradable vitrimers based on polycaprolactone (PCL), an aliphatic and biodegradable polyester, potentially derived from biomass fermentation. In detail, three different *ad-hoc* synthesized star-shaped acrylated PCLs, characterized by different number of arms and molecular weight, were synthesized from hydroxyl terminated polymers and used to prepare vitrimer systems. Indeed, the above polymers were crosslinked with a fast exchangeable diboronic ester dithiol ([2,2′-(1,4-phenylene)-bis[4-mercaptan-1,3,2-dioxaborolane], DBEDT), by exploiting a thiol-acrylate reaction without solvent. The formation of a dynamic network was proven by FT-IR, DSC, TGA, gel fraction, rheological and DMA measurements. In particular, the activation energies for the relaxation process of these materials were verified by rheological measurements in the range 44-62 kJ/mol. Moreover, all vitrimers, which were completely degraded by enzymatic hydrolysis within 12 days, exhibited excellent recyclability and self-healing properties when heated to 180 °C before processing.

9.2 Introduction

Covalent Adaptable Networks (CANs) have gained considerable attention because they combine some of the properties of thermosets, such as creep and solvent resistance, with the reprocessability typical of thermoplastic-like materials, thus bridging the gap between these two classes of materials [1]. Indeed, CANs have the unique ability to chemically break, reshape or reform their covalent network when exposed to external stimuli [2,3] and may represent one of the possible solutions to the thermoset recycling problem [4]. These systems can be divided into dissociative or associative, depending on how the density of cross-links changes following the stimulus application [1]. In dissociative CANs, which present variable cross-link density, dissociation of the cross-links after application of the stimulus leads to partial or complete depolymerization of the network. In contrast, associative CANs are characterized by a fixed cross-link density because a bond formation process

occurs prior to bond breaking, resulting in a dynamic and rapid exchange that softens the material when the stimulus is applied [2]. The concept of associative CANs was further extended by the introduction of vitrimers, which are characterized by an Arrhenius-like viscosity variation with temperature. Indeed, as with CANs in general, the reprocessability of vitrimers enables easy mechanical recycling, thus extending the life of the material and reducing its overall environmental impact [3]. Despite the above property, vitrimers may be exposed to similar scenarios as conventional plastics at the end of their life cycle, leading to their potential disposal in landfills or dispersion in the environment, and raising concerns about optical and chemical pollution [4], due to the release of toxic species or the formation of microplastics [5]. To reduce the environmental impact, many vitrimers are designed by exploiting the use of biobased building blocks [6], but this does not guarantee their biodegradability. Therefore, the development of sustainable systems is crucial to fully solve the problem of their dispersion in the environment. In this context, the use of polycaprolactone (PCL), an aliphatic polyester [7], is very interesting because it is not only biodegradable, but also potentially produced from 5-hydroxymethylfurfural (5-HMF), a molecule obtained by fermentation of biomass, thus closing the material's carbon loop [8]. In the literature, the majority of PCL-based CANs are mainly of dissociative type and are generally prepared by exploiting the Diels-Alder reaction [9–18]. Defize et al. used the above mechanism to prepare PCL-based dissociative networks starting from different furan/anthracene systems ad maleimide-bearing star-shaped PCLs [10–12]. Despite the dynamicity of the formed network, some drawbacks should be highlighted, such as the time-consuming synthesis, the toxicity of the maleimides [19], and the decrease of cross-linking density with temperature, leading to a relevant worsening of the rheological properties. For PCL-based vitrimers, a few examples were described in the literature, where the formation of a dynamic system was ensured by exchange reactions involving the ester bond of the polyester [20–22]. Thus, Vallin et. al developed a covalent associative nanocomposite network by combining star-shaped hydroxyl-terminated PCL and methylene diphenyl diisocyanate (MDI) in presence of reduced graphene oxide (rGO) by exploiting transesterification and transcarbamoylation reactions [23]. It was demonstrated that the rheological behaviour of the above material can be controlled by adjusting the OH:NCO ratio and by incorporating rGO as nanofiller. Similarly, Joe et al. prepared PCL-based 4D printable PCL-based, shape memory vitrimers by reacting a PCL printing resin with polyhexamethylene diisocyanate (PHMDI) and poly(styrene-co-allyl alcohol) (PSA) promoting the transesterification with $Zn(acac)_2$ [20]. In another work, linear commercial PCL was used together with thermoplastic polyurethane (TPU), cellulose nanocrystals (CNC) and a vitrimer (ESO-S) prepared by mixing epoxidized soybean oil (ESO) with 4,4′-diaminodiphenyldisulfide (APD). The presence of ESO-S was found to improve the interfacial compatibility between TPU, PCL, and CNC, while increasing

tensile strength and thermal stability of the material [24]. Despite the interesting properties of the obtained materials, the described approaches, generally applied for the preparation of PCL-based vitrimers, present some drawbacks mainly related to the use of organic- or metal-based catalyst, which can be harmful, and to the uncontrolled changes in the starting polymer topology towards random structures due to the transesterification exchange reactions on the polyester backbone [25,26]. On this basis, the incorporation of a biopolymer in a vitrimer preparation that does not use catalysts or solvents for its preparation while maintaining the degradability of the system is highly desirable. In this context, a promising reaction for vitrimer production is the one based on boronic esters, compounds first used by Cromwell et al. [27] to prepare exchangeable networks by boronic ester transesterification and later by Röttger et al. based on boronic ester metathesis [28]. These boron-based systems have the advantage of being easily hydrolysed through the B-O bond by the action of water or alcohols, producing a hydrolysate that can be recovered and reused to form a new polymer [29]. Nevertheless, boronic esters, which are also easy to prepare and exhibit low toxicity [30,31], have not yet been employed in combination with PCL-based systems, which may be potentially advantageous given the combination of the low melting temperature of this material (< 60 °C) and the fast metathesis exchange rate of boronic esters. The aim of this work was to develop biodegradable vitrimers, combining for the first time PCL with a boronic ester cross-linker, using an approach that does not require the use of solvents and catalysts. In order to verify the influence of polymer structure and molecular weight on the final material properties of vitrimers, three different star-shaped PCLs with acrylate end groups, characterized by four and six arms and different molecular weights were synthesized and applied in the formulation the respective systems. In detail, star-shaped PCLs were synthesized by ring opening polymerization of ε-caprolactone using pentaerythritol and dipentaerythritol as initiators in presence of tin octoate as catalyst (**Figure 9.1)**. The formed acryloyl-terminated star-shaped PCLs, prepared by acrylation of the hydroxyl end groups, were then cross-linked through a thiol-acrylate reaction, under solventless conditions, with a boronic ester cross-linker, i.e., [2,2′-(1,4-phenylene)-bis[4-mercaptan-1,3,2-dioxaborolane] (DBEDT). The formed systems were then characterized in terms of their thermal and rheological properties as well as their enzymatic degradation and recyclability.

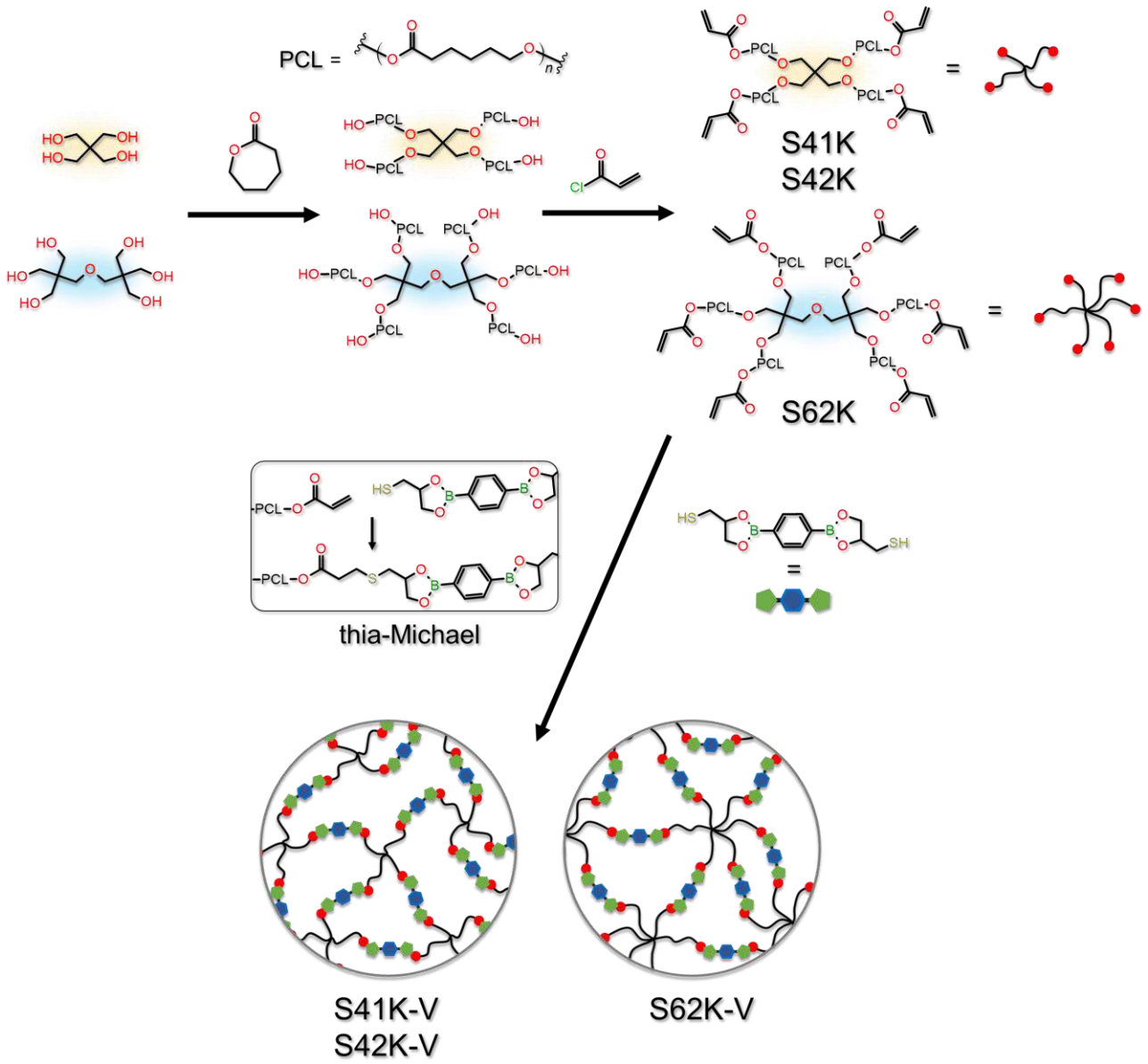

Figure 9.1. *Preparation of PCL-based vitrimeric networks starting from pentaerythritol or dipentaerythritol as initiators.*

9.3 Materials and methods

9.3.1 Materials

ε-caprolactone (ε-CL, purity = 97%), pentaerythritol (purity = 99%), tin octoate ($Sn(Oct)_2$, purity ≥ 96%), methanol (99.9%), acryloyl chloride (purity ≥ 99%), toluene (purity = 99.8%, anhydrous), dichloromethane (DCM, purity ≥ 99.8%, stabilized with amylene), thioglycerol (purity ≥ 97%), benzene-1,4-diboronic acid (purity ≥ 97%), ethanol (purity ≥ 99.8%), potassium carbonate (purity ≥ 99%) were purchased from Sigma Aldrich. High molecular weight commercial PCL, CAPA 6500® (M_w = 50000 g/mol) (PCL-L) was purchased from Perstorp. ε-caprolactone and DCM were purified prior to use by vacuum distillation over CaH_2 and stored under Ar atmosphere. Pentaerythritol and benzene-1,4-diboronic acid were dried in vacuum oven at 40 °C prior use. All the other reagents were of analytical grade and used without further purification. Cutinase Novozym 51032 was purchased from STREM chemicals.

9.3.2 Preparation of the boronic ester crosslinker

[2,2′-(1,4-Phenylene)-bis[4-Mercaptan-1,3,2-Dioxaborolane] (DBEDT) was prepared according to the procedure reported by Zych et al. by condensation of thioglycerol and benzene-1,4-diboronic acid in ethanol [32]. The material, after preparation, was stored in a desiccator prior to use.

9.3.3 Synthesis of star-shaped PCLs

Acrylated polymers were synthesized according to a previously reported two-step procedure, starting from the synthesis of star-shaped PCL with hydroxyl end groups [33–35] using pentaerythritol or dipentaerythritol as initiators (**Table 9.1** and **Figure 9.2**). The type of initiator was chosen to obtain 4- or 6- armed star-shaped structures, while its amount determined the molecular weight, which was set at 1000 and 2000 g/mol per arm. Successively, star-shaped acrylated PCLs were obtained by acrylation reaction of PCL-OH using an excess of acryloyl chloride (3 eq. respect terminal -OH groups) and K_2CO_3 (equimolar to acryloyl chloride) in DCM (1 mL/g respect hydroxyl terminated PCL) for 48 hours at 30 °C. After the reaction, the solids were removed by filtration and centrifugation and the product was precipitated in ice cold methanol (50 mL/g of acrylated PCL). The polymers were then vacuum dried in oven for several days at room temperature until a constant weight was

reached. **Table 9.1** describes the polymers prepared with the synthesis conditions, while the main ^{1}H-NMR and FT-IR of signals of S41K are given in **Table 9.2**. The other synthesized polymers were characterized by the same signals. The acrylated polymers were defined by specifying the number of arms and molecular weight in the code. The example S41K indicates a star-shaped polymer (S) prepared using pentaerythritol as initiator with 4 arms (4) and characterized by a molecular weight of 1000 g/mol (1K).

Table 9.1. *Properties of the synthesized PCL-OH.*

Sample code	Initiator	$M_{n\ theo}$ *[g/mol]	[ε-CL]/[I]	[ε-CL]/[cat]	$M_{n\ NMR}$* [g/mol]
S41K	Pentaerythritol	1000	35.04	5000	1536
S42K	Pentaerythritol	2000	70.08	5000	2254
S62K	Dipentaerythritol	2000	105.13	5000	2118

*:Theorethical molecular weight per single arm measured on the starting hydroxyl terminated star PCL.

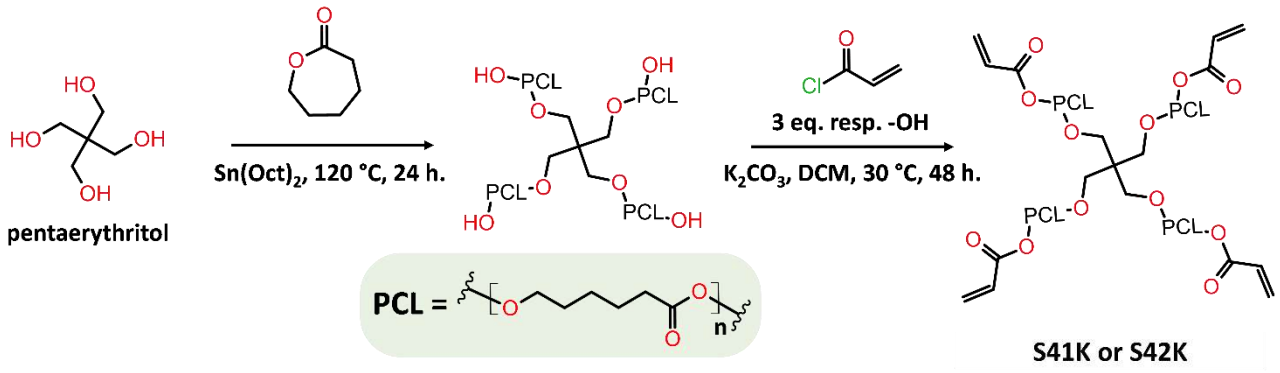

Fig. 9.2. *Scheme of the synthesis of S41K and S42K star-shaped polymers using pentaerythritol.*

Table 9.2*. FT-IR and ^{1}H-NMR signals of S41K polymers.*

FT-IR [cm^{-1}]
S41K (with -OH end groups): 2945 (asymmetric -**CH₂**- stretching); 2870 (symmetric -**CH₂**- stretching); 1725 (symmetric >**C=O** stretching); 1297 (-**C-O**- and -**C-C**- stretching); 1242 (asymmetric -**C-O-C**- stretching); 1179 (symmetric -**C-O-C**- stretching).
S41K (with acrylated end groups): 2945 (asymmetric -**CH₂**- stretching); 2870 (symmetric -**CH₂**- stretching); 1725 (symmetric >**C=O** stretching); 1641 (**-C=C-** stretching, acrylate unit); 1297 (-**C-O**- and -**C-C**- stretching); 1242 (asymmetric -**C-O-C**- stretching); 1179 (symmetric -**C-O-C**- stretching); 814 (**-CH=CH₂** twisting, acrylate unit).

^{1}H-NMR [ppm]
S41K (with -OH end groups): 4.09 (-C**H**$_2$- pentaerythritol, s); 4.05 (-C**H**$_2$-, t); 3.63 (-C**H**$_2$-OH PCL chain terminal, t); 2.29 (-C**H**$_2$-, t); 1.64 (-C**H**$_2$-, m); 1.38 (-C**H**$_2$-, m).
S41K (with acrylated end groups): 6.39 (acryloyl unit, dd), 6.11 (acryloyl unit, dd), 5.81 (acryloyl unit, dd), 4.15 (-C**H**$_2$-O-Acr, t); 4.09 (-C**H**$_2$- pentaerythritol, s); 2.29 (-C**H**$_2$-, t); 1.64 (-C**H**$_2$-, m); 1.38 (-C**H**$_2$-, m).

9.3.4 Vitrimer preparation

The PCL-based vitrimers, whose reaction scheme is shown in **Figure 9.3**, were obtained by carefully mixing PCL acrylates and finely ground DBEDT, which is a fairly coarse solid when prepared, and was weighed so that the final acrylate:thiol ratio was equal to one (**Table 9.3**). The materials were then homogeneised by a pre-mixing phase of 2 min at 120 °C to melt the polymer, solubilise DBEDT and obtain a clear and transparent system. Curing was then continued by pouring the mixture in pre-heated silicone moulds of the desired shape for an additional 24 hours at 120 °C. The cured vitrimers were then removed, cooled down to room temperature and stored in a desiccator prior to analysis. The coding of vitrimers follows that of the corresponding acrylates, i.e., the vitrimers prepared using S41K are coded S41K-V.

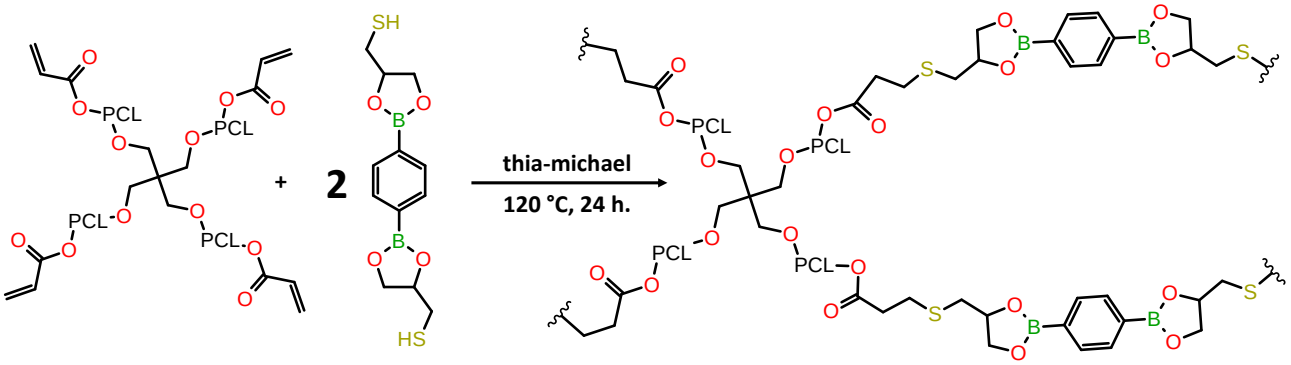

Figure 9.3. *Scheme of the synthesis of S41K-V and S42K-V.*

Table 9.3. *Preparation conditions of the vitrimer systems.*

Sample code	DBEDT/PCL ratio*[mg/g]
S41K-V	101.7
S42K-V	66.0
S62K-V	74.0

*: expressed as mg DBEDT needed to crosslink completely 1 g of PCL acrylate, considering thiol:acrylate = 1. This was calculated by considering the M_{nNMR} value of the star-shaped polymers.

9.3.5 Enzymatic degradation

Enzymatic hydrolysis of materials was performed by placing small rectangular vitrimer specimens (dimensions = 6x2x2 mm^3, initial weight = 25 mg, n = 4) in a 1.5 mL Eppendorf safe-lock tube followed by 1 mL of a 5 µM solution of cutinase in 0.1 M phosphate buffer solution (KPO), pH 8. Samples were incubated at 50 °C for 1, 3, 6 and 12 days, until complete degradation was observed. At the desired time point, the samples were removed from the enzyme solution, washed three times with an excess of milliQ water and then dried at 30 °C in vacuum oven until constant weight before performing the gravimetric measurement of the weight loss using an analytical scale (±0.0001 g).

9.3.6 Characterization

^{1}H-NMR spectra of hydroxyl and acrylated PCLs were recorded using a Jeol ECZ400R/S3 400 MHz using 10 mm NMR tubes and $CDCl_3$ as solvent. All the samples were dissolved in $CDCl_3$ at a concentration of 15 mg/mL and analyzed at room temperature. FT-IR spectra of the materials were acquired using a Bruker "Vertex 70®" in ATR mode from 400 to 4000 cm^{-1}. Thermal analysis was performed using a DSC1/TGA STAR^e System®. In detail, DSC thermograms were recorded in the range -100/+150 °C, using heating/cooling rates of ±10 °C/min under 20 mL/min nitrogen flow. TGA measurements were performed from 30 to 800 °C under a nitrogen flow of 80 mL/min. The crystallinity degree of the prepared materials (χ_c) was calculated based on their PCL content, Φ_{PCL}, by applying **Equation 9.1**, using the melting enthalpy values (ΔH_m) measured from the second heating scan.

$$\chi_c = \frac{\Delta Hm}{\Delta H_m^0 \cdot \Phi PCL} \quad \textbf{(9.1)}$$

where ΔH_m is the measured melting enthalpy, Φ_{PCL} is PCL weight fraction in the vitrimer and ΔH_m^0 is the melting enthalpy of the 100% crystalline PCL (139 J/g [36]). The gel fraction (GF) of vitrimers

were measured using anhydrous toluene, being a good solvent for both reagents. In detail, 50 mg of the samples were accurately weighed and immersed in 2 mL of solvent until constant weight. Then, the samples were dried at 25 °C for 24 h followed by another 24 h at 30 °C under vacuum. After this phase, the samples were weighed, and the GF was calculated using **Equation 9.2** where: M_d = weight of the dried sample, M_i = initial weight.

$$GF = \frac{M_d}{M_i} \cdot 100 \qquad (\mathbf{9.2})$$

Dynamic mechanical analysis (DMTA) were carried out on bars (nominal size 6x1.5x30 mm^3) working in tensile mode on a TA Instruments Q800 using a heating rate of 3°C/min in the range from 25 to 200 °C, in strain-controlled mode (frequency = 1 Hz, deformation amplitude = 0.05%, preload = 0.01 N). Plate-plate rheological analysis of the materials was performed using an ARES rheometer, using 25 mm diameter x 1 mm thickness disks. Specimens for both DMTA and rheology were obtained by curing the vitrimers within silicone molds with suitable geometries and keeping the materials in the desiccator until the tests. Dynamic strain sweep measurements were performed to confirm the linearity of the viscoelastic region up to 1% strain. Frequency sweeps measurements were carried out to measure the complex viscosity (η*), storage modulus (G') and dissipative modulus (G'') in the frequency range of 0.1–100 rad/s, between 90 °C and 210 °C with 30 °C steps. Isothermal relaxation tests were also carried out using 1% strain. Stress G(t) was normalized on G_0, namely the stress recorded at t = 0.5 s to get rid of instrumental transitory at the begin of the relaxation test. All the rheological measurements were performed under nitrogen flow to avoid oxidative and hydrolytic degradation of the materials.

9.4 Results and discussion

9.4.1 Study of the cross-linking reaction

The thiol-acrylate reaction (**Figure 9.3**) between the star-shaped acrylated PCLs and DBEDT was monitored by comparing the FT-IR spectra of the starting polymers with those of the respective cross-linked systems (**Figure 9.4**). The neat polymers exhibited typical signals associated with PCL chains at 2950 cm^{-1} and 2870 cm^{-1} (υ Csp^3- H methylenic unit), 1725 cm^{-1} (υ C=O), at 1295 cm^{-1} (υ C–O and C–C), 1242 cm^{-1} and 1171 cm^{-1} (υ C–O–C asymmetric/symmetric). Moreover, two additional bands were found at 1640 and 814 cm^{-1}, which can be attributed to C=C stretching and -CH=CH_2

twisting of acrylate units, respectively, as previously reported in other works [35,37]. As shown in Figure 2, the above two signals disappeared in the FT-IR spectra of the polymers after reaction with DBEDT. Indeed, as previously reported by Zych et al., this finding proves the good outcome of the thiol-acrylate reaction. Moreover, some shoulders around 1211 cm^{-1} and peaks at 652 cm^{-1} were found in the spectra of the cross-linked PCL, which can be attributed to the presence of B-O and B-O-B bonds of the boronic ester, respectively and which can be also observed as distinct peaks in the DBEDT spectrum (**Figure 9.5**) [38].

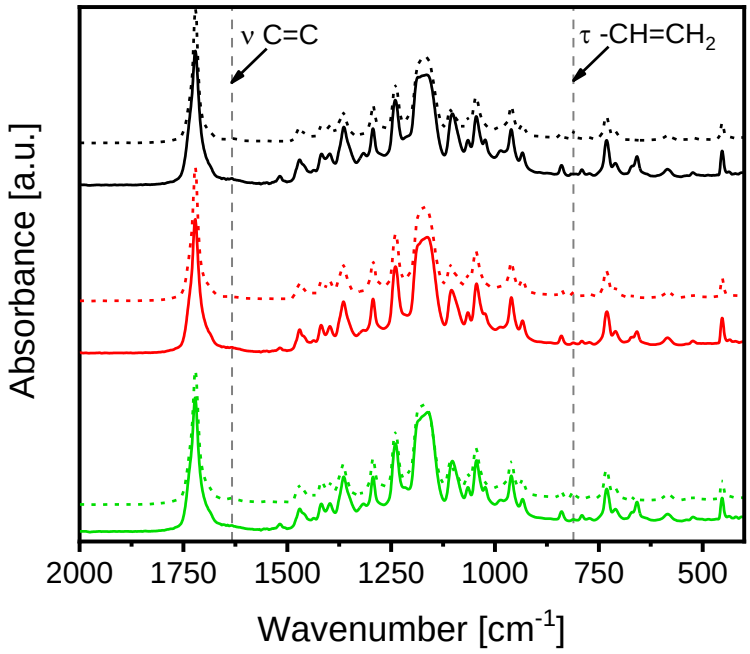

Figure 9.4. *FT-IR spectra of PCL acrylates (dashed line) and respective vitrimers (continuous line) obtained from S41K (black), S42K (red) and S62K (green) polymers.*

Macroscopically, the crosslinking process was evidenced by an increase in the systems viscosity, over time, while the mixture was being heated up. For all the systems the transition from liquid, pourable mixtures (**Figure 9.6a**), having viscosity comparable to those of melted PCL acrylates, to rubbery transparent solids (**Figure 9.6c**), able to slowly crystallize at room temperature (**Figure 9.6b**) was observed. Moreover, the gel fraction (GF) measurements performed on the materials showed values of 79%, 78% and 83% for S41K-V, S42K-V, S62K-V vitrimers respectively. These were comparable to the GF found for a similar system (81.9 ± 1.4%) reported in the literature [32], and previously confirmed results obtained by FT-IR analysis. These findings are consistent with the hypothesis of the formation of a crosslinked structure, thus confirming the positive outcome of the curing reaction.

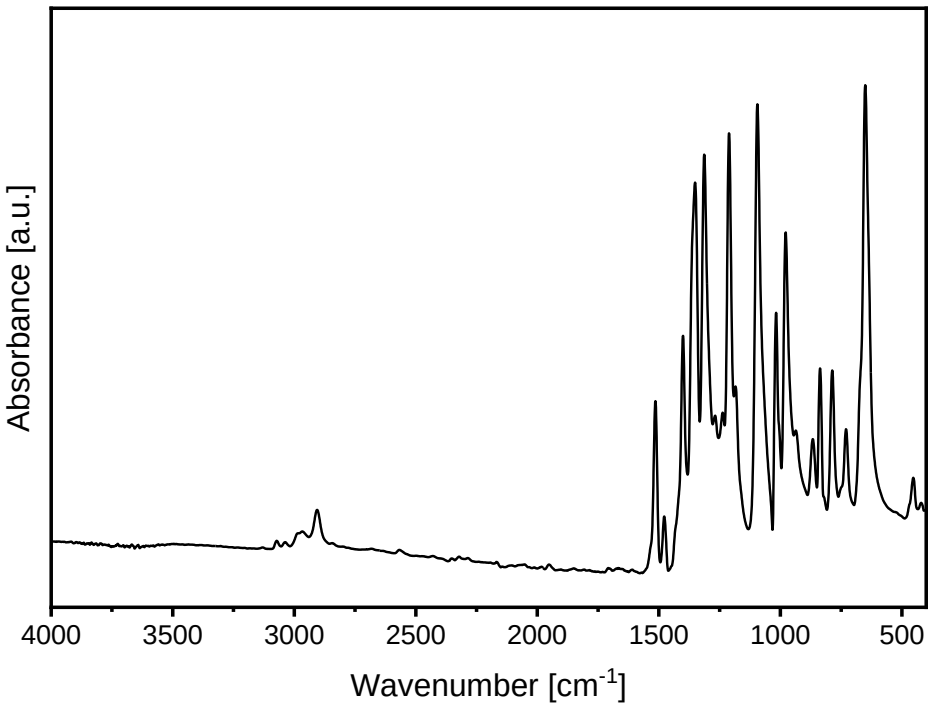

Figure 9.5. *FT-IR spectra of DBEDT powder.*

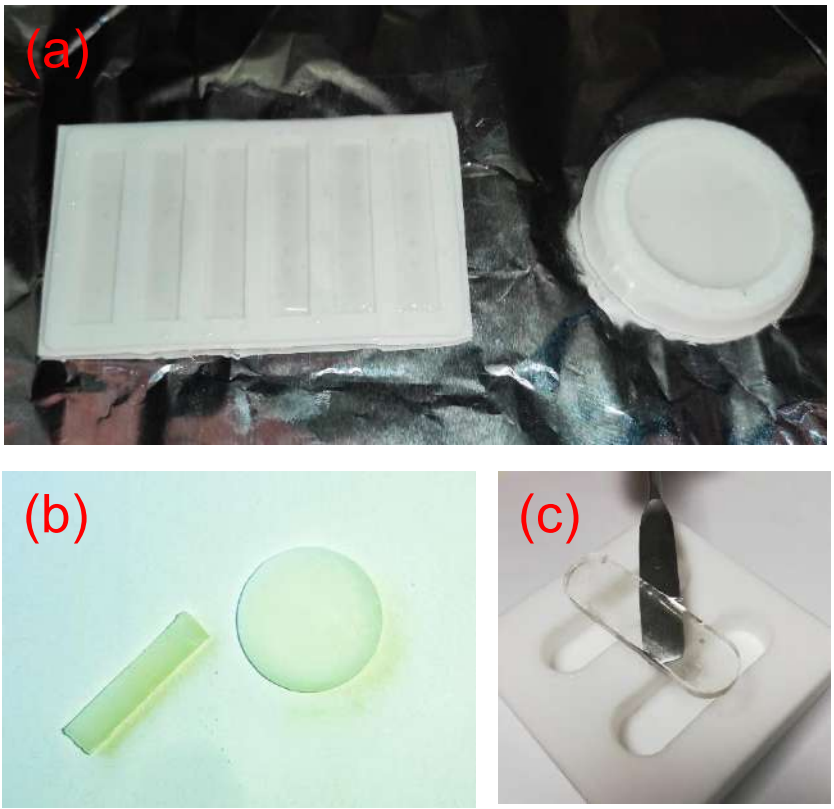

Figure 9.6. *Photos of S41K/DBEDT mixture during curing (a) and the resulting material, S41K-V, at room temperature (under PCL T_m) (b) and at 80 °C (above PCL T_m) (c).*

9.4.2 Study of the thermal properties

The thermal properties of the acrylated polymers and the corresponding cross-linked systems are reported in **Table 9.4**, while DSC and TGA traces are given in **Figure 9.7** and **Figure 9.8**. In particular, when comparing the DSC data of the different acrylated starting materials, it was found that the molecular weight as well as the number of arms of the star-shaped PCL affected the system thermal properties. In particular, the crystallinity (χ_c) of the acrylated polymers increased with increasing the molecular weight and the number of arms, from 40 % for S41K to 52% and 53 % for S42K and S62K, respectively. These samples show a different trend compared to linear high molecular weight polymers, where, in general, an increase in molecular weight leads to a decrease in crystallinity [39–43]. Indeed, in the case of branched or star-shaped polymers, the chain length enhances the structuring, at least at low molecular weights, showing an inverse behavior compared to linear polymers [44].

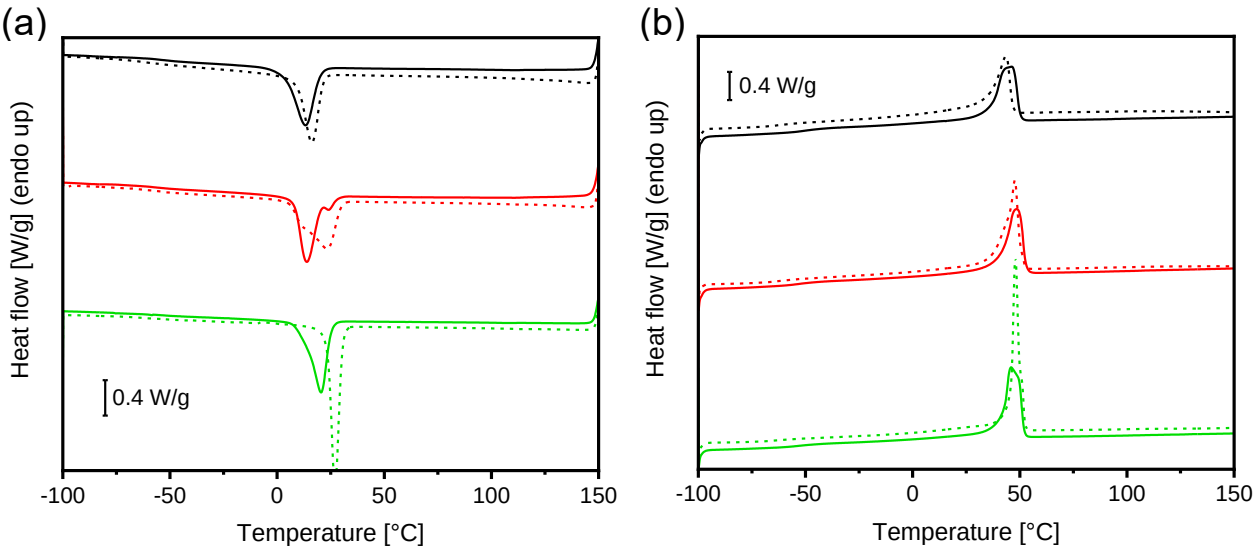

Figure 9.7. *DSC thermograms, cooling (left) and second heating (right) for PCL acrylates (dashed line) and respective vitrimers (continuous line) obtained from S41K (black), S42K (red) and S62K (green) polymers.*

This could be due to the fact that the structuring of the linear fraction predominates with increasing chain length compared to the crystallization disorder that develops around the branched core and could explain the same crystallinity of the 4-armed and 6-armed sample, S42K and S62K, respectively, characterized by the same molecular weight per single arm. In contrast, all the cross-linked samples seemed to maintain the same χ_c, which was lower than that of the pristine polymers for S42K-V and S62K-V. A slight difference among the samples was observed in the T_c, which decreased expecially for S42K after the cross-linking process.

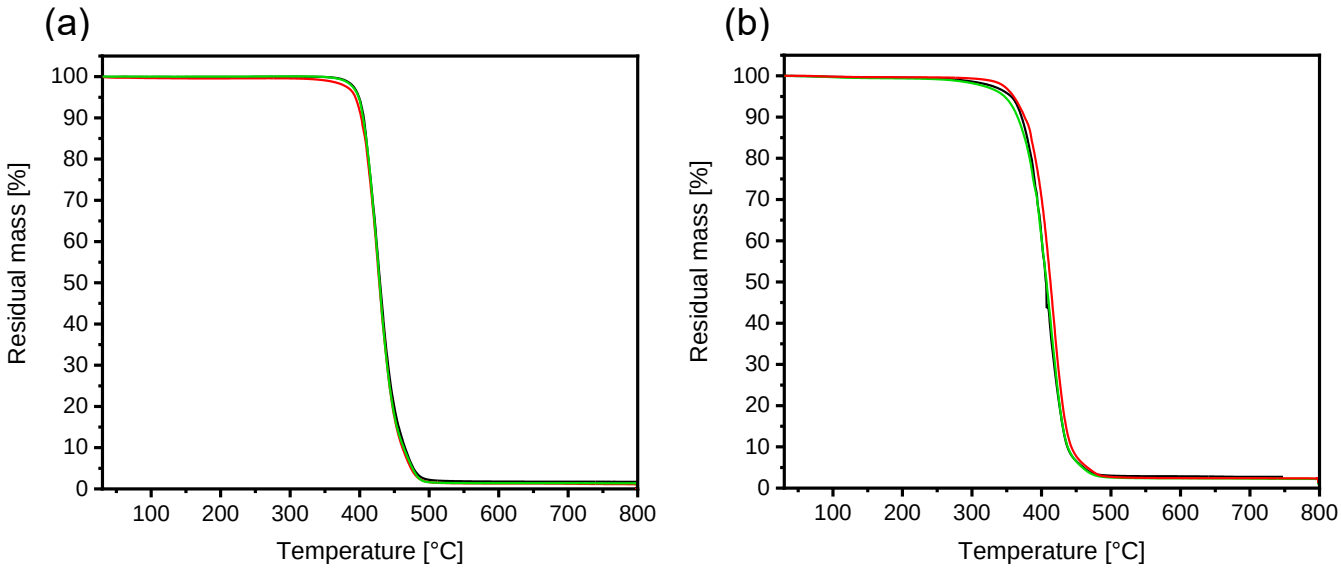

Figure 9.8. *TGA curves of PCL acrylates (a) and respective vitrimers (b) obtained from S41K (black), S42K (red) and S62K (green) polymers.*

The decrease in crystallinity and T_c in the cross-linked samples, which was observed mainly in the samples characterized by the highest molecular weights, namely S42K and S62K, could be related to to a decrease in the mobility of the macromolecular chains caused by the introduction of bonds at the ends of the star-shaped structures. Therefore, the above findings appear to support the formation of a network when the star-shaped polymers are reacted with DBEDT at high temperature. Although the crystallinity decreases in the cross-linked systems, it is worth underling that all the samples retain some degree of structuration even after the treatment with the cross-linking agent, a characteristic which may affect the final material's properties. The results of thermogravimetric analysis of the acrylated polymers revealed a similar onset degradation temperature ($T_{onset\ 5\%}$), which was around 390 °C, and an equal temperature of maximum rate of degradation (T_{max}) of 427 °C, which is in agreement with the values observed in other previous works for acrylated PCL [35,45] and related to a statistical chain scission by a β-elimination mechanism. In contrast, a general decrease in the thermal stability, in terms both of $T_{onset\ 5\%}$ and T_{max}, was observed after the cross-linking reaction. Indeed, the extent of this variation reflects the DBEDT content of the system. Considering the lower degradation temperature observed for neat DBEDT compared to the PCL acrylated polymers, this can be possibly attributed to its thermal degradation within the network structure.

Table 9.4. *Thermal characterization of acrylated polymers and vitrimers.*

Sample code	T_c [°C]	$\Delta H_{c\ CORR}$ [J/g]	T_m [°C]	$\Delta H_{m\ CORR}$ [J/g]	$\chi_{c\ CORR}$ [%]	$T_{onset\ 5\%}$* [°C]	T_{max}** [°C]
S41K	16	-52	43	55	40	399	427
S42K	23	-67	47	72	52	393	427
S62K	27	-68	48	73	53	398	427
S41K-V	13	-56	46	58	42	356	407
S42K-V	14	-56	48	59	42	359	416
S62K-V	20	-58	46	60	43	346	412
DBEDT	-	-	100	56	-	258	334/354

The subscript m CORR and c CORR indicate the values measured during melting and crystallization, respectively, considering the mass fraction of PCL contained in the materials. *:$T_{onset\ 5\%}$ was extrapolated from TGA curves as the point where the mass loss was equal to 5%. **:T_{max} was extrapolated from DTG curves as the points where the mass loss rate was at its maximum.

9.4.3 DMTA and rheological analyses

Thermomechanical properties of vitrimers (**Figure 9.9**) were investigated by dynamic mechanical thermal analyses on heating ramp. At room temperature, storage moduli in the range of 0.4±0.1 GPa were measured, which are consistent with that of a linear high molecular weight, PCL-L (**Figure 9.10)**. Beside the expected fall in stiffness across the melting of PCL, the high temperature storage modulus at high temperature can be correlated with the crosslinking of the PCL network. Indeed, a fully stable storage modulus plateau was observed for all vitrimeric formulations, in the range of 1 MPa, with limited differences between the different formulations. Such plateau confirms the crosslinked nature of the material, maintaining the shape of the specimens well above the melting temperature (**Figure 9.11**).

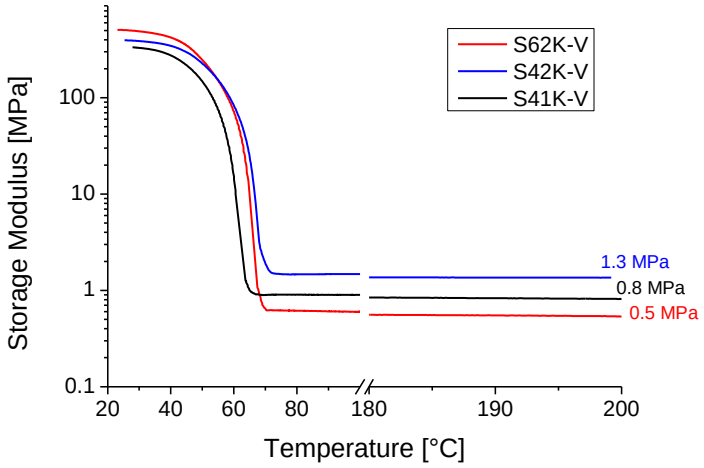

Figure 9.9. *DMTA plots on heating ramp for the different PCL vitrimers.*

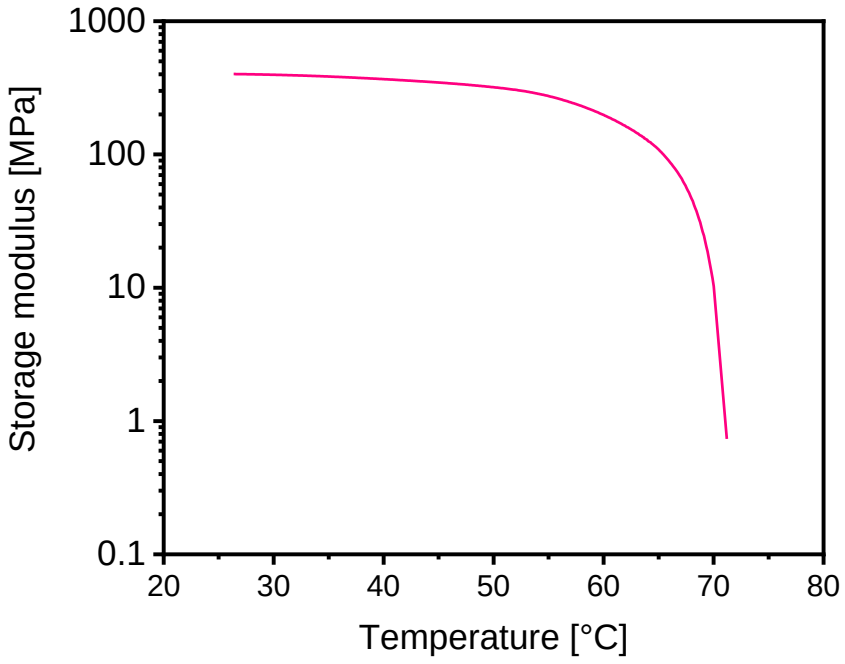

Figure 9.10. *DMTA analysis of high molecular weight PCL. The curve is interrupted at 70 °C due to sample melting.*

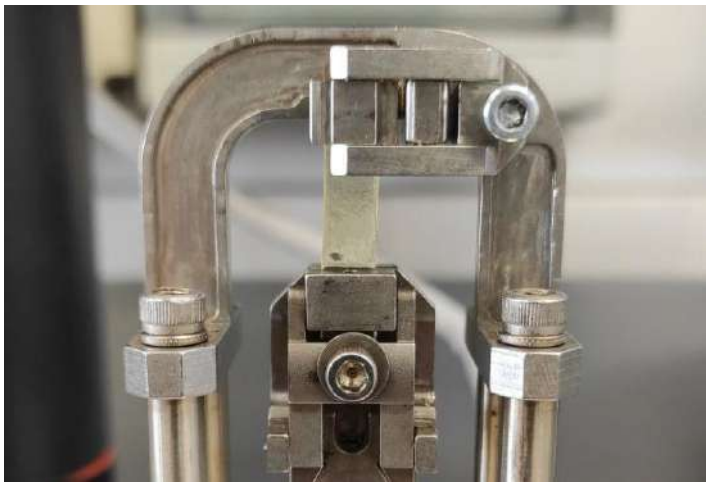

Figure 9.11. *Photo of S41K-V film at 80 °C (above PCL T_m), during DMTA analysis.*

To further investigate the bond exchange at high temperature, rheological test were carried out in frequency sweep at different temperatures, ranging from 90 to 210°C (**Figure 9.12**). At 90°C, S41K-V displayed a fully solid like behaviour, characterized by a constant value of storage modulus, higher than G''over the whole frequency range. Similarly, rheological behaviour for S42K-V and S62K-V is dominated by the elastic component, with only a slight decrease in the storage modulus at frequencies below 1 rad/s. At higher temperatures, the decay in storage modulus at low ω expectedly becomes progressively more important for all formulations, suggesting the existance of a relaxation phenomenon. This is further evidences by the appearance of a peak in the loss modulus, increasing in intensity and shifting towards higher frequency with temperature increase. Crossover between G' and G'' was observed only for S62K-V at 210°C (at 0.2 rad/s), whereas for lower temperatures it appears to fall below the minimum frequency applied. Similarly, crossover not observed in the explored frequency range for both S41K-V and S42K-V. This is in agreement with other boronic ester-crosslinked vitrimers, displaying crossover points below 0.1 rad/s [28].

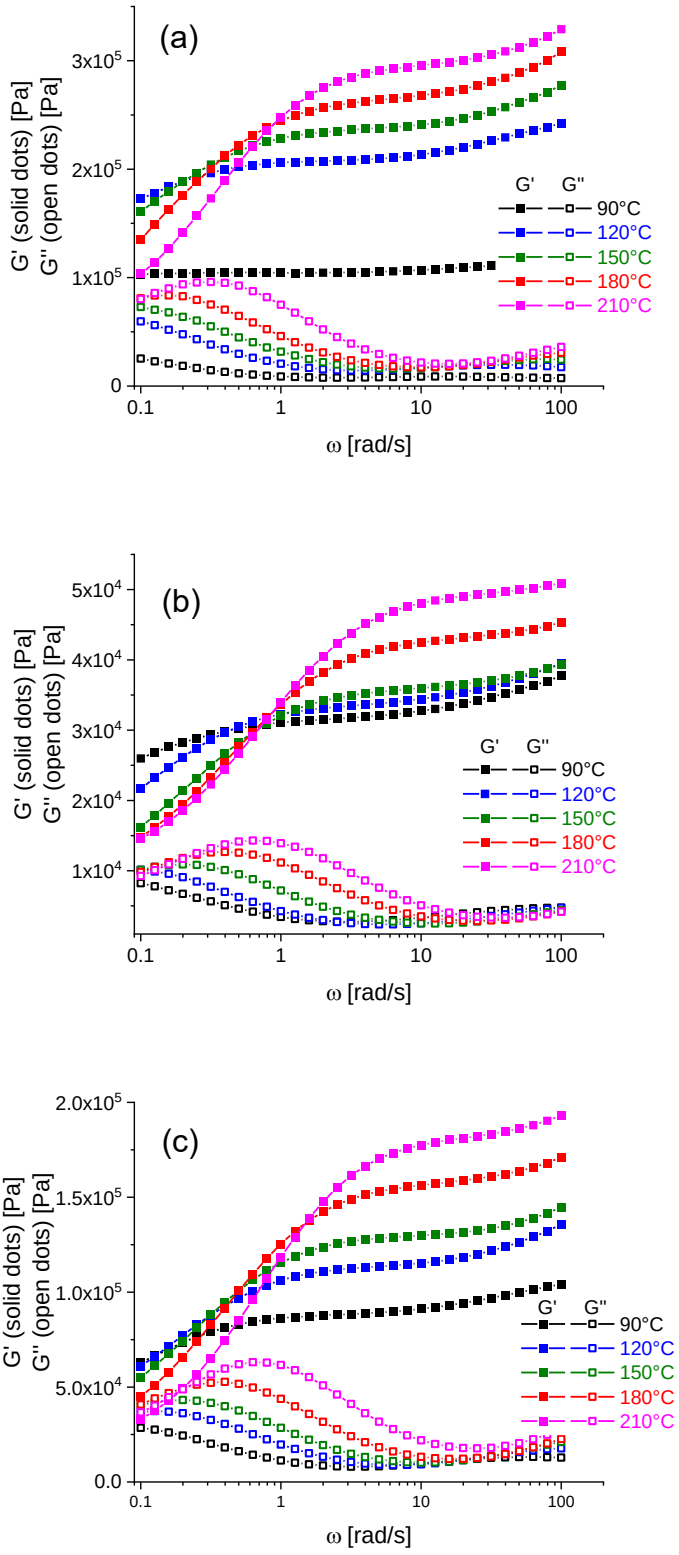

Figure 9.12. *Rheological plots for S41K-V (a), S42K-V (b) and S62K-V (c).*

To investigate the kinetics of the relaxation phenomena, stress relaxation tests were carried out at different temperatures (**Figure 9.13**). Relaxation times obtained are very well fitted by the Arrhenius plots, yielding activation energy for the relaxation process in the range of 60 kJ/mol for both S41K-V and S42K-V, while a lower value was obtained for S62K-V. As already observed for the rheological behavior, it is possible to hypothesize that the 6-arm PCL structure allows greater mobility, and the corresponding network is consequently characterized by a lower activation energy compared to systems prepared from 4-arm PCL. However, the activation energies for the relaxation of PCL boronic ester vitrimers are in agreement with previously reported results for similar systems [28,32].

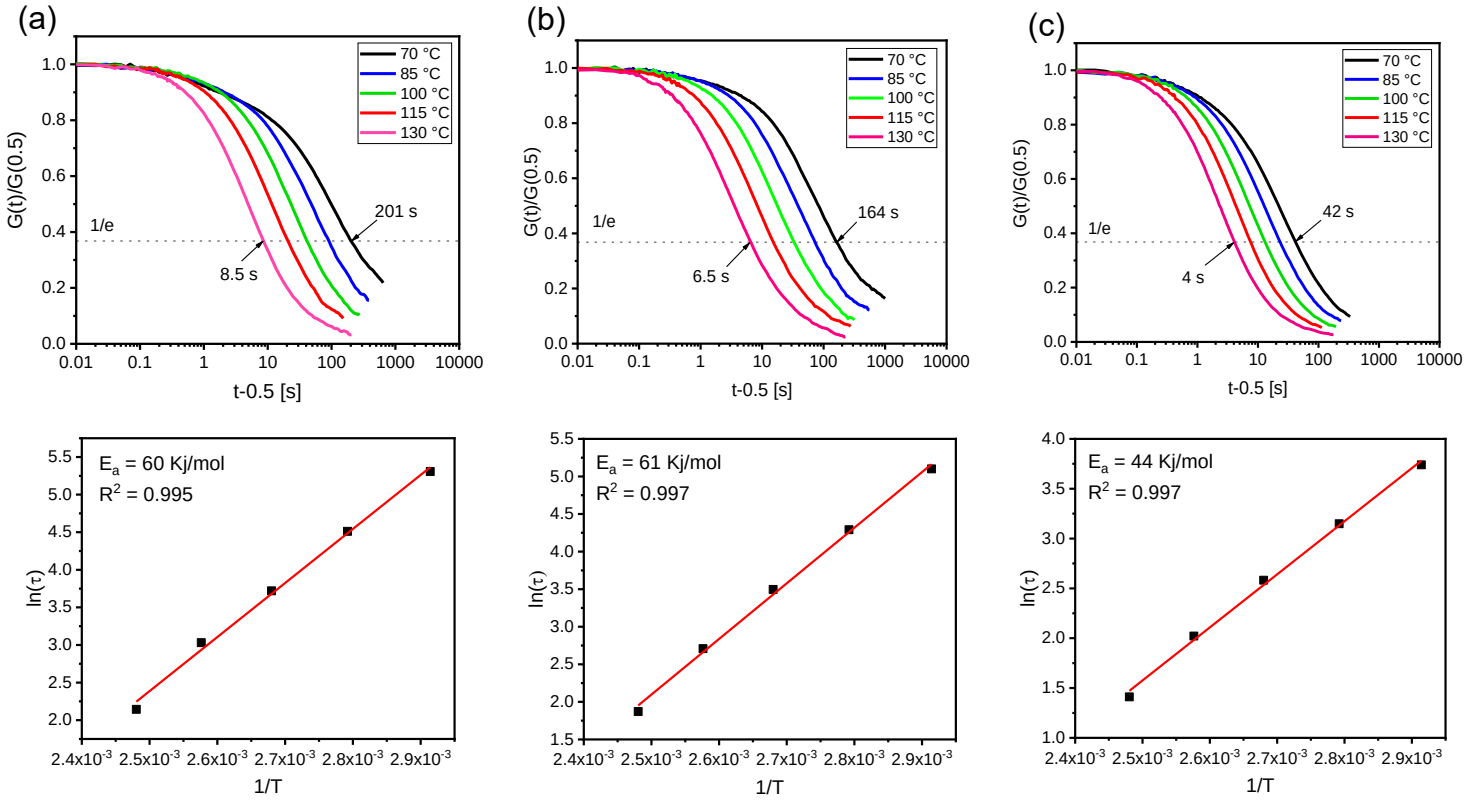

Figure 9.13. *Stress relaxation plots (top) for S41K-V (a), S42K-V (b) and S62K-V (c), along with the corresponding Arrhenius plots (bottom).*

9.4.4 Recyclability and self-healing test

In order to evaluate the recyclability of the developed systems (**Figure 9.14**), a piece of the cross-linked film (0.5 g) was manually cut into small pieces, which were then placed in a 3 x 3.5 cm^2 rectangular mould. To facilitate the material flow during the compression molding process, the sample was preheated to 180 °C for 3 minutes and then pressed at the same temperature for 5 minutes with a very low force (300 kgf). After this procedure, a homogeneous film identical to the original material

was successfully recovered. The self-healing test was similarly performed by cutting the film sample into two parts and using the same temperature without preheating. In this case, the sample was held in position in the mold with a small glass slide to keep both edges in perfect contact and prevent deformation due to heating. Also, in this case it was possible to obtain a homogeneous film. These observations clearly demonstrate that the bond exchange and macromolecular interdiffusion, as well as the viscosity of the materials under the conditions used for both tests, were sufficient to ensure good adhesion between the different pieces confirming the vitrimeric behaviour possessed by this new class of materials. Furthermore, the thermochemical stability of the materials was proved by the unchanged FT-IR spectra and TGA curves of the samples before and after recycling. **Figure 9.15** and **Figure 9.16** show the FT-IR spectra and TGA profiles of S41K-V as an example. Indeed, as demonstrated by this test, the high network dynamicity introduced by boronic ester metathesis provides a key advantage in terms of reprocessability, making these materials easily moldable and recycable without the use of catalysts (**Figure 9.17**). It is worth underling that some of these catalysts, especially the metal-based ones, such as tin octoate or zinc acetylacetonate, which are widely used in polyester/polyurethane vitrimers to promote transesterification and transcarbamoylation exchange reactions [23,46,47], are toxic or harmful even when employed in very low concentration, [48–51]. Moreover, their presence could lead to a decrease in the thermal stability of the system, since they are able to promote degradation by depolymerization or, in presence of water, by hydrolytic processes under the recycling conditions generally used [52–54]. Considering these aspects, the developed approach is promising when considered from the point of view of producing new sustainable materials with lower environmental impact.

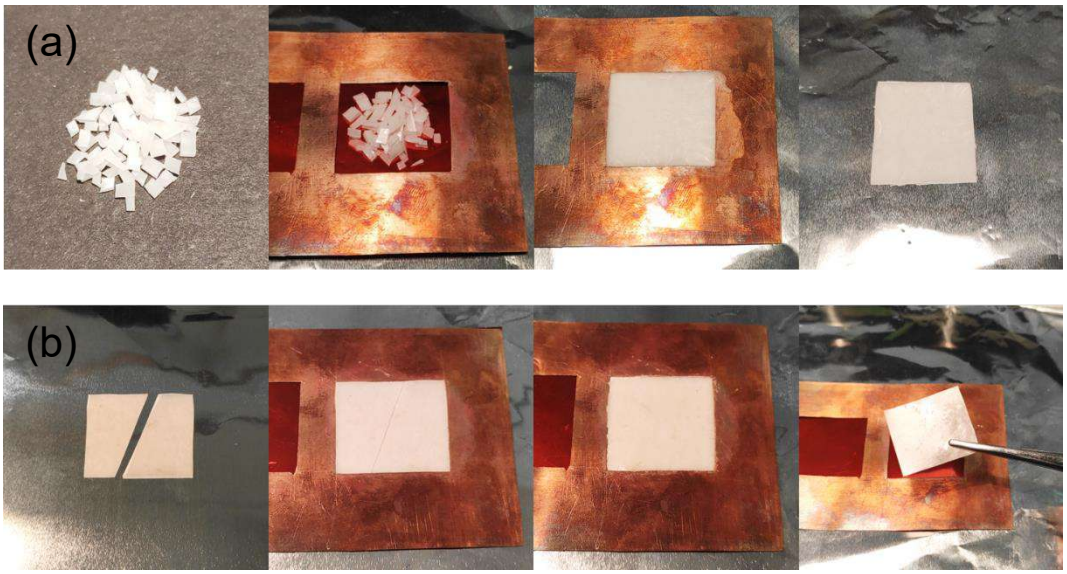

Figure 9.14. *Example of recyclability (a) and self-healing (b) tests performed on S42K-V vitrimer.*

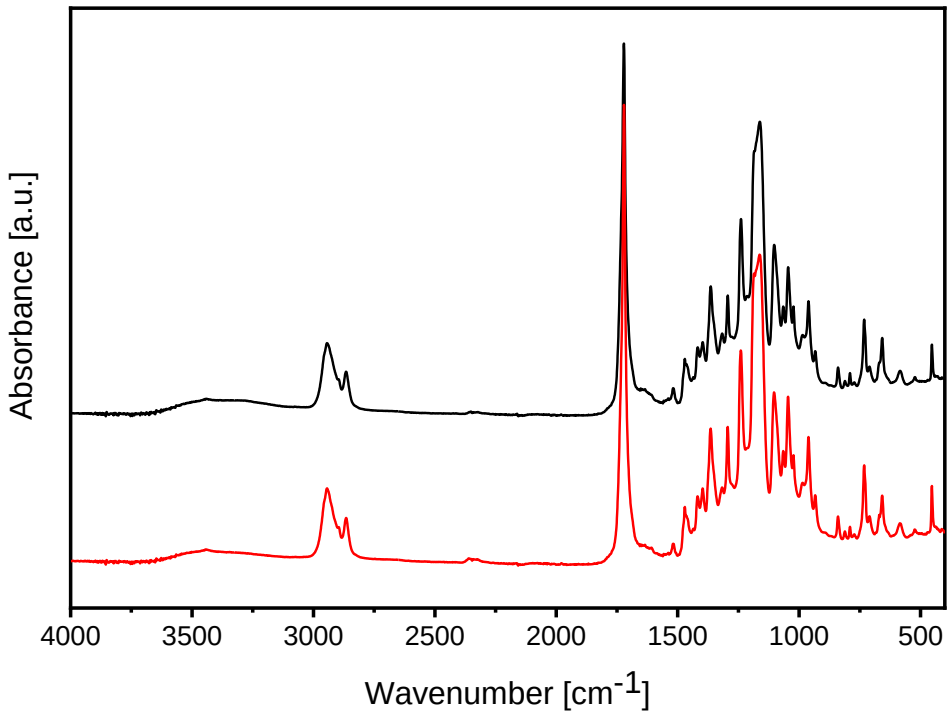

Figure 9.15. *FT-IR spectra of S41K-V before (black) and after (red) recycling test.*

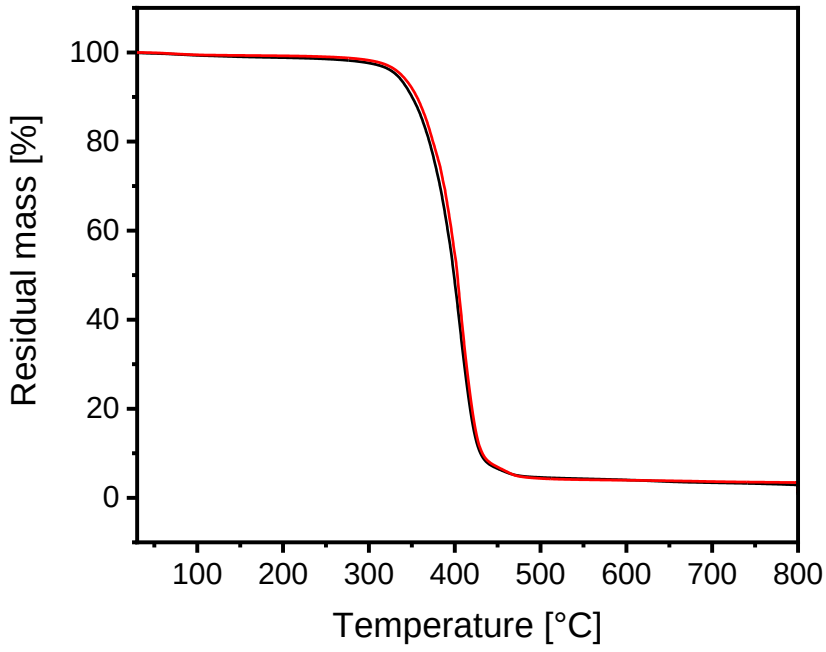

Figure 9.16. *TGA thermograms of S41K-V before (black) and after (red) recycling test.*

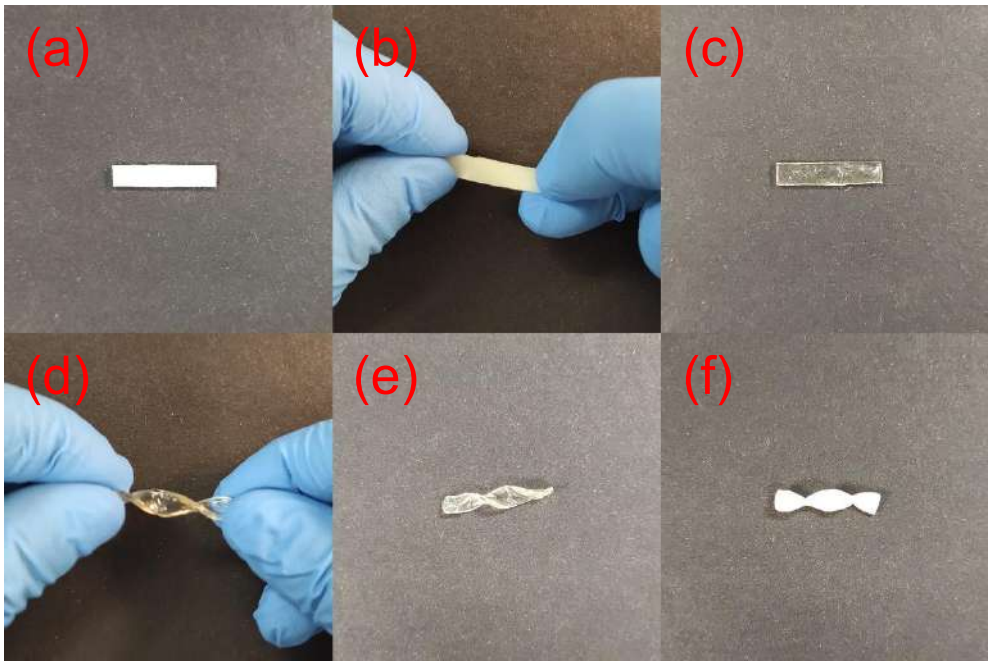

Figure 9.17. *Photos of: S41K-V film at room temperature (a), S41K-V film at room temperature under twisting test by hand (b), S41K-V film at 80 °C (c), S41K-V film at 80 °C under twisting test by hand (d), twisted S41K-V film during cooling (e) and twisted S41K-V film at room temperature (f).*

9.4.5 Enzymatic Degradation

The enzymatic degradation of the PCL vitrimers was carried out using a cutinase, a highly active hydrolytic enzyme belonging to the serin-hydrolases family known for its activity on polyesters [33,55–57]. To investigate the effect of crosslinking on the hydrolytical stability of the PCL-based vitrimers, we used a high molecular weight linear PCL, namely PCL-L, as a reference material (**Figure 9.18**). Not surprisingly, complete hydrolysis of PCL-L was observed after 3 days, demonstrating the effective depolymerization activity of this enzyme for PCL, as also reported in our previous work [33]. In contrast, the vitrimers exhibited slower degradation times, requiring 12 days to be completely degraded. Considering the melting behaviour of the linear PCL and vitrimers, a fast degradation rate could be expect for the latter systems, as the reaction temperature (50 °C) was well above the T_m of the PCL crystalline phase of the vitrimers and very close to the melting temperature reported in other works for PCL-L (57 °C) [33,58]. On this basis, the results suggest that the presence of cross-links in the polymer matrix is the main factor influencing the degradation rate of PCL at that temperature. Moreover, no significant differences in the degradation profile of the different vitrimers were observed, probably due to the limited differences in molecular weight and number of functionalities of the studied star-shaped polymers. Although the different degradation rate of the vitrimers compared to the linear polymer, the possibility of degradation of the crosslinked network,

opens up the possibility of exploiting this process in the formation, through enzymatic depolymerization, of monomers/oligomers that can be reused in the *ex novo* synthesis of polymers/vitrimers, making these materials appealing from a circular economy perspective [59,60].

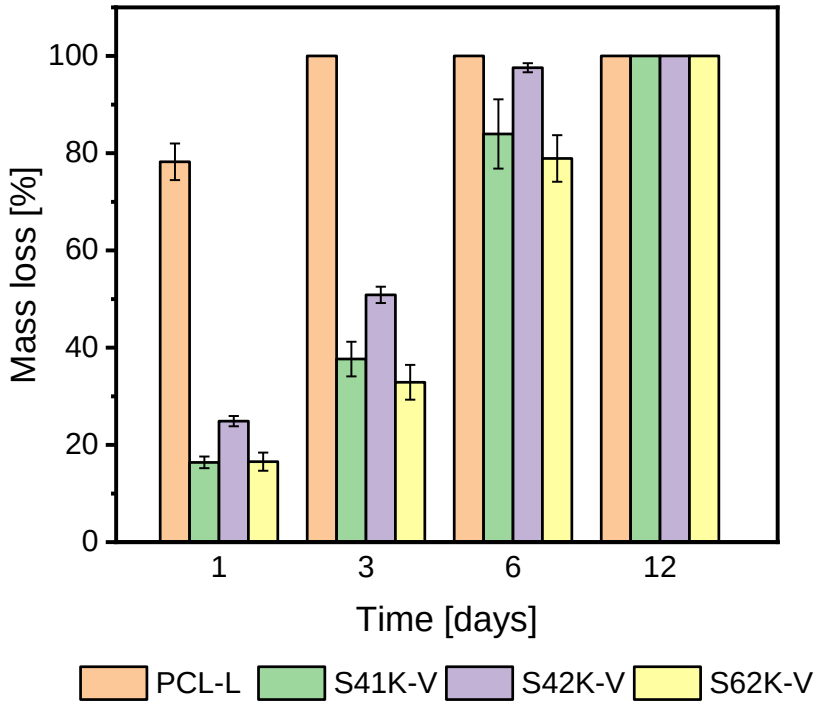

Figure 9.18. *Enzymatic hydrolytic degradation profile of: PCL-L polymer, S41K-V, S42K-V and S62K-V vitrimers in 5 μM cutinase solution in 0.1 M KPO buffer pH 8.*

9.5 Conclusions

In this work, novel vitrimer systems based on PCL were successfully developed. In the design of the formulation, various aspects related to both the manufacturing approach and the final properties of the material were considered to make the whole process environmentally friendly. First, starting from ad-hoc synthesized star-shaped PCL, a polymer potentially produced from renewable sources, a crosslinker was used that allowed the vitrimer production without the use of solvents and catalysts, it being based on a simple thiol-acrylate reaction. The behavior of the vitrimers, common to all systems produced and slightly influenced by the number of arms and the length of the star-shaped polymers, allowed easy recycling through a simple shaping process. In addition, an analysis of enzymatic hydrolysis highlighted the ability of the materials to degrade despite the formation of the network, a phenomenon due to the construction of the systems with PCL, a highly biodegradable polymer. The above property, which generally does not apply to all vitrimer systems, may clearly be of great interest for the end of life of the developed material.

9.6 References

[1] B.R. Elling, W.R. Dichtel, Reprocessable cross-linked polymer networks: are associative exchange mechanisms desirable?, ACS Cent. Sci. 6 (2020) 1488–1496. https://doi.org/10.1021/acscentsci.0c00567.

[2] A. Jourdain, R. Asbai, O. Anaya, M.M. Chehimi, E. Drockenmuller, D. Montarnal, rheological properties of covalent adaptable networks with 1,2,3-triazolium cross-links: the missing link between vitrimers and dissociative networks, Macromolecules 53 (2020) 1884–1900. https://doi.org/10.1021/acs.macromol.9b02204.

[3] T. Pajula, K. Behm, S. Vatanen, E. Saarivuori, Managing the Life Cycle to Reduce Environmental Impacts, in: Dyn. Long-Life Assets, Springer International Publishing, Cham, 2017: pp. 93–113. https://doi.org/10.1007/978-3-319-45438-2_6.

[4] E.L. Teuten, J.M. Saquing, D.R.U. Knappe, M.A. Barlaz, S. Jonsson, A. Björn, S.J. Rowland, R.C. Thompson, T.S. Galloway, R. Yamashita, D. Ochi, Y. Watanuki, C. Moore, P.H. Viet, T.S. Tana, M. Prudente, R. Boonyatumanond, M.P. Zakaria, K. Akkhavong, Y. Ogata, H. Hirai, S. Iwasa, K. Mizukawa, Y. Hagino, A. Imamura, M. Saha, H. Takada, Transport and release of chemicals from plastics to the environment and to wildlife, Philos. Trans. R. Soc. B Biol. Sci. 364 (2009) 2027–2045. https://doi.org/10.1098/rstb.2008.0284.

[5] K.-E. Peiponen, J. Räty, U. Ishaq, S. Pélisset, R. Ali, Outlook on optical identification of micro- and nanoplastics in aquatic environments, Chemosphere 214 (2019) 424–429. https://doi.org/10.1016/j.chemosphere.2018.09.111.

[6] M.A. Lucherelli, A. Duval, L. Avérous, Biobased vitrimers: Towards sustainable and adaptable performing polymer materials, Prog. Polym. Sci. 127 (2022) 101515. https://doi.org/10.1016/j.progpolymsci.2022.101515.

[7] V. Guarino, G. Gentile, L. Sorrentino, L. Ambrosio, Polycaprolactone: synthesis, properties, and applications, Enc. Polym. Sci. Tech. (2017). https://doi.org/10.1002/0471440264.pst658.

[8] S.H. Pyo, J.H. Park, V. Srebny, R. Hatti-Kaul, A sustainable synthetic route for biobased 6-hydroxyhexanoic acid, adipic acid and ϵ-caprolactone by integrating bio- and chemical catalysis, Green Chem. 22 (2020) 4450–4455. https://doi.org/10.1039/d0gc01454k.

[9] K. Ishida, V. Weibel, N. Yoshie, Substituent effect on structure and physical properties of semicrystalline Diels-Alder network polymers, Polymer 52 (2011) 2877–2882. https://doi.org/10.1016/j.polymer.2011.04.038.

[10] T. Defize, R. Riva, C. Jérôme, M. Alexandre, Multifunctional poly(ε-caprolactone)-forming networks by diels-alder cycloaddition: effect of the adduct on the shape-memory properties, Macromol. Chem. Phys. 213 (2012) 187–197. https://doi.org/10.1002/macp.201100408.

[11] T. Defize, R. Riva, J.M. Raquez, P. Dubois, C. Jérôme, M. Alexandre, Thermoreversibly crosslinked poly(ε-caprolactone) as recyclable shape-memory polymer network, Macromol. Rapid Commun. 32 (2011) 1264–1269. https://doi.org/10.1002/marc.201100250.

[12] T. Defize, J.-M. Thomassin, M. Alexandre, B. Gilbert, R. Riva, C. Jérôme, Comprehensive study of the thermo-reversibility of diels–alder based pcl polymer networks, Polymer 84 (2016) 234–242. https://doi.org/10.1016/j.polymer.2015.11.055.

[13] D. Pratchayanan, J.-C. Yang, C.L. Lewis, N. Thoppey, M. Anthamatten, Thermomechanical insight into the reconfiguration of diels–alder networks, J. Rheol. 61 (2017) 1359–1367. https://doi.org/10.1122/1.4997580.

[14] Z.P. Wang, W.H. Ruan, M.Z. Rong, M.Q. Zhang, Injection molding of highly filled microcrystalline cellulose/polycaprolactone composites with the aid of reversible diels-alder reaction, J. Mater. Sci. Technol. 170 (2024) 246–254. https://doi.org/10.1016/j.jmst.2023.07.017.

[15] M. Houbben, J.-M. Thomassin, C. Jérôme, Supercritical co2 blown poly(ε-caprolactone) covalent adaptable networks towards unprecedented low density shape memory foams, Mater. Adv. 3 (2022) 2918–2926. https://doi.org/10.1039/D2MA00040G.

[16] M. Houbben, C.P. Sànchez, P. Vanderbemden, L. Noels, C. Jérôme, MWCNTs filled PCL covalent adaptable networks: Towards reprocessable, self-healing and fast electrically-triggered shape-memory composites, Polymer. 278 (2023) 125992. https://doi.org/10.1016/j.polymer.2023.125992.

[17] J. Caprasse, R. Riva, J.-M. Thomassin, C. Jérôme, Hybrid covalent adaptable networks from cross-reactive poly(ε-caprolactone) and poly(ethylene oxide) stars towards advanced shape-memory materials, Mater. Adv. 2 (2021) 7077–7087. https://doi.org/10.1039/D1MA00595B.

[18] Y. Cao, M.Z. Rong, M.Q. Zhang, Covalent adaptable networks impart smart processability to multifunctional highly filled polymer composites, Compos. Part A Appl. Sci. Manuf. 151 (2021) 106647. https://doi.org/10.1016/j.compositesa.2021.106647.

[19] D.A. Cooney, H.A. Milman, R.G. Cable, R.L. Dion, V.H. Bono, K. Karrer, H.P. Friedl, Maleimide—biochemical, pharmacologic and toxicologic studies, Biochem. Pharmacol. 27 (1978) 151–166. https://doi.org/10.1016/0006-2952(78)90295-2.

[20] J. Joe, J. Shin, Y. Choi, J.H. Hwang, S.H. Kim, J. Han, B. Park, W. Lee, S. Park, Y.S. Kim, D. Kim, A 4d printable shape memory vitrimer with repairability and recyclability through network architecture tailoring from commercial poly(ε-caprolactone), Adv. Sci. 8 (2021) 2103682. https://doi.org/10.1002/advs.202103682.

[21] S. Bhusal, C. Oh, Y. Kang, V. Varshney, Y. Ren, D. Nepal, A. Roy, G. Kedziora, Transesterification in Vitrimer

Polymers Using Bifunctional Catalysts: Modeled with Solution-Phase Experimental Rates and Theoretical Analysis of Efficiency and Mechanisms, J. Phys. Chem. B. 125 (2021) 2411–2424. https://doi.org/10.1021/acs.jpcb.0c10403.
[22] W. Miao, W. Zou, Y. Luo, N. Zheng, Q. Zhao, T. Xie, Structural tuning of polycaprolactone based thermadapt shape memory polymer, Polym. Chem. 11 (2020) 1369–1374. https://doi.org/10.1039/C9PY01891C.
[23] A. Vallin, D. Battegazzore, G. Damonte, A. Fina, O. Monticelli, on the development of nanocomposite covalent associative networks based on polycaprolactone and reduced graphite oxide, Nanomaterials 12 (2022) 3744. https://doi.org/10.3390/nano12213744.
[24] G. Ye, J. Zhang, H. Bi, The effect of epoxy vitrimer on the structure and properties of thermoplastic polyurethane/polycaprolactone polymer composites, Polym. Eng. Sci. 63 (2023) 1828–1835. https://doi.org/10.1002/pen.26328.
[25] W. Zou, B. Jin, Y. Wu, H. Song, Y. Luo, F. Huang, J. Qian, Q. Zhao, T. Xie, Light-triggered topological programmability in a dynamic covalent polymer network, Sci. Adv. 6 (2020). https://doi.org/10.1126/sciadv.aaz2362.
[26] J. Lv, A. Wang, Y. Li, S. Xu, X. Li, Thermadapt shape memory pcl-co-pba network exhibiting tunable properties and dynamics of ester–ester exchange reactions, ACS Appl. Polym. Mater. (2023). https://doi.org/10.1021/acsapm.3c01496.
[27] O.R. Cromwell, J. Chung, Z. Guan, Malleable and self-healing covalent polymer networks through tunable dynamic boronic ester bonds, J. Am. Chem. Soc. 137 (2015) 6492–6495. https://doi.org/10.1021/jacs.5b03551.
[28] M. Röttger, T. Domenech, R. van der Weegen, A. Breuillac, R. Nicolaÿ, L. Leibler, High-performance vitrimers from commodity thermoplastics through dioxaborolane metathesis, Science 356 (2017) 62–65. https://doi.org/10.1126/science.aah5281.
[29] W. Niu, C. O'Sullivan, B.M. Rambo, M.D. Smith, J.J. Lavigne, Self-repairing polymers: poly(dioxaborolane)s containing trigonal planar boron, Chem. Commun. (2005) 4342. https://doi.org/10.1039/b504634c.
[30] M.A. Soriano-Ursúa, E.D. Farfán-García, Y. López-Cabrera, E. Querejeta, J.G. Trujillo-Ferrara, Boron-containing acids: preliminary evaluation of acute toxicity and access to the brain determined by raman scattering spectroscopy, Neurotoxicology 40 (2014) 8–15. https://doi.org/10.1016/j.neuro.2013.10.005.
[31] S.J. Baker, C.Z. Ding, T. Akama, Y.-K. Zhang, V. Hernandez, Y. Xia, Therapeutic potential of boron-containing compounds, Future Med. Chem. 1 (2009) 1275–1288. https://doi.org/10.4155/fmc.09.71.
[32] A. Zych, J. Tellers, L. Bertolacci, L. Ceseracciu, L. Marini, G. Mancini, A. Athanassiou, Biobased, Biodegradable, Self-healing boronic ester vitrimers from epoxidized soybean oil acrylate, ACS Appl. Polym. Mater. 3 (2021) 1135–1144. https://doi.org/10.1021/acsapm.0c01335.
[33] G. Damonte, B. Barsanti, A. Pellis, G.M. Guebitz, O. Monticelli, On the effective application of star-shaped polycaprolactones with different end functionalities to improve the properties of polylactic acid blend films, Eur. Polym. J. 176 (2022) 111402. https://doi.org/10.1016/j.eurpolymj.2022.111402.
[34] G. Damonte, A. Vallin, D. Battegazzore, A. Fina, O. Monticelli, Synthesis and characterization of a novel star polycaprolactone to be applied in the development of graphite nanoplates-based nanopapers, React. Funct. Polym. 167 (2021) 105019. https://doi.org/10.1016/j.reactfunctpolym.2021.105019.
[35] G. Damonte, L. Maddalena, A. Fina, D. Cavallo, A.J. Müller, M.R. Caputo, A. Mariani, O. Monticelli, On novel hydrogels based on poly(2-hydroxyethyl acrylate) and polycaprolactone with improved mechanical properties prepared by frontal polymerization, Eur. Polym. J. 171 (2022) 111226. https://doi.org/10.1016/j.eurpolymj.2022.111226.
[36] M.A. Woodruff, D.W. Hutmacher, The return of a forgotten polymer - polycaprolactone in the 21st century, Prog. Polym. Sci. 35 (2010) 1217–1256. https://doi.org/10.1016/j.progpolymsci.2010.04.002.
[37] E.E.L. Maassen, R. Anastasio, L.C.A. Breemen, R.P. Sijbesma, J.P.A. Heuts, Thermally reversible diels–alder bond-containing acrylate networks showing improved lifetime, Macromol. Chem. Phys. 221 (2020) 2000208. https://doi.org/10.1002/macp.202000208.
[38] M.K. Smith, B.H. Northrop, Vibrational properties of boroxine anhydride and boronate ester materials: model systems for the diagnostic characterization of covalent organic frameworks, Chem. Mater. 26 (2014) 3781–3795. https://doi.org/10.1021/cm5013679.
[39] M. Jayakannan, S. Ramakrishnan, Effect of branching on the thermal properties of novel branched poly(4-ethyleneoxy benzoate), J. Polym. Sci. Part A Polym. Chem. 38 (2000) 261–268. https://doi.org/10.1002/(SICI)1099-0518(20000101)38:1<261::AID-POLA31>3.0.CO;2-Z.
[40] F. Paquin, J. Rivnay, A. Salleo, N. Stingelin, C. Silva, Multi-phase semicrystalline microstructures drive exciton dissociation in neat plastic semiconductors, J. Mater. Chem. C. 3 (2015) 10715–10722. https://doi.org/10.1039/b000000x.
[41] E. Ergoz, J.G. Fatou, L. Mandelkern, Molecular weight dependence of the crystallization kinetics of linear polyethylene. i. experimental results, Macromolecules 5 (1972) 147–157. https://doi.org/10.1021/ma60026a011.
[42] L. Mandelkern, The relation between structure and properties of crystalline polymers, Polym. J. 17 (1985) 337–350. https://doi.org/10.1295/polymj.17.337.
[43] M.J. Jenkins, K.L. Harrison, The effect of molecular weight on the crystallization kinetics of polycaprolactone,

Polym. Adv. Technol. 17 (2006) 474–478. https://doi.org/10.1002/pat.733.
[44] A.A. Puchkov, N.G. Sedush, A.I. Buzin, T.N. Bozin, A. V. Bakirov, R.S. Borisov, S.N. Chvalun, Synthesis and characterization of well-defined star-shaped poly(l-lactides), Polymer 264 (2023) 125573. https://doi.org/10.1016/j.polymer.2022.125573.
[45] M. Unger, C. Vogel, H.W. Siesler, Molecular weight dependence of the thermal degradation of poly(ε-caprolactone): a thermogravimetric differential thermal fourier transform infrared spectroscopy Study, Appl. Spectrosc. 64 (2010) 805–809. https://doi.org/10.1366/000370210791666309.
[46] V. Solouki Bonab, V. Karimkhani, I. Manas-Zloczower, Ultra-fast microwave assisted self-healing of covalent adaptive polyurethane networks with carbon nanotubes, Macromol. Mater. Eng. 304 (2019). https://doi.org/10.1002/mame.201800405.
[47] A.E. Gerdroodbar, H. Alihemmati, M. Bodaghi, M. Salami-Kalajahi, A. Zolfagharian, Vitrimer chemistry for 4d printing formulation, Eur. Polym. J. 197 (2023) 112343. https://doi.org/10.1016/j.eurpolymj.2023.112343.
[48] X.F. Li, P.F. Wang, C.L. Feng, D.Q. Liu, J.K. Chen, F.C. Wu, Acute toxicity and hazardous concentrations of zinc to native freshwater organisms under different ph values in china, Bull. Environ. Contam. Toxicol. 103 (2019) 120–126. https://doi.org/10.1007/s00128-018-2441-2.
[49] A. Stjerndahl, A. Finne-Wistrand, A.C. Albertsson, C.M. Bäckesjö, U. Lindgren, Minimization of residual tin in the controlled Sn(II)octoate-catalyzed polymerization of ε-caprolactone, J. Biomed. Mater. Res. - Part A. 87 (2008) 1086–1091. https://doi.org/10.1002/jbm.a.31733.
[50] P.S. Giram, B. Garnaik, Evaluation of biocompatibility of synthesized low molecular weight plga copolymers using zinc l-proline through green route for biomedical application, Polym. Adv. Technol. 32 (2021) 4502–4515. https://doi.org/10.1002/pat.5452.
[51] M.C. Tanzi, P. Verderio, M.G. Lampugnani, M. Resnati, E. Dejana, E. Sturani, Cytotoxicity of some catalysts commonly used in the synthesis of copolymers for biomedical use, J. Mater. Sci. Mater. Med. 5 (1994) 393–396. https://doi.org/10.1007/BF00058971.
[52] O. Coulembier, S. Moins, J.M. Raquez, F. Meyer, L. Mespouille, E. Duquesne, P. Dubois, Thermal degradation of poly(l-lactide): accelerating effect of residual dbu-based organic catalysts, Polym. Degrad. Stab. 96 (2011) 739–744. https://doi.org/10.1016/j.polymdegradstab.2011.02.014.
[53] Y. Fan, H. Nishida, Y. Shirai, T. Endo, Racemization on thermal degradation of poly(L-lactide) with calcium salt end structure, Polym. Degrad. Stab. 80 (2003) 503–511. https://doi.org/10.1016/S0141-3910(03)00033-8.
[54] H. Nagahara, M. Ono, M. Konishi, Y. Fukuoka, Partial hydrogenation of benzene to cyclohexene, Appl. Surf. Sci. 121–122 (1997) 448–451. https://doi.org/10.1016/S0169-4332(97)00325-5.
[55] A. Pellis, E.H. Acero, H. Weber, M. Obersriebnig, R. Breinbauer, E. Srebotnik, G.M. Guebitz, Biocatalyzed approach for the surface functionalization of poly(L-lactic acid) films using hydrolytic enzymes, Biotechnol. J. 10 (2015) 1739–1749. https://doi.org/10.1002/biot.201500074.
[56] A. Gricajeva, A.K. Nadda, R. Gudiukaite, Insights into polyester plastic biodegradation by carboxyl ester hydrolases, J. Chem. Technol. Biotechnol. 97 (2022) 359–380. https://doi.org/10.1002/jctb.6745.
[57] K. Masaki, N.R. Kamini, H. Ikeda, H. Iefuji, Cutinase-like enzyme from the yeast cryptococcus sp. strain s-2 hydrolyzes polylactic acid and other biodegradable plastics, Appl. Environ. Microbiol. 71 (2005) 7548–7550. https://doi.org/10.1128/AEM.71.11.7548-7550.2005.
[58] G. Damonte, A. Vallin, A. Fina, O. Monticelli, On the development of an effective method to produce conductive pcl film, Nanomaterials 11 (2021) 1385. https://doi.org/10.3390/nano11061385.
[59] C. Siracusa, F. Quartinello, M. Soccio, M. Manfroni, N. Lotti, A. Dorigato, G.M. Guebitz, A. Pellis, On the selective enzymatic recycling of poly(pentamethylene 2,5-furanoate)/poly(lactic acid) blends and multiblock copolymers, ACS Sustain. Chem. Eng. 11 (2023) 9751–9760. https://doi.org/10.1021/acssuschemeng.3c01796.
[60] Y.-R. Oh, Y.-A. Jang, J.K. Song, G.T. Eom, Efficient enzymatic depolymerization of polycaprolactone into 6-hydroxyhexanoic acid by optimizing reaction conditions and microbial conversion of 6-hydroxyhexanoic acid into adipic acid for eco-friendly upcycling of polycaprolactone, Biochem. Eng. J. 185 (2022) 108504. https://doi.org/10.1016/j.bej.2022.108504.